A SYNTHETIC AND STRUCTURAL INVESTIGATION OF PNICTOGEN AND CHALCOGEN PERI-SUBSTITUTED NAPHTHALENES

Phillip Nejman

A Thesis Submitted for the Degree of PhD
at the
University of St Andrews

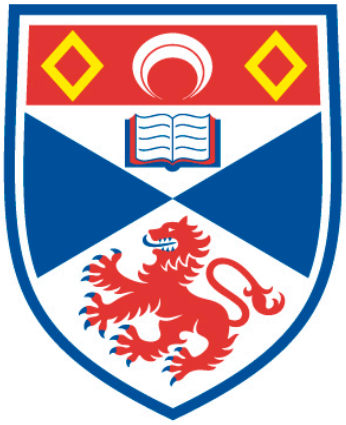

2017

A Synthetic and Structural Investigation of Pnictogen and Chalcogen *peri*-Substituted Naphthalenes

A thesis submitted by

Phillip S. Nejman

University of St Andrews

FOUNDED 1413

In Partial Fulfilment for the award of

Doctor of Philosophy

University of St Andrews, School of Chemistry

7th March 2017

Declarations

I, Phillip S. Nejman, hereby certify that this thesis, which is approximately 62,000 words in length, has been written by me, and that it is the record of work carried out by me, or principally by myself in collaboration with others as acknowledged, and that it has not been submitted in any previous application for a higher degree.

I was admitted as a research student in October 2013 and as a candidate for the degree of Doctor of Philosophy in August 2014; the higher study for which this is a record was carried out in the University of St Andrews between 2013 and 2017.

Collaboration Statement

I am grateful to Dr Kasun S. Athukorala Arachchige, Dr David B. Cordes and Professor Alexandra M. Z. Slawin for single crystal X-ray structure determinations, by collecting and solving the data. Elemental analyses were carried out by Mr Stephen Boyer at London Metropolitan University. Mass spectrometry was performed either by the analytical service within the University of St Andrews Chemistry department by Mrs Caroline E. R. Horsburgh or by the EPSRC National Mass Spectrometry Service in Swansea. The crystal structure of benzene-1,2-dithiol was provided by Mr Nicholas Black. Part of the work presented in Chapter 5 was carried out in collaboration with two honours research project students, Miss Bethany Lawson in 2014/15 and Miss Rhiann Ferguson in 2015/16. All compounds synthesised are numbered and ordered by chapter in order of their appearance in this work (e.g. C1-1, C2-1, C2-2... *etc.*). These are given in the laminated handout for convenience.

Date: 7th March 2017 Signature of Candidate: (P. S. Nejman)

2. Supervisor's declaration:

I hereby certify that the candidate has fulfilled the conditions of the Resolution and Regulations appropriate for the degree of Doctor of Philosophy (PhD) in the University of St Andrews and that the candidate is qualified to submit this thesis in application for that degree.

Date: 7th March 2017 Signature of Supervisor: (Dr P. Kilian)

3. Permission for publication:

In submitting this thesis to the University of St Andrews I understand that I am giving permission for it to be made available for use in accordance with the regulations of the University Library for the time being in force, subject to any copyright vested in the work not being affected thereby. I also understand that the title and the abstract will be published, and that a copy of the work may be made and supplied to any bona fide library or research worker, that my thesis will be electronically accessible for personal or research use unless exempt by award of an embargo as requested below, and that the library has the right to migrate my thesis into new electronic forms as required to ensure continued access to the thesis. I have obtained any third-party copyright permissions that may be required in order to allow such access and migration, or have requested the appropriate embargo below.

The following is an agreed request by candidate and supervisor regarding the publication of this thesis:

Embargo on both all of the printed and electronic copies for the fixed period of two years on the following grounds:

- Publication would preclude future publication

Date: 7th March 2017 Signature of Candidate: (P. S. Nejman)

Date: 7th March 2017 Signature of Supervisor: (Dr P. Kilian)

Abstract

Donor–acceptor complexes have been known for over a century and enjoy a long list of applications in chemistry. The work presented in this thesis explores the dative interaction between phosphorus and its heavier congener bismuth. Utilising *peri*-substitution, atoms can be forced in close proximity to one another resulting in a repulsive (non-bonding) interaction or an attractive (bonding) interaction. Hence, *peri*-substitution can be used to support traditionally ephemeral species. A range of phosphorus and bismuth containing *peri*-substituted compounds were synthesised and characterised using multi-nuclear NMR spectroscopy, mass spectrometry, elemental analysis and single crystal X-ray diffraction with the data for several structures collected and solved personally. Where the bismuth moiety contained two aryl groups, no bonding interaction between the phosphorus and bismuth was observed owing to the poor Lewis acidity of the bismuth. Upon increasing the Lewis acidity, by exchanging one of the aryl groups with a halogen, the formation of a donor–acceptor complex was observed. This series of compounds represents rare examples of structurally characterised phosphine–bismuthine donor–acceptor complexes. The formation of bismuth(V) derivatives proved to be incredibly challenging with only one compound obtained. The compound was identified as a phosphino–bismuthonium salt.

The coordination of *S*,*S* bidentate ligands remains an important area of chemistry. Complexes bearing this type of ligand have a number of industrial applications including catalysts in vulcanisation and lubricant additives. These complexes can also show a range of electrochemical properties and can support unusual magnetic properties. Two series of rhodium and iridium complexes were prepared using aromatic dithiolates of varying flexibility and size. These were characterised using multinuclear NMR spectroscopy, mass spectrometry, elemental analysis and single crystal X-ray diffraction with the data for most of the structures collected and solved personally. Bimetallic complexes were shown to form *via* bridging sulfur and/or chlorine atoms when the metal centre was coordinatively unsaturated. A large variation in the type of structure was observed depending on the flexibility of the aromatic backbone with an interesting tetrameric structure obtained when the biphenyl backbone was utilised. Monomeric forms of the complexes were obtained using a phosphorus donor to occupy the vacant site. The change in flexibility of the backbone was shown to have little effect on the structure formed. Altering the size and electronics of the phosphorus ligand was investigated with the electronic properties shown to overcome any steric restrictions imposed by an increased size as determined by the Tolman cone angle.

Acknowledgements

By the time my student card expires in September 2017 I will have been a registered student at the University of St Andrews for eleven years. To some that may seem idyllic and for the most part I'd tend to agree with them, I've certainly enjoyed my time here! I'm not the most conventional person in the world and my route to this PhD thesis is a testimony to that. In keeping with this my first acknowledgement is not to my supervisors, but, Prof. Alex Slawin whose sound advice and understanding led me to join the WooKiWin (**Woo**llins/**Ki**lian/Sla**win**) conglomerate.

I'm indebted to Dr Petr Kilian and Prof. Derek Woollins (alphabetical order, not favouritism) for taking me into their groups after my "false start". Your guidance and advice have helped me to achieve so much over the past three years from the seven publications to the supervision of all those project students and everything in-between. I know a lot of people think doing a PhD is really stressful and requires you to have practically no life outside of the lab. That has certainly not been my experience which is a testament to the way in which you both manage your research groups. For that, and all the enlightening conversations we've had over the years I thank you both. I'd also like to take the opportunity to thank Dr David Cordes and Prof. Alex Slawin for their help regarding everything relating to single crystal X-ray diffraction. Whether it was running and solving the data for me or helping me out when the MINI decided to have "one of those days". Finally I'd like to thank Dr Iain Smellie who has provided me with excellent advice and been a sounding board for so many things over the years.

I have met so many wonderful people within the research groups I've been in during my time at St Andrews. I'd like to make a special mention of Dr Lorenz Obrecht, Dr Roy McBurney and Dr Upulani Somisara who all made my first couple of years researching so entertaining. The PhD students and Postdocs of the WooKiWin conglomerate have all made my time in the group memorable for so many different reasons. Laurence provided endless comedy with his graveyard of cafetieres (he's got a plastic one now) and killing of keyboards *via* coffee packet explosions. Nick was always up for a trip to the Whey Pat for a game of darts or a session of "bin ball" in the office. Paula (now Dr Paula Sanz Camacho) could always be relied on for a good chat about everything and anything going on within the department. To all the other members of the groups past and present thanks for making my time unforgettable. Hopefully I haven't missed anyone out but if I have then apologies, either that, or you weren't as important as you think you were!

A large amount of my time (some might say too much) over the last few years has been taken up with lab demonstrating, school outreach programmes and honours research project supervision. The

UG teaching labs were always a source of entertainment with the rule, there is no such thing as a stupid question, being pushed to its limit on occasion. Lab demonstrating provided a perfect distraction from failed research experiments partly down to the, for want of a better word, insanity of the UG students. I have also had the joy of helping honours research project students all of whom, whether they believe it or not, taught me more lessons and skills then I ever did them. So Rhiann, Bethany, Paul and Christina (alphabetical by last name guys!) thanks for everything over the last couple of years. This includes, but is not limited to; producing NMR spectra with more grease than compound in it and using the same word/phrase in your reports to describe everything.

Outside of the lab I've been fortunate to meet some great people through both the eleven-a-side and six-a-side football teams I've been a part of. So thanks to the Whipp Inn Boys (with special mention to Euan "sicknote" Shaw for introducing me to the team), Studs N Balls and the various chemistry based teams I've played in.

Staying even moderately sane during a PhD is important and whilst I'm sure the next person I'm going to thank will disagree, I reckon I did not too bad on that front. I know that the lifts to play golf at 9am on a Sunday morning, having someone to complete all the Lego games I own and listen to my inane drivel have been major factors in that endeavour. So thanks Siobhan for all of that and so much more besides which, incidentally, includes putting the vast majority of the commas in this thesis!

Finally I would like to make mention of the person who inspired me to undertake a PhD who sadly passed away in 2011, Dr Nigel Botting. I was fortunate enough to conduct my final year project within his research group in 2010/2011 which is when I decided that going on to do a PhD was what I wanted. His attitude towards both teaching and research is one I have tried to emulate over the last five years and I will continue to do so for many more to come. If I thought this thesis good enough I'd dedicate it to him but to me that would be arrogant. Instead, I will just say thank you Dr Nigel Botting.

Contents

Declarations i
Abstract iii
Acknowledgements iv
Contents vi
Abbreviations xii
General Abbreviations xii
Spectroscopic Abbreviations xiii
Overview xiv
Chapter 1 – General Introduction 1
1.1 – Bismuth: Not Your Everyday Element 1
1.1.1 – The occurrence of bismuth in nature and its uses 2
1.2 – Donor–Acceptor Complexes 4
1.2.1 – Donor–Acceptor complexes involving phosphorus 4
1.2.2 – Donor–Acceptor complexes involving bismuth 7
1.3 – *peri*-Substitution 11
1.3.1 – *peri*-substitution in the formation of novel bonding motifs 13
1.4 – Through-Space Spin-Spin Coupling 18
1.4.1 – ^{13}C–^{31}P through-space coupling 19
Chapter 2 – Phosphorus–Bismuth *peri*-Substituted Acenaphthenes 21
2.1 – Introduction to *peri*-Substituted Bismuth Compounds 21
2.2 – Building a *peri*-Substituted Compound 25
2.3 – Bismuth starting materials preparation 26
2.4 – Synthesis and Characterisation of a Geminally Substituted Tris(acenaphthyl) Bismuthine 28
2.4.1 – Spectroscopic analysis of C2-2 28
2.4.2 – Crystallographic characterisation of C2-2 31
2.4.3 – Varying the ratio of bismuth trichloride 33
2.5 – *peri*-Substituted Unsymmetrical Triaryl Bismuthines: A Synthetic and Structural Study. 34
2.5.1 – Spectroscopic analysis of C2-5 and C2-6 36
2.5.2 – Crystallographic characterisation of C2-5 and C2-6 38

2.6 – Phosphine–Bismuthine Donor–Acceptor Complexes: A Synthetic, Spectroscopic and Structural Examination 40
2.6.1 – Spectroscopic analysis of C2-7−10 42
2.6.2 – Crystallographic characterisation of C2-7, C2-8, C2-9 and C2-10 46
2.6.2.1 – $(^{i}Pr)_2$P-Acenap-BiI_2, the surprise crystal structure 50
2.6.3 – Examining the solid state structural types of Bi(III) compounds 52
2.6.4 – Improved synthesis of C2-6 53
2.7 – Towards *peri*-Substituted Bismuth(V) Compounds 56
2.7.1 – Spectroscopic analysis of C2-12 58
2.7.2 – Crystallographic characterisation of C2-12 60
2.8 – Conclusions 61
Chapter 3 – General Introduction 63
3.1 – A Brief History of Sulfur 63
3.2 – Sulfur in Nature 64
3.3 – Types of Sulfur Donor Ligands 66
3.3.1 – Complexes containing the sulfide ligand 66
3.4 – Dithiolato Ligands in Complexation Chemistry 68
3.4.1 – Alkyl dithiolato transition metal complexes 69
3.4.2 – Aromatic dithiolato transition metal complexes 70
3.4.2.1 – Aromatic dithiolate ligands in hydrogenase mimics 71
3.4.2.2 – Naphthalene dithiolate based transition metal complexes 73
3.4.2.3 – Biphenyl dithiolate based transition metal complexes 79
3.4.2.4 – Acenaphthene dithiolate based transition metal complexes 80
3.4.2.5 – Binaphthalene dithiolate based transition metal complexes 81
Chapter 4 – Structural Diversity in Bimetallic Rhodium and Iridium Dithiolato Complexes 83
4.1 – Introduction to Bimetallic Dithiolato Complexes 83
4.1.1 – Bimetallic complexes using alkyl dithiolato ligands 84
4.1.2 – Bimetallic complexes using aromatic dithiolato ligands 86
4.2 – Constructing a Bimetallic System: Building Blocks 88
4.2.1 – Starting material preparation and new structural characterisation 89

4.2.1.1 – Crystallographic characterisation of H_2A-D 92
4.3 – Constructing a Bimetallic System: The Assembly 95
4.3.1 – Neutral bimetallic complexes 96
4.3.1.1 – Crystallographic characterisation of C4-3a'/b and C4-4a/b 99
4.3.2 – Cationic bimetallic complexes 104
4.3.2.1 – Crystallographic characterisation of C4-3c/4c and C4-5b/6b 106
4.3.3 – Dicationic multimetallic complexes 109
4.3.3.1 – Crystallographic characterisation of C4-3d 110
4.4 – Conclusions 112
Chapter 5 – Monomeric Rhodium and Iridium Dithiolato Complexes with Neutral Phosphine/Phosphite Donors 114
5.1 – Introduction to Monomeric Dithiolato Complexes 114
5.1.1 – Dithiolato rhodium and iridium complexes with phosphorus ligands 115
5.2 – Synthetic Routes to Monomeric Dithiolato Complexes 118
5.2.1 – Starting material preparation and new structural characterisation 119
5.2.1.1 – Crystallographic Characterisation of C5-3/4 and C5-8–C5-11 122
5.3 – Varying the Size and Flexibility of the Aromatic Backbone 126
5.3.1 – Monomeric rhodium dithiolato complexes with a PMe_3 ligand 126
5.3.1.1 – Crystallographic characterisation of C5-11b–e 129
5.4 – Examining the Role of the Phosphorus Ligand in Monomeric Rhodium and Iridium Dithiolato Complexes 132
5.4.1 – Spectroscopic and structural analysis of triethylphosphine containing complexes 134
5.4.1.1 – Crystallographic characterisation of C5-3b–d and C5-4b–d 136
5.4.2 – Spectroscopic and structural analysis of triphenylphosphine containing complexes 139
5.4.2.1 – Crystallographic characterisation of C5-5b/d and C5-6b/d 141
5.4.3 – Spectroscopic and structural analysis of triethyl phosphite containing complexes 143
5.4.3.1 – Crystallographic characterisation of C5-7b/7d and C5-8b/8d 146
5.4.4 – Spectroscopic and structural analysis of triphenyl phosphite containing complexes 147
5.4.4.1 – Crystallographic characterisation of C5-9b/d and C5-10d 151
5.5 – Conclusions 153

Chapter 6 – Experimental 155
6.1 – Chapter 2 Experimental Procedures 157
6.1.1 – Triphenylbismuth ($BiPh_3$) 157
6.1.2 – Diphenylbismuth chloride ($BiPh_2Cl$) 158
6.1.3 – Dichloro(phenyl)bismuth ($BiPhCl_2$) 159
6.1.4 – 5,6-dibromoacenaphthene ($AcenapBr_2$) 160
6.1.5 – $(^iPr)_2$P-Acenap-Br (C2-1) 161
6.1.6 – $((^iPr)_2$P-Acenap-$)_3$Bi (C2-2) 162
6.1.7 – $(^iPr)_2$P-Acenap-$BiPh_2$ (C2-5) 163
6.1.8 – $((^iPr)_2$P-Acenap-$)_2$BiPh (C2-6) 165
6.1.9 – $[(^iPr)_2$P-Acenap-BiPh$]^+$ $[BF_4]^-$ (C2-7) 167
6.1.10 – $(^iPr)_2$P-Acenap-BiPhCl (C2-8) 168
6.1.11 – $(^iPr)_2$P-Acenap-BiPhBr (C2-9) 169
6.1.12 – $(^iPr)_2$P-Acenap-BiPhI (C2-10) 171
6.1.13 – $[(^iPr)_2$P-Acenap-$BiPh_3]^+$ $[BiPh_2Cl_2]^-$ (C2-12) 172
6.2 – Chapter 4 Experimental Procedures 173
6.2.1 – Benzene-1,2-dithiol (H_2A) 173
6.2.2 – Naphtho[1,8-*cd*]-1,2-dithiole (S_2B) 174
6.2.3 – 5,6-dihydroacenaphtho-[5,6-*cd*]-1,2-dithiole (S_2C) 175
6.2.4 – Dibenzo-[*c*,*e*]-1,2-dithiine (S_2D) 176
6.2.5 – Naphthalene-1,8-dithiol (H_2B) 177
6.2.6 – Acenaphthene-5,6-dithiol (H_2C) 178
6.2.7 – [1,1'-biphenyl]-2,2'-dithiol (H_2D) 179
6.2.8 – Pentamethylcyclopentadienylrhodium(III) chloride (SM-1) 180
6.2.9 – Pentamethylcyclopentadienyliridium(III) chloride (SM-2) 180
6.2.10 – $[Cp^*Rh(BenzS_2)]_n$ (n = 1 or 2) (C4-3a) 181
4.2.11 – $[Cp^*Ir(BenzS_2]$ (C4-4a) 183
6.2.12 – $[Cp^*Rh(NaphthS_2)]_2$ (C4-3b) 184

6.2.13 – [Cp*Ir(NaphthS$_2$)]$_2$ (C4-4b) 185
6.2.14 – [(Cp*Rh)$_2$(AcenapS$_2$)Cl]$^+$ Cl$^-$ (C4-3c) 186
6.2.15 – [(Cp*Ir)$_2$(AcenapS$_2$)Cl]$^+$ Cl$^-$ (C4-4c) 187
6.2.16 – [(Cp*Rh)$_4$(μ^2-BiphenS$_2$)$_2$(μ^4-BiphenS$_2$)]$^{2+}$ 2Cl$^-$ (C4-3d) 188
6.2.17 – [(Cp*Rh)$_2$(NaphthS$_2$)Cl]$^+$ Cl$^-$ (C4-5b) 189
6.2.18 – [(Cp*Ir)$_2$(NaphthS$_2$)Cl]$^+$ Cl$^-$ (C4-6b) 190
6.3 – Chapter 5 Experimental Procedures 191
6.3.1 – [Cp*RhCl$_2$PEt$_3$] (C5-3) 191
6.3.2 – [Cp*IrCl$_2$PEt$_3$] (C5-4) 192
6.3.3 – [Cp*RhCl$_2$PPh$_3$] (C5-5) 193
6.3.4 – [Cp*IrCl$_2$PPh$_3$] (C5-6) 194
6.3.5 – [Cp*RhCl$_2$P(OEt)$_3$] (C5-7) 195
6.3.6 – [Cp*IrCl$_2$P(OEt)$_3$] (C5-8) 196
6.3.7 – [Cp*RhCl$_2$P(OPh)$_3$] (C5-9) 197
6.3.8 – [Cp*IrCl$_2$P(OPh)$_3$] (C5-10) 198
6.3.9 – [Cp*Rh(NaphthS$_2$)PMe$_3$] (C5-11b) 199
6.3.10 – [Cp*Rh(AcenapS$_2$)PMe$_3$] (C5-11c) 200
6.3.11 – [Cp*Rh(BiphenS$_2$)PMe$_3$] (C5-11d) 201
6.3.12 – [Cp*Rh(2,2'-BinapS$_2$)PMe$_3$] (C5-11e) 202
6.3.13 – [Cp*Rh(NaphthS$_2$)PEt$_3$] (C5-3b) 203
6.3.14 – [Cp*Ir(NaphthS$_2$)PEt$_3$] (C5-4b) 204
6.3.15 – [Cp*Rh(AcenapS$_2$)PEt$_3$] (C5-3c) 205
6.3.16 – [Cp*Ir(AcenapS$_2$)PEt$_3$] (C5-4c) 206
6.3.17 – [Cp*Rh(BiphenS$_2$)PEt$_3$] (C5-3d) 207
6.3.18 – [Cp*Ir(BiphenS$_2$PEt$_3$] (C5-4d) 208
6.3.19 – [Cp*Rh(NaphthS$_2$)PPh$_3$] (C5-5b) 209
6.3.20 – [Cp*Ir(NaphthS$_2$)PPh$_3$] (C5-6b) 210
6.3.21 – [Cp*Rh(BiphenS$_2$)PPh$_3$] (C5-5d) 212

6.3.22 – [Cp*Ir(BiphenS_2)PPh_3] (C5-6d) 213

6.3.23 – [Cp*Rh(NaphthS_2)P$(OEt)_3$] (C5-7b) 214

6.3.24 – [Cp*Ir(NaphthS_2)P$(OEt)_3$] (C5-8b) 215

6.3.25 – [Cp*Rh(BiphenS_2)P$(OEt)_3$] (C5-7d) 216

6.3.26 – [Cp*Ir(BiphenS_2)P$(OEt)_3$] (C5-8d) 217

6.3.27 – [Cp*Rh(NaphthS_2)P$(OPh)_3$] (C5-9b) 219

6.3.28 – [Cp*Ir(NaphthS_2)P$(OPh)_3$] (C5-10b) 220

6.3.29 – [Cp*Rh(BiphenS_2)P$(OPh)_3$] (C5-9d) 221

6.3.30 – [Cp*Ir(BiphenS_2)P$(OPh)_3$] (C5-10d) 222

General Conclusions and Future Scope 224

Publications List 226

References 228

Abbreviations

General Abbreviations

∑αβγ	Sum of the *peri*-Region Angles
3c–4e	Three-centre four-electron
Å	Ångström (1×10^{-10} m)
ABB	Aromatic Backbone
Acenap	Acenaphthene-5,6-diyl
ACS	Acetyl Coenzyme A Synthase
APCI	Atmospheric Pressure Chemical Ionisation
Ar	General aryl group
ATP	Adenosine Triphosphate
b.p	Boiling Point
Bu	Butyl
Calcd.	Calculated
cod	1,5-cyclooctadiene
CODH	Carbon Monoxide Dehydrogenase
Cp	Cyclopentadienyl
Cp*	Pentamethylcyclopentadienyl
CSD	Cambridge Structural Database
Cy	Cyclohexyl
DCE	1,2-dichloroethane
DCM	Dichloromethane
DFT	Density Functional Theory
dmit	2-thioxo-1,3-dithiole-4,5-dithiolate
dmp	2,6-Dimesitylphenyl
dppb	1,4-*Bis*(diphenylphosphino)butane
dppe	1,2-*Bis*(diphenylphosphino)ethane
dppm	1,1-*Bis*(diphenylphosphino)methane
dppp	1,3-*Bis*(diphenylphosphino)propane
DMSO	Dimethyl Sulfoxide
edt	Ethane-1,2-dithiolate
EDTA	Ethylenediaminetetracetic acid
ES	Electrospray
Et	Ethyl
ether	Diethyl Ether
eq.	Equivalent
Fc	Ferrocenyl ($C_{10}H_8Fe$)
HOMO	Highest Occupied Molecular Orbital
HCDTN	hexachlorodithionaphthalene
HRMS	High Resolution Mass Spectrometry
^{i}Pr	isopropyl
IR	Infrared
K	Kelvin
kcal	kilocalorie
M	Molar (mol/L)
Nap	Naphthalene-1,8-diyl
n-Bu	n-Butyl
NBS	*N*-Bromosuccinimide
NHC	*N*-Heterocyclic carbene
NMR	Nuclear Magnetic Resonance
NSI	Nanospray Ionisation
Me	Methyl
MeCN	Acetonitrile
Mes	Mesityl (2,4,6-trimethylphenyl)
meso	Meso Isomer
mol	Moles
m.p	Melting Point
μ	Bridging
O/N	Overnight

OCS	Carbonyl Sulfide
OTf	Trifluoromethanesulfonate
p	*para*
PaphyH	2-pyridinecarboxaldehyde-2-pyridylhydrazone
Ph	Phenyl
Phen	1,10-phenanthroline
Pn	Pnictogen (Group 15 element)
ppm	parts per million ($1/10^6$)
Pr	Propyl
rac	Racemic
r_{cov}	Covalent radii
r.t	Room temperature (*ca.* 16−25 °C)
r_{vdw}	van der Waals radii
Σr_{vdW}	Sum of the van der Waals radii
^{t}Bu	tertiary-butyl
TCNQ	7,7,8,8-tetracyano-*p*-quinodimethane
TCTTN	Tetrachlorotetrathionaphthalene
THF	Tetrahydrofuran
TMEDA	*N,N,N',N'*-tetramethylethylene-1,2-diamine
Tol	Tolyl (4-methylphenyl)
triphos	*Bis*(2-diphenylphosphinoethyl) phenylphosphine
TTF	Tetrathiafulvalene
TTN	Tetrathionaphthalene
tto	Tetrathiooxalate
TTT	Tetrathiotetracene

Spectroscopic Abbreviations

ArC	Aromatic Carbon
ArH	Aromatic Hydrogen
br	Broad
COSY	Correlation Spectroscopy
d	Doublet
dd	Doublet of Doublets
dq	Doublet of Quartets
dt	Doublet of Triplets
HMBC	Heteronuclear Multiple Bond Coherence
HSQC	Heteronuclear Single Quantum Correlation
Hz	Hertz
h	Heptet
J	Scalar Coupling Constant
m	Multiplet (NMR) or Medium (IR)
$^{xts}J_{AA}$	Through-Space Coupling (X = Formal Bond Separation, A = Coupling Nuclei)
ppm	Chemical Shift
*p*t	*pseudo* Triplet
*p*td	*pseudo* Triplet of Doublets
*p*p	*pseudo* Pentet
C_q	Quaternary Carbon
q	Quartet
s	Singlet (NMR) or Strong (IR)
t	Triplet
tt	Triplet of Triplets
v	Stretch
vs	Very Strong
w	Weak

Overview

Part 1 – A Synthetic, Spectroscopic and Structural Examination of *peri*-Substituted Phosphorus–Bismuth Acenaphthenes

Chapter 1 – General Introduction: This chapter aims to provide a brief overview of the history and chemistry of bismuth as well as the chemistry of main group donor–acceptor complexes including those developed within the Kilian research group. Short discussions of major concepts relating to this work such as *peri*-substitution and through-space coupling are also included.

Chapter 2 – Phosphorus–Bismuth peri-Substituted Acenaphthenes: A short discussion of the chemistry of *peri*-substituted compounds containing bismuth is provided. The synthesis of novel *peri*-substituted phosphorus–bismuth systems, including examples of donor–acceptor complexes, and their characterisation is presented.

Part 2 – Aromatic Dithiolate Ligands in the Formation of Rhodium and Iridium Complexes: A Synthetic, Spectroscopic and Structural Investigation

Chapter 3 – General Introduction: This chapter aims to provide a brief overview of the history, natural occurrence and coordination chemistry of sulfur. Several types of sulfur donor ligands are explored with a focus on those incorporating an aromatic backbone.

Chapter 4 – Structural Diversity in Bimetallic Rhodium and Iridium Dithiolato Complexes: A short introduction to bimetallic systems using dithiolato ligands is presented. The synthetic approach to bimetallic rhodium and iridium complexes using aromatic dithiolate of varying flexibility is discussed, drawing attention to the differing structures adopted in the solid state.

Chapter 5 – Monomeric Rhodium and Iridium Dithiolato Complexes with Neutral Phosphine/Phosphite Donors: A brief introduction into the use of phosphorus as a ligand relating specifically to dithiolato complexes is presented. The synthesis and characterisation of several series of monomeric rhodium and iridium complexes incorporating a phosphorus ligand are discussed.

Part 3 – Synthetic Protocols

Chapter 6 – Experimental Procedures: This chapter provides the experimental procedures and characterisation data for all the compounds presented in this research.

Part 1 – A Synthetic, Spectroscopic and Structural Examination of *peri*-Substituted Phosphorus–Bismuth Acenaphthenes

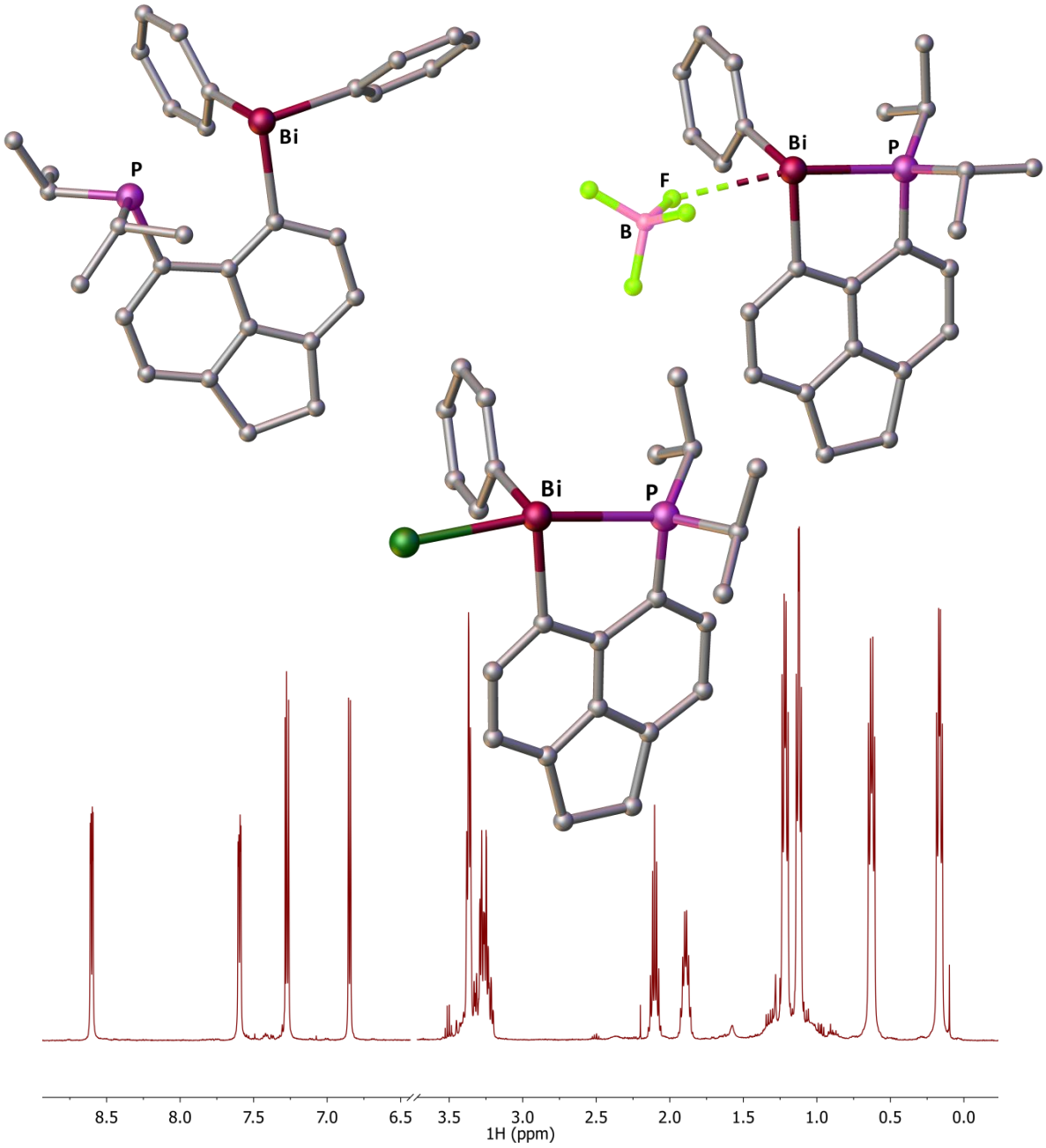

Chapter 1 – General Introduction

1.1 – Bismuth: Not Your Everyday Element

The part played in ancient civilisations by gold, silver, copper, iron, lead, tin, mercury, carbon and sulfur is well known. Certain other elements have a history that extends back through the centuries, albeit not quite as far, to the times of the alchemists. In this group may be mentioned the group 15 elements arsenic, antimony, bismuth and phosphorus. The early history of most of these elements is shrouded in so much uncertainty that only in the case of phosphorus is it possible to assign the discovery definitively to any one person.[1] Bismuth was known as the metal at least by 1480, however, its history in the Middle Ages is difficult to unravel because the element was so often confused with lead, tin, antimony or even gold.[2]

Figure 1: Bismite, Bi_2O_3 (left) and an artificially grown bismuth crystal showing the stair-step crystal structure (right).

The name bismuth is variously attributed to the Arabic *wiss majaht*, which refers to its ease of melting; the Persian *sipedak* or *isfidaz*, which means white; or the German terms *blei-weiss*, meaning white lead or *weisse masse* (*wismut*), which is an old mining term for white mass.[3] The sixteenth century German scholar G. Agricola latinised the name *wismut* to *bisemutum* around 1530. It was Agricola himself who first postulated that *bisemutum* was a specific metal itself with most others at the time believing it to be a kind of lead. However, credit for showing bismuth to be distinct from lead is actually attributed to the 18th century French scientist Claude Geoffroy the Younger.[4] Bismuth exists mostly in α-form (α-Bi) at standard pressure and temperature which is isostructural with rhombohedral black phosphorus with several other polymorphs known. Of the various known

forms of bismuth the only other well characterised form is ζ-Bi which has a body centre cubic structure in which each bismuth has eight nearest neighbours.[2] The colour seen in the crystal of bismuth (Figure 1, right) comes from the oxide tarnish and is iridescent showing many colours from yellow to blue.

1.1.1 – The occurrence of bismuth in nature and its uses

Bismuth can be found in both its native form and distributed within the earth's crust in a variety of minerals. Compared to other elements the abundance of bismuth within the earth's crust is extremely low at approximately 0.001−0.002 g t^{-1}. This value is similar to some of the more common platinum group metals and gold. As is common with the post-transition element metals bismuth is a chalcophile occurring in association with the chalcogens sulfur, selenium and tellurium as well as oxides and silicates. Bismuth mainly occurs as bismite (Bi_2O_3) (Figure 1, left), bismuthinite (Bi_2S_3) and bismutite ($(BiO)_2CO_3$) in association with lead, silver and cobalt ores.[2,4]

The main commercial source of bismuth is as a by-product obtained during the processing of complex ores which produce copper, lead, zinc, tin, gold and silver. The motivation for the removal of bismuth is the quality specified for these various base metals which requires the application of effective refining processes. World production figures for bismuth in 2015 were 8,500 tonnes with the vast majority (90%) being produced by China.[5] Two main methods used for the removal of bismuth are the Betterton-Kroll and Betts processes,[4,6] with the former responsible for over 90% of bismuth metal and is widely used around the world. The Betterton-Kroll process relies on the formation of compounds such as Ca_2Bi_2 and Mg_3Bi_2 which both have low densities and high melting points. During the refining process these compounds float to the surface of the molten lead and can be skimmed off as dross. Chlorination of the dross to remove calcium and magnesium followed by treatment with caustic soda produces bismuth with purity up to 99.95%. Sulfide ores are roasted to the oxide and then reduced by iron or charcoal. Because of its low melting point, very low solubility in Fe and fairly high oxidative stability in air Bi can be melted and cast in iron and steel vessels. The metal is too brittle to roll, draw or extrude at room temperature but above 225 °C bismuth can be worked quite well.

Generally bismuth is not used as a base metal, instead, its ability to form intermetallic compounds with unique properties has led to their use for specialised purposes. One of the earliest documented uses of a bismuth alloy was in 1450 when the Gutenberg printing presses started using type cut from such an alloy. The main use of bismuth is in the manufacture of low melting point alloys, many of

which will melt at temperatures below 100 °C. A well-known example is Woods metal (contains 26.7% Bi) which melts at 70°C, although there is another composition that melts at only 47 °C. These fusible alloys have several industrial applications, one of which is in automatic safety devices such as fire sprinklers, boiler plugs and controls for furnaces. A eutectic alloy is selected for this purpose as it has enough strength at ambient temperatures to hold parts together. Whilst at a specific elevated temperature it will melt thereby disconnecting the parts and making them safe or in the case of a fire sprinkler releasing the suppressant. Mixtures containing bismuth also have uses as solders and in bearing alloys. Several ceramic materials containing bismuth have displayed superconductive properties.[4]

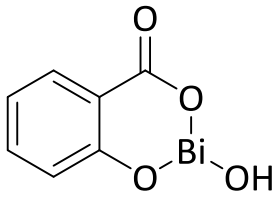

bismuth subsalicylate

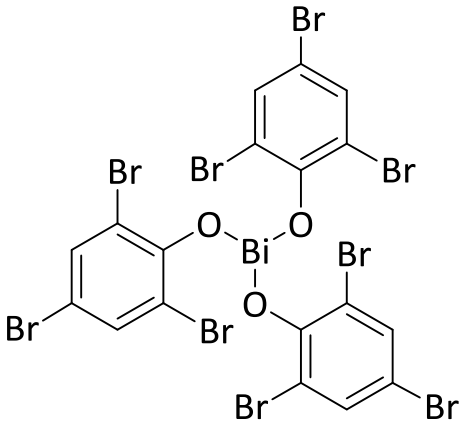

bismuth tribromophenate

Figure 2: Structure of Pepto-Bismol® and bismuth tribromophenate.

Unlike arsenic[7] and antimony,[8] bismuth[9] has an unusually low toxicity compared to other heavy elements such as lead.[10] As a consequence of the interest in the heavier group 15 elements as antiparasitic agents it became accepted that many of these preparations were antibacterial and had certain antiseptic properties. The low toxicity of bismuth in mammals made it especially suitable for incorporation into simple medical preparations for both internal use and as topical pastes for external use. The most widely known use of bismuth in medicine is bismuth subsalicylate (Figure 2) otherwise known as Pepto-Bismol® which is an antacid used to treat stomach discomforts. Other uses include BIPP® (bismuth subnitrate iodoform paraffin paste) which has been incorporated into dressings for wounds and xeroform, which contains bismuth tribromophenate (Figure 2), used for burn and skin graft dressings.[4]

1.2 – Donor–Acceptor Complexes

Donor-acceptor complexes are formed as a result of an attractive interaction between two molecules in which electron density is transferred from one to the other. The molecule which donates the electrons is labelled the donor whilst the molecule receiving them is known as the acceptor.[11] Although he did not realise it at the time, it was Louis Josef Gay-Lussac in 1809 who prepared the first donor acceptor complex by synthesising $H_3N{\cdot}BF_3$.[2] It wasn't until 1958 that Shore and Parry were able to prepare and isolate an ammonia borane adduct ($H_3N{\cdot}BH_3$) by reaction of gaseous ammonia with diborane which resulted in a white solid (Scheme 1).[12]

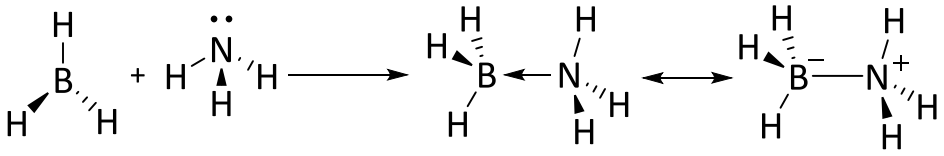

Scheme 1: The synthesis and resonance structures of ammonia borane.

This adduct can be drawn in two different ways, either as the dative structure showing the donation of the amine lone pair into a vacant p-orbital of the borane or as the zwitterion in which the nitrogen atom gains a positive charge with the boron atom becoming negative.

1.2.1 – Donor–Acceptor complexes involving phosphorus

Like amines, phosphines also have a lone pair which is capable of being donated to another molecule to form a bond. This is most commonly observed within transition metal chemistry where vast numbers of complexes have been formed using phosphine ligands. Phosphines are also π acids able to accept electron density from the metal orbitals into its own σ* orbitals. By altering the R groups of the phosphines the electronic and steric properties of the ligand are tuned to the requirements of the complex.[13] Alkyl phosphines are the poorest π acids due to the higher energy of their σ* orbitals, as the R groups become more electronegative π acidity increases (PR_3 < PAr_3 < $P(OR)_3$ < $P(OAr)_3$ < PCl_3 < PF_3). A common synthetic application which uses this donating ability is the protection of air sensitive phosphines by reacting them with a borane source such as $Me_2S{\cdot}BH_3$ resulting in a phosphine–borane adduct which is air stable. The borane is easily removed by reacting the adduct with an amine to deprotect the phosphine.[14-16]

Whilst many phosphorus donors are known it is also possible to make good acceptor molecules containing phosphorus. Phosphorus pentahalides (PX_5) are excellent acceptors which react readily

with neutral donors to form neutral P-hexacoordinate donor–acceptor complexes. An early example of this is the adduct (1:1) formed by the reaction of pyridine with PCl_5 (Figure 3).[17] There are a number of other adducts containing phosphorus(V) halides acting as Lewis acids with examples shown in Figure 3.[18,19]

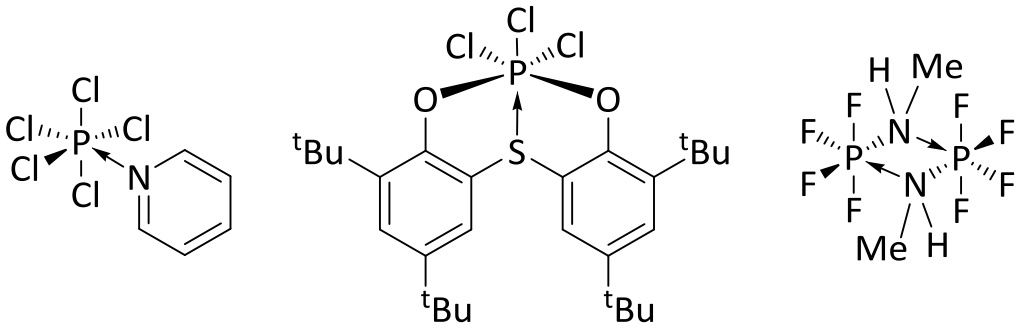

Figure 3: Phosphorus(V) halides acting as acceptors in donor–acceptor complexes.

Given the ability of phosphorus containing molecules to act as both donors and acceptors, it is plausible that two such molecules would combine to form a phosphine–phosphine donor–acceptor complex. In 1958 Holmes and Bertaut reported on a series of reactions to form donor–acceptor complexes using PMe_3, NMe_3 and NEt_3 as donors, with acceptors such as PCl_3, $AsCl_3$ and $SbCl_3$, $SbCl_5$ and $SnCl_4$.[20] They believed that the expected donor–acceptor adducts would be formed. The reactions resulted in the formation of white powdery solids at temperatures of less than 0 °C however at elevated temperatures decomposition occurred resulting in a clear liquid. A second report by Spangenberg and Sisler studying the reaction between selected trialkylphosphines and chlorophosphines proposed a different result. They found that in the majority of cases the alkyl phosphine was chlorinated by the chlorophosphines producing a trialkyldichlorophosphorane and a cyclophosphine (Scheme 2).[21]

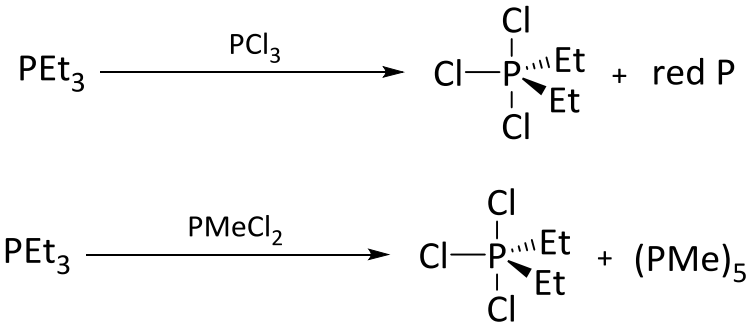

Scheme 2: Reactions reported by Spangenberg and Sisler.

Analysis of the compounds formed using infrared and Raman spectroscopy indicated that a 2:1 adduct had been formed between PMe_3 and PBr_3. The proposed structure was a single phosphorus tribromide acceptor adopting a *pseudo*-octahedral geometry with two donating trimethylphosphine molecules in the trans positions.[22] The first ^{31}P NMR evidence for the formation of these types of complexes appeared in 2001 suggesting both the 1:1 and 2:1 adducts were formed in the reaction between PMe_2Bz' (Bz' = 3,5-dimethylbenzyl) and PBr_3. In the same paper the first 1:1 phosphine–phosphine donor–acceptor complexes were structurally characterised (Figure 4), unfortunately the 2:1 complexes could not be crystallised due to their thermal decomposition above −40°C.[23]

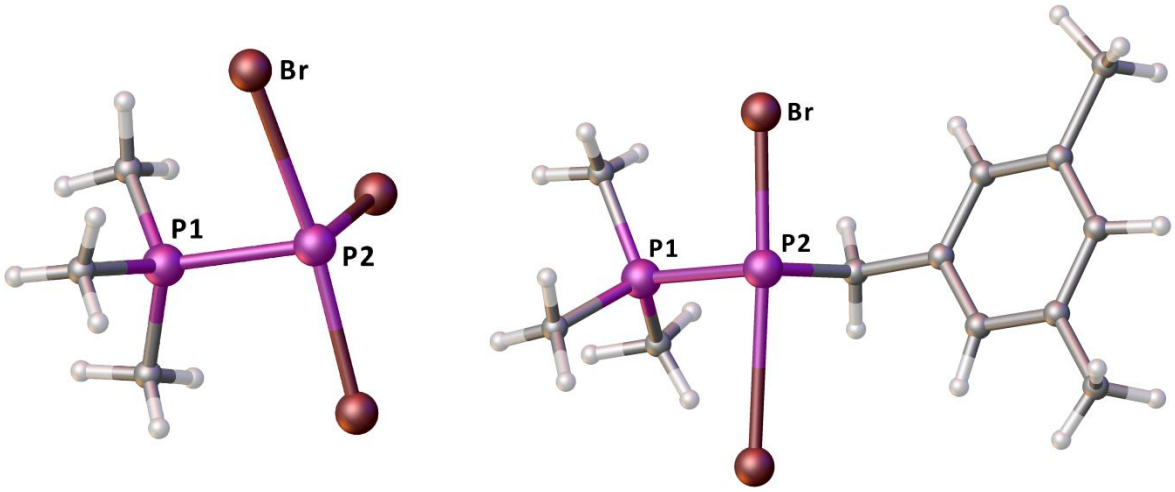

Figure 4: Crystal structures of the 1:1 adducts of PMe_3 and PBr_3 (left) and PBr_2Bz' (right).

A common feature of the phosphine–phosphine donor–acceptor complexes presented above is their lack of thermal stability at ambient temperatures. The first ambient temperature stable phosphine–phosphine donor–acceptor complex was isolated within the Kilian research group in 2009.[24] During the quenching of lithium phenolate, formed during the reaction shown in Scheme 3, with chlorotrimethylsilane the phenoxy groups were substituted for chloride groups yielding the donor–acceptor complex.[24]

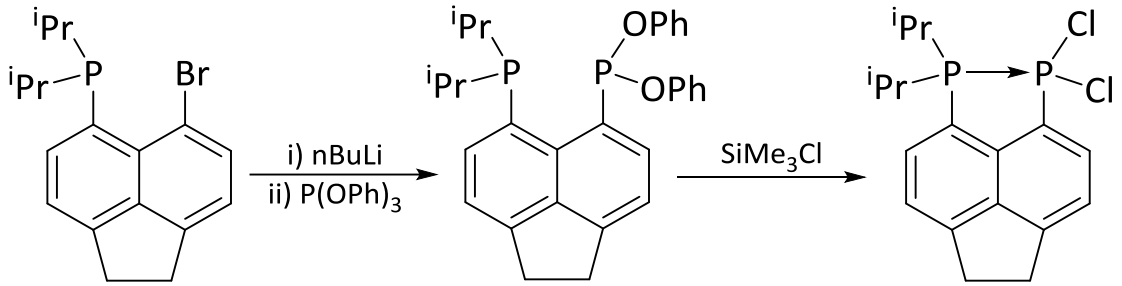

Scheme 3: Synthetic route to the first ambient temperature stable phosphine–phosphine donor–acceptor complex.

The compound was structurally characterised using single crystal X-ray diffraction which confirmed the bonding nature of the phosphine–phosphine interaction. Within the structure the donor phosphorus atom adopts a distorted tetrahedral geometry with the acceptor atom attaining a *pseudo*-trigonal bipyramidal geometry. The P–P distance within the structure of 2.2570(14) Å is typical for a P–P single bond as determined from the Cambridge Structural Database (CSD) (2.22 Å).[25,26]

1.2.2 – Donor–Acceptor complexes involving bismuth

There is relatively little in the literature regarding the use of bismuth in donor–acceptor complexes with only a limited number being structurally characterised. As mentioned in section 1.2.1 the early work investigating donor–acceptor complexes involving a phosphine and a heavier pnictogen was conducted by Holmes and Bertaut[20] followed by Summers and Sisler.[27] Just like the arsenic and antimony trihalides, bismuth trihalides can also act as good acceptors owing to their Lewis acidity. One of the first studies using bismuth trihalides as acceptors was performed by Alonzo and Consiglio in 1985.[28] They used both bidentate nitrogen (Phen) and phosphorus (dppe) ligands alongside the tridentate nitrogen ligand PaphyH in reactions with various bismuth trihalides (BiX_3, X = Cl, Br, I). In nearly all cases a 1:1 adduct was formed with the only exceptions being the complexes $[BiCl_3(Phen)_{1.33}]$ and $[BiCl_3(dppe)_{1.5}]$. The compounds all displayed similar properties in that they were poorly soluble in common organic solvents meaning analysis was conducted using IR spectroscopy, mass spectrometry and elemental analysis. Further work by Willey and co-workers on the reactions of bidentate phosphines with bismuth trichloride resulted in the crystal structures of $[Bi_2Cl_6(dppm)_2]$ and $[Bi_2Cl_6(dppe)_2]$ (Figure 5).[29] Both structures were similar in that they can be described as adopting an edge-shared bioctahedral geometry. In the case of $[Bi_2Cl_6(dppm)_2]$ all the halogens lie in an equatorial plane. More recently Burford and co-workers investigated the reaction of triphos with sources of $Pn(OTf)_3$ (Pn = P, As, Sb, Bi) discovering the first stable triphosphine complexes of both Sb(III) and Bi(III).[30]

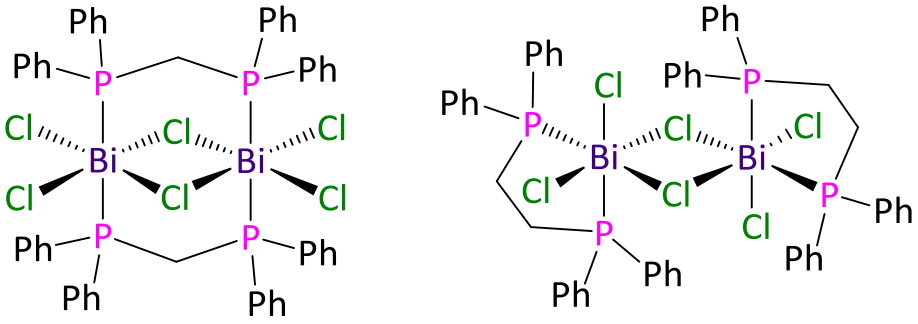

$[Bi_2Cl_6(dppm)_2]$ **$[Bi_2Cl_6(dppe)_2]$**

Figure 5: The phosphorus–bismuth complexes structurally characterised by Willey and co-workers.

Norman and co-workers have investigated a wide range of phosphine–bismuth donor–acceptor complexes.[31,32] Several structural types have been identified through the use of single crystal X-ray diffraction. The neutral complex formed between triethylphosphine and bismuth tribromide has the empirical formula $[BiBr_3(PEt_3)]$. Analysis of the crystal structure showed the complex exists as a tetramer in the solid state with each bismuth centre octahedrally coordinated (Figure 6, left). A large phosphine *trans* influence was observed as the Bi–Br bonds *trans* to the phosphine were longer by approximately 0.2 Å compared to the other bismuth to bridging bromine bonds.[32] Compounds with the general formula $[BiX_3(PR_3)_2]$ in which two phosphine ligands are present for each bismuth centre are also known. They all adopt the edge-shared bioctahedral structure shown in Figure 6 (right). Once again the *trans* influence of the phosphorus donor is observed within the complex.[31,32]

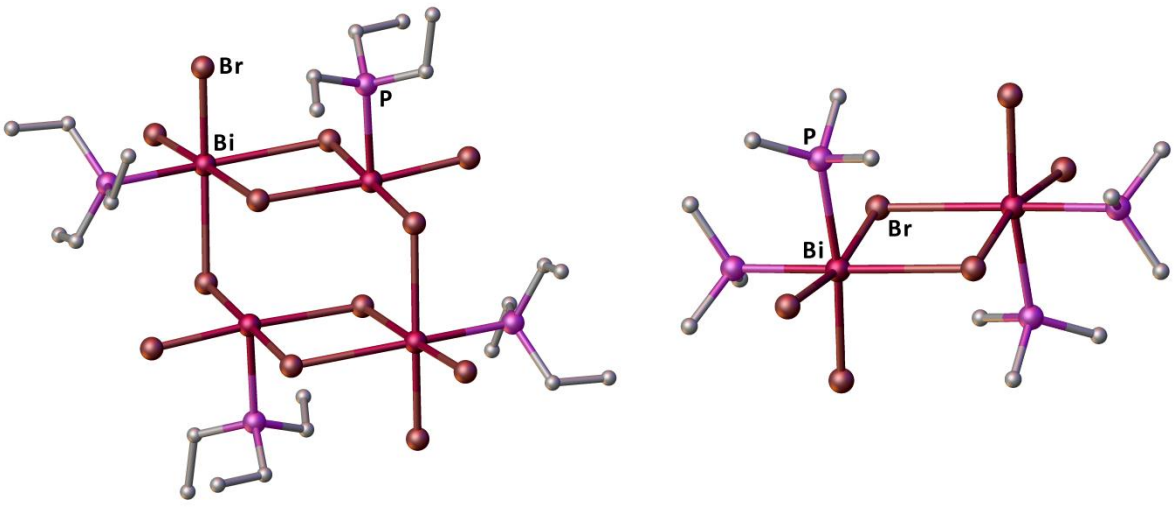

Figure 6: Crystal structures of phosphorus–bismuth donor–acceptor complexes prepared by Norman and co-workers ($[Bi_4Br_{12}(PEt_3)_4]$, left and $[Bi_2Br_6(PMe_3)_4]$, right).

In addition to the neutral compounds described above, Norman and co-workers also prepared the monoanionic complexes, $[\{PMe_3H\}\{Bi_2Br_7(PMe_3)_2\}]$ and $[\{PPh_4\}\{BiI_4(PMe_2Ph)_2\}]$, which were structurally characterised.[33,34] The anionic component $[Bi_2Br_7(PMe_3)_2]^-$ (Figure 7) was found to be polymeric with the repeating unit adopting an edge-shared bioctahedral form. The units are linked *via* linear bromine bridges with both Bi–Br bonds being *trans* to a trimethylphosphine donor and therefore elongated. The structure of the anion $[BiI_4(PMe_2Ph)_2]^-$ (Figure 7) is monomeric with the coordination around the bismuth centre being close to octahedral.

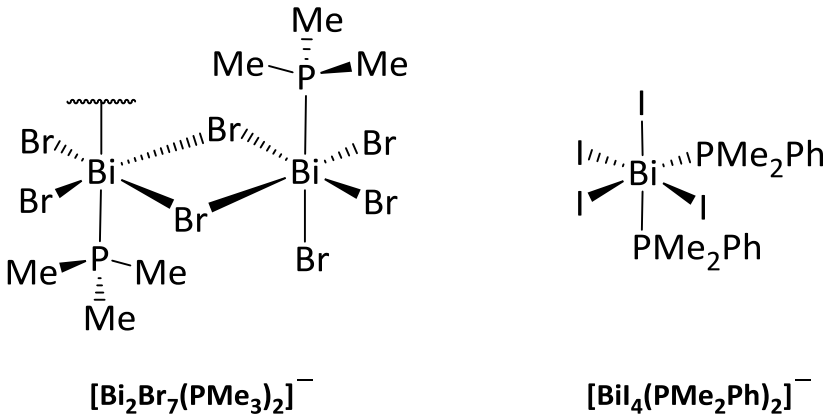

Figure 7: The bismuth anions $[Bi_2Br_7(PMe_3)_2]^-$ (left) and $[BiI_4(PMe_2Ph)_2]^-$ (right).

In 2007 Stranger and Wild showed that diorgano-arsenium, -stibenium and, -bismuthenium ions form stable adducts of the type $L{-}{>}ER_2^+X^-$ when reacted with triphenylphosphine (L).[35] The two electron donor L occupies a coordination site orthogonal to the trigonal plane of the six electron ER_2^+ group. They described the synthesis, structural characterisation and bonding within a series of triphenylphosphine-stabilised arsenium, stibenium and bismuthenium complexes of the types $[(Ph_3P)EPh_2]PF_6$ (E = As, Sb, Bi) and $[(Ph_3P)_2EPh_2]PF_6$ (E = Sb, Bi) (Figure 8). The coordination geometries around the central pnictogen elements are distorted trigonal pyramidal in the mono(triphenylphosphine) complexes and distorted trigonal bipyramidal in the *bis*(triphenylphosphine) complexes. In each case the stereochemically active lone pair of the six-electron, angular diphenyl-arsenium, -stibenium or –bismuthenium ion occupies an equatorial position in the trigonal plane containing the C–E–C bonds. For the mono(triphenylphosphine) complexes computational results (PBE/TZP level) for the cations are consistent with the dative covalent formulation $[Ph_3P{\rightarrow}PnPh_2]^+$, especially for E = As and Sb. However for the *bis*(triphenylphosphine) complexes the bonding between the phosphine and stibenium or bismuthenium ions is best described as an induced dipole–ion interaction.[35]

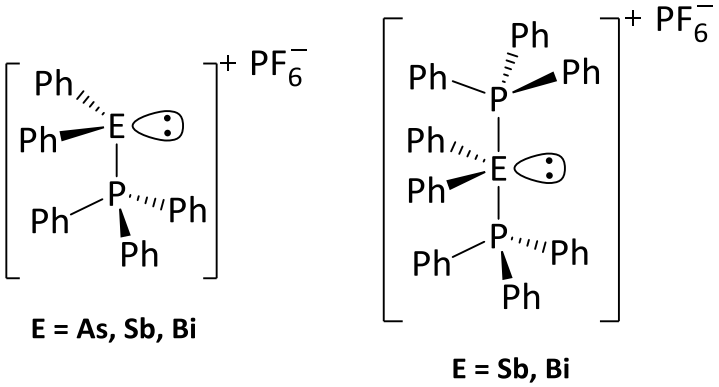

Figure 8: The triphenyl-stabilised diphenyl cationic pnictogen salts characterised by Wild and Stranger in 2007.

So far the examples where bismuth acts as an acceptor have contained phosphorus based donor ligands. In 2001 Reid and co-workers investigated the use of bi- and tri-dentate arsines alongside diphosphines in the formation of antimony(III) and bismuth(III) complexes.[36] This work was built upon their previous research into antimony(III) and bismuth(III) complexes with di- or tri- thio- or seleno-ethers and thio- or seleno-ether macrocycles.[37-40] In several examples a 1,2-substituted benzene ring was used as a scaffold for the diarsine or diphosphine in the hope of increasing the stability of the formed complex in solution. Additionally, it was anticipated that higher ligand:Sb/Bi ratios would be observed compared to complexes formed using more flexible aliphatic linkers. The complexes prepared were poorly soluble in chlorocarbons, acetonitrile and nitromethane with the ^{1}H NMR spectra obtained being relatively uninformative. IR spectra were used to confirm the absence of oxidation of the phosphine or arsine groups. Several crystal structures were obtained confirming that it was 1:1 adducts that had been formed with a distorted octahedral geometry. The reason suggested for the lack of any higher ligand:Sb/Bi ratios was that the primary interactions within the systems are in the pyramidal MX_3 units. The remaining sites on the distorted octahedron are filled by weaker (secondary) bonding to the neutral ligands and the longer distance bridging X-group. A recent review by Burt, Levason and Reid provides an excellent overview of the main group complexes formed using phosphine, arsine and stibine ligands.[41]

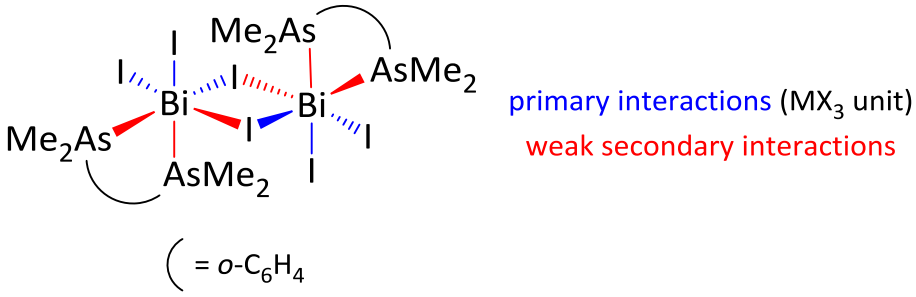

Figure 9: $[Bi_2I_6\{o\text{-}C_6H_4(AsMe_2)_2\}_2]$ showing the primary MX_3 unit in blue and the weaker long range bonding interactions in red.

1.3 – *peri*-Substitution

The double substitution in the 1, 8 and 5, 6 positions of naphthalene and acenaphthene (and related systems) respectively is known as *peri*-substitution.[42] Naphthalene itself is a rigid planar molecule with all the angles being *ca*. 120° with very little difference in C–C bond lengths.[43] As a result of this rigidity the exocyclic *peri*-bonds are aligned near perfectly parallel at a distance of 2.44 Å (Figure 10).[44] Acenaphthene has an ethylene bridge between the 1 and 2 positions creating a fused 5 membered ring. This causes the C1–C1a–C2 angle to decrease (112.4(1)°) whilst the C5–C5a–C6 angle increases (128.4(1)°). As such the exocyclic *peri*-bonds are no longer near parallel and the resulting *peri*-distance is increased to 2.67 Å (Figure 10).[45] Despite this difference between the two molecules they share similar reactivities and are interchangeable in many reactions.[46]

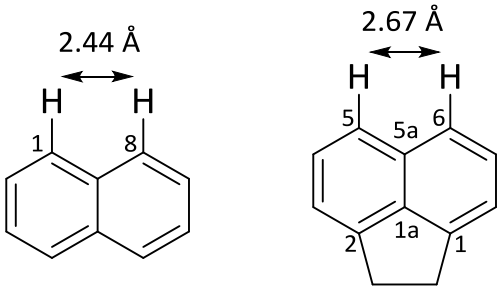

Figure 10: Naphthalene and acenaphthene with the *peri*-distances shown.

Only hydrogen atoms fit in the *peri*-region as the sum of their van der Waals radii is less than the *peri*-distance ($\sum r_{vdW}$ = 2.18 Å).[47] Any other atom placed in these positions experience varying degrees of steric strain which can be relieved in different ways. The first way is through distortion of the rigid carbon skeleton which can occur as both in-plane and out-of-plane distortions. Secondly, the formation of an attractive interaction between the two *peri*-atoms removes their need to be

further apart.[24,42] Any repulsive interaction between the two *peri*-atoms can result in very large distortions and deformations within the whole molecule as a result of the two atoms trying to adopt positions as far apart as possible. This occurs as the two atoms try to minimise the overlap of their occupied orbitals.[42,44,46]

One of the best ways to study the effects different atoms have in the *peri*-positions is by using single crystal X-ray diffraction to determine the crystal structure of the molecule. There are several measurements which can be made within the structure which provides information regarding the nature of the interaction between the *peri*-atoms and the level of strain within the molecule (Figure 11). By comparing the angles and distances around the *peri*-region to those of the unsubstituted naphthalene system these properties can be quantified. The in-plane distortion can be measured in several ways, firstly by comparing the sum of the *peri*-angles (∑αβγ) to the ideal value of 360° and secondly by comparing the C1–C8a–C8 angle between the unsubstituted and substituted derivatives. An alternative way of quantifying this is through the determination of the splay angle; this is calculated by taking the sum of the bay region angles and subtracting 360. A positive value implies a repulsive (non-bonding) interaction whilst a negative (bonding) suggests an attractive interaction. This measurement is reliable for atoms where the sum of their covalent radii does not exceed the *peri*-distance. If this becomes the case then this measurement becomes less reliable since even large proximate atoms with attractive interactions will still have a positive splay angle.[42,48]

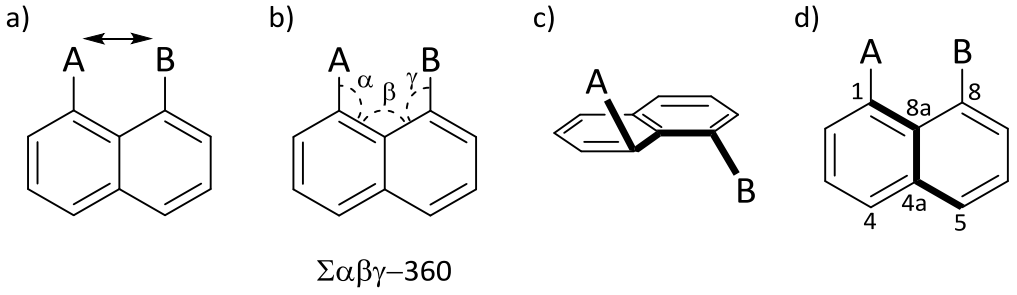

Figure 11: Measurements made to determine the interactions and strain within a *peri*-substituted molecule: a) the *peri*-distance, b) the splay angle, c) out-of-plane distortions of the *peri*-atoms and d) the torsion angles A–C1···C8–B and C1–C8a–C4a–C5.

The out-of-plane distortions can be measured by looking at the distance by which the *peri*-atoms deviate above and below the mean C_{10} plane of the naphthalene ring system. Looking at the A–C1···C8–B torsion angle also gives information regarding this, generally where an attractive interaction is present this torsion angle is normally <15°. If there is a large repulsive interaction between the two *peri*-atoms then the central naphthalene ring system buckles to release the strain.

This level of deformation can be measured by looking at the C1–C8a–C4a–C5 and C8–C8a–C4a–C4 torsion angles. All of these measurements provide a picture of the interaction between the *peri*-atoms.

1.3.1 – *peri*-substitution in the formation of novel bonding motifs

One of the main reasons to study *peri*-substitution within main group chemistry is the ability to stabilise traditionally ephemeral species. In the context of the donor–acceptor complexes discussed in section 1.2.1 this stabilisation effect, in part, arises as the system goes from being bimolecular to unimolecular. Thus, if a donor-acceptor complex is formed between two *peri*-substituted atoms the entropy change within the system is lessened compared to the bimolecular case. As mentioned above, further stabilisation occurs owing the release of strain within the rigid backbone upon the formation of an attractive interaction between the *peri*-atoms.

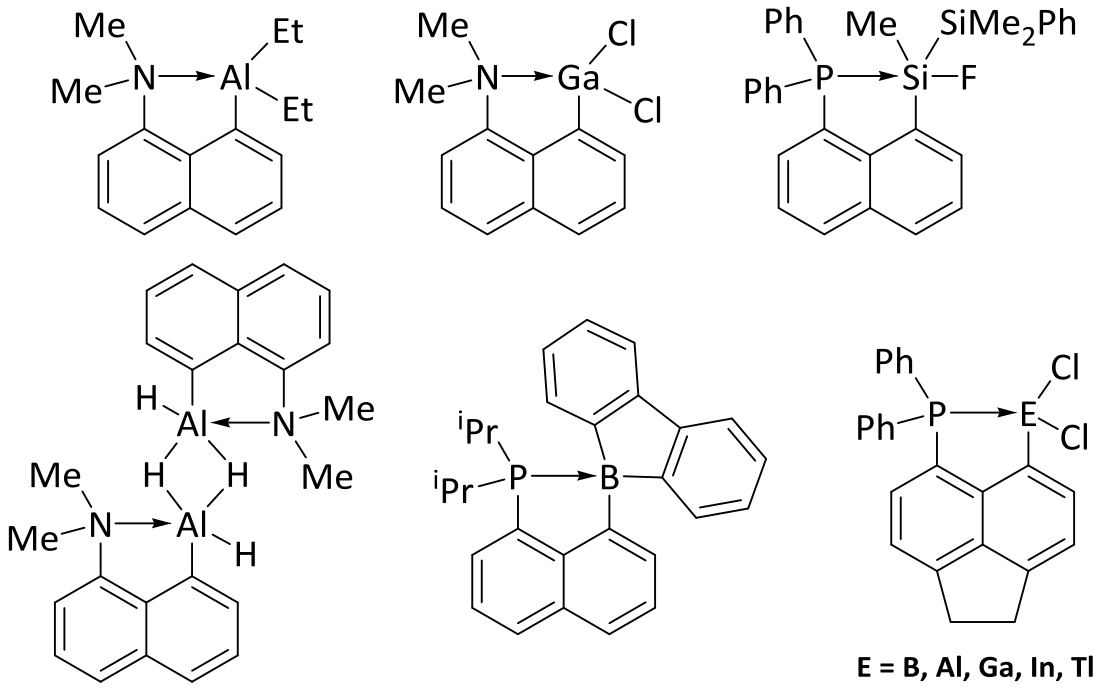

Figure 12: Selected examples of donor–acceptor complexes utilising the naphthalene skeleton.

As mentioned in section 1.2.1 the first room temperature stable phosphine–phosphine donor–acceptor complex was achieved through the stabilising effects of *peri*-substitution.[24] Between the late 1960s and early 2000s a vast number of *peri*-substituted organic compounds were synthesised.[49-51] Compounds containing elements from groups 13–16 have been heavily reviewed with many of them displaying novel bonding interactions or unusual reactivity attributed to the

stabilising effect of *peri*-substitution. Figure 12 shows examples of these donor–acceptor complexes containing acceptors with elements from group 13 and 14.[42,44,46,52-59]

The highly basic nature of $Nap(NR_2)_2$ (Nap = naphthalene-1,8-diyl) compounds have led them to be named "proton sponges". This high basicity of 1,8-diaminonaphthalenes is due to the stabilisation gained from the relaxation of the naphthalene system when a bonding interaction is formed across the *peri*-gap.[60-62] Through the formation of intramolecular hydrogen bonds from the mono-protonation of these compounds the strain on the naphthalene ring is relaxed. The distance between the two nitrogen atoms decreases significantly upon protonation (Scheme 4).[63,64]

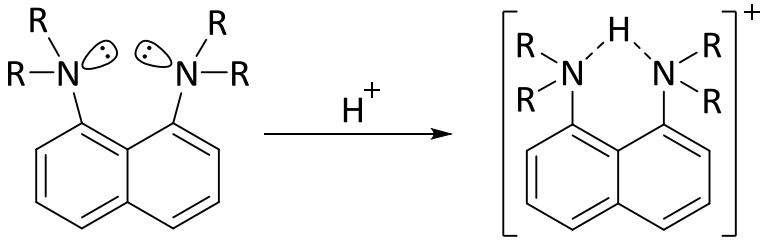

Scheme 4 Protonation of 1,8-diaminonaphthalene to form the proton bridged compound.

The Kilian and Woollins research groups have a strong interest in the *peri*-substitution of naphthalene and its related derivatives, predominantly with group 15 and 16 elements as well as combinations of these with tin substituents.[42,65-67] Through the stabilising effects of *peri*-substitution a compound containing a rare example of a $\sigma^4P–\sigma^6P$ bond was isolated in 2003 (Scheme 5).[68] The reaction of excess chlorine gas on $NapP_2S_4$ was designed as a synthetic route towards $Nap(PCl_2)_2$, which is inaccessible from the direct reaction of $NapLi_2$ and PCl_3.[69] The previous synthetic route to $Nap(PCl_2)_2$ was *via* the reaction of HCl gas with $Nap(P(NEt_2)_2)_2$ however the reaction yield was very low at 9%.[70] An improvement in the synthesis was published by Schmidbaur in 2004.[71] The desirable synthon $Nap(PCl_2)_2$ can be prepared in a 93% yield from $NapP_2Cl_6$ by reacting it with a slight excess of methyldichlorophosphite resulting in the volatile by-products phosphoryl chloride and chloromethane (Scheme 5).[72]

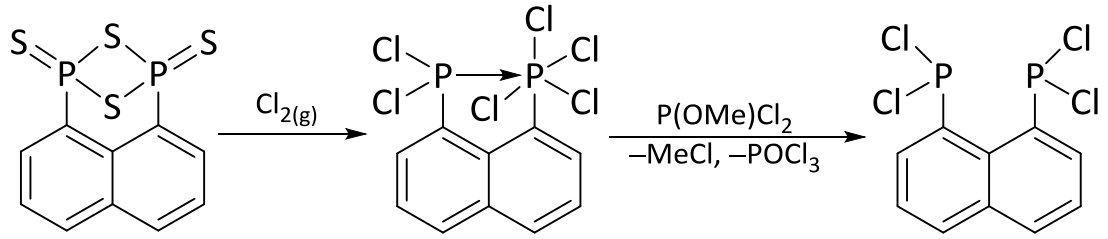

Scheme 5: Synthetic route to $Nap(PCl_2)_2$ from $NapP_2S_4$ *via* the $NapP_2Cl_6$ intermediate.

One of the remarkable features of $NapP_2Cl_6$ is that the donor group is the Lewis acidic PCl_2 group. Under normal circumstances the PCl_2 group would not be regarded as a strong donor, the formation of the donor–acceptor complex is attributed to the rigid constraints enforced by the naphthyl framework. As a result, the P–P bond length is at the upper end of the range for a typical P–P single bond. The $^{31}P\{^1H\}$ NMR of the compound at room temperature consists of very broad signals, cooling to 213 K results in the appearance of two doublets which indicates the formation of an ionic phosphonium–phosphoranide structure. The chemical shifts of the two doublets are similar to those observed for the PCl_4^+ and PCl_6^- ions.[68]

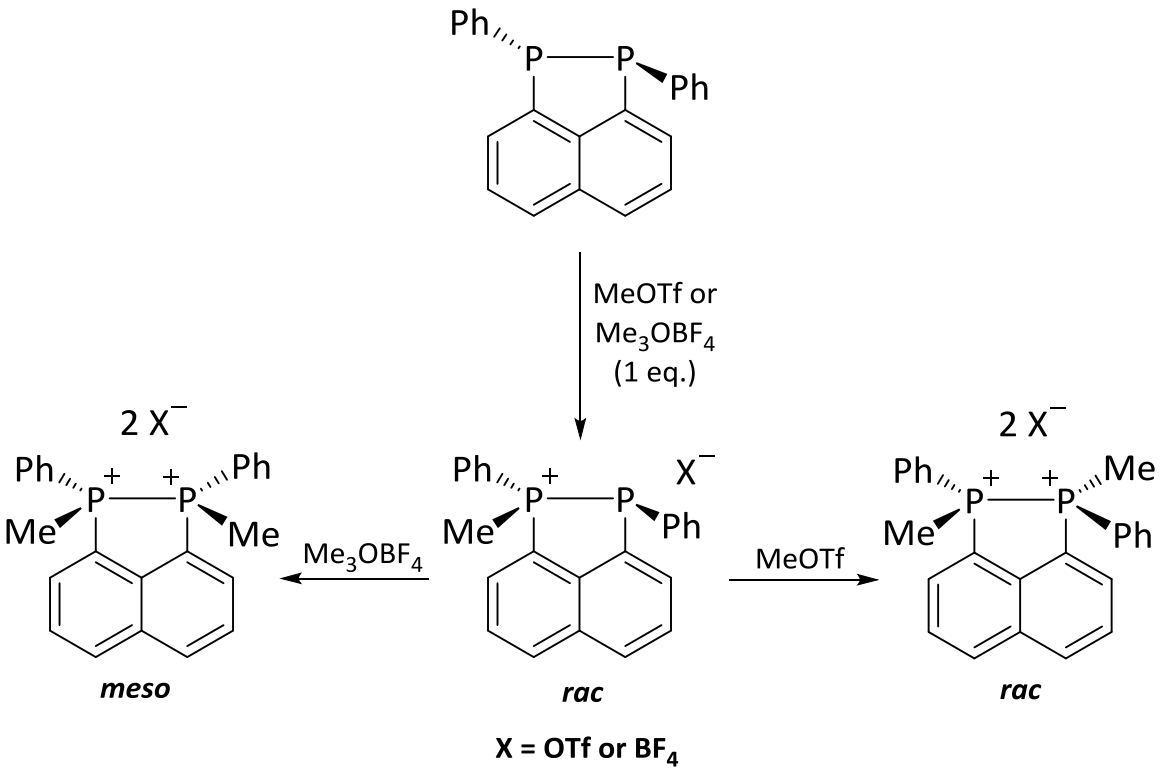

Scheme 6: Synthetic routes to 1,2-diphosphonium dications using different methylating agents.

There are very few species with two cationic centres located at two directly connected atoms which possess kinetic stability. The most stable 1,2-dications are produced by removal of electrons from

non-bonding orbitals at the central atoms, thus the examples that do exist usually have either nitrogen or chalcogens as the central atoms. In 2011 the Kilian research group used *peri*-substitution to stabilise 1,2-diphosphonium cations (Scheme 6). Computational studies (B3LYP/6-31+G* level of DFT) supported the notion that extra stabilisation is gained from the rigid naphthalene backbone.[73]

A phosphinidene is an example of an organopnictogen species in oxidation state +1 with the general formula RP. They were first observed in the 1960s by Schmidt who utilised a disulfide (EtS–SEt) to trap phenylphosphinidene resulting in a phenylphosphonodithioite. However, investigations into the chemistry surrounding them was difficult due to their high reactivity and sensitivity to air.[74] Phosphinidenes are six electron species with a triplet ground state and a large singlet-triplet gap of approximately 22±3 kcal mol^{-1} (phenylphosphinidene).[75] These ephemeral species, which rapidly oligomerise even at cryogenic temperatures, have never been isolated in the monomeric form. Mathey and co-workers developed a way to stabilise the singlet state by complexation to a transition metal centre. In this way one of the lone pairs is sequestered through coordination to the metal centre (Figure 13, top left).[76]

Metal-free phosphinidene complexes are also known with one of the first being discovered by Protasiewicz and co-workers. They isolated the compound dmpP=PMe_3 as an air sensitive yellow solid (Figure 13, top right).[77,78] This phosphanylidene–σ^4–phosphorane (also known as phospha-Wittig reagent) is a type of base-stabilised phosphinidene with two stereochemically active lone pairs. The compound dmpP=PMe_3 is one of only two structurally characterised compounds of this type. The second compound of this type to be structurally characterised was prepared within the Kilian research group in 2012.[79] By using *peri*-substitution the donor group ($^{i}Pr_2P$) is held in close proximity to the phosphinidene group allowing it to be stabilised (Figure 13, bottom). The crystal structure obtained showed that in the solid state the ylide form is the dominant species. Despite being air sensitive it is stable indefinitely in hydrocarbon solvents such as benzene and in the solid state, unlike dmpP=PMe_3, which decomposes over time. Compared to dmpP=PMe_3, *peri*-stabilised phosphanylidene–σ^4–phosphorane is sterically unshielded around the phosphinidene atom leaving it essentially “naked”, allowing for a wide range of reactivities to be investigated. It was shown to react with a variety of chalcogens (O, S, Se, Te) as well as being active in coordination chemistry with a number of metals (Pt, Au, Mo, Rh, Pd).[80]

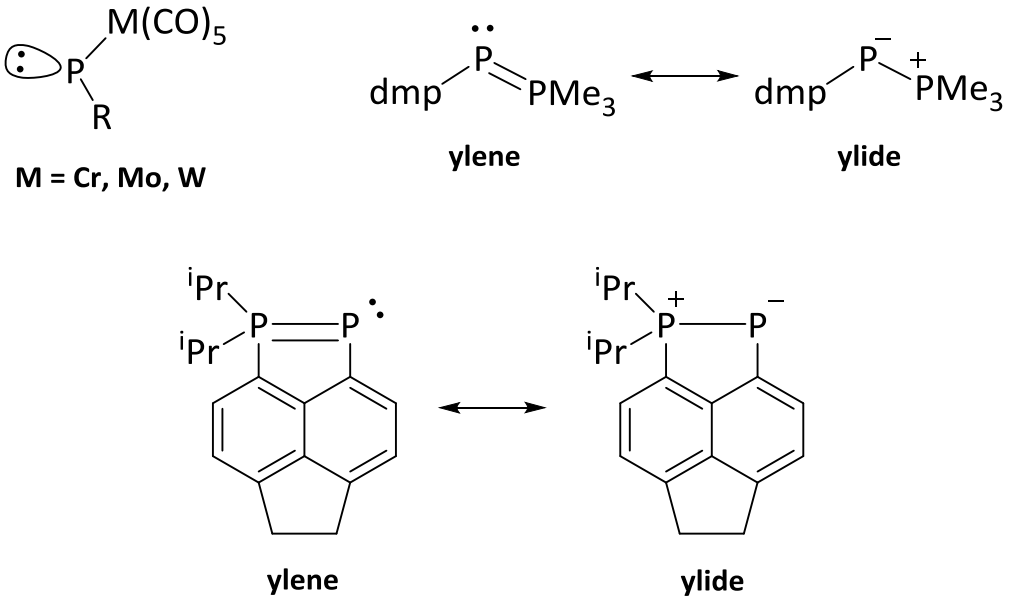

Figure 13: Mathey's metal-stabilised phosphinidene (top left), Protasiewicz's metal-free phosphinidene (top right) and Kilian's "naked" phosphinidene (bottom).

Beckmann and co-workers also have an interest in using *peri*-substitution to form donor–acceptor complexes; in their case they use a diphenylphosphino donor group. They recently published a series of compounds with a variety of p-block dichloride acceptors (ECl_2, E = B, Al, Ga, In, Tl, P, As, Sb, Bi).[59] This crystallographic and DFT study provides a useful insight into the donor–acceptor properties of the p-block elements. Two different synthetic routes were employed, one utilised low temperature lithium halogen exchange followed by salt elimination whilst the other uses transmetallation of a trialkyltin precursor (Scheme 7).[59]

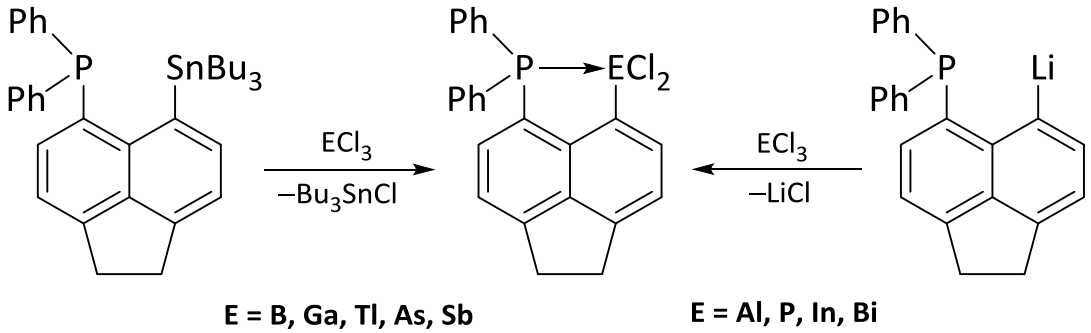

Scheme 7: Synthetic routes to the p-block containing donor–acceptor complexes by Beckmann.

This section contains but a few from a large array of *peri*-substituted naphthalene and acenaphthene compounds. The recent reviews by Kilian and Woollins on group 15 and 16 *peri*-substituted systems and their reactivity towards metals provide an excellent overview of the field.[42,46]

1.4 – Through-Space Spin-Spin Coupling

Nuclear magnetic resonance (NMR) spectroscopy has become an essential analytical tool within chemistry over the last sixty years. NMR spectra provide information about the chemical environment of a particular nucleus based on both its chemical shift and spin-spin coupling. The transfer of nuclear spin information between nuclei occurs *via* the interaction of the electrons between the coupled atoms. Traditionally the transfer of magnetic spin information was thought to occur only through unambiguous covalent bonds. Theoretical studies conducted in the 1950s proposed the existence of through-space spin-spin coupling interactions between non-bonded nuclei.[81] Whilst examining the ^{19}F NMR spectra of some organofluorine compounds in 1956 Saika and Gutowski observed a set of unexpected multiplets, this turned out to be the first example of through-space spin-spin coupling.[82] Years later similar observations were made by Roberts and Lutz.[83]

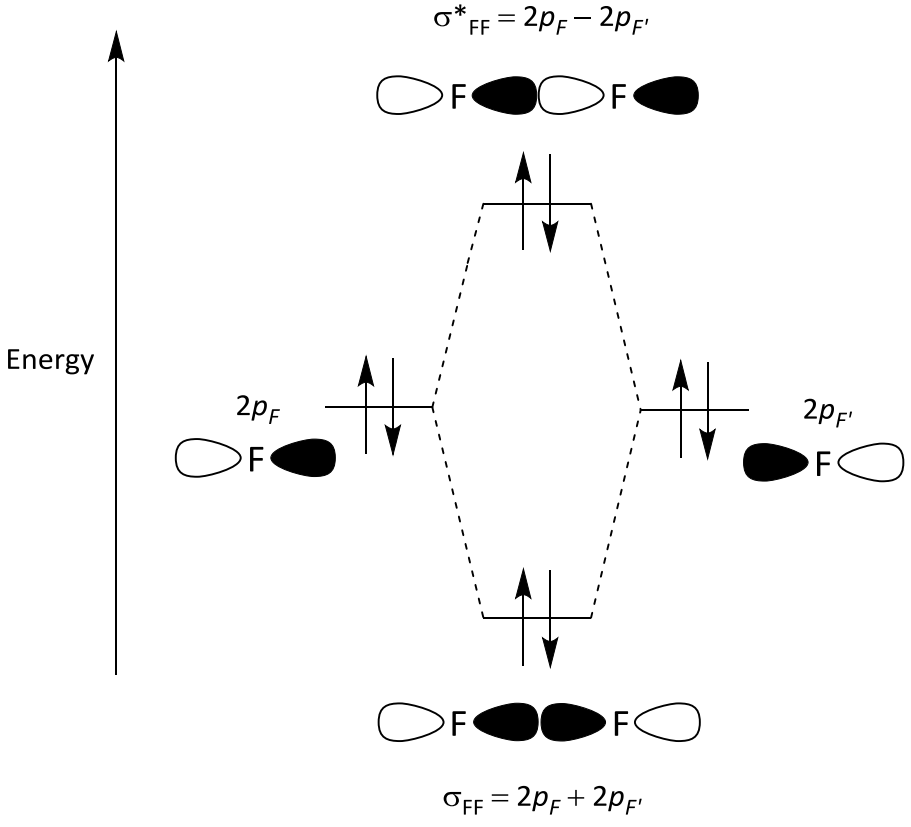

Figure 14: Molecular Orbital diagram showing the bonding and anti-bonding orbitals formed by the overlap of two fluorine lone pair orbitals.

A detailed study using ^{19}F NMR spectroscopy of fluorine compounds which were both *peri*- and bay-substituted was conducted by Mallory in 2000.[84] By using the geometric constraints imposed by the

rigid frameworks the through-space coupling between the two formally non-bonded fluorine atoms could be investigated. Mallory proposed the transfer of magnetisation occurs through the overlap of two lone pair orbitals resulting in an in-phase and out-of-phase combination (Figure 14). Looking at the molecular orbital diagram (Figure 14) we can see that both the bonding and anti-bonding orbitals are filled, i.e. the bond order is zero. Despite this an interaction between the two fluorine atoms is still formed as shown by ^{19}F NMR spectroscopy. The coupling constant, J_{FF} arises from the combination of both the through-bond (^{tb}J) and through-space (^{ts}J) couplings as shown in Eq. 1.

$$J_{FF} = {}^{ts}J_{FF} + {}^{tb(\pi)}J_{FF} + {}^{tb(\sigma)}J_{FF} \qquad \textbf{(Eq. 1)}$$

The conclusion reached by Mallory was that for fluorine atoms separated by four or more bonds the contribution from both through-bond components was sufficiently small that it could be omitted. Mallory observed $^{4ts}J_{FF}$ values of between 28−85 Hz and $^{5ts}J_{FF}$ values of between 165−175 Hz. It was clear that the F···F distance within the molecule played an important role in the magnitude of the $^{ts}J_{FF}$ observed as the phenanthrene derivatives gave larger values than the naphthalene or acenaphthene versions. Mallory confirmed an exponential relationship between the magnitude of ^{ts}J and the interatomic distance of the atoms using *ab initio* calculations modelling two hydrogen fluoride molecules at varying distances.[84]

1.4.1 – ^{13}C–^{31}P through-space coupling

Of particular interest to the work presented in chapter 2 is through-space coupling between ^{13}C and ^{31}P nuclei. It is more commonly seen within ^{13}C NMR spectra since the relative abundance of ^{13}C is 1.11%, as such, its isotopologues only appear as tiny satellites in the ^{31}P NMR spectrum. One of the first examples of through-space ^{13}C–^{31}P coupling was observed by Pascal and co-workers within a cyclophane system. Coupling was observed between the carbon atoms in the central aromatic ring and the phosphorus atom. They proposed this occurred as the phosphorus lone pair interacts with the delocalised p-orbitals which make up the arene π-cloud, thus allowing the transfer of magnetisation (Figure 15, left).[85]

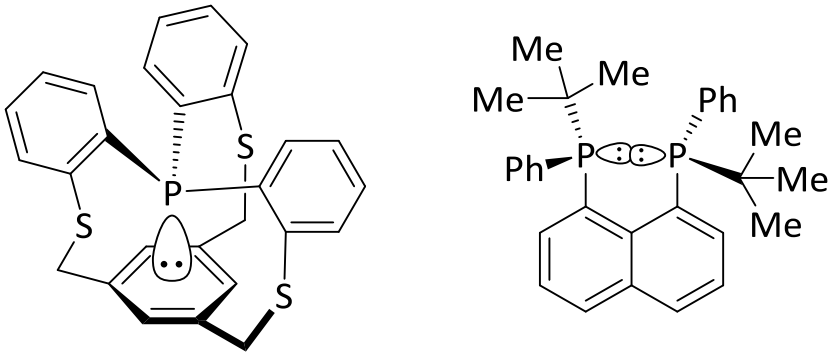

Figure 15: Examples of compounds displaying through-space $^{13}C–^{31}P$ coupling (Pascal, left), (Schmutzler, right).

Examples of $^{13}C–^{31}P$ though-space coupling have also been seen in *peri*-substituted naphthalene compounds as shown by Schmutzler (Figure 15, right).[86] From the $^{13}C\{^{1}H\}$ NMR spectra both $^{5ts}J_{CP}$ (3.6 Hz) and $^{6ts}J_{CP}$ (9.0 Hz) are observed owing to the quasi-linear arrangement of the P···P–C motif. During the work presented in chapter 2 through-space coupling was observed within the $^{13}C\{^{1}H\}$ NMR spectra of several compounds. The presence of such coupling showed a level of interaction between the two *peri*-substituents that would otherwise have gone unnoticed.

Chapter 2 – Phosphorus–Bismuth *peri*-Substituted Acenaphthenes

2.1 – Introduction to *peri*-Substituted Bismuth Compounds

Examples of donor–acceptor complexes with heavier pnictogen atoms acting as acceptors are rare. Recently the Kilian group has focused on synthesising donor–acceptor systems with heavier pnictogens (As, Sb) acting as acceptors.[87,88] By using *peri*-substitution to stabilise these systems several room temperature stable donor–acceptor complexes were synthesised and characterised using single crystal X-ray diffraction.[87,88] Examples where bismuth has been used as an acceptor are even rarer within the literature, as mentioned in section 1.2.2. The aim of this work was to expand this field and investigate the nature of the interaction between the two *peri*-atoms when bismuth was used as an acceptor.

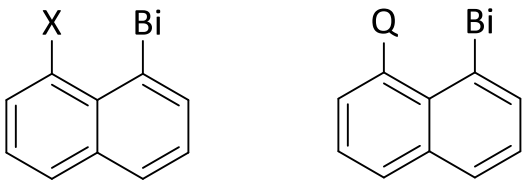

X = any atom **Q = any atom except H or C**

Figure 16: The initial substructure (left) and more refined substructure (right) used in the search for *peri*-substituted bismuth substances.

A search using the Scifinder® web portal for the substructure shown in Figure 16 (left) resulted in 72 substances which had at least one reference available.[89] A large number of these compounds are either simple triarylbismuthines or halogenobismuthines which contain either the naphthyl group or one of its larger derivatives. The type of compounds with most relevance to the work presented here are *peri*-substituted bismuth containing naphthalenes or acenaphthenes where the second *peri*-position is occupied by an element other than carbon or hydrogen (Figure 16, right). By applying this filter to the 72 substances identified only eight compounds remain. One of the compounds is a published substance synthesised and characterised as part of the work presented in this thesis. Of the remaining seven, three appear as part of a computational study on the role of the lone pair in non-bonded *bis*(chalcogen)-1,8-naphthalenes.[90] This left only four compounds of which two,

$(Mes)_2B$-Naphth-$BiPh_2$ and Ph_2P-Acenap-$BiCl_2$, have been structurally characterised by single crystal X-ray diffraction.

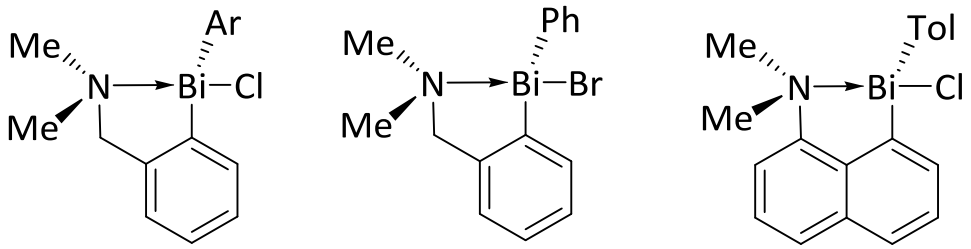

Figure 17: Nitrogen–bismuth donor–acceptor complexes synthesised by Suzuki and co-workers.

One of the first reported *peri*-substituted compounds containing a bismuth atom was prepared by Suzuki and co-workers in 1993.[91] The work mainly focused on the synthesis of chiral chlorobismuthines which were stabilised by intramolecular coordination of a *N*,*N*-dimethylamino group to form a donor–acceptor complex (Figure 17). The majority of the compounds synthesised were based upon an *N*,*N*-dimethylbenzylamine scaffold. By reacting this with n-BuLi and adding in a chlorobismuthine a triaryl bismuthine was prepared. A subsequent fluorodearylation was conducted using boron trifluoride diethyl etherate followed by halogen exchange of the resulting compound with brine to regenerate the chlorobismuthine (Scheme 8).

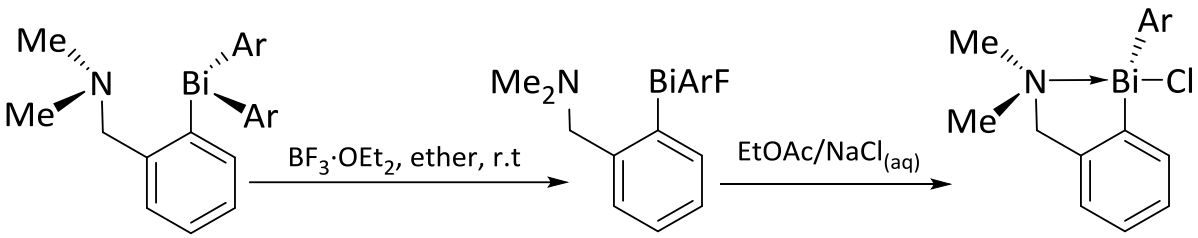

Scheme 8: Synthetic route used by Suzuki in the formation of chiral chlorobismuthines.

The NMe_2 and CH_2 groups of these chlorobismuthines were observed to be diastereotopic within their ^1H NMR spectra. Variable temperature ^1H NMR studies of the series showed the coalescence temperature for the NMe_2 signal was approximately 70 °C in d_8-toluene for all but one of the compounds. Changing the halogen from chlorine to bromine had little effect on the coalescence temperature. Two processes to explain the coalescence of the NMe_2 signals were proposed. Firstly, through dissociation of the intramolecular N–Bi coordination bond followed by rotation around the CH_2–N bond (180°) and subsequent restoration of the N–Bi bond. Secondly, through inversion at the chiral bismuth centre without prior N–Bi dissociation, the first process was believed to be the most likely.

The *peri*-substituted compound shown in Figure 17 (right) was prepared in a similar manner starting from *N*,*N*-dimethyl-1-naphthylamine. Variable temperature ^{1}H NMR studies of this compound showed no coalescence of the NMe_2 signals even at 110 °C. This is due to the rigid nature of the naphthalene backbone preventing dissociation of the N–Bi bond and subsequent rotation around the CH_2–N bond. Only the tolyl version of the benzylamine based compounds was characterised crystallographically. The bismuth centre was shown to have a distorted *pseudo*-trigonal bipyramidal geometry with the two carbon atoms and lone pair occupying the equatorial positions whilst the nitrogen and chlorine take up the axial positions. The N–Bi distance (2.525(6) Å) was much shorter than the sum of their van der Waals radii (N–Bi 3.6 Å)[92] suggesting a strong interaction. The Bi–Cl bond length was longer than those seen in other chlorobismuthines and sulfonyl-stabilised chlorobismuthines which reflects the donation of the nitrogen atom's lone pair into the σ*(Bi–Cl) orbital.

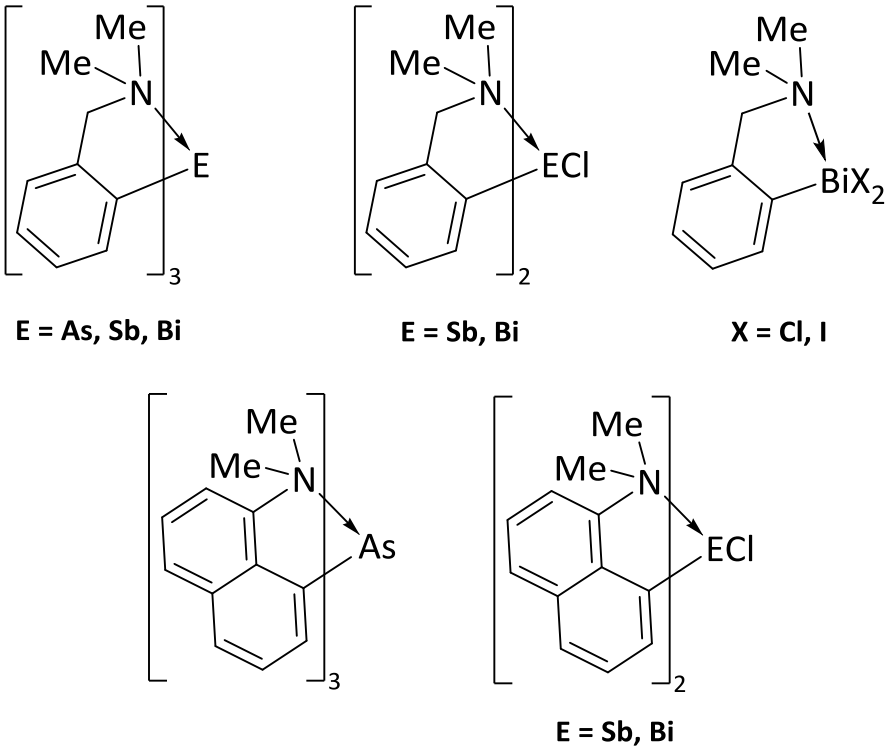

Figure 18: Nitrogen–pnictogen donor–acceptor complexes synthesised by Cowley and co-workers.

Further work using the same backbones substituted with a range of pnictogens was carried out by Cowley and co-workers in the mid-1990s.[93,94] A series of compounds based upon both the *N*,*N*-dimethylbenzylamine backbone of the type $(Me_2N(CH_2)C_6H_4)_3E$ (E = As, Sb, Bi), $(Me_2N(CH_2)C_6H_4)_2ECl$ (E = Sb, Bi) and, $(Me_2N(CH_2)C_6H_4)BiX_2$ (X = Cl, I) and the *N*,*N*-dimethyl-1-naphthylamine backbone of the type (Me_2N-Naphth-)$_3$E (E = As) and (Me_2N-Naphth-)$_2$ECl (E = Sb, Bi) were synthesised (Figure 18).

Nearly all of the compounds were characterised using single crystal X-ray diffraction which aided in the determination of the interaction between the nitrogen and pnictogen atoms. As we saw before, donor–acceptor interactions were detected in all of the derivatives. In the $(Me_2N(CH_2)C_6H_4)_3E$ (E = As, Sb, Bi) and $(Me_2N\text{-Naphth-})_3E$ (E = As) compounds the geometry around the pnictogen atom is that of a distorted octahedron in which the distortion arises from an opening on the N_3E face where the pnictogen lone pair is believed to be situated. Compared to the $(Me_2N(CH_2)C_6H_4)_2ECl$ (E = Sb, Bi), $(Me_2N\text{-Naphth-})_2ECl$ (E = Sb, B), $(Me_2N(CH_2)C_6H_4)BiX_2$ (X = Cl, I) and, the previous compounds described above the interaction between the nitrogen and pnictogen atoms are weaker due to the decreased Lewis acidity of the pnictogen centre. Such a trend is consistent with the view that the Lewis acidity of these complexes is associated with the σ*(E–X) orbitals through which the amine coordinates and that σ*(E–C) orbitals are weaker acceptors than the σ*(E–X) orbitals.

By using the more rigid naphthalene backbone in the tri-substituted compounds, shorter N–E distances were observed. Within the EAr_2Cl series of compounds the same trigonal bipyramidal geometry around the pnictogen centre was observed with the lone pair occupying an equatorial position. Interestingly the $BiArI_2$ compound crystallised as a centrosymmetric dimer *via* bridging iodine atoms resulting in a geometry around the bismuth best described as distorted square-based pyramidal. The same structure was not observed for the arsenic and antimony derivatives, instead the previously seen trigonal bipyramidal geometry was found in the crystal.

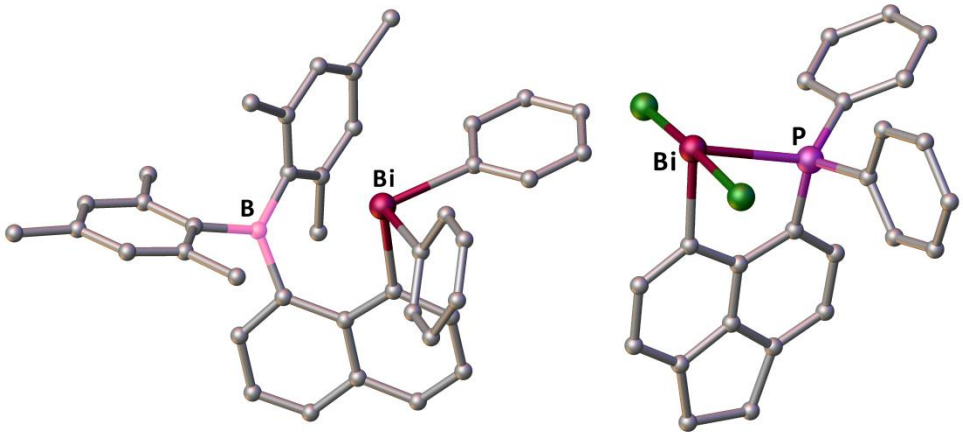

Figure 19: Crystal structures of the *peri*-substituted boron–bismuthine synthesised by Gabbai (left) and phosphine–bismuthine synthesised by Beckmann (right).

As we saw in section 1.3.1, Beckmann and co-workers recently prepared a range of *peri*-substituted compounds of the type $Ph_2P\text{-Ace-}ECl_2$ (E = B, Al, Ga, In, Tl, P, As, Sb, Bi).[59] The bismuth containing compound was structurally characterised by single crystal X-ray diffraction (Figure 19, right). The

crystal structure showed the complex exists in a dimerised form *via* bridging chlorine atoms resulting in a distorted square-based pyramidal geometry around the bismuth centre. For simplicity the monomeric form is shown in Figure 19 (right).

The final example to be discussed shows that within a donor–acceptor complex the bismuth centre can also act as a donor. Gabbai and co-workers published a paper in 2011 which contained the synthesis and crystal structures (bismuth derivative in Figure 19, left) of two boron/pnictogen naphthalene compounds, supported by computational analysis.[95] Boron is well known as being an excellent acceptor within a number of *peri*-substituted boron nitrogen/phosphorus compounds.[96-98] Given that the strength of the bonds formed by p-block elements decreases as you descend a group, Gabbai wanted to investigate the use of heavier pnictogens as donors. The ^{1}H NMR data obtained for each compound was consistent with the formation of a donor–acceptor complex as the six methyl groups all appeared as separate signals. Interestingly the ^{11}B NMR spectra showed broad signals with typical shifts for triarylboranes suggesting the boron centres remained trigonal planar without significant electron pair donation from the pnictogen atoms. The crystal structures supported the presence of a B–Pn interaction as the distance between the two atoms (B–Sb 3.216(6) and B–Bi 3.330(6) Å) was significantly less than the sum of their van der Waals radii (B–Sb 4.0 Å; B–Bi 4.1 Å).[92] The geometry around the boron was confirmed as remaining trigonal planar with the pnictogen centre adopting a *pseudo*-trigonal bipyramidal geometry. The computational study (B3LYP/6-31G level of DFT) which included geometry optimisation and natural bond order analysis supported the observations made experimentally.

2.2 – Building a *peri*-Substituted Compound

In order to synthesise a *peri*-substituted compound each motif needs to be added to the acenaphthene backbone in a sequential manner. This requires the preparation of the principal starting material 5,6-dibromoacenaphthene (**AcenapBr$_2$**) which was synthesised following a literature procedure (Scheme 9).[99] The characterisation data obtained matched that reported in the literature. To introduce the first substituent **AcenapBr$_2$** was reacted with one molar equivalent of n-BuLi at −78 °C, resulting in the formation of 5-lithio-6-bromoacenaphthene. Subsequent addition of diisopropylchlorophosphine resulted in the formation of (^{i}Pr)$_2$P-Acenap-Br (**C2**-**1**) with the elimination of lithium chloride (Scheme 9).[24]

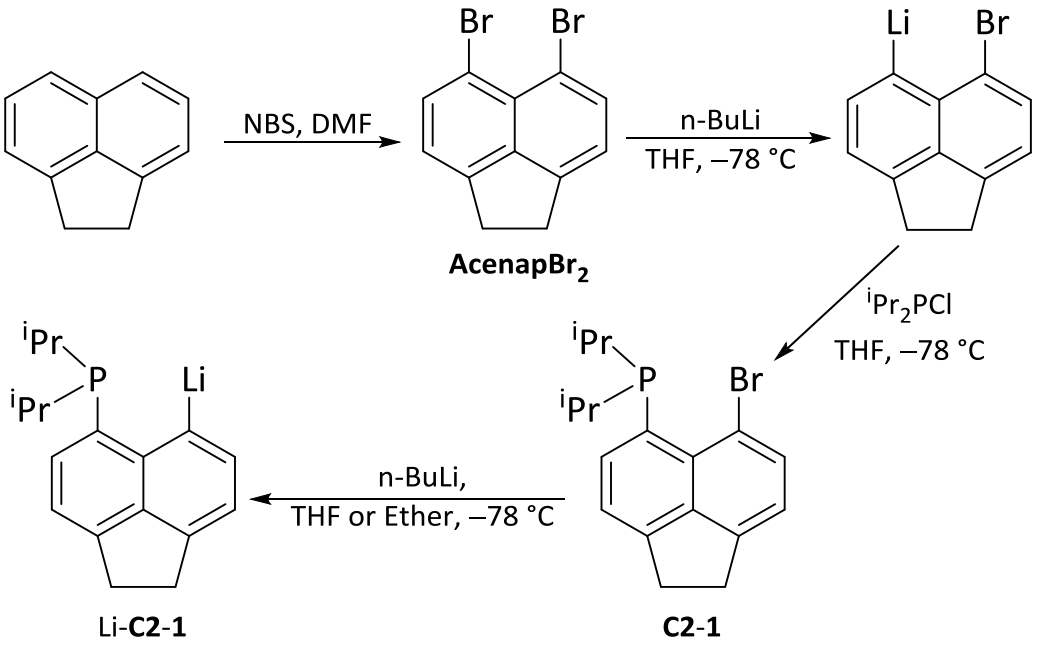

Scheme 9: Synthetic route to building a *peri*-substituted acenaphthene.

A second low temperature lithium halogen exchange to form Li-**C2**-**1** (Scheme 9) followed by a salt elimination reaction, allowed a second group to be added in the remaining *peri*-position. The diisopropylphosphine moiety is an excellent Lewis base (strong σ donor) making it an ideal group in the attempts to form donor–acceptor complexes. The synthesis of **C2**-**1** was first reported by the Kilian group in 2009,[24] the compound is only mildly air sensitive with the recrystallisation step able to be performed in air. The $^{31}P\{^{1}H\}$ NMR spectrum shows a singlet at δ_P −2.2 ppm with the expected signals from the acenaphthene backbone and isopropyl groups observed within the ^{1}H and $^{13}C\{^{1}H\}$ NMR spectra.

2.3 – Bismuth starting materials preparation

In the synthesis of **C2**-**1**, the addition of a group into the *peri*-position requires reaction of the lithiated acenaphthene compound with an electrophilic species such as a chlorophosphine. The focus of this chapter is on the synthesis and characterisation of *peri*-substituted phosphorus–bismuth acenaphthenes. Thus, a series of bismuth starting materials were required to react with Li-**C2**-**1**. Previous work within the group has utilised various mono- and dichloro pnictogens to add into the second *peri*-position.[66] Some bismuth analogues of these compounds were identified as potential reagents along with the commercially available compound bismuth trichloride (Figure 20). In the case of both bismuth trichloride and dichloro(phenyl)bismuthine the ratio of lithiated

acenaphthene to bismuth reagent could be altered allowing for various degrees of substitution to be achieved.

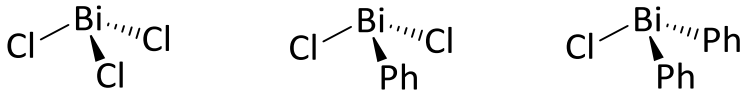

$BiCl_3$ **$BiCl_2Ph$** **$BiClPh_2$**

Figure 20: Bismuth compounds selected for study.

Both dichloro(phenyl)bismuthine and chlorodiphenylbismuthine are known compounds prepared by redistribution reactions between triphenylbismuthine and bismuth trichloride.[100,101] Triphenylbismuthine was synthesised *via* the reaction of three equivalents of phenylmagnesium bromide with bismuth trichloride. This reaction is amenable to a large scale synthesis with good yields and excellent purity obtained from reactions conducted on the tens of grams scale. The characterisation data obtained matched that reported within the literature.[101,102]

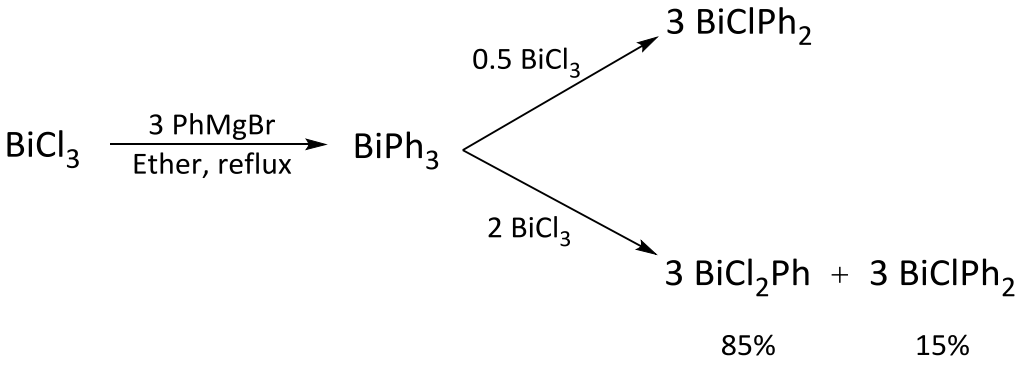

Scheme 10: Synthetic route to $BiClPh_2$ and $BiCl_2Ph$ including the preparation of $BiPh_3$.

Scheme 10 shows the synthetic route to $BiCl_2Ph$ and $BiClPh_2$ including the synthesis of $BiPh_3$. The redistribution reactions to form the two chlorobismuthines were met with varied success. The redistribution to form $BiClPh_2$ proceeded smoothly and resulted in analytically pure material (confirmed by elemental analysis) following the procedure found in the literature.[101] The redistribution reaction to form $BiCl_2Ph$ proved to be much more difficult which was surprising given the number of publications reporting the preparation of this compound. Several attempts were made with variation of the reaction conditions but in all cases the material isolated at the end was a mixture of both the desired $BiCl_2Ph$ and $BiClPh_2$. Analysis of the ^1H NMR spectrum showed the mixture to contain 85% $BiCl_2Ph$ and 15% $BiClPh_2$ which was the case for nearly all attempts. No

explanation for this problem is offered as the same $BiCl_3$ and $BiPh_3$ used in the other redistribution reaction were used here. Attempts to purify the compound by recrystallisation were unsuccessful so this mixture was used in further syntheses. The solubility of both compounds is poor in most common solvents with the only solvent suitable for obtaining NMR data being d_6-acetone and d_6-DMSO.

2.4 – Synthesis and Characterisation of a Geminally Substituted Tris(acenaphthyl) Bismuthine

The first synthetic target was the *tris*(acenaphthyl) bismuthine analogous to the arsenic containing compound prepared by Cowley and co-workers shown in Figure 18 (page 23).[94] This was prepared by reaction of Li-**C2**-**1** with ⅓ of an equivalent of bismuth trichloride at low temperature (−78 °C) (Scheme 11). Following filtration of the reaction and washing with diethyl ether, then degassed water, **C2**-**2** was isolated as a white solid in a 32% yield.

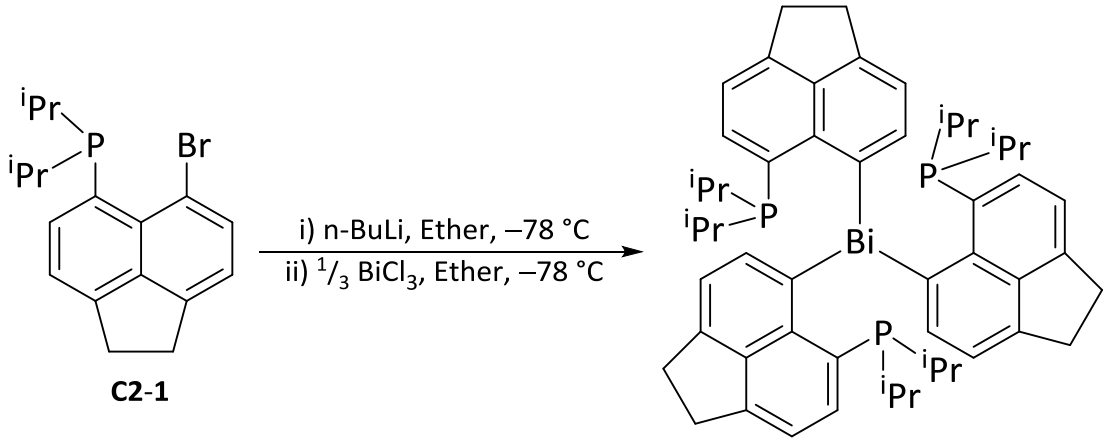

Scheme 11: Synthetic route to tris(*peri*-substituted) bismuthine **C2**-**2**.

2.4.1 – Spectroscopic analysis of C2-2

The $^{31}P\{^1H\}$ NMR spectrum of **C2**-**2** shows a single peak at δ_P −21.3 ppm strongly suggesting that there is no bonding interaction between the phosphorus and bismuth atoms. Because of the crowded, propeller-like geometry of **C2**-**2** (determined from the crystal structure discussed below) a low temperature (222 K) $^{31}P\{^1H\}$ NMR spectrum was obtained. No observable line broadening or other notable changes were seen indicating no additional interlocking takes place at this temperature.

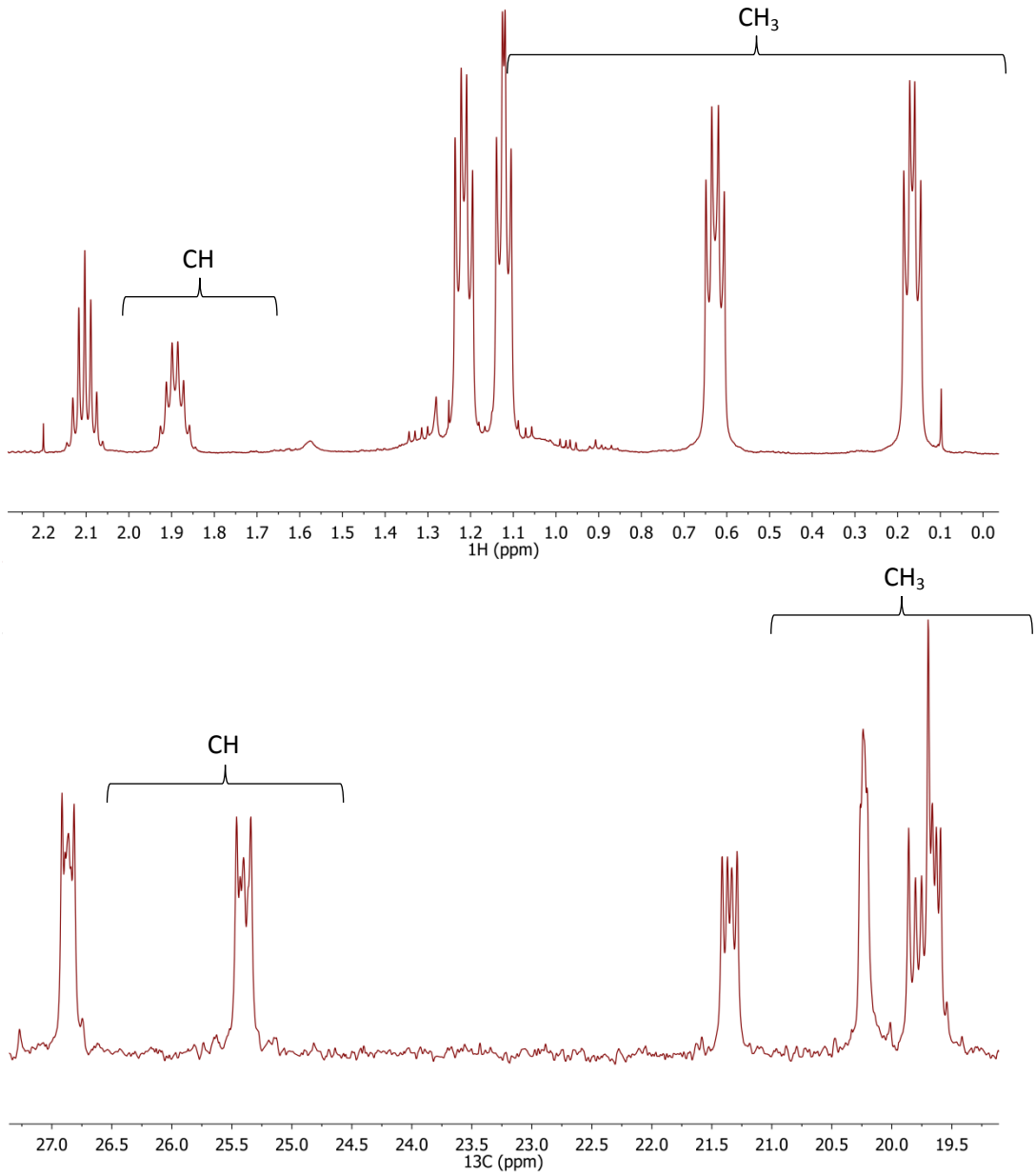

Figure 21: The alkyl region of the ^{1}H NMR spectrum ($CDCl_3$, 500 MHz) (top) and $^{13}C\{^{1}H\}$ NMR DEPT-Q–135 spectrum ($CDCl_3$, 125 MHz) (bottom) of **C2**-**2**.

Because of the crowded nature of **C2**-**2** the ^{1}H and $^{13}C\{^{1}H\}$ NMR spectra display multiple anisochronous signals for chemically equivalent groups. Four and three methyl environments are observed in the ^{1}H and $^{13}C\{^{1}H\}$ NMR spectra respectively owing to the restricted rotation present within the compound. Thus, the four methyl and two CH groups become magnetically inequivalent. Within the ^{1}H NMR spectrum four doublets of doublets are seen between δ_H 1.30–0.10 ppm corresponding to the methyl groups. The $^{3}J_{HP}$ coupling constants range from 10.1–14.4 Hz and are similar to those seen in related systems prepared within the Kilian research group.[103] Two signals corresponding to the CH of the isopropyl groups are observed with one appearing as a septet and

the other as a doublet of septets (Figure 21, top). As expected four signals appear in the aromatic region along with the expected coupling which corresponds to the acenaphthene backbone.

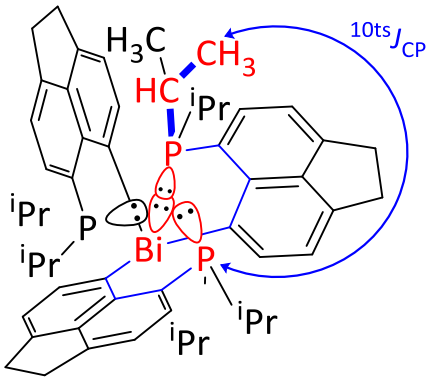

Figure 22: Graphical representation of the magnetisation transfer pathway in **C2**-**2** for long-range couplings ($^{10ts}J_{CP}$). Bonds (formally) involved in the transfer are coloured blue with lone pairs involved in the transfer (through space) coloured red.

The most interesting features of the NMR data obtained were seen within the $^{13}C\{^{1}H\}$ NMR spectrum. The signals of methyl carbon atoms (δ_C 21.5–19.5 ppm) are second order multiplets, corresponding to AA'A''X spin systems (A = ^{31}P, X = ^{13}C) (Figure 21). This is because methyl carbons couple not only with ^{31}P atoms separated by two bonds ($^{2}J_{CP}$), but also have non-negligible couplings with more distant phosphorus atoms. These two, formally $^{10}J_{CP}$ couplings, have different magnitudes, which results in a complex second order signal. The shape of the signals is very sensitive to subtle changes of the coupling constants, which made the iterative fitting impossible. Whilst we cannot determine exact magnitude of these long range couplings, we can confirm both these $^{10}J_{CP}$ couplings are very likely non-negligible (i.e. > 2 Hz) and different in each of the four diastereotopic methyl groups in **C2**-**2**. The through-bond component (through ten bonds, ^{10}J), is likely to be very small.[104] Hence, it is highly likely that the couplings involve two through space components (through two *peri*-gaps), i.e. the magnetisation is transferred due to the overlap of lone pairs on each of the two phosphorus atoms with the lone pair on central bismuth atom (Figure 22). In a similar vein, the isopropyl CH environments (δ_C 27.0–25.3 ppm) display complex multiplets, corresponding to AA'A''X spin systems (Figure 21). The remaining signals within the $^{13}C\{^{1}H\}$ NMR spectrum of **C2**-**2** are consistent with that expected from the acenaphthene skeleton. These observations made in all the NMR spectra were mirrored in the arsenic and antimony analogues recently synthesised within the Kilian group.[105]

Both the IR and Raman spectra showed the expected peaks with the analytical purity of the compound confirmed by means of elemental analysis. The mass spectrum ($APCI^+$) showed a peak corresponding to $[M+H]^+$ at *m/z* 1017.4254 providing further evidence for the proposed compound.

2.4.2 – Crystallographic characterisation of C2-2

Crystals suitable for single crystal X-ray diffraction (for brevity the term X-ray work will be used from now on in place of single crystal X-ray diffraction) were obtained from a saturated solution of **C2-2** in DCM at 0 °C. Two molecules crystallised within the asymmetric unit alongside four molecules of DCM. The large amount of co-crystallised solvent is due to both the size and almost spherical shape of the molecule, thus, the crystal has large voids which can easily accommodate solvent.

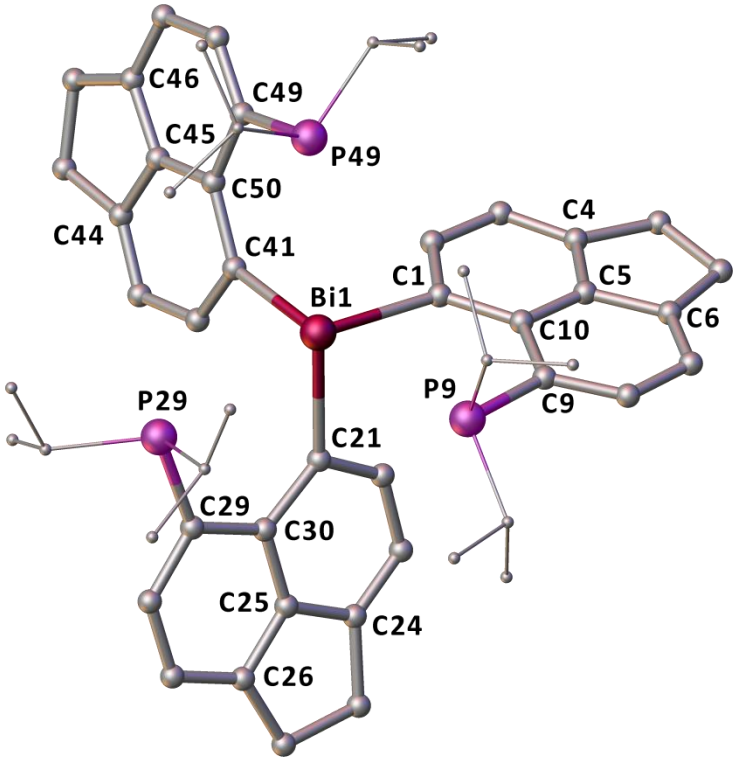

Figure 23: Crystal structure of **C2-2** with hydrogen atoms omitted for clarity. The second molecule within the asymmetric unit and the four co-crystallised solvent molecules (DCM) are also omitted for clarity.

The crystal structure of **C2-2** is shown in Figure 23 with selected structural parameters in Table 1. Both of the pnictogen atoms adopt a trigonal pyramidal geometry if sub-van der Waals non-bonding interactions are ignored. The angles around the bismuth atom (C–Bi1–C) show a greater deviation than those around the phosphorus centre (C–P–C) compared to the ideal angle of 107°. This is due to the purely p-orbital overlap that is responsible for the bonds to the bismuth centre. Thus the

angles around the bismuth centre are expected to be close to 90°. The purely p-orbital overlap from the bismuth centre is due to the diffuse nature of *n*p-orbitals relative to the *n*s-orbitals (n > 2) and their spatial incompatibility relative to 2s and 2p orbitals. Therefore, no hybridisation between the 6s and 6p orbitals occur. No strong dative interactions are formed between the Lewis basic *i*Pr_2P groups and the central bismuth atom as indicated by P···Bi distances which range between 3.2 and 3.3 Å. Both the C_{Ace}–P (1.80(2)−1.85(1) Å) and C–Bi (2.31(1)−2.34(1) Å) bond lengths are comparable to others of this type.[95,106] This difference in bond lengths may contribute to the lack of interaction between the bismuth and phosphorus atoms as the bismuth sits further above the acenaphthenediyl backbone. Positive splay angles (15.7(9)−16.0(9)°) provide further evidence that there is no interaction between the phosphorus and bismuth centres. Despite three bulky *peri*-groups being attached to the bismuth centre in **C2**-**2**, there are no major distortions of acenaphthene rings, with only moderate to medium in-plane and out-of-plane displacement of the *peri*-atoms observed. Due to the specifics of the *peri*-substitution, all P···Bi distances are significantly sub-van der Waals (76–77% using r_{vdW} = 1.95 (P) and 2.30 (Bi) Å).[92] Taking these short contacts into account, the central bismuth atom could also be viewed as attaining a distorted octahedral geometry with its lone pair protruding one of the octahedral faces. A collinear arrangement of all C_{Ace}–Bi···P motifs observed within the crystal structures of **C2**-**2** is consistent with the onset of a n(P)→σ*(E–C) 3c–4e interaction. However, given the other parameters discussed above, the strength of this interaction is likely to be small.

Table 1: Selected bond lengths [Å], angles [°], torsion angles [°] and displacements [Å] for **C2**-**2**.

C_{Ace}–P	1.80(2)−1.85(1)	P9···Bi1	3.240(3) [3.279(4)]
C–Bi1	2.31(1)−2.34(1)	P29···Bi1	3.250(4) [3.218(3)]
P···P	5.066(6)−5.484(5)	P49···Bi1	3.250(3) [3.242(4)]
C–Bi1–C	91.7(5)−96.0(5)	P···Bi1···P	103.3(1)−115.1(1)
C–P–C	95.0(9)−104.8(6)		
splay angle[a]	15.9(9) [16.0(9)]	P–C···C–Bi1	2.8(7) [2.5(7)]
	15.9(9) [15.7(9)]		1.5(7) [6.3(7)]
	16.0(8) [16.0(9)]		7.4(7) [8.6(8)]
Out of plane displacements			
P	0.025−0.338	Bi1	0.027−0.442

[a] calculated as the sum of the bay region angles–360.

[] denotes data from second molecule in asymmetric unit.

2.4.3 – Varying the ratio of bismuth trichloride

Having successfully prepared the tri-subsisted bismuthine **C2**-**2**, the next step was to investigate the synthesis of the di- and mono-substituted derivatives. Similar work has been carried out within the Kilian group before with the mono-substituted phosphorus,[24] arsenic[87] and antimony[88] derivatives published in 2009, 2014 and 2015 respectively. As mentioned in the introduction to this chapter, Cowley and co-workers have prepared di- and mono-substituted pnictogen derivatives using the *N*,*N*-dimethyl-1-naphthylamine backbone.[93] This was achieved by reacting the correct stoichiometric amount of 8-(Me_2N)$C_{10}H_6$Li with the desired pnictogen trihalides at low (−78 °C) temperatures. Similarly, Beckmann and co-workers prepared an analogous acenaphthene based compound, Ph_2P-Acenap-$BiCl_2$, by reacting their lithiated species with a fivefold excess of bismuth trichloride at −78 °C.[59] Using these papers coupled with our own experience of preparing similar compounds the reaction shown in Scheme 12 was attempted.

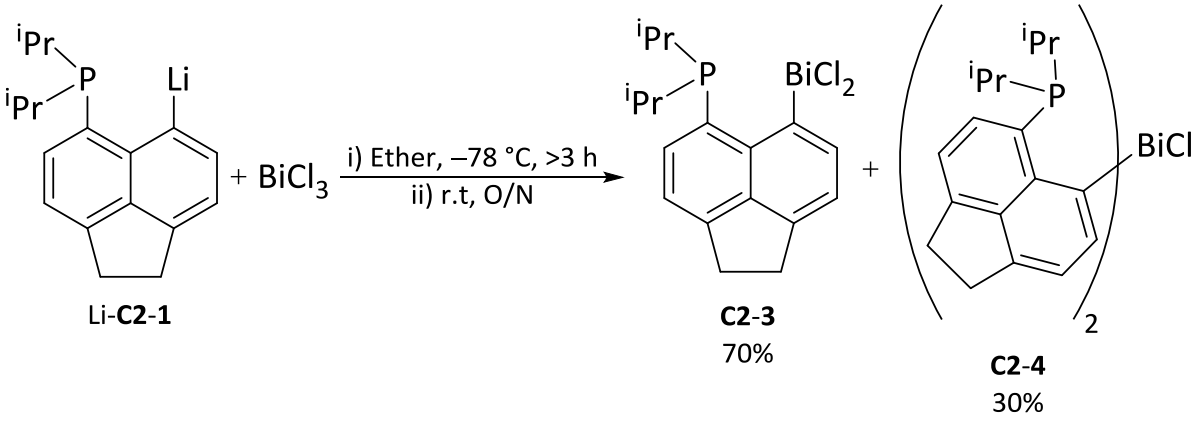

Li-**C2**-**1**

C2-**3**
70%

C2-**4**
30%

Scheme 12: Synthetic route followed in the attempted preparation of **C2**-**3**. The products shown are proposed based on data obtained and previous work conducted within the Kilian group. Percentages estimated using the $^{31}P\{^1H\}$ NMR data obtained.

The lithiated species Li-**C2**-**1** was prepared as before (Scheme 9) and kept at −78 °C. Separately a suspension of bismuth trichloride in diethyl ether was cooled to −78 °C and stirred vigorously. The lithiated suspension was added *via* cannula in small portions over 3 h to the bismuth trichloride suspension. Once the addition was complete the reaction was allowed to warm to room temperature and stirred overnight. A beige suspension formed which was filtered, washed with diethyl ether and then dried under vacuum. The solid obtained was contaminated with lithium chloride (formed as a by-product) and as such the NMR sample prepared ($CDCl_3$) was filtered before being run. The $^{31}P\{^1H\}$ NMR spectrum obtained contained two signals at δ_P 84.1 and 8.3 ppm in a 70:30 ratio. Comparing these signals to those we have observed for other related pnictogen

compounds we proposed that the peak at δ_P 84.1 ppm was likely to be from the desired product **C2-3**. The related systems containing arsenic and antimony have signals in their $^{31}P\{^1H\}$ NMR spectra at δ_P 65.3 and 51.0 ppm respectively.[87,88] Based on the reaction conditions the second product was presumed to be the di-substituted compound **C2-4**. The ^1H NMR spectra had a large number of signals which could correspond to the isopropyl groups of the two proposed products. Also observed were a number of aromatic peaks which supported the presence of two separate compounds. Additionally the weakness of the obtained spectrum could be due to the poor solubility of the products which would correspond to observations made by others in similar bismuth compounds.[59,93]

Attempts to grow crystals from the sample were unsuccessful and mostly resulted in decomposed material as determined by a change in colour to black. The synthetic route used by Beckmann was also attempted which used an excess of bismuth trichloride.[59] This was unsuccessful with only a sticky black substance obtained after the work up which proved to be insoluble in common solvents. In a final attempt the solvent was changed to THF to see if solvent choice would affect the outcome of the reaction. Again, only insoluble black material was obtained, as such, no further attempts were made to prepare the dichlorobismuthine derivative.

Some of the work presented in section 2.4 has contributed to the following publication:

Geminally Substituted Tris(acenaphthyl) and Bis(acenaphthyl) Arsines, Stibines and Bismuthine: A Structural and Nuclear Magnetic Resonance Investigation : Brian A. Chalmers, Christina B. E. Meigh, Phillip S. Nejman, Michael Buhl, Tomas Lebl, J. Derek Woollins, Alexandra M. Z. Slawin, Petr Kilian, *Inorg. Chem.*, **2016**, *55*, 7117–7125.

2.5 – *peri*-Substituted Unsymmetrical Triaryl Bismuthines: A Synthetic and Structural Study.

In section 2.3 attempts to prepare two bismuth starting materials which could be reacted with Li-**C2-1** to form a triaryl bismuthine were described. One of the desired compounds was isolated with an acceptable purity whilst the second proved harder to prepare. Recent work within the Kilian group has focused on developing the synthesis of *peri*-substituted unsymmetrical triaryl pnictogens containing either one or two acenaphthene units.[88,105] This was achieved by reaction of the analogous pnictogen starting materials to those prepared in section 2.3 with Li-**C2-1**. Based upon the

results obtained in the previous work we expected the reactions with $BiClPh_2$ and $BiCl_2Ph$ to proceed in a similar fashion. The reaction with the impure $BiCl_2Ph$ compound was still attempted as it was hoped that separation of the expected products could be achieved. Scheme 13 shows the synthetic route followed to the expected products ($(^iPr)_2$P-Acenap-$BiPh_2$ (**C2**-**5**) and (($(^iPr)_2$P-Acenap-)$_2$BiPh (**C2**-**6**). As mentioned previously (section 2.3) the bismuth reagents $BiClPh_2$ and $BiCl_2Ph$ are both poorly soluble compounds. We found that their solubility was slightly better in THF than diethyl ether thus this solvent was used for reactions involving these reagents.

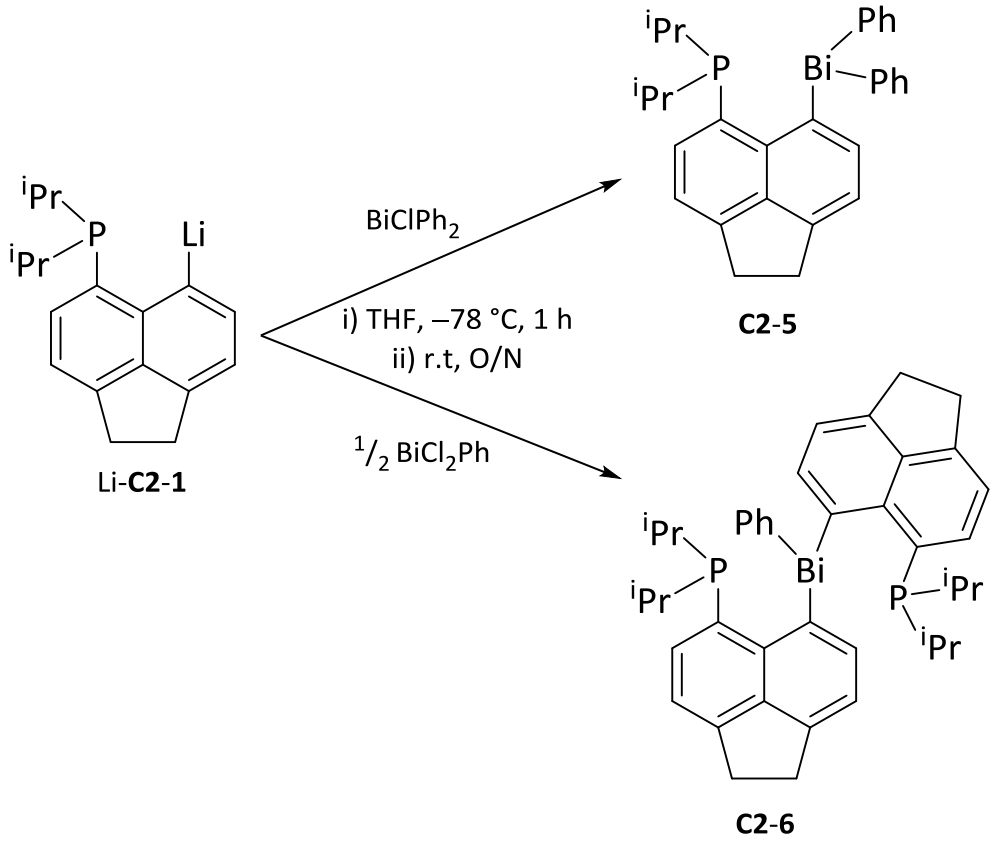

Scheme 13: Synthetic routes to *peri*-substituted triaryl bismuthines **C2**-**5** and **C2**-**6**.

The reaction between Li-**C2**-**1** and $BiClPh_2$ proceeds as expected with the formation of **C2**-**5** in a 60% isolated yield. Following completion of the reaction in THF by stirring O/N at room temperature, the solvent was removed and replaced with diethyl ether. Washing of the diethyl ether suspension with degassed water and subsequent separation and drying of the organic layer resulted in a clear solution. Removal of the solvent afforded a very viscous/near solid material which became an off white solid upon addition of MeCN. Collection of the product by filtration and subsequent drying afforded **C2**-**5** as an off white solid. Recrystallisation from hot MeCN resulted in analytically pure colourless crystals of **C2**-**5**. The same procedure was followed for the synthesis of **C2**-**6**. The

antimony analogue of **C2**-**5** was able to act as a bidentate ligand in the formation of platinum and molybdenum complexes.[107] Attempts to use **C2**-**5** in the same manner by reacting it with [Pt(cod)Cl_2] and [Mo(nbd)$(CO)_4$] proved to be unsuccessful. The $^{31}P\{^1H\}$ NMR showed no change with the signal for **C2**-**5** being the only thing observed after stirring at room temperature for twenty four hours. Heating the reaction mixture caused decomposition of **C2**-**5** as determined by several additional peaks in the $^{31}P\{^1H\}$ NMR spectrum of the reaction mixture. The inert pair effect is likely to be the main cause for this lack of reactivity. Owing to poor shielding of the 4f electrons, the 6s electrons experience an increased effective nuclear charge. This makes the 6s electrons less likely to form a dative bond as they are held tightly by the bismuth nucleus. Additionally, the size of the bismuth atom may be preventing the metal from coming in close enough for **C2**-**5** to act as a bidentate ligand.

2.5.1 – Spectroscopic analysis of C2-5 and C2-6

The signals in the $^{31}P\{^1H\}$ NMR spectra of **C2**-**5** and **C2**-**6** appear at δ_P −23.6 and −22.2 ppm respectively with both appearing as broad singlets. Within the $^{31}P\{^1H\}$ NMR spectra of the reaction mixture after preparation of **C2**-**6** a signal corresponding to **C2**-**5** was also observed, interestingly a second impurity signal at δ_P −20.7 ppm was also present. This second signal could correspond to **C2**-**2**, which is to be expected if the $BiCl_2Ph$ reagent was contaminated with bismuth trichloride. These two impurities made up approximately 10% of the mixture as determined by the $^{31}P\{^1H\}$ NMR spectrum. Since **C2**-**2**, **C2**-**5** and **C2**-**6** can all be recrystallised from hot MeCN and other organic solvents tested, purification of the compound obtained in the formation of **C2**-**6** *via* this method was unsuccessful.

In the ^1H NMR spectrum of **C2**-**5** only two doublets of doublets (δ_H 1.07 and 0.61 ppm) are observed corresponding to the methyls of the isopropyl groups indicating a higher degree of symmetry than in **C2**-**2**. This is further supported by the presence of only one signal arising from the CH of the isopropyl groups. The rest of the signals from the acenaphthene backbone and the two phenyl groups appear as expected. Due to the steric clash between the two large $(^iPr)_2$P-Acenap- groups, some of the alkyl signals in the ^1H NMR spectrum of **C2**-**6** are broadened at 298 K (25 °C). This is especially noticeable for the methyls from the isopropyl groups three of which appear as broad singlets (Figure 24). This broadening can be attributed to the moderately fast rotation of the two acenaphthene units around the Bi–C_{Ace} bond on the NMR timescale. These observations made within the ^1H NMR spectrum of **C2**-**6** mirror those made for both the arsenic and antimony derivatives.[105] The signals in the aromatic region were not broadened and appear as sharp signals with the

expected coupling observed. An improved synthetic method is presented in section 2.6.4 which resulted in analytically pure **C2**-**6**.

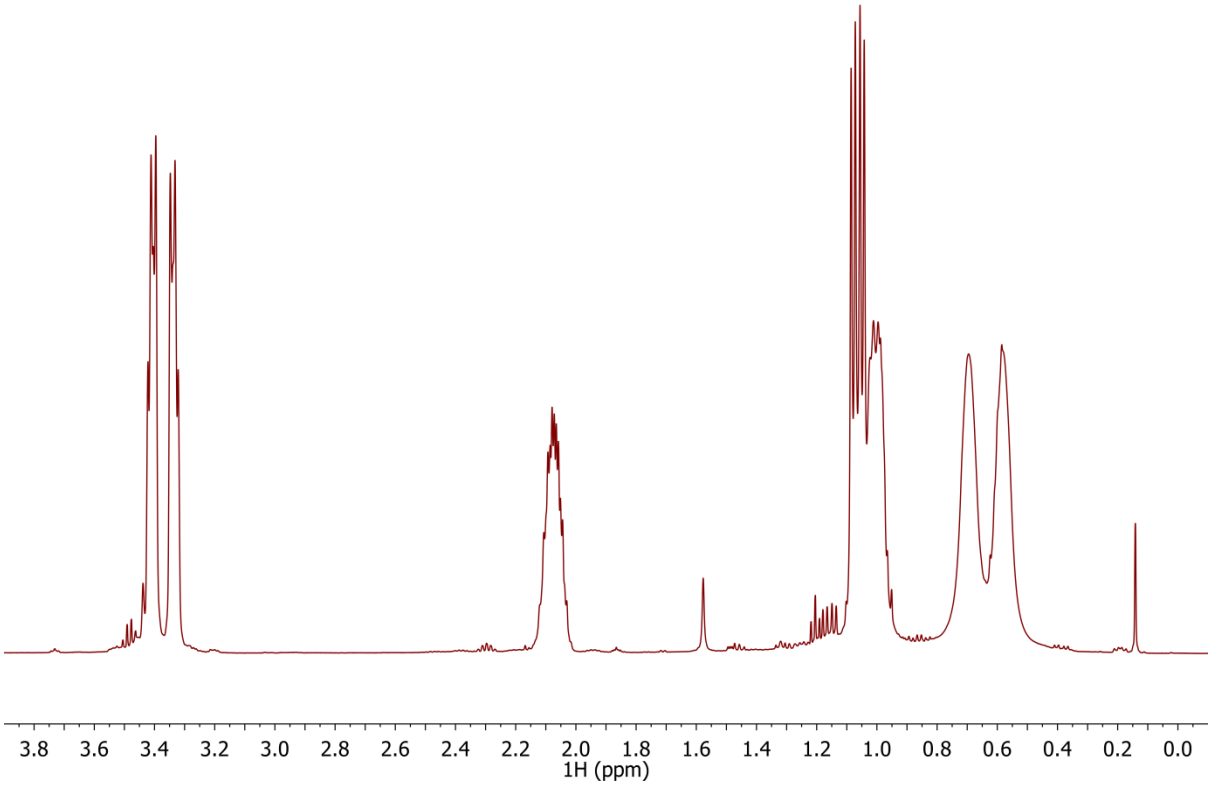

Figure 24: The alkyl region of the ^{1}H NMR spectrum ($CDCl_3$, 500 MHz) of **C2**-**6** showing the broad signals observed. The signal at δ_H 0.09 ppm is due to a silicone grease impurity.

As expected the $^{13}C\{^{1}H\}$ NMR spectrum of **C2**-**5** shows only two signals for the methyl and one for the CH fragments of the isopropyl groups. The deshielding effect of the bismuth atom results in the phenyl *ipso*-carbon appearing at δ_C 167.3 ppm. Interestingly this signal appears as a doublet through coupling to the phosphorus atom. The large $^{5ts}J_{CP}$ value of 42.2 Hz is most likely composed entirely of a through-space component due to the overlap of the phosphorus lone pair and the σ*(Bi–C) orbital (Figure 25). This indicates the onset of a 3c–4e type interaction, however, given the shielded nature of the phosphorus signal within the $^{31}P\{^{1}H\}$ NMR spectrum of **C2**-**5** this interaction is likely to be weak. The $^{13}C\{^{1}H\}$ NMR spectrum of **C2**-**6** is not broadened as the arsenic and antimony derivatives were,[105] however detailed analysis was not possible on this sample owing to the impurities present. A more detailed discussion of the $^{13}C\{^{1}H\}$ NMR spectrum of **C2**-**6** is provided in section 2.6.4.

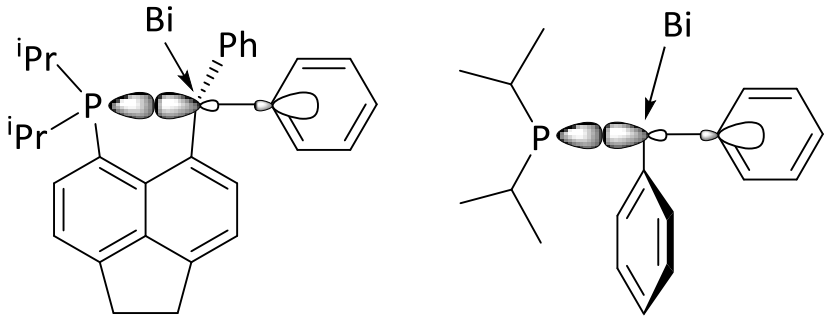

Figure 25: A view of **C2**-**5** orthogonal to the acenaphthene plane (left) and along the acenaphthene plane (right) showing the 3c–4e interaction of the phosphorus lone pair and the σ*(Bi–C) orbital.

Further analysis of **C2**-**5** was achieved through elemental analysis and APCI$^+$ HRMS (*m/z* 555.1646 [M−Ph]$^+$). The impurities within **C2**-**6** using this synthetic route precluded elemental analysis however the APCI$^+$ HRMS did show the [M+H]$^+$ signal at *m/z* 825.3192 with the base peak matching that expected for [M−Ph]$^+$ (*m/z* 747.2752).

Within the Kilian research group an antimony analogue of **C2**-**5** has been prepared.[88] The $^{31}P\{^1H\}$ NMR spectrum showed a singlet at δ_P −21.9 ppm which is similar to **C2**-**5** albeit shifted slightly downfield ($\Delta\delta_P$ 1.7 ppm). This subtle shift difference could be down to the difference in the relative Lewis acidities of the two pnictogen centres with the bismuth being a weaker Lewis acid.

2.5.2 – Crystallographic characterisation of C2-5 and C2-6

Crystals suitable for X-ray work were obtained for both **C2**-**5** and **C2**-**6** from boiling MeCN. The crystal structures of the two compounds are shown in Figure 26 with selected structural parameters in Table 2 (**C2**-**5**) and Table 3 (**C2**-**6**).

Table 2: Selected bond lengths [Å], angles [°], torsion angles [°], and displacements [Å] for **C2**-**5**.

P9···Bi1	3.291(2)	Bi1–C	2.26(1)–2.309(7)
P–C	1.849(8)–1.88(1)		
C–P9–C	102.6(4)–103.9(4)	C–Bi1–C	92.4(3)–94.4(3)
C9–P9···Bi1	91.4(3)	C1–Bi1···P9	70.8(2)
C13–Bi1···P9	161.2(2)	C19–Bi1···P9	78.3(2)
P9–C9···C1–Bi1	8.9(4)	Splay angle[a]	16.8(8)
C1–C10–C5–C6	179.1(8)	C9–C10–C5–C4	177.8(8)
Out of plane displacements			
P9	0.244	Bi1	0.139

[a] calculated as [(P9–C9–C10 + C9–C10–C1 + C10–C1–Bi1)–360].

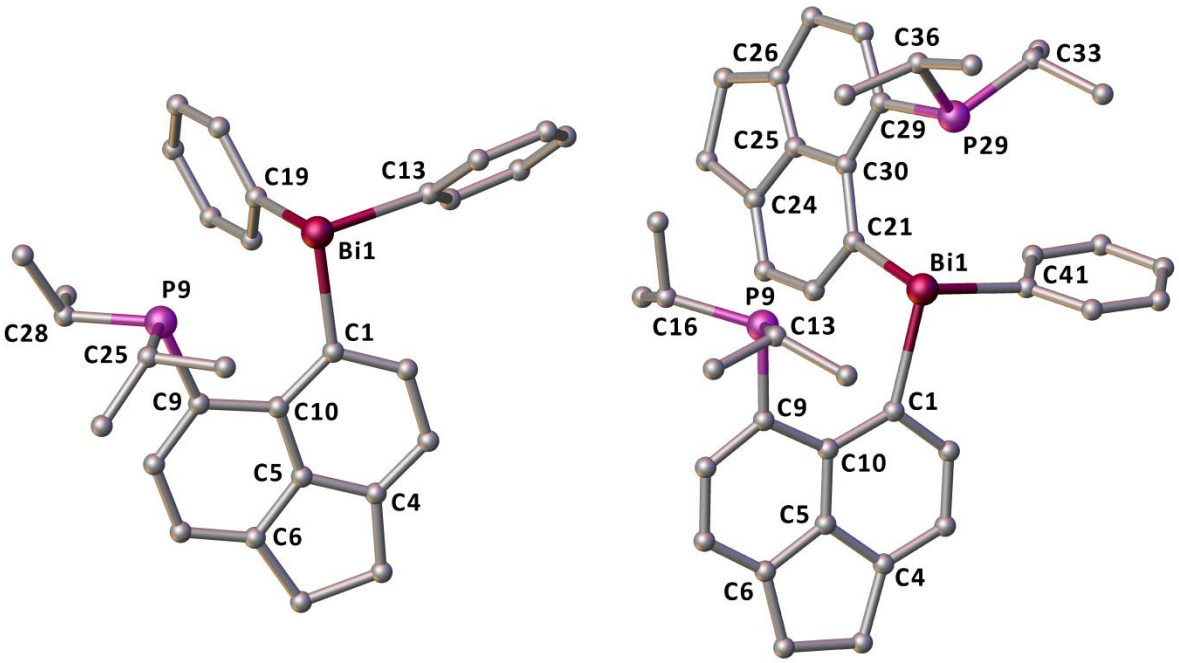

Figure 26: Crystal structures of **C2**-**5** (left) and **C2**-**6** (right) with hydrogen atoms omitted for clarity. The co-crystallised solvent (MeCN) molecule from **C2**-**5** is also omitted for clarity.

The structure of **C2**-**5** shows both pnictogen atoms adopting a trigonal pyramidal geometry if non-bonding sub-van der Waals interactions are ignored. As we saw within the structure of **C2**-**2** the angles around the bismuth atom are close to 90° owing to the purely p-orbital bonding of the bismuth atom. As we determined from the NMR data, there is no bonding interaction between the phosphorus and bismuth atoms with a P···Bi distance of 3.291(2) Å and a large positive splay angle (16.8(8)°). The quasi-linear P9···Bi1–C13 interaction (161.2(2)°) suggests the onset of a 3c–4e type interaction which is in agreement with the large through-space coupling observed within the $^{13}C\{^{1}H\}$ NMR spectrum for C13. The slightly elongated Bi1–C13 bond (2.309(7) Å) with respect to the Bi1–C19 bond (2.26(1) Å) adds further support to the formation of this interaction. The phosphorus and bismuth atoms display a modest distortion out of the mean C_{12} acenaphthene plane with a P9–C9···C1–Bi1 torsion angle of 8.9(4)°.This deviation coupled with the weak 3c–4e interaction seems to alleviate the expected strain within the acenaphthene framework when repulsive *peri*-interactions arise. The lack of strain within the acenaphthene backbone is evidenced by the small deviations from the ideal torsion angle of 180° for the C1–C10–C5–C6 and C9–C10–C5–C4 torsion angles. As with **C2**-**2** the P···Bi distance is significantly sub-van der Waals (77%). Looking at the angles around the bismuth centre, if this interaction is taken into account we see large variation of the C–Bi···P angles (C1–Bi1···P9 70.8(2)° and C19–Bi1···P9 78.3(3)°). This variation is a product of the distinctly different P–C_{Ace} and Bi–C_{Ace} bond lengths present within the structure.

Table 3: Selected bond lengths [Å], angles [°], torsion angles [°] and displacements [Å] for **C2**-**6**.

P···Bi1	3.227(2)/3.238(3)	Bi1–C	2.293(7)–2.35(1)
P–C	1.83(1)–1.884(9)		
C–P–C	101.2(4)–105.4(4)	C–Bi1–C	92.7(3)–95.4(3)
C–Bi1···P (*trans*)	163.6(2)/165.5(2)	C–Bi1···P (*cis*)	70.5(2)–80.7(2)
P9···Bi1···P29	112.49(6)		
P9–C9···C1–Bi1	0.5(4)	P29–C29···C21–Bi1	9.2(4)
Splay angle[a]	15.0(7)	C1–C10–C5–C6	179.2(8)
	15.1(7)	C21–C30–C25–C26	178.8(9)
Out of plane displacements			
P9/P29	0.219/0.190	Bi1	0.174/0.170

[a] calculated as the sum of the bay region angles – 360°.

Within the structure of **C2**-**6** neither of the phosphorus atoms forms a dative bond with the bismuth centre just like in **C2**-**5**. The P···Bi distances are 3.227(2) and 3.238(2) Å, which although non-bonding, do fall within the sum of the van der Waals radii. Considering the quasi-linear arrangement of the P···Bi–C bonds (P9···Bi1–C41 163.6(2)°; P29···Bi1–C1 165.5(2)°) and the sub-van der Waals P···Bi distances, a weak 3c–4e interaction may contribute to the conformation observed in the solid state. Evidence for an attractive non-bonding interaction between the *peri*-atoms can be shown by the small P–C···C–Bi torsion angles (0.5(4)° and 9.3(4)°) and small out-of-plane displacements of around 0.17–0.22 Å of the phosphorus and bismuth atoms from the mean acenaphthene plane. The out-of-plane distortions are also very small, deviating very slightly from the ideal 180° (C1–C10–C5–C6 179.2(8)°). However, the relatively poor Lewis acidity of the bismuth centre means the interactions between the phosphorus and bismuth atoms are clearly non-bonding due to the large positive splay angles (15.0(7)° and 15.1(7)°) and large P···Bi separations. This is in good agreement with the analogous arsenic and antimony derivatives the Kilian group published recently.[105]

2.6 – Phosphine–Bismuthine Donor–Acceptor Complexes: A Synthetic, Spectroscopic and Structural Examination

So far all the phosphorus–bismuth acenaphthenes synthesised have shown no strong attractive interaction between the two *peri*-atoms. This is due to the poor Lewis acidity of the triaryl bismuth centre in these compounds. In order to increase the Lewis acidity one or both of the other bismuth substituents could be replaced with an electronegative atom such as chlorine. All of the examples in section 2.1, where a donor–acceptor complex has been formed, contain a dihalo-bismuthine as the acceptor. In section 2.4.2 little success was encountered when trying to utilise bismuth trichloride to

form the desired halo-bismuthine, this method had been successful for all of the lighter pnictogens used previously.[24,87,88] Suzuki and co-workers utilised a fluorodearylation reaction to form a nitrogen–bismuth donor–acceptor complex. This was achieved starting from Me_2N-Naphth-$Bi(Tol)_2$ using boron trifluoride diethyl etherate, followed by washing with an aqueous sodium chloride solution.[91] With **C2**-**5** synthesisable in good quantities, this seemed a plausible route towards the desired halo-bismuthine.

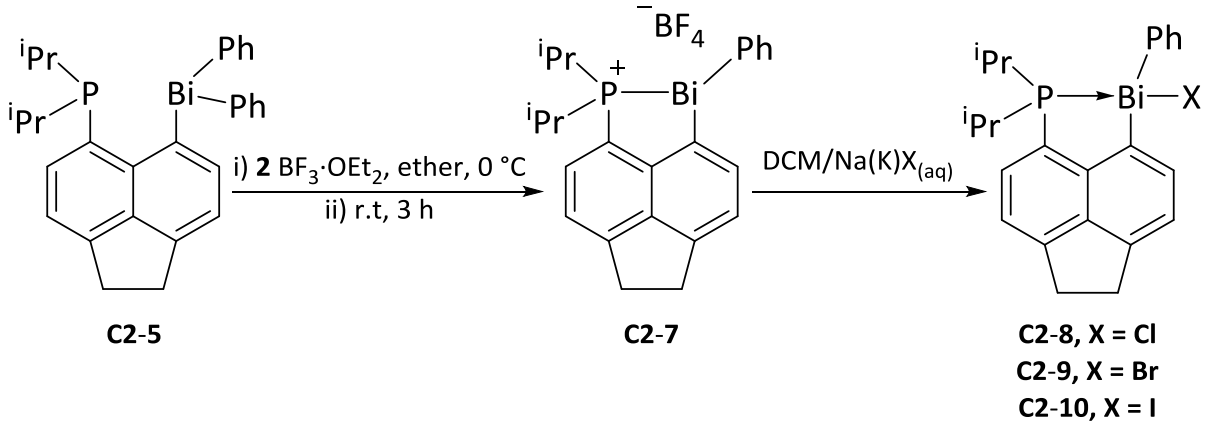

Scheme 14: Synthetic routes to the bismuthino-phosphonium salt **C2**-**7** and donor–acceptor complexes **C2**-**8**/**9**/**10**.

Suzuki and co-workers proposed the product from the fluorodearylation reaction was Me_2N-Naphth-Bi(Tol)F, with the fluorine atom bound to the bismuth centre. They never isolated this intermediate. When we have applied the same reaction sequence to **C2**-**5**, we found the product to actually be the bismuthino-phosphonium tetrafluoroborate salt **C2**-**7,** shown in Scheme 14. The structure of the compound was confirmed using multinuclear NMR spectroscopy, single crystal X-ray diffraction and elemental analysis. Dissolving **C2**-**7** in DCM followed by washing with a saturated aqueous solution of either a sodium or potassium halide resulted in the donor–acceptor complexes **C2**-**8**/**9**/**10**. The work up was straightforward with the organic layer separated then dried over magnesium sulfate. Filtration, followed by removal of the solvent under vacuum, afforded the compounds as either white (**C2**-**8** and **C2**-**9**) or yellow (**C2**-**10**) solids. In all cases the compounds required no further purification. The compounds were found to be stable in solution ($CDCl_3$) for several days before decomposition products started to appear in both the ^1H and $^{31}P\{^1H\}$ NMR spectra. Several attempts were made to prepare the fluorine derivative by washing with a saturated aqueous potassium fluoride solution. On each occasion, a different shift in the $^{31}P\{^1H\}$ NMR spectrum of the obtained

solid was observed with several impurities present. For this reason this synthetic target was not pursued further.

2.6.1 – Spectroscopic analysis of C2-7–10

The $^{31}P\{^{1}H\}$ NMR spectra of **C2**-**7** and **C2**-**8**–**10** are shown in Figure 27. The identification **C2**-**7** could not be performed using the NMR data collected alone. The $^{31}P\{^{1}H\}$ NMR spectrum of **C2**-**7** shows a signal at δ_P 56.7 ppm, which has shifted dramatically downfield compared to **C2**-**5** ($\Delta\delta_P$ 83.3 ppm). This deshielding of the phosphorus centre was initially attributed to the formation of a strong donor–acceptor complex due to the similarity of the chemical shift with previously reported systems. The arsenic compound $(^{i}Pr)_2$P-Acenap-$AsCl_2$ and antimony derivative $(^{i}Pr)_2$P-Acenap-$SbCl_2$ display signals at δ_P 65.3 and 51.0 ppm respectively.

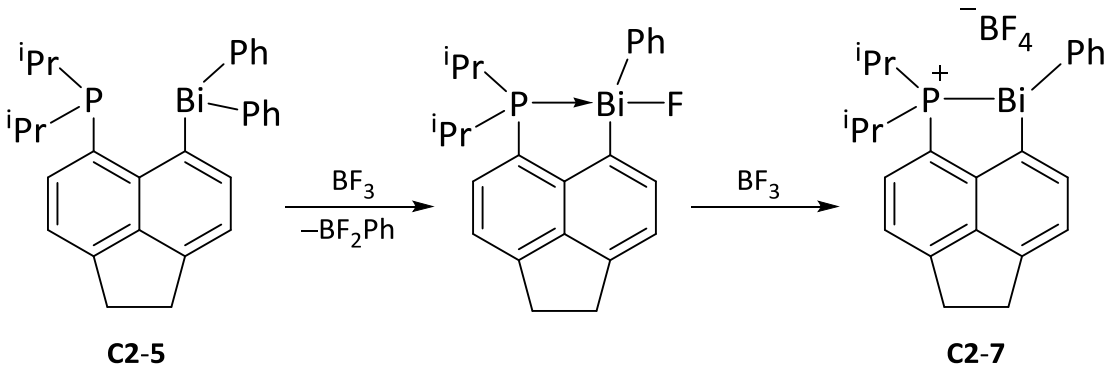

C2-**5** **C2**-**7**

Scheme 15: Plausible route to **C2**-**7** *via* a strong donor–acceptor complex.

Only after the crystal structure was determined did the full explanation become available. The formation of this bismuthino-phosphonium salt as shown in Scheme 14 is most likely due to the ability of boron trifluoride to act as a halide abstractor. Additionally, this helped explain the requirement for two molar equivalents of the boron trifluoride diethyl etherate. A two-step process is proposed, firstly, one molecule of boron trifluoride reacts with **C2**-**5** to replace a phenyl group with a fluorine atom. Secondly, due to the strength of the interaction between the phosphorus and bismuth centres a second boron trifluoride abstracts the fluorine from the bismuth to create the phosphonium salt (Scheme 15). The chemical shift of **C2**-**7** is also similar to the related phosphino-phosphonium derivative (δ_P 60.0 ppm) previously prepared within the group.[66]

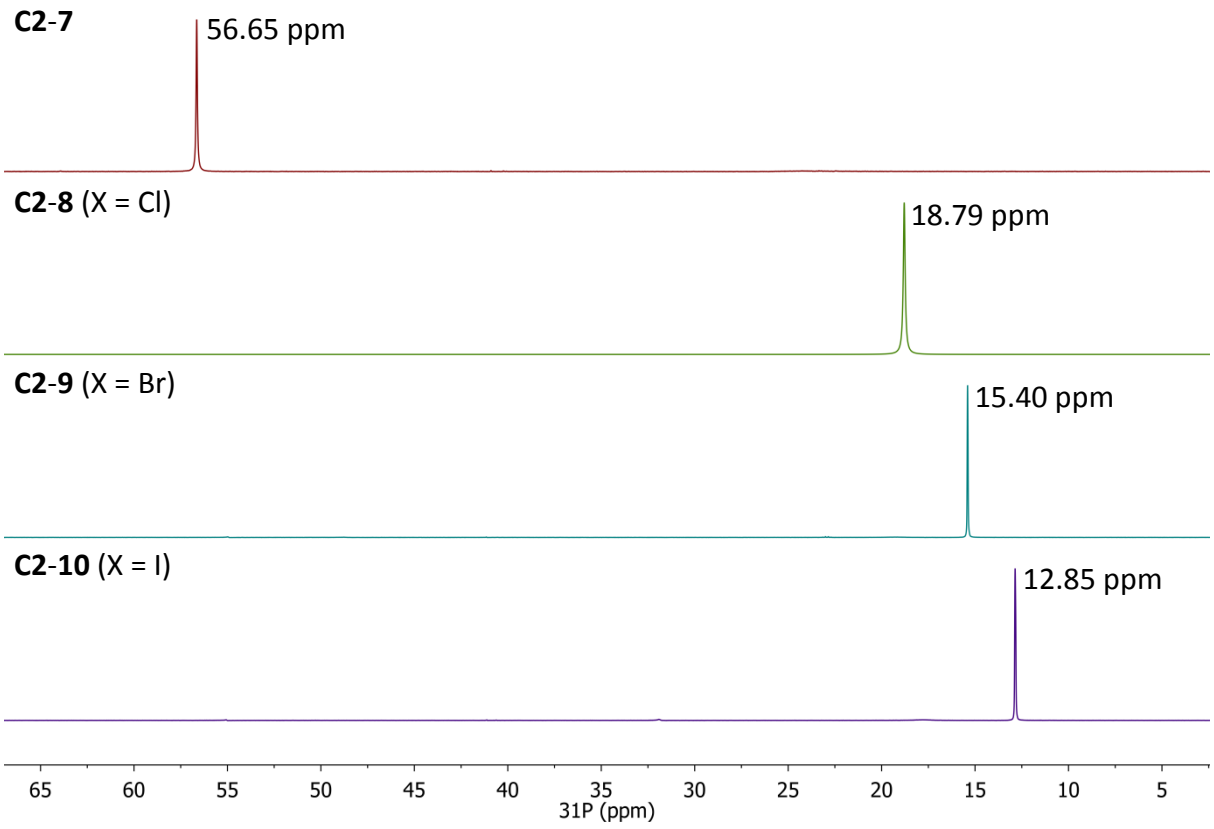

Figure 27: $^{31}P\{^{1}H\}$ NMR spectra ($CDCl_3$, 202 MHz) of **C2**-**7** and **C2**-**8**–**10**.

The compounds **C2**-**8**, **C2**-**9** and **C2**-**10** all display signals shifted significantly downfield compared to **C2**-**5** whilst being shifted significantly upfield compared to **C2**-**7**. This is easily explained as the formation of the donor–acceptor complex puts these systems between the two extremes of bonding (**C2**-**7**) and non-bonding (**C2**-**5**) between the phosphorus and bismuth atoms. The Lewis acidity of the bismuth centre decreases (Acenap-BiPh**Cl** > Acenap-BiPh**Br** > Acenap-BiPh**I**) as you go down the halogens group. This means the donation of the phosphorus lone pair into the σ*(Bi–X) orbital is less effective and as such the phosphorus nuclei becomes more shielded ongoing from **C2**-**8** to **C2**-**10**. Both the arsenic and antimony derivatives of **C2**-**8** have been synthesised recently within the Kilian group,[66,88,107] the addition of **C2**-**8** to this series allows comparisons between the heavier pnictogens to be made. Figure 28 shows the completed series of compounds and their $^{31}P\{^{1}H\}$ NMR chemical shifts.

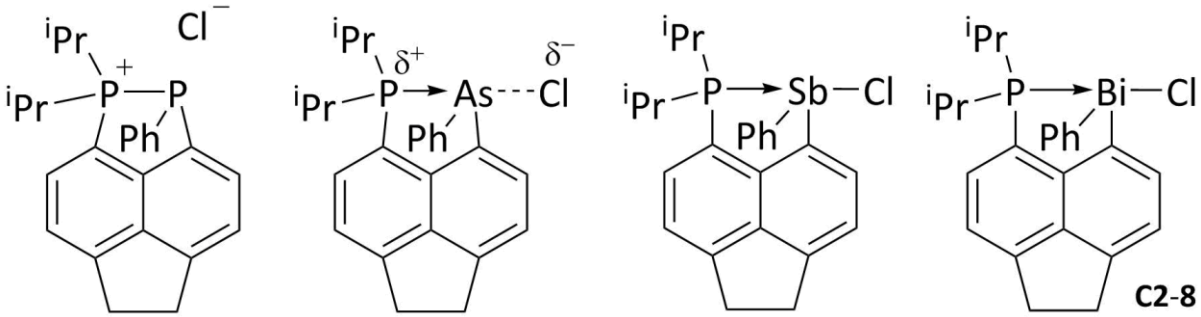

Figure 28: Pnictogen compounds of the type (^{i}Pr)$_2$P-Acenap-PnPhCl (Pn = P, As, Sb, Bi) and their ^{31}P{^{1}H} chemical shifts.

Looking at the figure there is a distinct difference between both the phosphorus/arsenic and antimony/bismuth analogues. The phosphorus congener exists as the phosphino-phosphonium salt[66] hence its downfield chemical shift. The arsenic system[107] appears to exist in the same form in the solution state due to the similar ^{31}P{^{1}H} chemical shift. Within the solid state there is a distinct interaction between the arsenic and chlorine atoms as determined by single crystal X-ray diffraction. For the antimony derivative a significant shift upfield is observed in the ^{31}P{^{1}H} NMR spectrum as the ionic character is significantly decreased.[88] Comparing the antimony and bismuth (**C2**-**8**) congeners there is a downfield shift on changing from antimony to bismuth. This implies a stronger phosphorus–pnictogen interaction which was unexpected owing to the decreased Lewis acidity of the bismuth centre compared to the antimony derivative.

The ^{1}H NMR of **C2**-**7** supports the formation of a bond between the phosphorus and bismuth atoms as four doublets of doublets are observed corresponding to the isopropyl CH_3 groups (δ_H 0.50–1.31 ppm). Furthermore, two distinct signals for the isopropyl CH groups are observed at δ_H 3.06 and 2.97 ppm. The remaining signals from the acenaphthene backbone and phenyl substituent appear with coupling constants as expected for the structure. In the donor–acceptor complexes **C2**-**8**–**10** the same asymmetry is observed for the isopropyl groups within their respective ^{1}H NMR spectra. The remaining aromatic signals are also consistent with the proposed structures. This implies that the interaction between the phosphorus and bismuth atoms is preserved in solution.

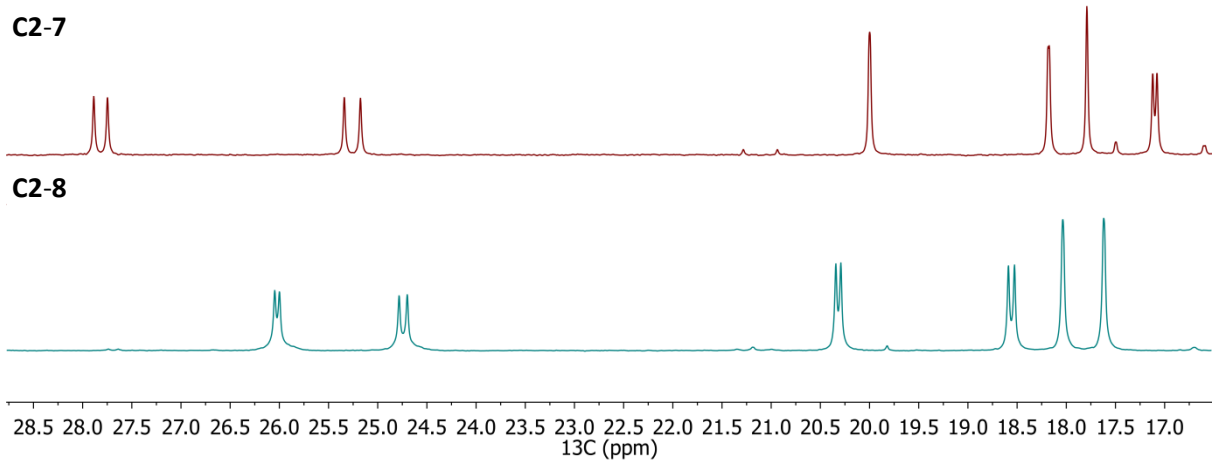

Figure 29: Alkyl region of the $^{13}C\{^{1}H\}$ NMR DEPT-Q–135 spectra ($CDCl_3$, 125 MHz) of **C2**-**7** (top) and **C2**-**8** (bottom).

The $^{13}C\{^{1}H\}$ NMR spectra of **C2**-**7**–**10** display a number of interesting features. As predicted by their ^{1}H NMR spectra, two and four signals are present corresponding to the CH and CH_3 parts, respectively, of the isopropyl groups (Figure 29). This confirms that the interaction between the two *peri*-atoms remains in solution. Interestingly, whilst all the CH signals observed appear as doublets the magnitude of the coupling in **C2**-**7** (J_{CP} 17.4 and 20.4 Hz) is greater than that seen in **C2**-**8**–**10** (J_{CP} ranges from 4.3 to 10.9 Hz). Additionally, only one of the four signals arising from the methyl groups appears as a doublet in **C2**-**7** (J_{CP} 5.4 Hz) with the rest as slightly broadened singlets. For **C2**-**8**–**10** two of the four signals are doublets (J_{CP} ranges from 6.7 to 7.8 Hz) with the other two again being slightly broadened. The anticipated aromatic signals are present within all the spectra, along with the expected coupling constants. In **C2**-**7** the bonding interaction between the two *peri*-atoms means that the *ipso*-carbon of the phenyl ring couples strongly to the phosphorus atom. Such coupling is also observed within **C2**-**8**–**10** owing to the strong attractive interaction between the *peri*-atoms (Figure 30). The magnitude of this coupling constant decreases as the Lewis acidity of the bismuth moiety decreases owing to a weaker interaction between the *peri*-atoms ($^{2}J_{CP}$ 12.8 (**C2**-**7**), 8.4 (**C2**-**8**), 7.3 (**C2**-**9**), 6.2 (**C2**-**10**) Hz).

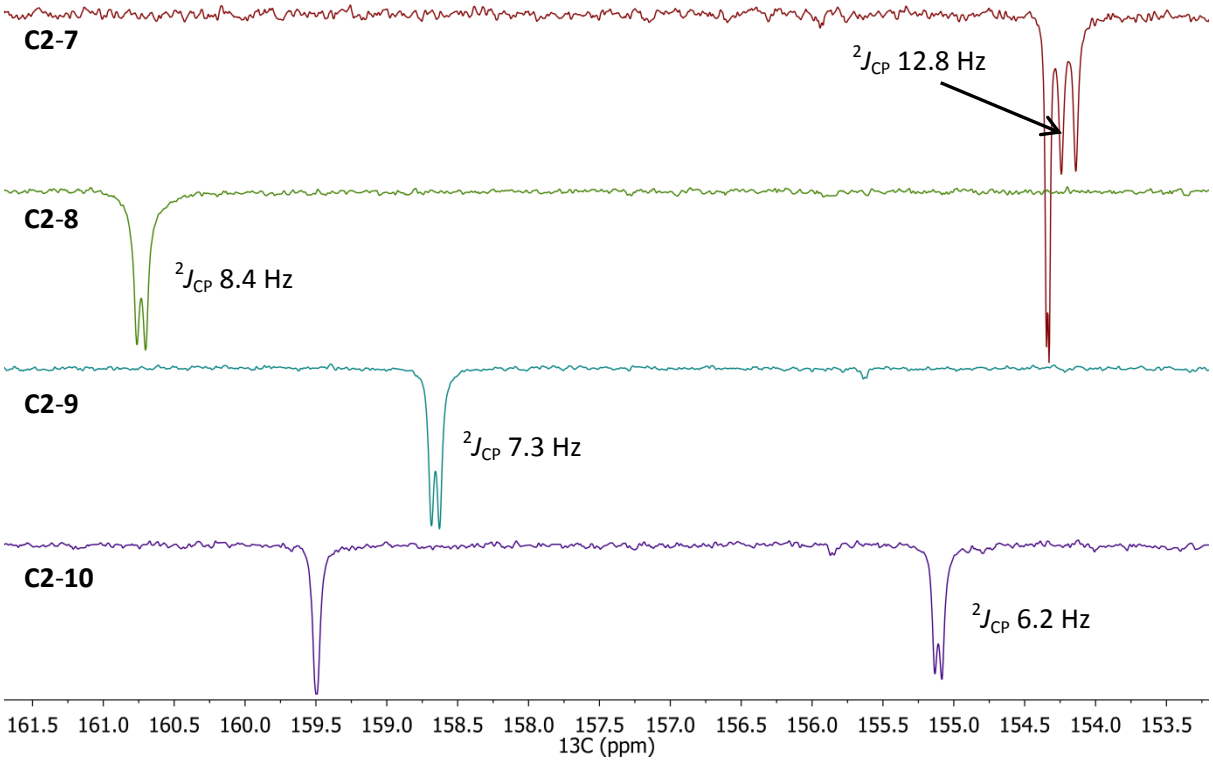

Figure 30: Aromatic region of the $^{13}C\{^1H\}$ NMR DEPT-Q–135 spectra ($CDCl_3$, 125 MHz) of **C2**-**7**–**10** showing the coupling between the phenyl ring *ipso*-carbon and phosphorus atom.

The presence of a tetrafluoroborate counterion in **C2**-**7** is supported by signals in the IR spectrum at ν_{max} 1084, 1056 and 519 cm^{-1}. These correspond to FBF deformations (ν_{max} 1084 and 1056 cm^{-1}) and B–F stretch vibrations (ν_{max} 519 cm^{-1}) which are similar to other literature compounds bearing the tetrafluoroborate anion.[108] The IR spectra of the donor–acceptor compounds (**C2**-**8**–**10**) appeared as expected. The mass spectra of **C2**-**7**–**10** all displayed base peaks which corresponded to $[(^iPr)_2$P-Acenap-BiPh$]^+$ (*m/z* 555.1654); in the case of **C2**-**7** this was $[M]^+$ whilst for **C2**-**8**–**10** this was the $[M-X]^+$ fragment. Interestingly for **C2**-**9** the $[M+H]^+$ peak was observed at *m/z* 635.0916 (^{79}Br) and 637.0898 (^{81}Br) with less than 1% intensity. The analytical purity of all the compounds was confirmed by elemental analysis.

2.6.2 – Crystallographic characterisation of C2-7, C2-8, C2-9 and C2-10

Crystals suitable for X-ray work were obtained for the compounds **C2**-**7**, **C2**-**8**, **C2**-**9** and **C2**-**10** *via* slow diffusion of ether into a concentrated DCM solution containing the compound. In all cases only one molecule was present within the asymmetric unit. The crystal structures of **C2**-**7**–**10** are shown in Figure 32 with selected structural parameters in Table 4.

The crystal structure of **C2**-**7** confirms that the proposed bonding interaction between the phosphorus and bismuth atoms exists. The P–Bi bond length is 2.674(2) Å which is less than the average single bond length from structures within the Cambridge Structural Database (2.733 Å).[25,26] It is similar to the bond lengths observed in the coordination complexes of bismuth triflates with diphosphine ligands reported by Burford and co-workers (Figure 31).[109]

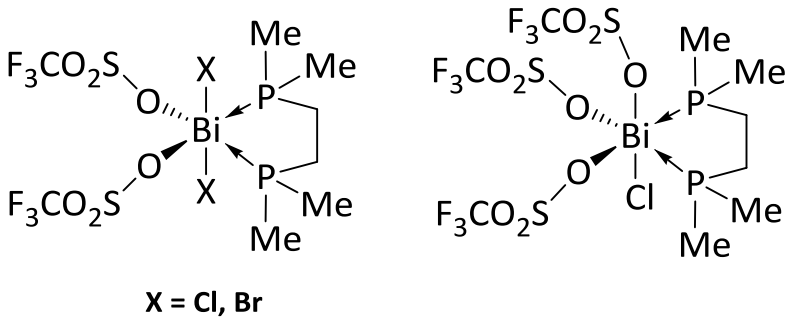

Figure 31: Coordination complexes of bismuth triflates reported by Burford and co-workers.

From the structure we can see an interaction between the bismuth centre and one of the fluorine atoms of the tetrafluoroborate. The Bi–F distance is 2.736(4) Å which although being less than the $\sum r_{vdW}$ (using r_{vdW} = 1.50 (F) and 2.30 (Bi) Å) is far longer than any other Bi–F bond reported in the CSD (Bi–F; mean = 2.331 Å, range = 2.0890−2.5940 Å).[25,26] Additionally the Bi–F distance in **C2**-**7** is far longer than the sum of the covalent radii (2.28 Å, using r_{cov} = 0.64 (F) and 1.48 (Bi) Å),[110] as such this is assumed to be a weak interaction.

The phosphorus atom adopts a tetrahedral geometry. The angles around the bismuth atom are again close to 90° owing to the purely p-orbital overlap that is responsible for the bonds to the bismuth centre. The most distorted angle from the expected 90° is C1–Bi1–P9 (78.43(17)°) due to both the rigid acenaphthene framework and the large difference in the P9–C9 and Bi1–C1 bond lengths. The splay angle is close to zero (1.5(5)°) as would be expected with such a large atom in the *peri*-position. The analogous phosphorus compound has a splay angle of −8.85(18)°.[66] Overall the molecular geometry of the acenaphthene ring is relaxed with a low P9–C9···C1–Bi1 torsion angle (3.3(3)°) and only moderate distortions in the central ring torsions. Additionally, the out-of-plane displacements of both pnictogen atoms are relatively small. One last observation within the structure is the presence of weak H···π interactions between two of the methyl environments and the phenyl ring of the bismuth centre. This may explain why two of the methyl signals in the ^{1}H NMR of **C2**-**7** were more shielded than the others.

Table 4: Selected bond lengths [Å], angles [°], torsion angles [°] and displacements [Å] for **C2**-**7**, **C2**-**8**, **C2**-**9** and **C2**-**10**.

	C2-**7**	**C2**-**8**	**C2**-**9**	**C2**-**10**
P9–Bi1	2.674(2)	2.816(2)	2.805(2)	2.798(1)
Bi1–X1	2.736(4)	2.767(2)	2.9410(8)	3.1980(6)
P9–C9	1.806(6)	1.823(7)	1.801(8)	1.818(4)
Bi1–C1	2.258(6)	2.284(6)	2.258(6)	2.281(4)
C1–Bi1–C13	95.0(2)	92.7(3)	96.7(3)	91.6(1)
C1–Bi1–P9	78.43(17)	76.2(2)	76.52(18)	76.54(10)
C13–Bi1–P9	92.73(16)	86.30(19)	87.91(17)	86.88(10)
C1–Bi1–X1	–	90.8(2)	92.2(2)	94.2(1)
C13–Bi1–X1	–	89.6(2)	89.8(2)	91.6(1)
P9–Bi1–X1	–	166.13(6)	168.17(4)	170.56(2)
splay angle[a]	1.5(5)	4.5(7)	5.1(6)	5.3(4)
P9–C9···C1–Bi1	3.3(3)	8.1(3)	2.4(3)	4.0(2)
C1–C10–C5–C6	176.0(6)	179.7(8)	177.7(7)	178.9(4)
C9–C10–C5–C4	177.8(6)	179.8(8)	179.4(7)	179.0(4)
Out of plane displacements				
Bi1	0.117	0.028	0.053	0.043
P9	0.231	0.243	0.151	0.093

[a] calculated as [(Bi1–C1–C10)+(C1–C10–C9)+(C10–C9–P9)−360].

The crystal structures of **C2**-**8**, **C2**-**9** and **C2**-**10** are isostructural which is not unexpected given the only change is in the halogen attached to the bismuth centre. The successful formation of a donor–acceptor complex is confirmed in all cases owing to the presence of a P–Bi dative bonding interaction. Across the series the P–Bi lengths vary little (P–Bi = 2.816(2) (Cl), 2.805(2) (Br), 2.798(1) (I) Å) and are slightly longer than the average length reported in the CSD (P–Bi 2.733 Å).[25,26] This suggests the change in relative Lewis acidities of each bismuth centre is quite small. The trend observed contradicts the $^{31}P\{^{1}H\}$ NMR data with the P–Bi distance decreasing as you descend the halogens, suggesting the Lewis acidity of the acceptor group is in fact increasing in the order **C2**-**8** < **C2**-**9** < **C2**-**10**. However, the difference between the chloro- and iodo-compounds is so small (0.018 Å) it is likely crystal packing effects are playing a part. For all the compounds the Bi–X bonds are lengthened compared to their respective trihalides ΔBi–X 0.267 (Cl), 0.281 (Br) and 0.128 (I) Å.[4] This is expected as the n(P)→σ*(Bi–X) interaction causes a weakening of the Bi–X bond and thus a longer distance. In the case of **C2**-**8** the Bi–Cl bond length is similar to that reported for the related Me_2N-Naphth-Bi(Tol)Cl compound (Bi–Cl 2.700(2) Å).[91] In the case of **C2**-**8** and **C2**-**9** these values are still greater than those seen when the halogens adopt axial positons in $BiPh_3X_2$ (Bi–Cl 2.529−2.615 Å, Bi–Br 2.7261(9)−2.7600(9) Å).[111,112]

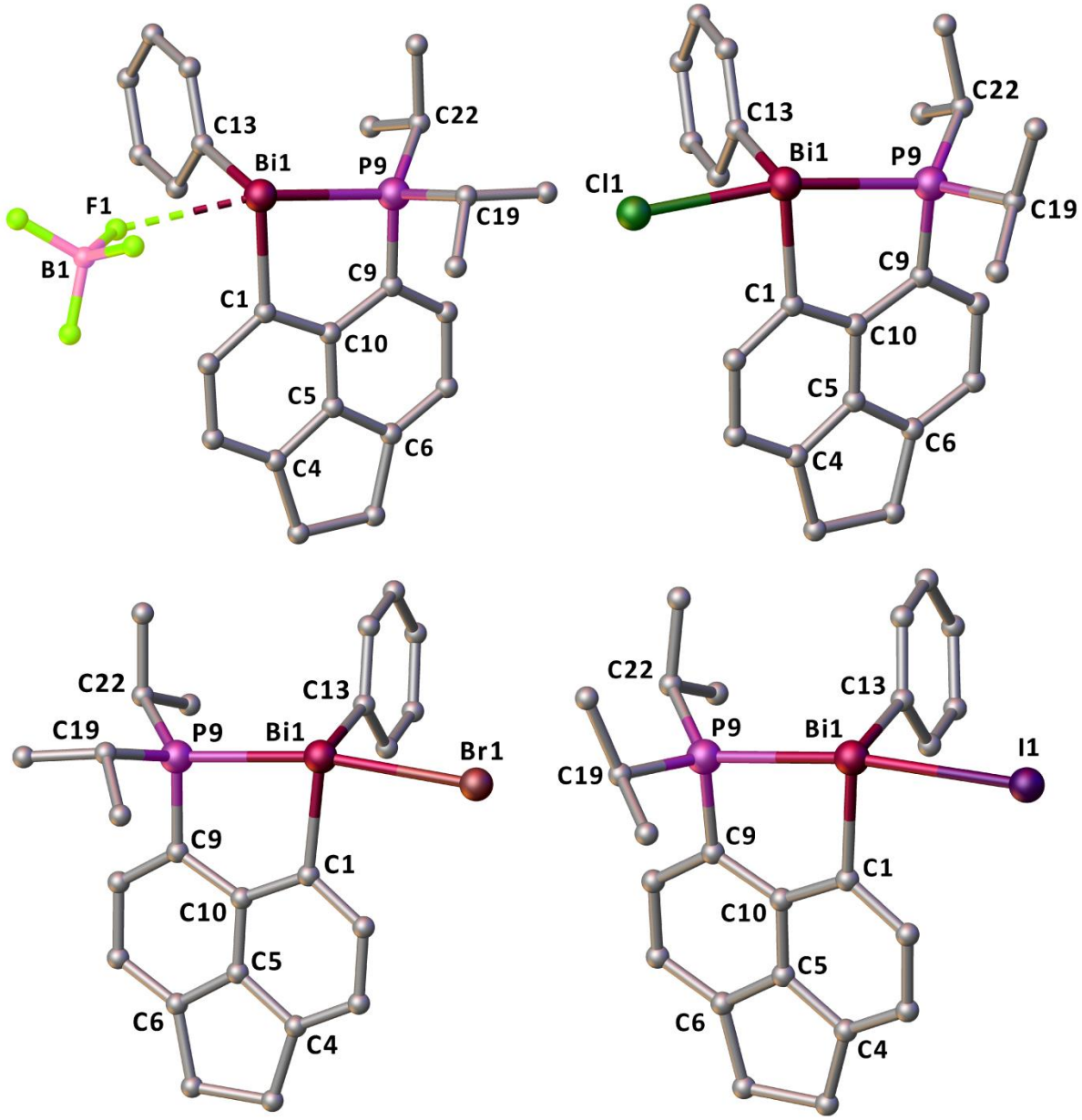

Figure 32: Crystal structures of **C2**-**7** (top left) and **C2**-**8** (top right), **C2**-**9** (bottom left) and **C2**-**10** (bottom right) with hydrogen atoms omitted for clarity.

As with **C2**-**7** the phosphorus centre adopts a tetrahedral geometry within all the structures owing to the formation of the dative P–Bi bond. The presence of this dative interaction now means the bismuth centre adopts a trigonal bipyramidal geometry with the phosphorus and halogen atoms in the axial positons. The angles around the bismuth atom are again close to 90° with the most acute being the C1–Bi1–P9 (**C2**-**8** 76.2(2)°, **C2**-**9** 76.52(18)°, **C2**-**10** 76.54(10)°) in all cases. The linearity of the axial substituents is also compromised with the P···Bi–X angle getting closer to 180° as the halogen changes from Cl to Br to I. As we saw before, both of these observations are in part due to the difference in the P–C and Bi–C bond lengths. The strength of the out-of-plane distortion, as

measured by the P9–C9···C1–Bi1 torsion angle, is greatest for **C2**-**8** being approximately double that seen for **C2**-**10** and 3½ times that of **C2**-**9**. The large P9–C9···C1–Bi1 torsion in **C2**-**8** helps explain why this compound displays the longest P–Bi length. The trend is reversed when the in-plane distortion is measured using the splay angle as this value increase across the series **C2**-**8**–**10**. As with the previously reported structures in sections 2.4.2 and 2.5.2 the central acenaphthene ring system exhibits only weak to moderate distortions.

2.6.2.1 – (^{i}Pr)$_2$P-Acenap-BiI$_2$, the surprise crystal structure

During one of the attempts to obtain crystals of **C2**-**10**, an interesting result was obtained. The structure observed was that of (^{i}Pr)$_2$P-Acenap-BiI$_2$ (now assigned the compound number **C2**-**11**). It is possible this has been formed during the crystallisation process *via* a redistribution reaction between two molecules of **C2**-**10** resulting in the observed product and **C2**-**5**. The structure contains co-crystallised solvent molecule ($CHCl_3$) and forms a centrosymmetric dimer *via* bridging iodine atoms. Similar dimers have been observed for other related pnictogen dihalides, prepared within the Kilian group, and Ph_2P-Acenap-$BiCl_2$ recently reported by Beckmann and co-workers.[59,87,88] The crystal structure is shown in Figure 33 with selected structural parameters in

Table 5.

Table 5: Selected bond lengths [Å], angles [°], torsion angles [°] and displacements [Å] for **C2**-**11**.

Distances			
P9–Bi1	2.735(1)	P9–C9	1.798(3)
Bi1–I1	3.0271(4)	Bi1–I2	3.1128(4)
Bi1–C1	2.245(3)	Bi1'–I2	3.4755(5)
C1–Bi1–I1	88.47(9)	C1–Bi1–I2	87.12(9)
I1–Bi1–I2	171.95(1)	P9–Bi1–I1	90.08(2)
P9–Bi1–I2	95.58(2)	P9–Bi1–I2'	174.95(2)
Splay angle[a]	3.9(3)	P9–C9···C1–Bi1	1.7(2)
C1–C10–C5–C6	178.8(3)	C9–C10–C5–C4	177.8(3)
Out of plane displacements			
P9	0.069	Bi1	0.014

[a] calculated as [(Bi1–C1–C10)+(C1–C10–C9)+(C10–C9–P9)−360].

Analysis of the structure shows it to be similar with the related compound $BiArI_2$ (Ar = 2-(Me_2NCH_2)C_6H_4) synthesised by Cowley and co-workers.[93] The phosphorus atom adopts the expected tetrahedral geometry donating its lone pair into the bismuth atom, which consequently adopts a *pseudo*- trigonal bipyramidal geometry. The P–Bi bond length is 2.735(1) Å which is close to

the average length for single P–Bi bonds mentioned previously. The two Bi–I bonds differ in length Bi1–I1 3.0271(4) and Bi1–I2 3.1128(4) with the Bi1–I2 length being slightly longer owing to this acting as the bridging iodine in the formation of the dimer. Both of these lengths are shorter than those seen in **C2**-**10** (3.1980(6) Å) owing to the formation of a different structural architecture where the two iodine atoms now take up the axial positions. Thus the phosphorus lone pair is no longer donating into the σ*(Bi–I) orbital meaning no weakening of the Bi–I bond. The Bi1'–I2 distance is 3.4755(5) confirming the weak nature of the dimeric interaction.

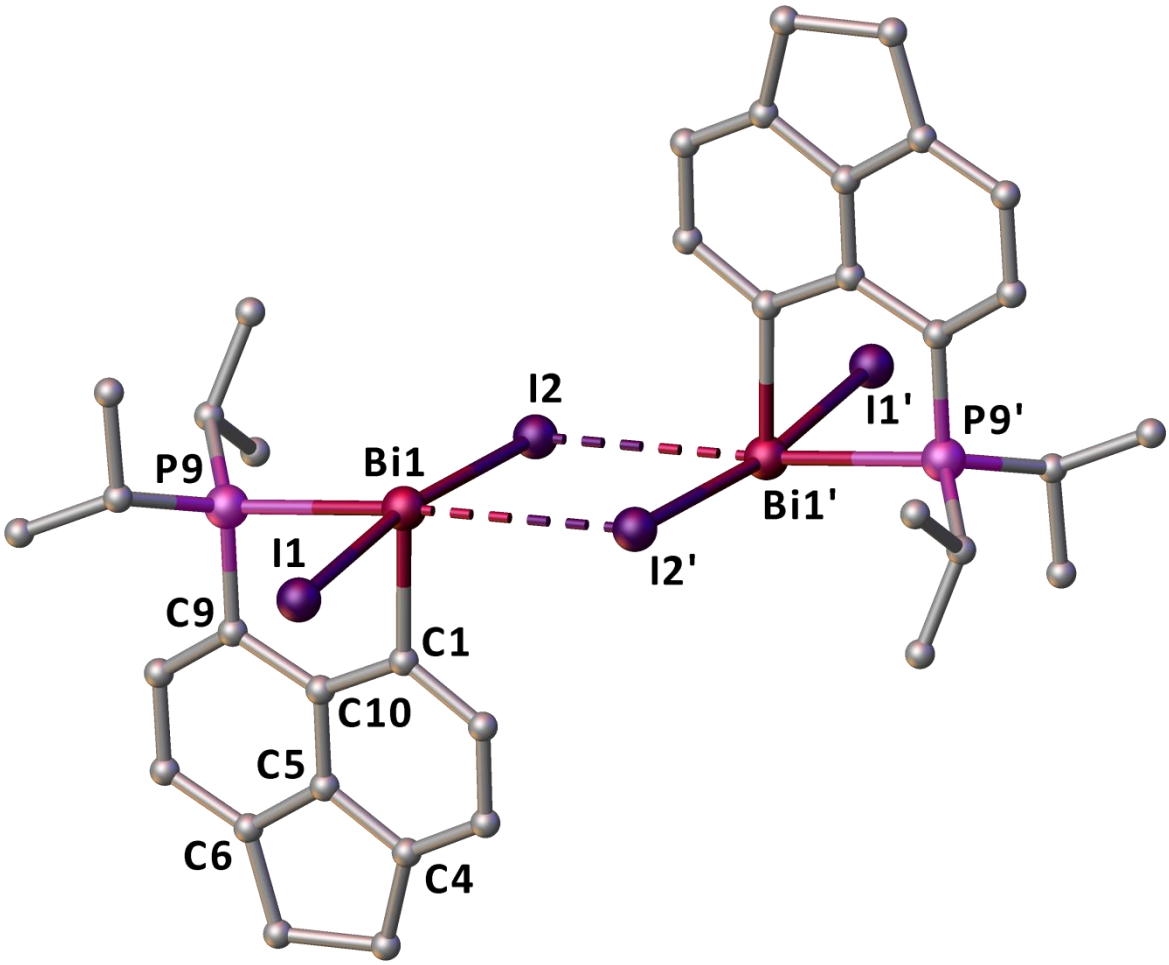

Figure 33: Crystal structure of **C2**-**11** with hydrogen atoms omitted for clarity. The co-crystallised solvent molecule ($CHCl_3$) is also omitted for clarity.

The level of in-plane distortion within **C2**-**11** is less than that seen in the compounds **C2**-**8**–**10**. This is most likely due to the stronger interaction between the phosphorus and bismuth atoms. Both the splay angle (3.9(3)°) and P9–C9···C1–Bi1 torsion (1.7(2)°) confirm this low distortion level. Additionally, the out-of-plane displacements of the two pnictogen atoms from the acenaphthene ring system are only minor. The acenaphthene backbone itself experiences only small distortions as

seen by the central C1–C10–C5–C6 and C9–C10–C5–C4 torsions. The positioning of the two iodine atoms in the axial positions is confirmed by the I1–Bi1–I2 angle of 171.95(1)°. Compound **C2**-**11** forms a centrosymmetric dimer through secondary Bi···I interactions. Taking these interactions into account the bismuth geometry becomes distorted square-based pyramidal. The iodine atoms occupy the meridional positions with a close to linear arrangement of the P9–Bi1···I2′ motif (174.95(2)°).

2.6.3 – Examining the solid state structural types of Bi(III) compounds

So far in this chapter we have seen two distinct structural types (**X** and **Y**) adopted by the bismuth compounds synthesised (Figure 34). Looking at the most Lewis acidic analogue **C2**-**11** we can see that structural type **X** is adopted. This is in agreement with other similar pnictogen derivatives and other diiodo-bismuth systems.[59,88,93] As we decrease the Lewis acidity of the bismuth centre through the replacement of one of the halogen atoms with a phenyl group the structural type changes to **Y**. The driving force for this changes is the formation of a 3c–4e bond by the donation of the phosphorus lone pair into the σ*(Bi–X) orbital. Indeed, 3c–4e bonding has been shown to drive conformational preferences in a wide range of *peri*-substituted species.[42] Finally, if no bonding interaction between the two *peri*-atoms is present then structural type **Y** is again preferred as seen in the crystal structure of **C2**-**5** where little or no attractive interaction takes place.

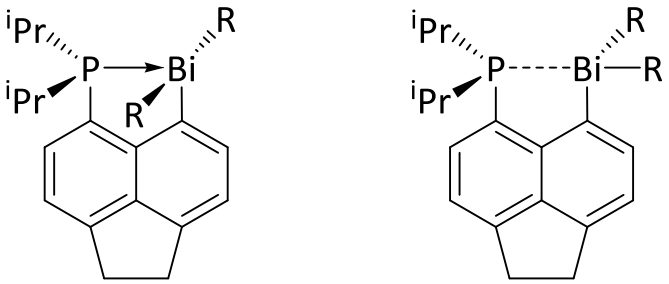

structural type **X** structural type **Y**

Figure 34: The two structural types identified in the reported Bi(III) series (**X** and **Y**).

Within the series of compounds presented in this chapter we have seen interactions between the *peri*-atoms ranging from covalent bonds through weaker dative bonds to non-bonding. When the interaction is classed as covalent structural type **X** is preferred whereas if only a weaker dative or non-bonding interaction is present then structural type **Y** is adopted. Therefore structural type **X** will be formed when a strong Lewis base and strong Lewis acid are situated in the *peri*-positions. Concurrently, if the Lewis acidity of the acceptor drops a sufficient amount causing the interaction to become weaker then structural type **Y** will be adopted.

2.6.4 – Improved synthesis of C2-6

As mentioned in section 2.5 a number of small impurities were present within **C2**-**6** because the starting material, $BiCl_2Ph$, could not be isolated in pure form. In section 2.6 the synthesis of **C2**-**8** was described, this compound is similar to the starting material $BiClPh_2$ as they are both chloro bismuthines with two aromatic groups. It was expected that reacting Li-**C2**-**1** with **C2**-**8** would result in the formation of **C2**-**6**. Scheme 16 outlines the synthetic protocol used. Reacting one equivalent of Li-**C2**-**1** with **C2**-**8** at −78 °C followed by extraction of the desired compound using ether, then subsequent washing with hot MeCN, afforded **C2**-**6** as an off white solid. The analytical purity of the product was confirmed by elemental analysis. The ^{1}H, $^{13}C\{^{1}H\}$ and ^{31}P NMR spectra as well as the $APCI^{+}$ HRMS were consistent with that obtained following the previous synthetic route.

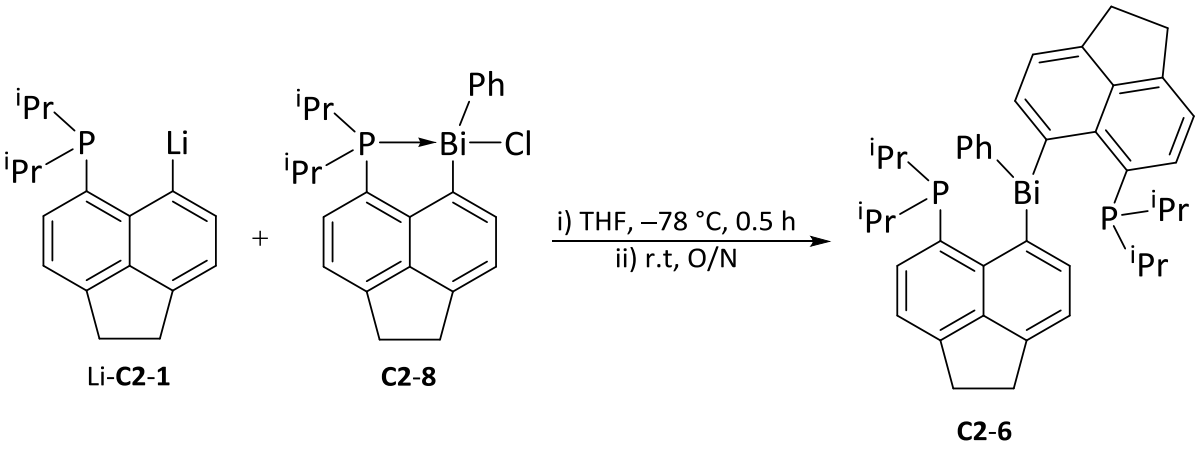

Scheme 16: Improved synthetic route to **C2**-**6**.

As mentioned previously some of the alkyl signals within the ^{1}H NMR spectrum of **C2**-**6** are broadened. The $^{13}C\{^{1}H\}$ NMR spectrum of **C2**-**6** does not show such extensive broadening of the signals. The quaternary carbon of the acenaphthene group directly bound to the phosphorus atom was the only signal not visible within the spectrum. As we saw in **C2**-**5** the signal from the *ipso*-carbon of the phenyl ring is split by through-space coupling to the phosphorus atoms. This results in a triplet with a large coupling constant of 34.7 Hz which is most likely composed entirely of through-space component due to the overlap of the phosphorus lone pair and the σ*(Bi–C) orbital.

Within the Kilian group both the arsenic and antimony derivatives of **C2**-**6** have been previously prepared.[105] Comparing the arsenic, antimony and bismuth analogues the bismuth centre was the least Lewis acidic with the most shielded phosphorus signal (δ_P −10.5 (As, 373 K), −17.5 (Sb, 363 K), −22.5 (Bi, 298 K)). The room temperature $^{31}P\{^{1}H\}$ NMR spectra of these compounds show how the larger pnictogen centre imposes less steric restriction on the acenaphthene substituents (Figure 35).

The arsenic derivative displays two broad signals at δ_P −11.6 and −14.4 ppm showing the asymmetry of the two acenaphthene units due to the restricted rotation of the acenaphthene units around the central pnictogen. For the antimony system room temperature is close to the coalescence temperature as shown by the very broad single obtained (δ_P −18.9 to −22.8 ppm). The larger antimony atom allows more freedom for the acenaphthene units to rotate and thus the two phosphorus atoms become magnetically equivalent. Finally, **C2**-**6** displayed the broadened singlet mentioned earlier at δ_P −22.2 ppm. Due to the size of the bismuth atom there are no appreciable steric restrictions placed upon the acenaphthene units, thus, they can easily interconvert at room temperature.

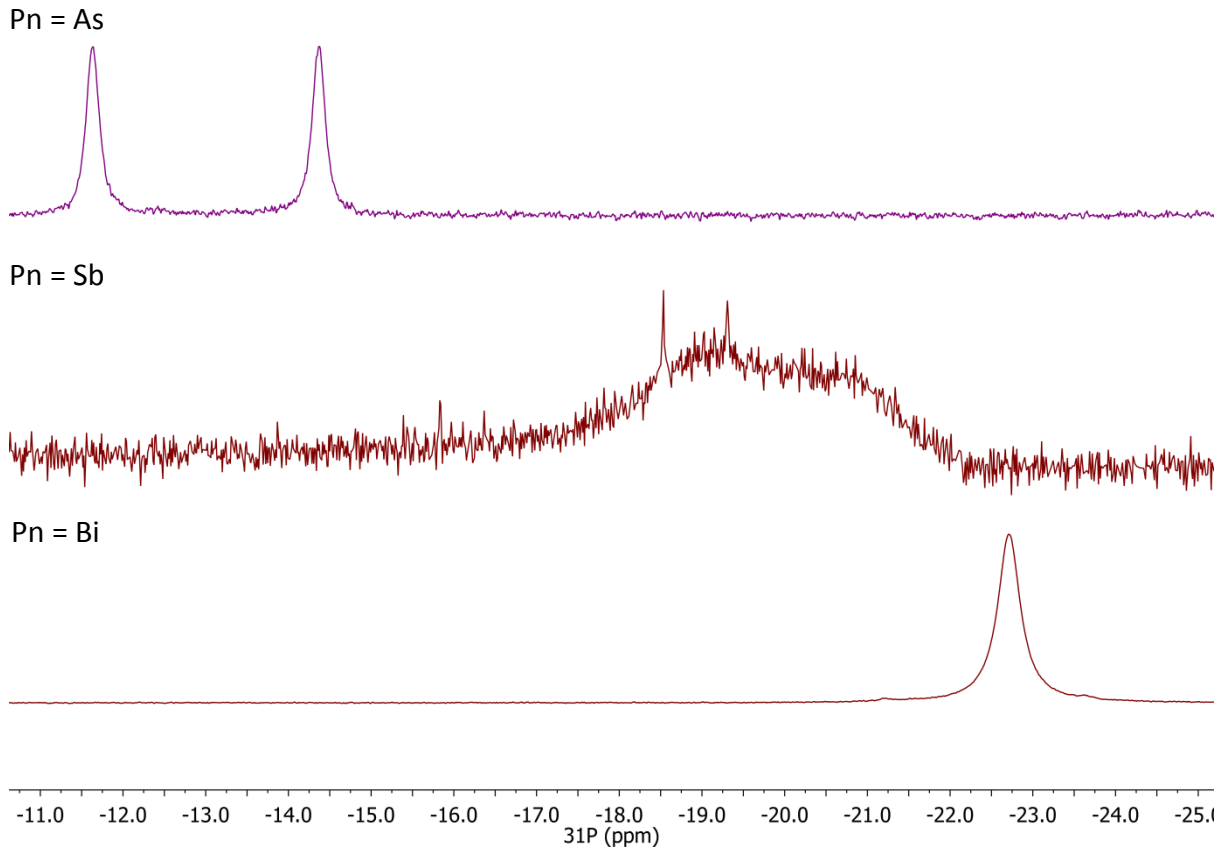

Figure 35: $^{31}P\{^1H\}$ NMR spectra (298 K, $CDCl_3$ (Pn = As), d_8-toluene (Pn = Sb) and CD_2Cl_2 (Pn = Bi), 202 MHz (Pn = As, Bi) and 109 MHz (Pn = Sb)) of the pnictogen compounds $((^iPr)_2P\text{-Acenap})_2\text{-PnPh}$, Pn = As (top), Sb (middle), Bi (bottom).

Variable temperature NMR studies had been conducted previously on the arsenic and antimony derivatives.[105] Using the coalescence method (Eq. 2) the rotational barrier of the arsenic and antimony derivatives were determined at their respective coalescence temperatures. The rotational barrier, $\Delta G^{\ddagger}$, calculated for the arsenic derivative (coalescence temperature = 340 K) was 62.3 kJ

mol^{-1} with the antimony derivative (coalescence temperature = 303 K) determined to be 57.7 kJ mol^{-1}.

$$\Delta G^{\ddagger} = aT\left[9.972 + \log\left(\frac{T_c}{\Delta\nu}\right)\right] \qquad \textbf{(Eq. 2)}$$

In order to calculate this value for the **C2**-**6** a variable temperature NMR study was conducted in the range of 185−295 K (Figure 36). As **C2**-**6** already displays a singlet in its room temperature $^{31}P\{^{1}H\}$ NMR spectrum the sample only required cooling, to allow the determination of both the coalescence temperature and Δν of the slow motion regime (where Δν is the maximum peak separation of the slow motion regime in Hertz). Using Eq. 2 ($a = 1.914 \times 10^{-2}$ for units of kJ mol^{-1}, T/T_c = 262 K and Δν = 797.8 Hz) an estimation of the rotational barrier for **C2**-**6** was calculated, $\Delta G^{\ddagger}$ = 47.6 kJ mol^{-1}. Whilst the values for each pnictogen containing compound are not directly comparable owing to the use of the coalescence method the observed trend of $\Delta G^{\ddagger}$ (As > Sb > Bi) is what would be expected. The larger bismuth atom was expected to result in a lower barrier to rotation at the coalescence point compared to the antimony and arsenic derivatives.

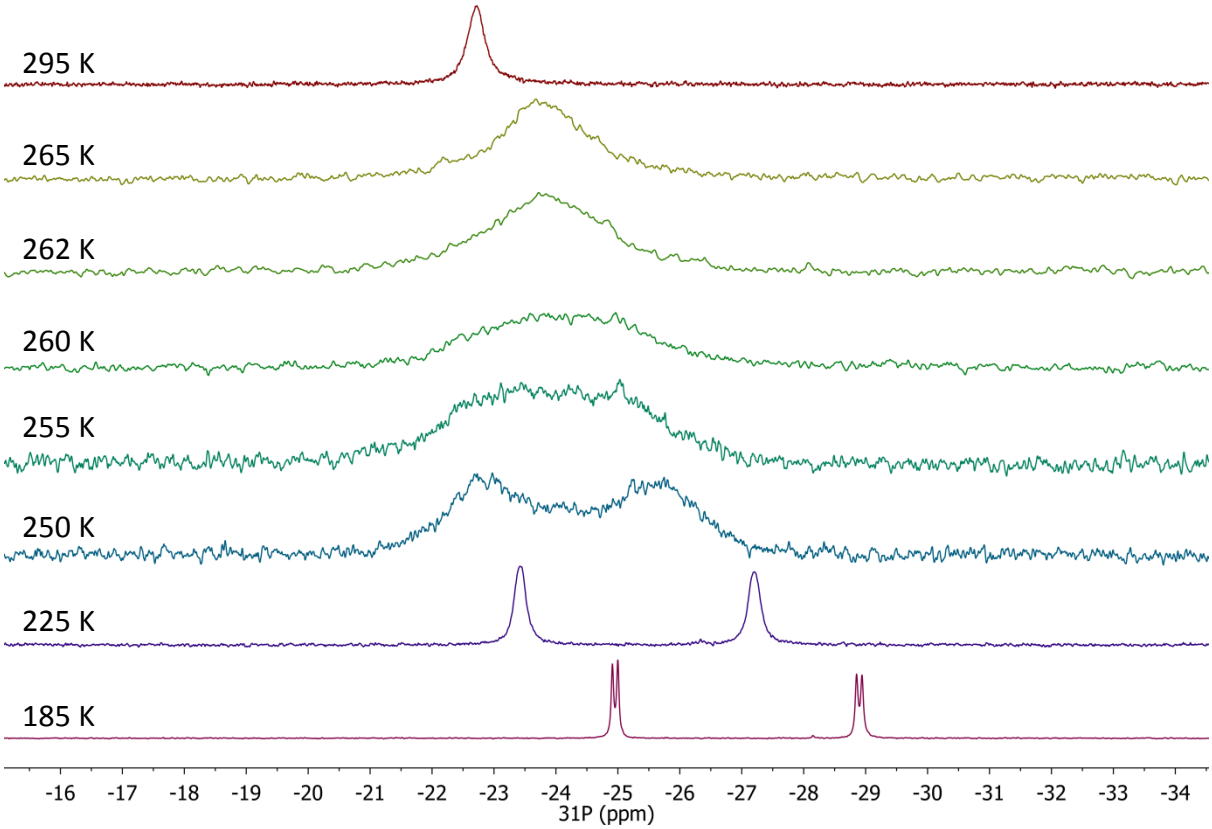

Figure 36: Variable temperature $^{31}P\{^{1}H\}$ NMR spectra of **C2**-**6** (CD_2Cl_2, 202 MHz).

The low temperature (slow motion regime) $^{31}P\{^{1}H\}$ NMR spectrum (185 K) of **C2-6** displays two sharp doublets ($^{8ts}J_{PP}$ 17.8 Hz) at δ_P −24.9 and −28.9 ppm (Figure 36, bottom) consistent with a simple AX spin system. The magnitude of $^{8ts}J_{PP}$ is remarkable as there is no direct overlap of the lone pairs on the phosphorus atoms. This coupling constant most likely consists of an entirely through-space component. The transfer of magnetisation is highly likely to involve two through-space interactions because of the overlap of the two phosphorus lone pairs with the diffuse bismuth lone pair (Figure 37).

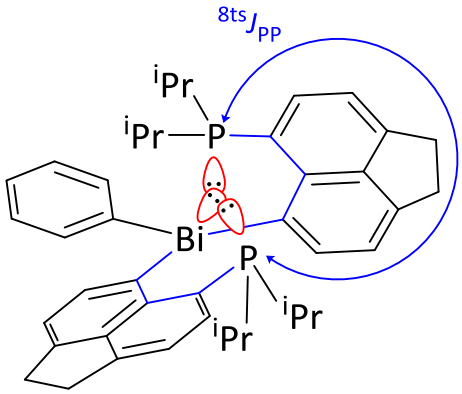

Figure 37: Graphical representation of the magnetisation transfer pathway in **C2-6** for long-range couplings ($^{8ts}J_{PP}$). Bonds (formally) involved in the transfer are coloured blue with lone pairs involved in the transfer (through space) coloured red.

2.7 – Towards *peri*-Substituted Bismuth(V) Compounds

So far the compounds prepared have contained only bismuth(III). As is characteristic of the pnictogens the other commonly seen oxidation state is bismuth(V). The final part of the work presented here involved trying to incorporate a bismuth(V) centre into our *peri*-substituted systems. At first we investigated the possibility of oxidising a Bi(III) centre already attached to the acenaphthene backbone. Triphenylbismuth dichloride $BiPh_3Cl_2$ is easily prepared by chlorinating triphenylbismuth using sulfuryl chloride and isolable in excellent yields.[101] As such we thought the same chlorination procedure could be used on our tri-aryl bismuthines (**C2-2**, **C2-5** and **C2-6**). Compound **C2-5** was selected first as it represented the least sterically demanding system and therefore be the most likely to react favourably. Scheme 17 shows the synthetic procedure followed. The obtained solid showed a number of signals within the $^{31}P\{^{1}H\}$ NMR spectrum. No clear assignments could be made regarding the nature of the products; additionally, the ^{1}H NMR spectrum was highly crowded. It's likely the phosphorus centre is reacting with the sulfuryl chloride giving rise

to undesired side products. Several attempts were made varying the reaction conditions to try and control the reactivity however none of these were successful. The difficulty experienced attempting to oxidise the Bi(III) centre can be explained by the inert pair effect. There is a large increase between the 3rd and 4th ionisation energies of bismuth. This is due to the increased effective nuclear charge experienced by the 6s electrons owing to inefficient shielding of the 4f electrons.[11]

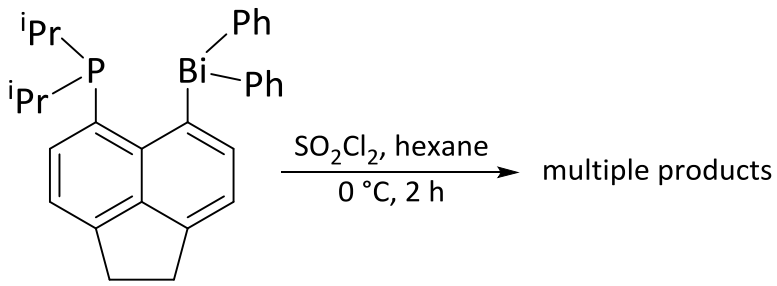

C2-5

Scheme 17: Synthetic route followed to chlorinate **C2-5**.

Since the oxidation of the bismuth centre after it has been attached to the acenaphthene backbone proved unsuccessful we chose to try and add the bismuth(V) moiety directly. This would be achieved by reacting one equivalent of Li-**C2-1** with $BiPh_3Cl_2$ at low temperature (Scheme 18). A beige precipitate formed which was collected by filtration and washed with ether. The expected product, $(^iPr)_2P$-Acenap-$BiPh_3Cl$, was not obtained, instead the phosphino-bismuthonium salt **C2-12** was isolated. The nature of the product was only established after single crystal X-ray analysis, coupled with ^1H NMR spectroscopy.

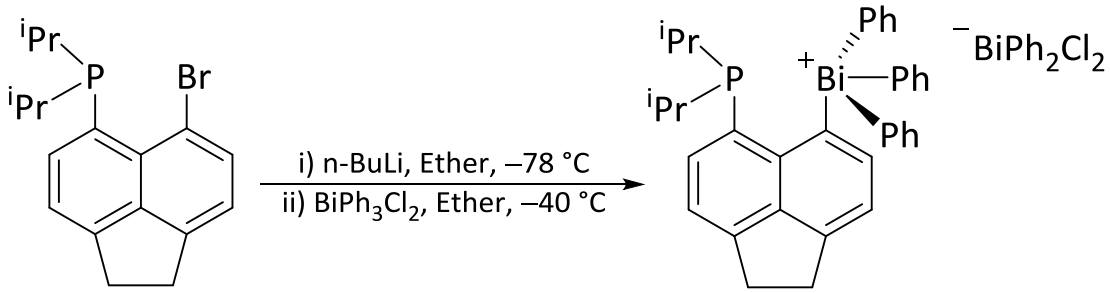

C2-1 **C2-12**

Scheme 18: Synthetic route to the phosphino-bismuthonium salt **C2-12**.

2.7.1 – Spectroscopic analysis of C2-12

The $^{31}P\{^{1}H\}$ NMR spectrum of **C2-12** is shown in Figure 38 (top) where we can see a very broad signal at δ_P −46.3 ppm. This is consistent with an increased shielding of the phosphorus centre *cf*. the bismuth(III) examples we have seen previously. The decreased Lewis acidity of the bismuth(V) versus the bismuth(III) centre may be reason for this. As such, no dative interaction between the phosphorus and bismuth atoms is expected. The chemical shift of this compound compares well to other pnictogen analogues such as the antimony derivative which has δ_P −42.3 ppm.[88]

The ^{1}H NMR spectrum of the product obtained after the reaction was initially confusing. Two doublets of doublets were observed corresponding to the methyl groups of the isopropyl groups (Figure 38, bottom), supporting potential restricted rotation around the P–C_{Ace} bond. However, examination of the integrals for the aromatic signals compared to the alkyl region suggested more aromatic environments were present. Following the determination of the crystal structure these extra aromatic environments were easily explained by the presence of the $[BiPh_2Cl_2]^-$ counterion. The aromatic region mostly consists of overlapping multiplets making full assignment impossible.

No through-space coupling between the *ipso*-carbon of the phenyl rings is observed in the $^{13}C\{^{1}H\}$ NMR spectrum. This could be due in part to the slightly broadened nature of the signals arising due to the slow interchange of the phenyl rings on the NMR timescale. Due to the formation of a bismuthonium cation the *ipso*-carbon signal appears at δ_C 183.9 ppm. The remaining signals corresponding to the proposed structure were all present and consistent with those seen in previous compounds. The NSI^+ mass spectrum provided further evidence of the formation of a bismuthonium cation with the $[M]^+$ peak observed at *m/z* 709.2426.

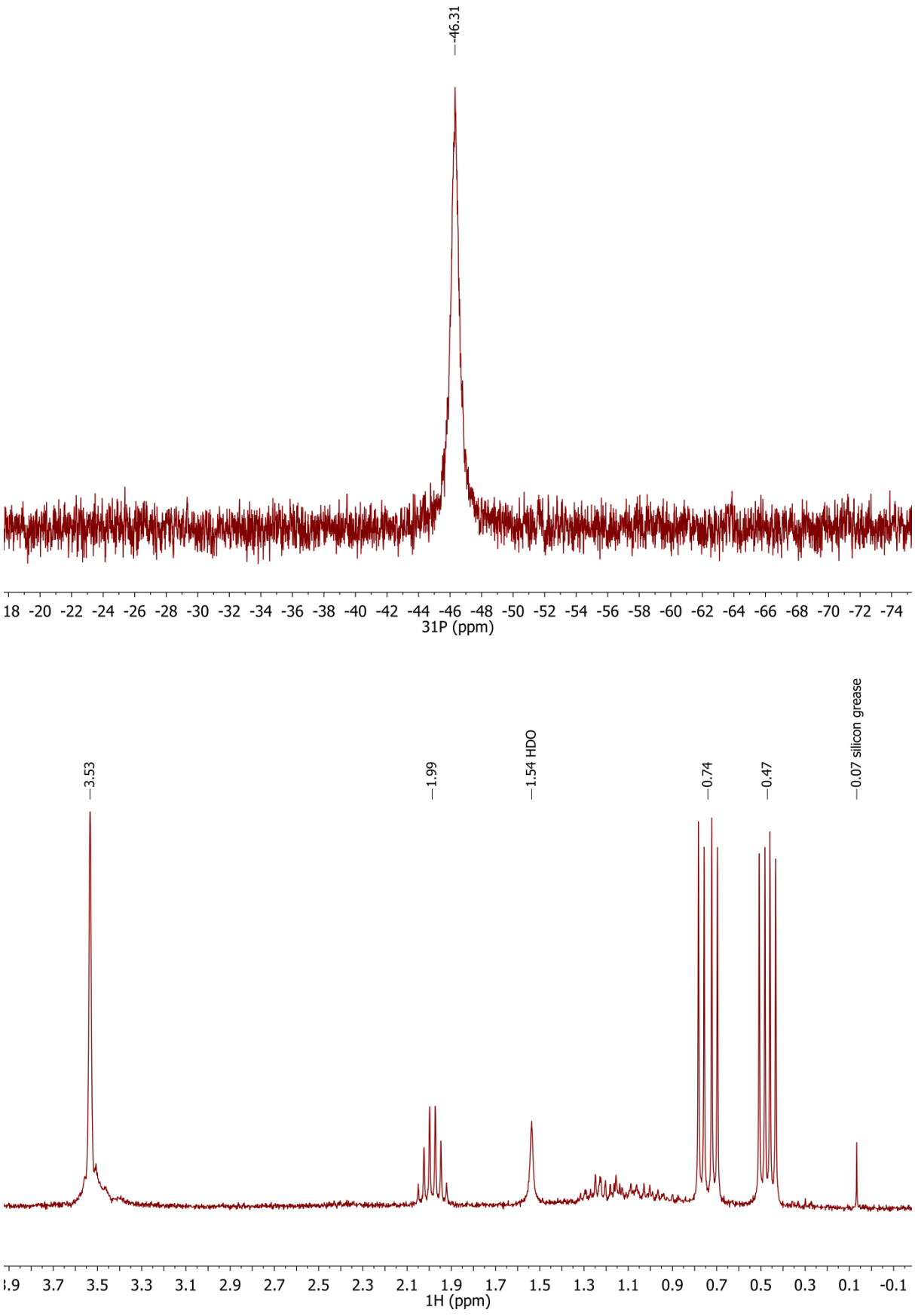

Figure 38: The $^{31}P\{^{1}H\}$ NMR spectrum ($CDCl_3$, 162 MHz) (top) and alkyl region of the ^{1}H NMR spectrum ($CDCl_3$, 400 MHz) (bottom) of **C2**-**12**.

2.7.2 – Crystallographic characterisation of C2-12

Crystals suitable for X-ray work were obtained *via* slow diffusion of ether into a concentrated solution of **C2-12** in DCM. Only one molecule crystallises within the asymmetric unit with a co-crystallised solvent molecule (C_6H_6). The identification of the counterion as $[BiPh_2Cl_2]^-$ proved to be crucial in explaining the spectroscopic data obtained. Two views of the crystal structure are shown in Figure 39 with selected structural parameters in Table 6.

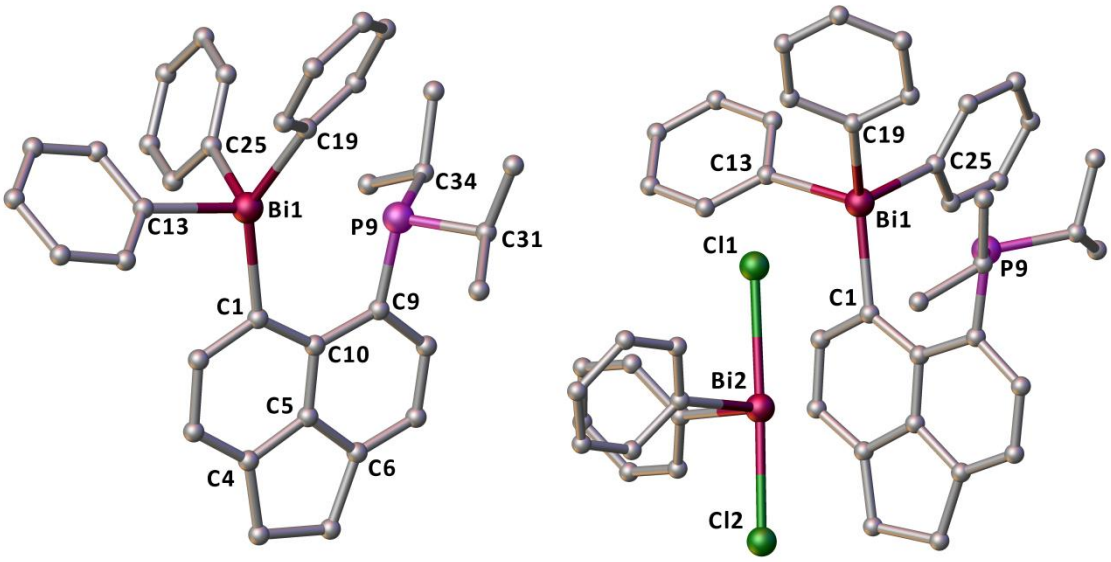

Figure 39: Two views of the crystal structure of **C2-12** with the $[BiPh_2Cl_2]^-$ counterion omitted (left) and included (right). Hydrogen atoms and the co-crystallised solvent molecule (C_6H_6) are omitted from both views for clarity.

The distance between the two *peri*-atoms is the longest seen thus far at 3.223(3) Å. This is due to both the decreased Lewis acidity of the bismuth centre making the formation of a dative bond unfavourable and the increased steric bulk around the bismuthonium cation. The Bi1–Cl1 distance, 3.256(2) Å, is also too large to be considered a covalent bond (average Bi–Cl bond length in $BiPh_3Cl_2$ is 2.570 Å).[111] The interaction mimics that of the Bi–P in so much as it should be considered weak. Both the P–C and Bi–C bond lengths observed are similar to those seen in the previous compounds. The phosphorus atom adopts the usual *pseudo*-tetrahedral geometry (the lone pair points towards the bismuth atom) with only small deviations from the ideal angle (109°) observed. The bismuth atom adopts a distorted tetrahedral geometry if we exclude interactions between the phosphorus and chlorine atoms. If we do take into account the sub van der Waals interactions between the bismuth and both the chlorine and phosphorus atoms, then we now have a distorted octahedral geometry around bismuth.

Table 6: Selected bond lengths [Å], angles [°], torsion angles [°] and displacements [Å] for **C2**-**12**.

P9···Bi1	3.223(3)	P9–C9	1.843(10)
Bi1–C1	2.242(10)	Bi1–C_{Ph}	2.223(9)–2.264(8)
Bi1–Cl1	3.256(2)	Bi2–Cl1	2.840(2)
Bi2–Cl2	2.670(3)		
C–P9–C	100.0(4)–104.3(5)	C–Bi1–C	98.1(3)–141.2(3)
C1–Bi1···P9	72.2(2)	C1–Bi1···Cl1	74.7(2)
C13–Bi1···P9	175.9(2)	C13–Bi1···Cl1	84.4(2)
C19–Bi1···P9	82.7(2)	C19–Bi1···Cl1	77.1(2)
C25–Bi1···P9	85.4(2)	C25–Bi1···Cl1	176.6(2)
P9···Bi1···Cl1	91.92(6)		
P9–C9···C1–Bi1	3.9(4)	Splay angle[a]	16.56(6)
C1–C10–C5–C6	177.6(9)	C9–C10–C5–C4	179.4(8)
Out of plane displacements			
P9	0.127	Bi1	0.022

[a] calculated as [(Bi1–C1–C10)+(C1–C10–C9)+(C10–C9–P9)–360].

2.8 – Conclusions

Utilising *peri*-substitution a series of compounds containing phosphorus and its heavier congener, bismuth, have been prepared. The reaction of Li-**C2**-**1** with ⅓ $BiCl_3$ afforded the expected tri-substituted product **C2**-**2** which was spectroscopically studied and examined in the solid state using single crystal X-ray diffraction. Using the bismuth starting materials $BiPh_2Cl$ and $BiPhCl_2$ and reacting them with Li-**C2**-**1** in a 1:1 and 2:1 ratio respectively afforded unsymmetrical tri-aryl bismuthines **C2**-**5** and **C2**-**6**. Due to impurities present within $BiPhCl_2$ **C2**-**6** was not isolated in a pure form using this method. Both of these were characterised in a similar fashion with **C2**-**6** showing fast interchange of the acenaphthene groups on the NMR timescale compared to the arsenic and antimony derivatives. Only a weak interaction between the phosphorus and bismuth atoms was observed in these compounds owing to the poor Lewis acidity of the bismuth moiety. Despite this several examples of long range through-space coupling was observed within the $^{13}C\{^1H\}$ NMR spectra of **C2**-**2** and **C2**-**5**.

By using **C2**-**5** as a starting point, the bismuthino-phosphonium salt **C2**-**7** was prepared, followed by the series of phosphine–bismuthine donor–acceptor complexes **C2**-**8**–**10**. This was achieved *via* fluorodearylation using boron trifluoride diethyl etherate to obtain **C2**-**7** then subsequent anion exchange with a sodium or potassium halide to form **C2**-**8**–**10**. The change in Lewis acidity of the bismuth centre was seen within the $^{31}P\{^1H\}$ NMR spectra of the **C2**-**8**–**10** series, with the signal shifting upfield as you go from chlorine to bromine to iodine. Within the donor–acceptor series the

bismuth adopts a *pseudo*-trigonal bipyramidal geometry owing to the formation of the dative bond between the two *peri*-atoms. A surprising crystal structure was also obtained of the diiodo species **C2**-**11** which was shown to form a centrosymmetric dimer within the solid state *via* bridging iodine atoms. For several of the compounds the single crystal X-ray diffraction data was collected and solved by myself. The reactivity of **C2**-**8** was also investigated with a second synthetic route to **C2**-**6** devised using **C2**-**8** as the starting material. The new synthetic route resulted in analytically pure material following purification.

Investigations into preparing bismuth(V) *peri*-substituted systems proved to be challenging owing to the inert pair effect, with only one compound obtained. The phosphino-bismuthonium salt **C2**-**12** was spectroscopically characterised and examined using single crystal X-ray diffraction. The bismuth centre adopted a distorted tetrahedral geometry with two possible long range interactions; one to the phosphorus centre and the other to a chlorine atom within the counterion.

Part 2 – Aromatic Dithiolate Ligands in the Formation of Rhodium and Iridium Complexes: A Synthetic, Spectroscopic and Structural Investigation

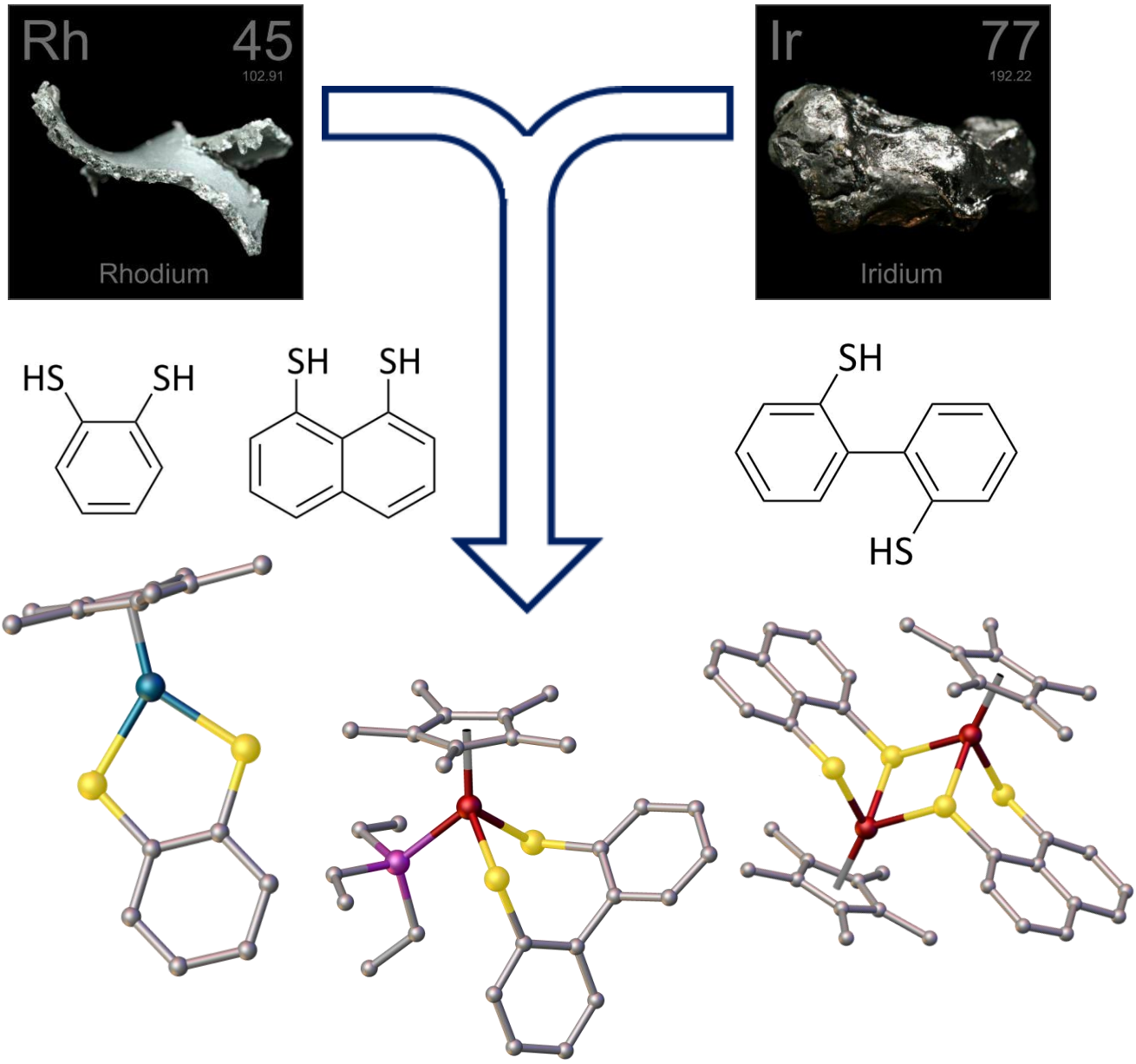

Chapter 3 – General Introduction

3.1 – A Brief History of Sulfur

The history of sulfur is part of antiquity with prehistoric humans using it as a pigment for cave painting and one of the first recorded instances of medication being the use of sulfur as a tonic. The first practical and industrial use of sulfur is credited to the Egyptians who used sulfur dioxide for bleaching cotton as early as 1600 BC. The use of sulfur in manufacture of explosives dates back to China around 500 BC. For centuries, sulfur, along with mercury and salt was believed to be a component of all metals and formed the basis of alchemy. Antoine Lavoisier proposed that sulfur was an element in 1777, however, in 1808 Humphry Davy disputed this saying it contained hydrogen. Unfortunately for Davy his sample was impure and when Louis Josef Gay-Lussac and Louis Jacques proved it to be an element the following year, Davy eventually agreed.

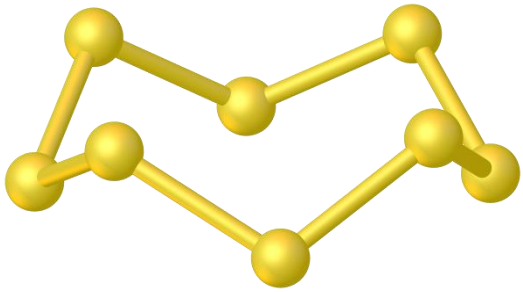

Figure 40: Crystal structure of α-sulfur (S_8).

Pure sulfur is a tasteless, brittle solid that is pale yellow in colour, a poor conductor of electricity and insoluble in water. Sulfur occurs naturally as the element, often in high concentrations around volcanic areas. It is also found in many minerals including iron pyrites, galena, gypsum and Epsom salts. There are several allotropes of sulfur; the most common at standard temperature and pressure is α-sulfur (S_8) which is a yellow solid consisting of S_8 puckered rings (Figure 40). Elemental sulfur was once commercially recovered from wells by the Frasch process. This involved forcing super-heated steam (160−170 °C) into the underground deposits causing the sulfur to melt allowing it to be pumped to the surface as a liquid. These days modern sulfur production is almost entirely from the various purification processes used to remove sulfur form natural gas, oil and tar sands.

Sulfur has a wide range of applications and is used in the vulcanisation of rubber, as a fungicide and in gunpowder manufacture. The greatest use of sulfur is in the production of sulfuric acid, arguably

one of the most important chemicals manufactured in the world. One reason for this is that one of sulfuric acids many uses is in the production of phosphoric acid to make phosphate fertilisers.[113,114]

3.2 – Sulfur in Nature

Sulfur is a minor constituent of a number of proteins and is an essential element for life with typical human consumption ≈100 mg per day.[115] Sulfur has been found in the hooves of pigs and oxen, in the feathers of birds, in sheep's wool and in the hair of rabbits, calves, horses and man. Overall, ≈1% of a humans body weight comprises sulfur and it is the eighth most abundant element in the body after hydrogen, carbon, oxygen, nitrogen, calcium, phosphorus and potassium.[116,117] Plant life also contains an array of sulfur compounds with sulfur present in appreciable amounts amongst residues following combustion. Over 90% of the sulfur obtained exists in the chemical form of the sulfur containing amino acids methionine and cysteine. Cysteine is an important feature of many living things and is essential for the maintenance of protein systems both in a structural and catalytic sense. Fibrous proteins, such as keratins, which are major components of biological tissues such as hair, horns, hooves, wool and nails, owe their hardness to the high cysteine content present (human hair is 14% cysteine). The ability of cysteine to dimerise through the formation of a disulfide bond makes this amino acid unique, in so much that it allows cross-bridging to occur when built into a primary sequence of a linear polypeptide. Oxidised sulfur in the form of sulfate esters of organic compounds occur within animals as steroid sulfates, phenol sulfates and polysaccharide sulfates. Within higher animals these sulfated polysaccharides are used to provide a matrix for cellular structures such as cartilage and skin.[118]

There are a number of bioactive substances containing sulfur which itself acts as the essential active component. Generally, these molecules act as catalytic assistants allowing reactions to occur more favourably by the production, stabilisation and transfer of reactive intermediates and as conduits for the flow of electrons in redox situations. Several of the most important ones are discussed below; Figure 41 shows some of the structures of these molecules.

Coenzyme A acts as a carrier of activated acyl groups which can be transferred to or from amides, esters and anhydrides.[119] It is biochemically constructed by a series of soluble enzymes within numerous organisms from pantothenic acid, L-cysteine and adenosine triphosphate in the presence of magnesium ions. A wide range of enzymes utilise the coenzyme A protein including hydrolases, isomerases, lyases, lygases, oxidoreductases and transferases.[120] It is essential in the metabolism of

fatty acids and carbohydrates due to its role as an acyl group activator. Coenzyme A esters also have a number of other important functions such as the formation of acetylcholine, acyl carnitines and triglycerides.[121] Lipoic acid has a well-defined function as a coenzyme used in fatty acid and carbohydrate metabolism occurring in the highly organised multi-enzyme complexes pyruvate dehydrogenase and α-ketoglutarate dehydrogenase.[118] It is present in a wide range of living organisms and is tightly bound to a protein. The biological activity of this molecule depends upon the high reactivity of the disulfide bond present within the five membered ring. This five membered dithiolane ring is extremely strained as the sulfur lone pairs try to move away from one another.

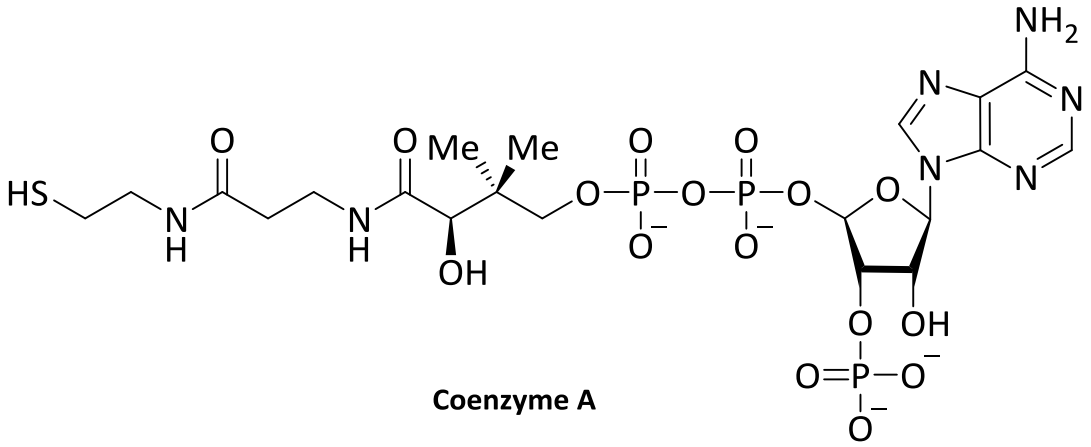

Coenzyme A

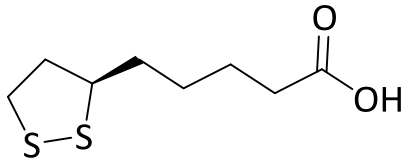

Lipoic Acid

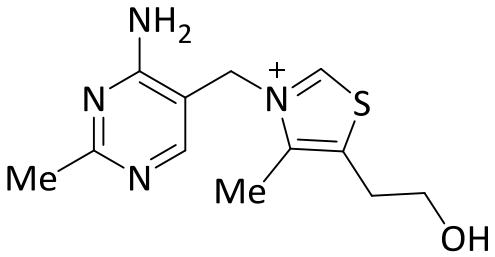

Thiamine (Vitamin B_1)

Figure 41: Bioactive molecules containing sulfur.

Thiamine, also known as Vitamin B_1, occurs in mammals as a mixture of the free form (Figure 41), monophosphate, diphosphate (major form) and triphosphate derivatives.[122] It is active in non-redox enzyme reactions that involve proton transfer, usually aided by acid-base catalysis. It is a coenzyme for reactions such as aldol condensations and both oxidative and nonoxidative decarboxylations, all of which involve the making or breaking of carbon–carbon bonds. Sulfur compounds can be metabolised by microorganisms in a variety of ways which involve either oxidation, reduction, or both. The ability to move electrons is therefore required for these reactions to occur; this need is

met by electron transfer proteins. Examples of electron carrier proteins are the cytochromes, sirohemes and nonheme iron–sulfur proteins such as rubredoxins and ferredoxins.[123]

3.3 – Types of Sulfur Donor Ligands

Sulfur donor ligands are classed as soft and bind particularly well to Class B metals such as those found in the second and third row of the d-block. They are very versatile being able to form mononuclear, polynuclear and cluster compounds.[124] There are numerous types of ligands ranging from the simple sulfide anion (S^{2-}) to thiolates, dithiolates, dithiolenes and dithiocarbamates (Figure 42).

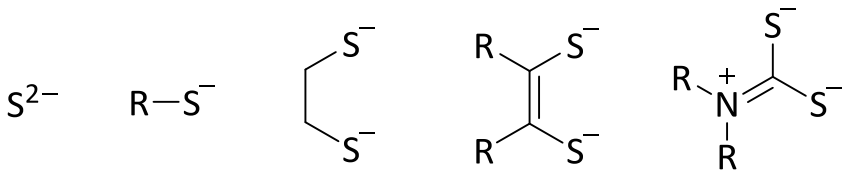

Figure 42: Examples of sulfur donor ligands.

3.3.1 – Complexes containing the sulfide ligand

The situation for the simplest sulfur complexes incorporating the sulfide anion is rare due to their lack of stability. For this reason, metallosulfanes [$L_nM–S–ML_n$] and metal sulfides [$L_nM=S$] are found almost exclusively with d^{10} and d^0 metals,[125] two such examples are shown in Figure 43 (left, centre).[126,127] One example where the d-shell is neither filled nor empty is the cobalt complex shown in Figure 43 (right).[128] The tungsten complex shown and the numerous thiometalates of the d^0 species occupy a special position insofar as their lack of d-electrons mean they behave more like main group elements.[125]

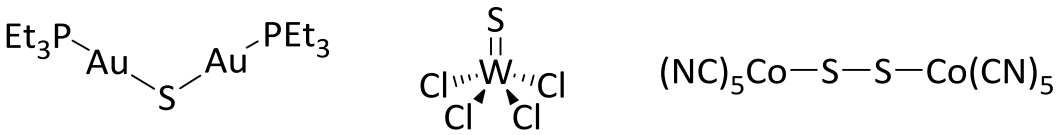

Figure 43: Simple transition metal sulfur complexes.

In these metallosulfanes and metal sulfides, the sulfur behaves as either a one or two electron donor. This results in the lone pairs being unused, and therefore reactive, and is the most likely cause for the lack of stability observed in these types of complexes. Isolable complexes are obtained

by using good π-acceptor ligands around the metal and by raising the coordination number of both the sulfur and metal.

A more common situation is for the sulfide anion to act as bridging ligand between either two or three metal centres as a two or four electron donor respectively. In the dinuclear examples the bridging sulfur atom spans a metal–metal bond to form an M_2S triangle (Figure 44). More common is the M_2S_2 fragment where two sulfur atoms bridge two metal atoms (Figure 44); examples with and without metal–metal bonds are known. Included in this class of compound is the longest known metal–sulfur complex, the red Roussain salt $K_2[Fe_2S_2(NO)_4]$.[129] The structure of its anion was postulated by Seel[130] in 1942 and later confirmed by structural analysis of the red Roussain ethyl ester.[131] The added stability of the M_2S_2 unit allows the appearance of metallosulfane and metal sulfide type bonds which, as mentioned before, are otherwise unseen for d^n-metals ($n \neq 0, 10$).[132]

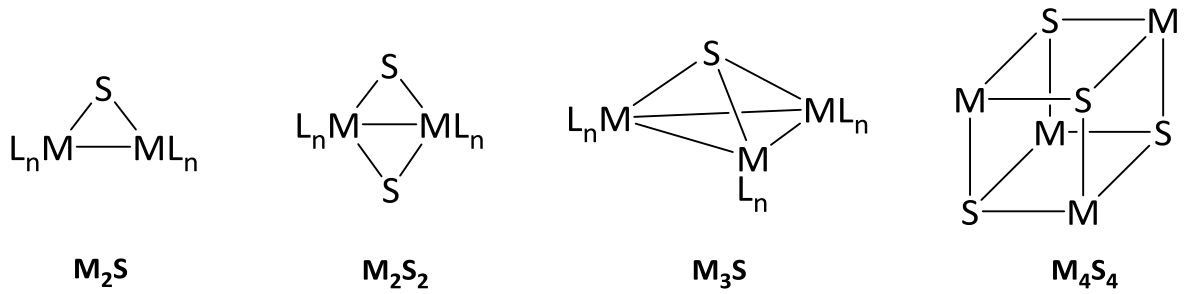

Figure 44: Structural arrangements of sulfide ligands bridging two or three metal centres.

The bonding situation where the sulfur atom bridges three metal centres results in some of the most stable transition metal sulfide complexes. Since the sulfur atom has used one of its lone pairs and forms three covalent bonds, the reactivity of the sulfur is reduced. In addition, the M_3S structural unit (Figure 44) represents a close approximation to the structure of sulfidic solids. The M_3S atomic arrangement has a favourable geometry with the three metals and the remaining lone pair forming an approximate tetrahedral coordination around the sulfur atom. This type of bonding is so favourable that it allows an enormous variation in the nature and electron configuration of the metals. When the sulfur is counted as a four-electron donor then for the majority of cases the 18-electron rule is observed. Deviations from this are possible due to the highly favourable nature of the M_3S and M_3S_2 (the latter bridged on both sides) structural arrangements. Another type of arrangement where the sulfur joins three metal centres is in the M_4S_4 cubane skeleton (Figure 44). This structure permits the optimal M_3S bonding for the sulfur whilst satisfying the metal's need for

bonding to several sulfur atoms. Interactions between the metals within the structure are also possible.

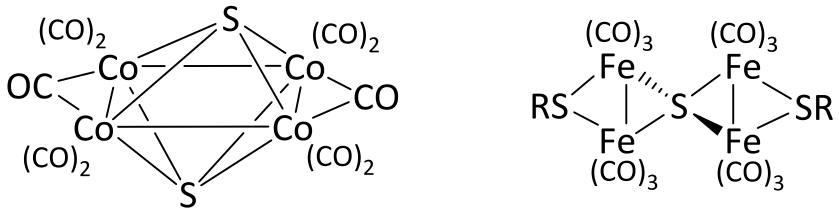

Figure 45: Sulfide ligands bridging four metal centres.

Examples were the sulfide ligand bridges four metal centres are less frequent. One example where the sulfur atom sits above the plane of the four metals is the cobalt complex $[Co_4S_2(CO)_{10}]$ (Figure 45).[133-135] In most of the other complexes of this type the sulfur atom lies in a tetrahedral hole between four metal centres. The sulfur atom no longer has any lone pairs since all of its valence electrons are required for the four metal–sulfur bonds. One such example of this arrangement is the iron complex shown in Figure 45.[136]

3.4 – Dithiolato Ligands in Complexation Chemistry

The coordination of *S*,*S* bidentate ligands remains an important area of chemistry. Complexes bearing this type of ligand have a number of industrial applications including catalysts in vulcanisation[137,138] and lubricant additives.[139] These complexes also show a range of electrochemical properties.[140,141] In addition *S*,*S* donors can support unusual magnetic properties[142,143] and are important in biological systems.[115]

The complexation chemistry of dithiolate ligands has been extensively studied with examples incorporating most of the transition metals known. The thiolate anion can exhibit a number of different binding modes in so much as the full negative charge can form a covalent bond to a metal, then the two lone pairs can also form dative bonds to other metal centres as neutral donors. This has already been observed in section 3.3.1 when discussing the use of sulfide as a ligand. When it comes to the binding modes of ligands in coordination chemistry there are a several types of nomenclature used to describe each situation.

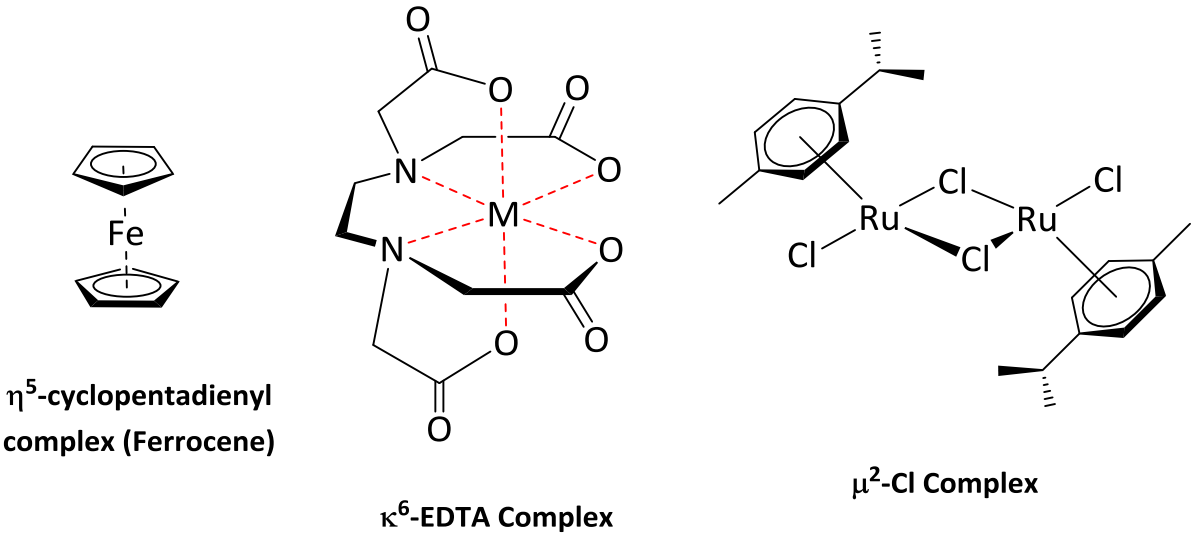

η^5-cyclopentadienyl complex (Ferrocene)

κ^6-EDTA Complex

μ^2-Cl Complex

Figure 46: Examples of hapticity (left), denticity (centre) and a bridging ligand (right).

Hapticity is the term used to describe a ligand which is bound to a metal centre through a serious of contiguous atoms. The Greek letter eta (η) is used followed by a superscript number which denotes the number of atoms involved in bonding. For example, the ligand cyclopentadienyl can coordinate through five carbon atoms so would be described as η^5-cyclopentadienyl. Ferrocene is the most famous example incorporating this ligand (Figure 46).[144] Denticity differs from hapticity, in this case polydentate ligands coordinating *via* multiple sites which are not contiguous would be described using the kappa notation (κ). The superscripted number which follows the kappa letter denotes the number of atoms involved in bonding to the metal within the complex. EDTA is a common ligand (Figure 46) used to sequester metal ions with both industrial and medical applications.[145,146] It is a hexadentate ligand bonding through six atoms so would be described as κ^6. The final situation needed to describe our sulfur donor atoms is when the ligand is bridging two or more atoms, usually metals. In this case the Greek letter mu (μ) is used with a superscript number denoting the number of metals bound to the bridging ligand. Most of the time μ^2 is simply denoted as μ. If the complex contains some ligands that are bridging and some that are not then the latter are described as terminal ligands. The bridging chloride ligands in the ruthenium complex (Cymene)ruthenium dichloride dimer would be described as μ^2 bridging ligands (Figure 46).[147]

3.4.1 – Alkyl dithiolato transition metal complexes

Alkyl dithiolate containing complexes have been known for well over 50 years.[148] A large amount of the early work was performed on structurally simple ligands such as ethane-1,2-dithiolate or propane-1,3-dithiolate. A wide range of metals have been used in the study of these ligands with a variety of binding motifs observed.[148-156] As with most new areas of interest in chemistry, the early

work on the use of alkyl dithiolate ligands in transition metal complexes was focused on the scope and structural characterisation of these new systems. During the mid-1980s Holm and co-workers investigated complexes of ethane-1,2-dithiolate (edt) with the first row transition metals. Their work, coupled with that of others, produced approximately 19 structural determinations of edt complexes and revealed the following stereochemical pattern: $[M(edt)_2]^{2-}$, planar (M = Cr(II), Co(III)), tetrahedral (M = Mn(II), Co(II), Zn(II), Cd(II)); $[VX(edt)_2]^{2-}$, pyramidal (X = O, S); $[Ti(edt)_3]^{2-}$, trigonal octahedral; $[M_2(edt)_4]^{2-}$, tetrabridged six-coordinate nonoctahedral (M = V(III)), double bridged planar (M = Mn(III), Fe(III)); $[Ni_2(edt)_3]^{2-}$, doubly bridged planar; $[Cu_3(edt)_3]^{3-}$, nonplanar Cu_3S_3 ring (selected examples in Figure 47).[154] Further study on the stability of these systems, their electron transfer capabilities and the preparation of bridged polynuclear species was then carried out.[157]

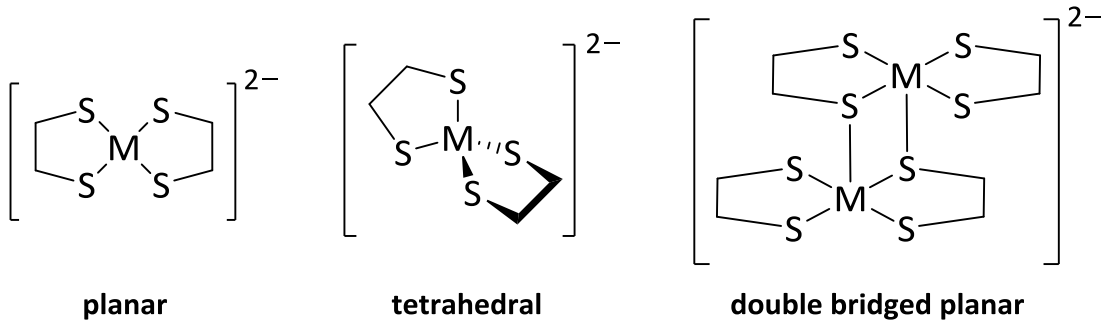

Figure 47: Structural variation in edt transition metal complexes.

The edt ligand has also found use in catalytically active transition metal complexes. Rhodium complexes containing this ligand have been investigated as catalyst precursors in the hydroformylation of hex-1-ene. A study of varying alkyl chain lengths was conducted from ethyl to n-butyl and in all cases catalytic hydroformylation was achieved.[158] Another interesting use of the edt ligand was in the formation of both monomeric and dimeric rhenium complexes of the type $[ReOCH_3(edt)PPh_3]$ and $[ReOCH_3(edt)]_2$ respectively.[159]

3.4.2 – Aromatic dithiolato transition metal complexes

Both aromatic and polyaromatic dithiolate ligands represent an interesting area of chemistry with a diverse structural and chemical range of complexes formed. These complexes have been studied for their electronic properties,[160] intramolecular interactions[161] and the formation of stable $16e^-$ species.[162] The most avid area of research for these ligands in recent years has been their use in creating hydrogenase catalytic site models.[163] By far the most widely studied ligand of this type is benzene-1,2-dithiolate ($BenzS_2$); this ligand also falls under the label of a dithiolene and has seen extensive research as such. Other ligands that are of particular interest to the work presented here

are naphthalene-1,8-dithiolate ($NapS_2$), acenaphthene-5,6-dithiolate ($AcenapS_2$), [1,1'-biphenyl]-2,2'-dithiolate ($BiphenS_2$) and [2,2'-binaphthalene]-1,1-dithiolate (2,2'-$BinapS_2$) (ligand precursors shown in Figure 48).

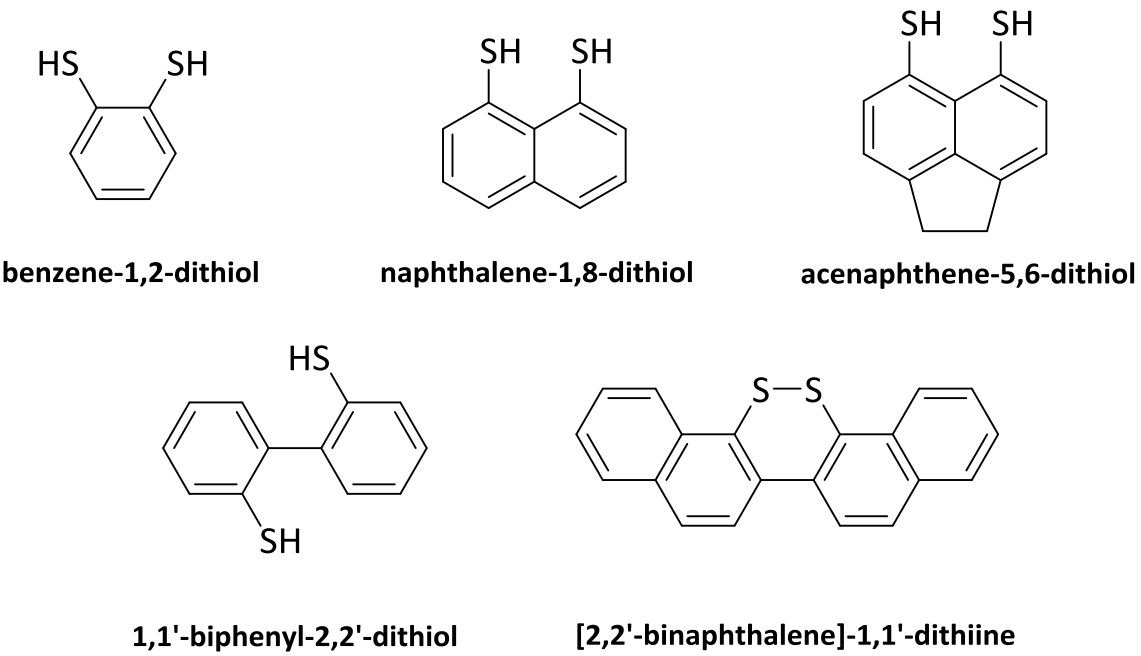

benzene-1,2-dithiol **naphthalene-1,8-dithiol** **acenaphthene-5,6-dithiol**

1,1'-biphenyl-2,2'-dithiol **[2,2'-binaphthalene]-1,1'-dithiine**

Figure 48: Aromatic and polyaromatic ligand precursors of interest to this research.

One qualitative way of examining the difference in the amount of research done using these ligands is through the use of the SciFinder® web portal.[89] Using the sub-structure search function and limiting the results to those containing any metal atom attached to the sulfurs provided results which were not surprising. For the $BenzS_2$ ligand 949 compounds were found, $NapS_2$ provided 103 results and $BiphenS_2$ resulted in 45 hits (this required filtering compounds containing the binaphthalene motif and other related structures). The $AcenapS_2$ ligand yielded only 17 results and of the seven references related to these compounds, only one came from out with research conducted by the Woollins group.[164] Finally, the 2,2'-$BinapS_2$ ligand produced only two hits, both of which were complexes the Woollins group had published.[165,166] Given the vast difference between the aromatic and polyaromatic examples the rest of this section will deal mainly with the polyaromatic ligands in the literature. The $BenzS_2$ ligand will be covered only in relation to the growing field of [FeFe] hydrogenase mimics.

3.4.2.1 – Aromatic dithiolate ligands in hydrogenase mimics

There is a growing interest in the development of catalysts for the production of hydrogen for use as an energy source. Platinum catalysts are ideally suited to this task from a chemical standpoint

however due to the high cost of platinum the idea of using this for a future “hydrogen economy” remains unappealing. In nature three types of hydrogenase enzymes, [Fe], [FeFe] and [NiFe] catalyse the formation and oxidation of hydrogen.[167-170] Of these, the [FeFe] hydrogenases are the most efficient catalysts generating hydrogen with high turnover frequencies of 6000–9000 s^{-1} at low overpotentials.[171-174] Crystallographic investigations of the active site within the enzyme have revealed two iron centres bridged by a dithiolate ligand in addition to CO and CN^- ligands and a cysteine linked [4Fe4S] cluster.[168,175-177] In an attempt to model the enzyme active site and design efficient and stable catalysts, a large number of complexes containing bridging dithiolate ligands and a combination of CO and σ-donating ligands have been reported (Figure 49).[163]

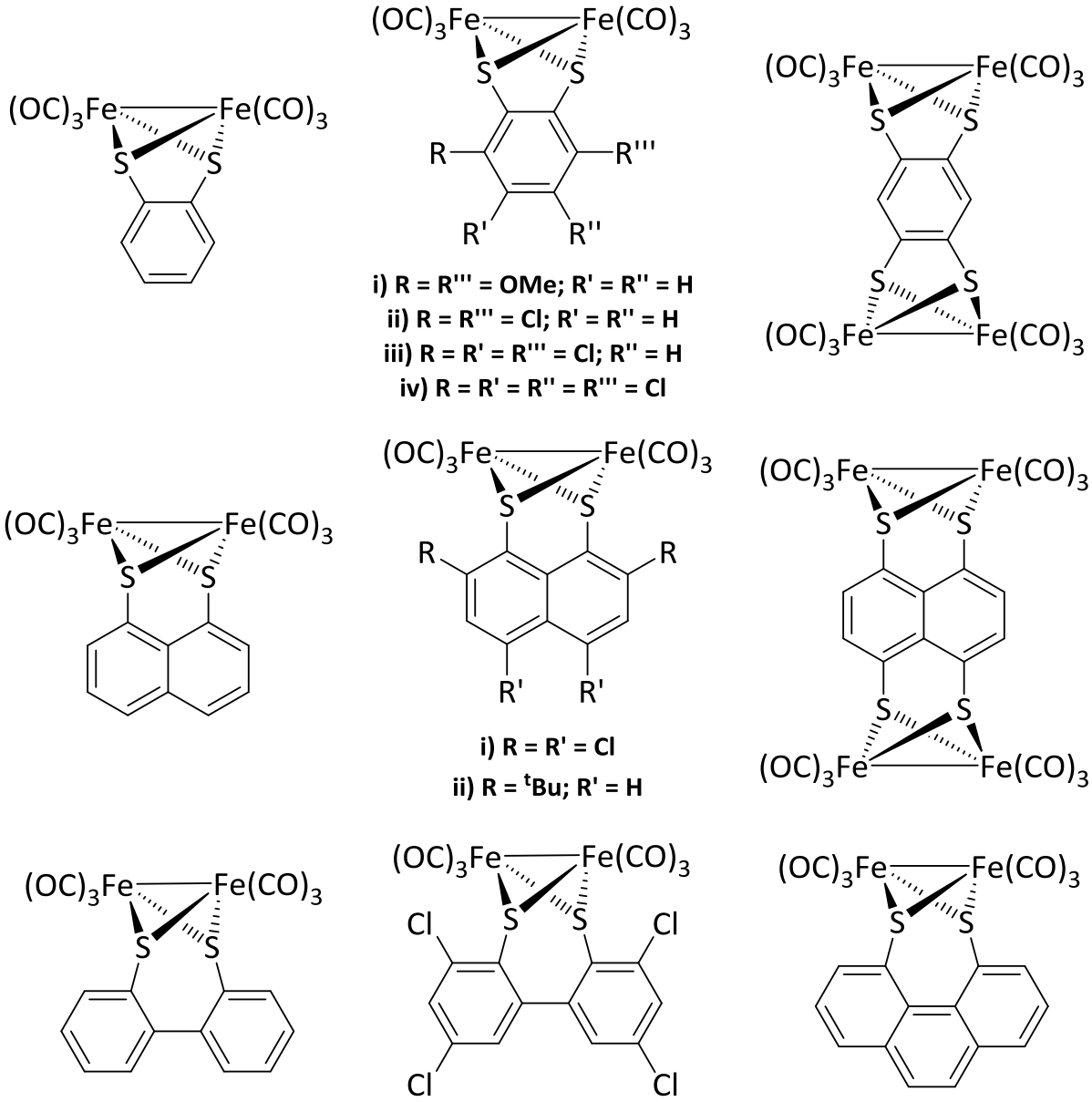

Figure 49: Selected examples of [FeFe] hydrogenase mimics containing aromatic dithiolate ligands.

Making use of these dithiolate ligands results in more stable reduction products and isolable hydride intermediates when compared to aliphatic analogues. Despite not exactly mimicking the enzyme active site, these complexes are still of great interest. These complexes have shown the ability to reduce protons both electrochemically and photochemically. To date these systems still have large problems to overcome as catalytically they are of low efficiency and require large overpotentials. In addition, the poor stability of the diiron based catalysts remains a major limitation to practical applications. Despite their limitations these systems have shown reversible reduction processes. The ability to tune the ligands by the addition of electron withdrawing groups, resulting in dramatic changes in the reduction potentials and electron transfer processes, makes them an attractive prospect in the future.[178,179]

3.4.2.2 – Naphthalene dithiolate based transition metal complexes

The coordination chemistry of naphthalene dithiolate and its derivatives has been largely overlooked out with the Woollins group research and that of the iron hydrogenase mimics discussed in section 3.4.2.1. Some of the first examples of complexes using the naphthalene dithiolate ligand, and the structurally similar compounds tetrathionaphthalene (TTN), tetrachlorotetrathionaphthalene (TCTTN) and tetrathiotetracene (TTT) (Figure 50), were published by Teo and co-workers in the late 1970s and early 1980s. They investigated the complexation chemistry of these ligands to a variety of low-valent metal substrates.

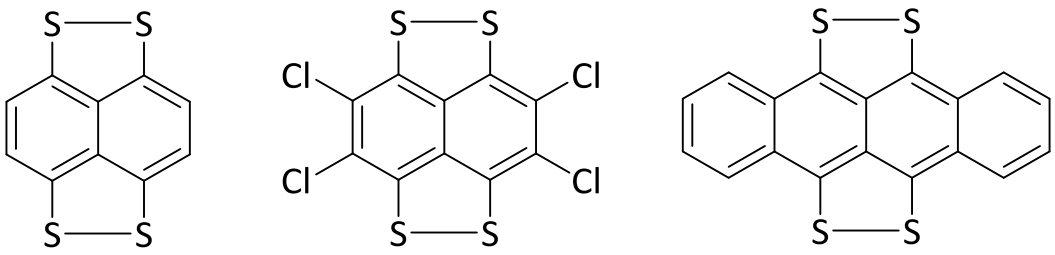

Figure 50: Structures of TTN, TCTTN and TTT.

All of these ligands have been successfully coordinated to platinum through an oxidative addition reaction with $[Pt(PPh_3)_4]$.[180,181] In all cases this resulted in a dimeric complex with a bridging tetrathiolene ligand (example reaction shown in Scheme 19); the single crystal X-ray structures for these complexes were determined.[182]

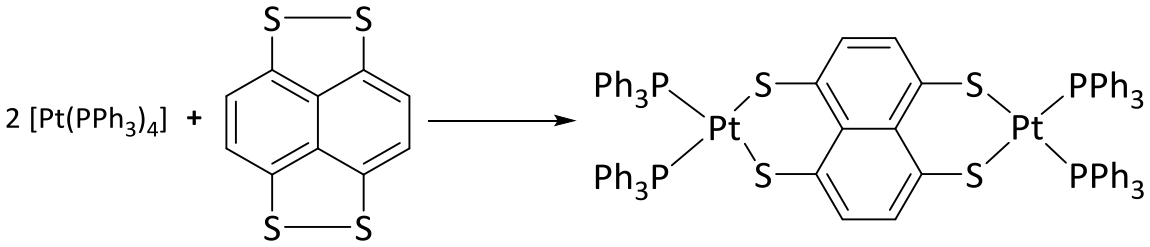

Scheme 19: Oxidative addition of TTN to $[Pt(PPh_3)_4]$.

Iridium is another metal whose coordination chemistry to these ligands has been extensively studied. Attempts at creating a similar dimeric complex to that seen above were conducted by reacting two equivalents of *trans*-$[Ir(PPh_3)_2(CO)Br]$ with TTN.[183] The complex isolated did not contain a bridging tetrathiolene moiety; instead one of the dithiolato groups was bound to both iridium atoms, which also contained an iridium–iridium bond (Figure 51, left). The analogous complex containing the TCTTN ligand was further reacted, firstly, with two equivalents of $[IrH(CO)(PPh_3)_3]$, then secondly with $[Pt(PPh_3)_4]$ to form a tetrameric iridium complex (Figure 51, centre) and a hetero tri-metallic species (Figure 51, right) respectively.[184]

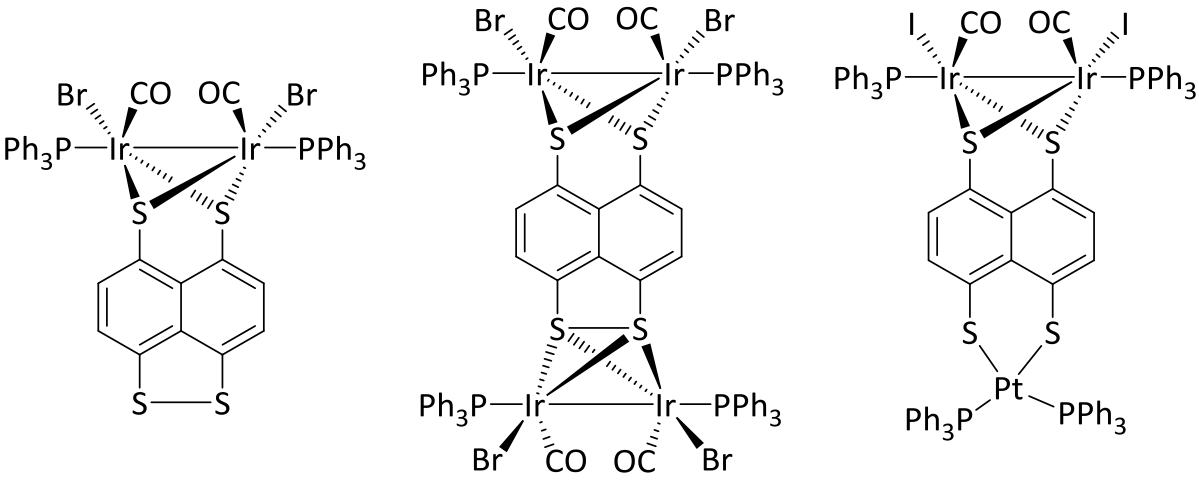

Figure 51: Dimeric and tetrameric iridium complexes and a tri-metallic hetero (Ir & Pt) species.

A monomeric iridium complex was synthesised by reacting TCTTN with one equivalent of $[IrCl(CO)(PPh_3)_3]$ in the presence of a small amount of PPh_3 to prevent dimerisation (Scheme 20).[184] The single crystal X-ray structure of this complex was reported three years later.[185]

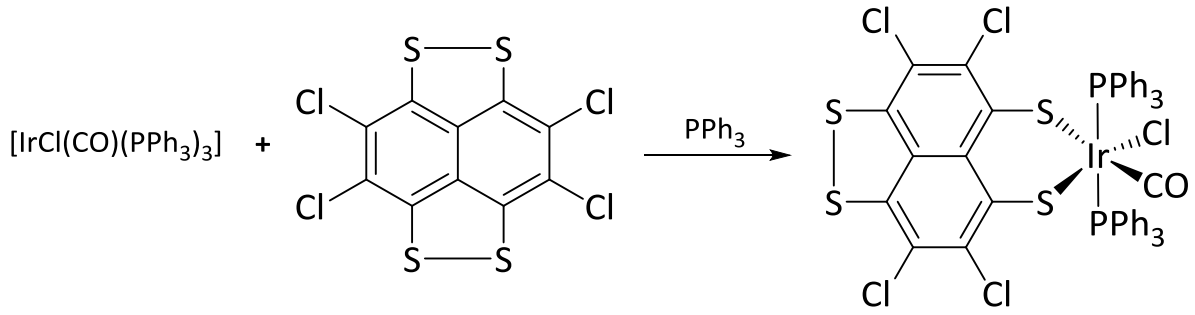

Scheme 20: Synthesis of a monomeric iridium complex by oxidative addition of TCTTN.

The coordination of TTN to nickel, cobalt and iron carbonyls has been examined, resulting in a pair of inorganic semiconductors (nickel and cobalt) and a homo tetra-metallic iron complex which greatly resembles the iron hydrogenase mimics discussed earlier. The nickel and cobalt complexes were found to be a linear polymeric structures of general formula ….Ni TTN Ni TTN…. and ….$Co_2(CO)_2$ TTN $Co_2(CO)_2$ TTN….[186]

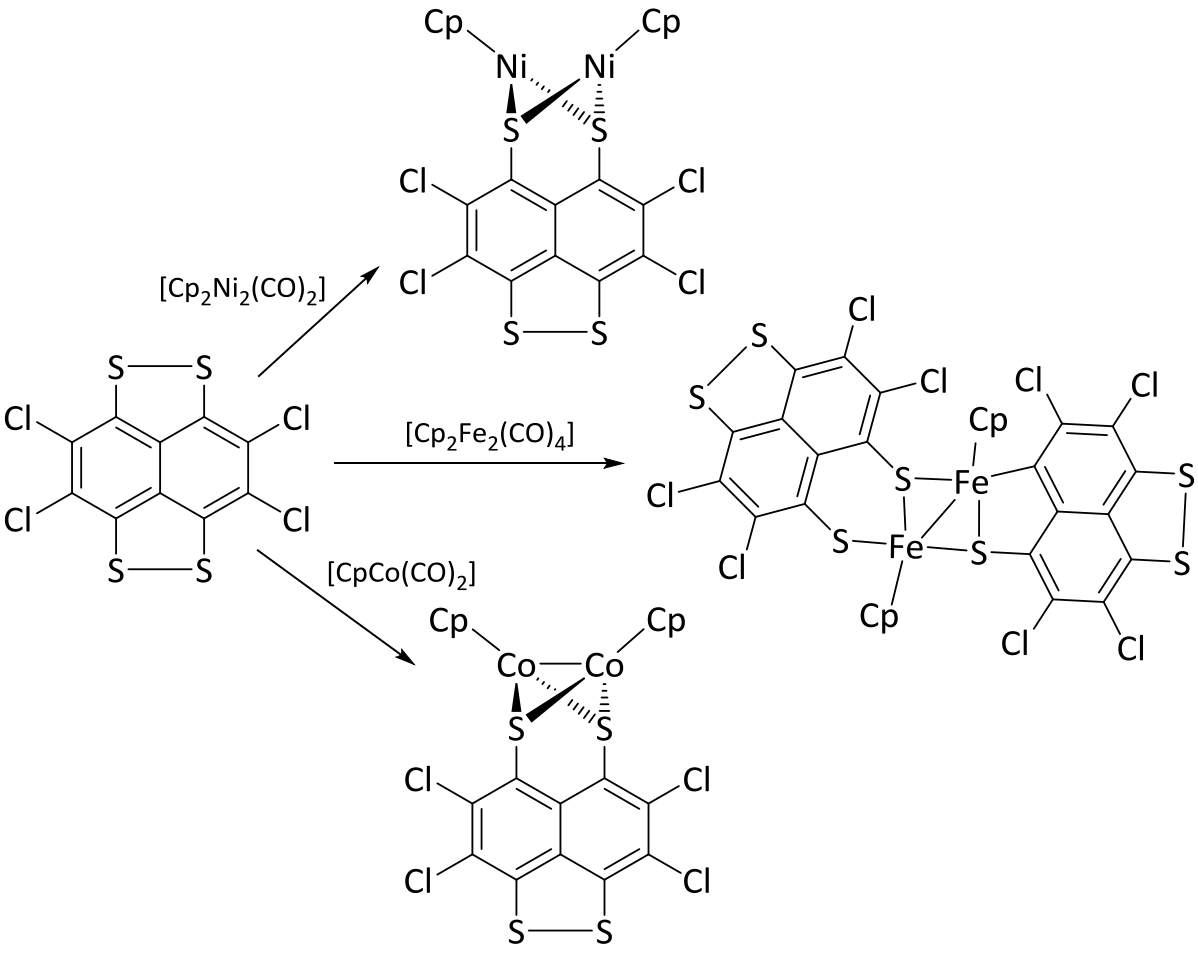

Scheme 21: Ferrocene, cobaltocene and nickelocene complexes with TCTTN.

One of the last investigations by Teo on these ligand types was a series of metallocene complexes. TCTTN was reacted with two equivalents of $[Cp_2Fe_2(CO)_4]$, $[CpCo(CO)_2]$ and $[Cp_2Ni_2(CO)_2]$ respectively as shown in Scheme 21.[187] The reaction with the ferrocene species gave an interesting dimeric complex where one of the TCTTN ligands has undergone a desulfurisaton reaction. This leaves one of the ligands bound to the Fe centre by a carbon atom with an iron–iron single bond also present. The nickel and cobalt derivatives behaved more conventionally with a metal–metal bond present in the cobalt complex but not the nickel one.

The related ligand hexachlorodithionaphthalene (HCDTN) which contains only one dithiolate binding site has been studied with a variety of metals. Treatment of HCDTN with $[Pd(PPh_3)_3]$ or $[Pt(PPh_3)_4]$ (Figure 52, left) results in mononulcear square planar complexes *via* an oxidative addition reaction.[188] Oxidative addition also occurs upon treatment of HCDTN with $[RhCl(PPh_3)_3]$ forming a complex containing a Rh(III) centre (Figure 52, centre). In contrast to this the reaction of HCDTN with $[Ni(cod)_2]$ in the presence of triphenylphosphine results in an unusual homometallic trinuclear nickel(II) complex (Figure 52, right).[189]

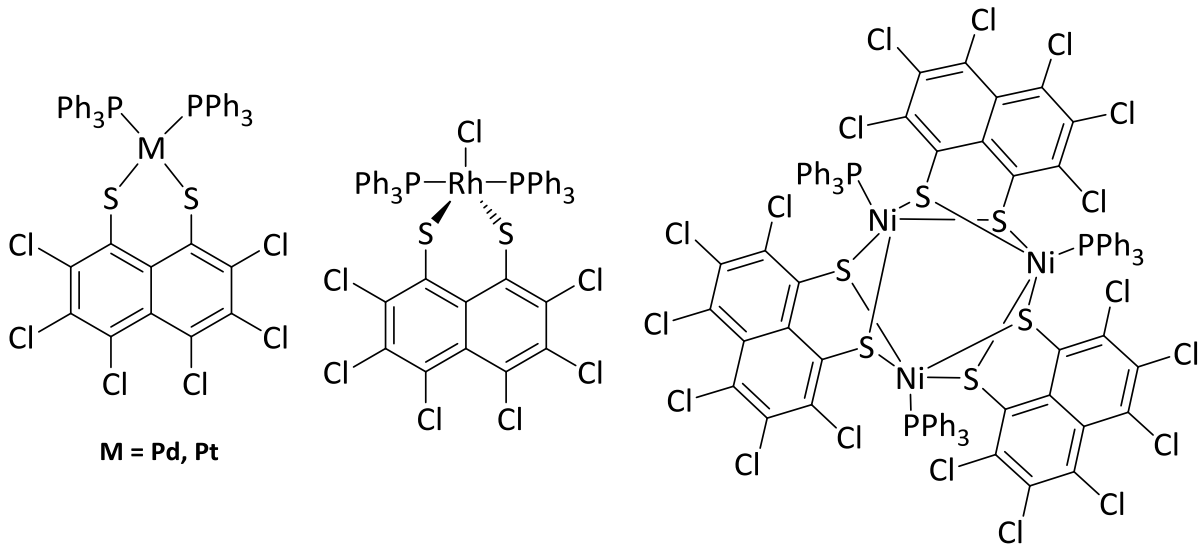

Figure 52: Oxidative addition products of HCDTN with Pd & Pt (left), Rh (centre) and Ni (right).

The Woollins group have previously published a comprehensive series of mononuclear platinum(II) complexes with a range of naphthalene dithiolates and their related oxides. The oxidative addition reactions were carried out by treating the respective dithioles with zero-valent platinum species such as $[Pt(PPh_3)_4]$ and $[Pt(C_2H_2)(PMe_3)_2]$ (Scheme 22).[190] Both the triphenylphosphine and trimethylphosphine derivatives of the parent naphthalene dithiole were also prepared by metathesis reactions. The dithiole was reduced *in situ* using lithium triethylborohydride then reacted with the appropriate platinum(II) dichloride ($[PtCl_2(PMe_3)_2]$ or $[PtCl_2(PPh_3)_2]$).[190]

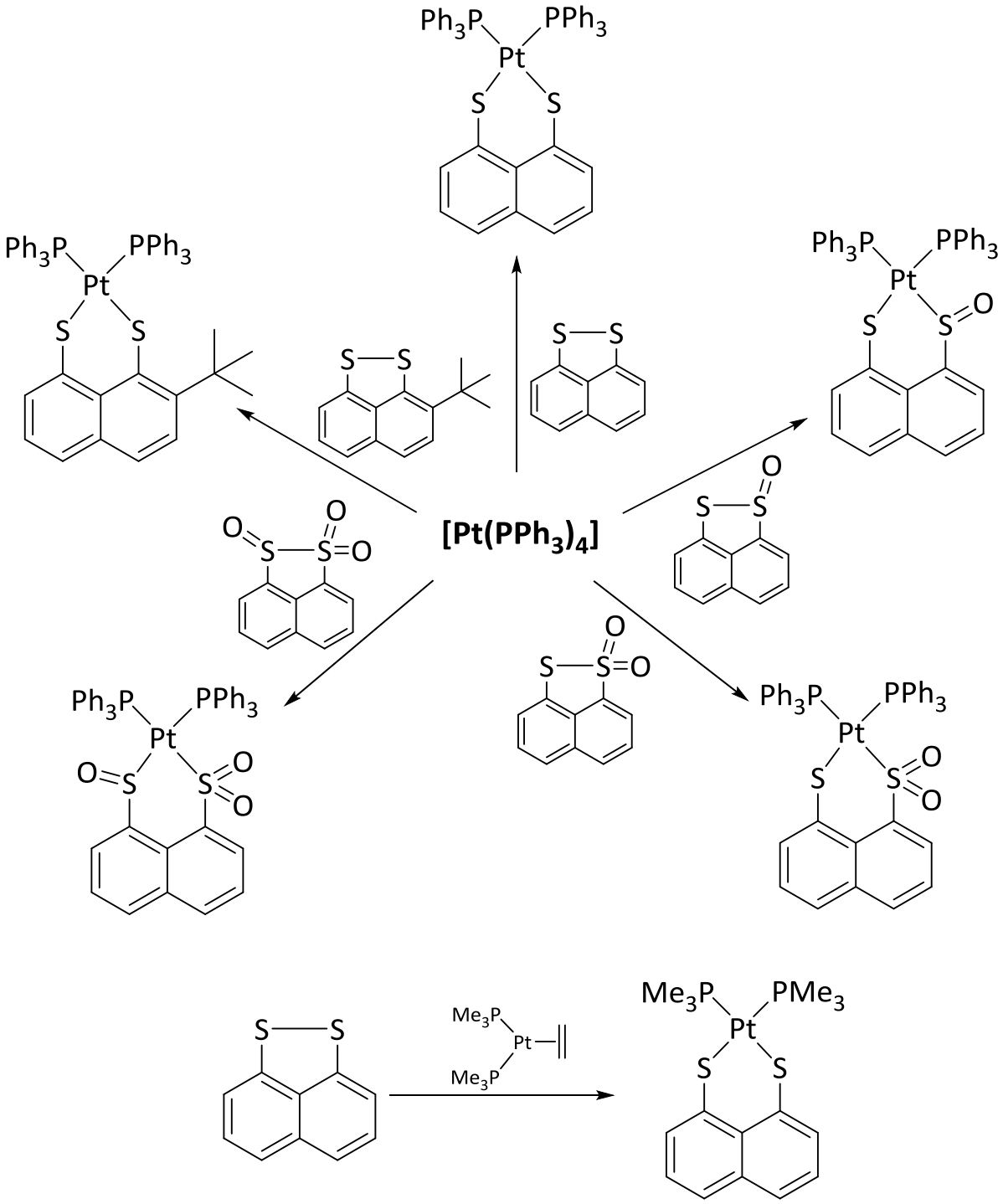

Scheme 22: Synthesis of platinum complexes bearing naphthalene dichalcogenolates and their oxides by oxidative addition reactions.

The Woollins group also published a series of dinuclear iridium(II) complexes using similar ligands to those shown above (Figure 53).[191] Again, oxidative addition reactions were used utilising [{Ir(μ-Cl)(cod)}$_2$] as the iridium source. All the products contained an iridium–iridium bond and provided suitable precursors to building more complex architectures.

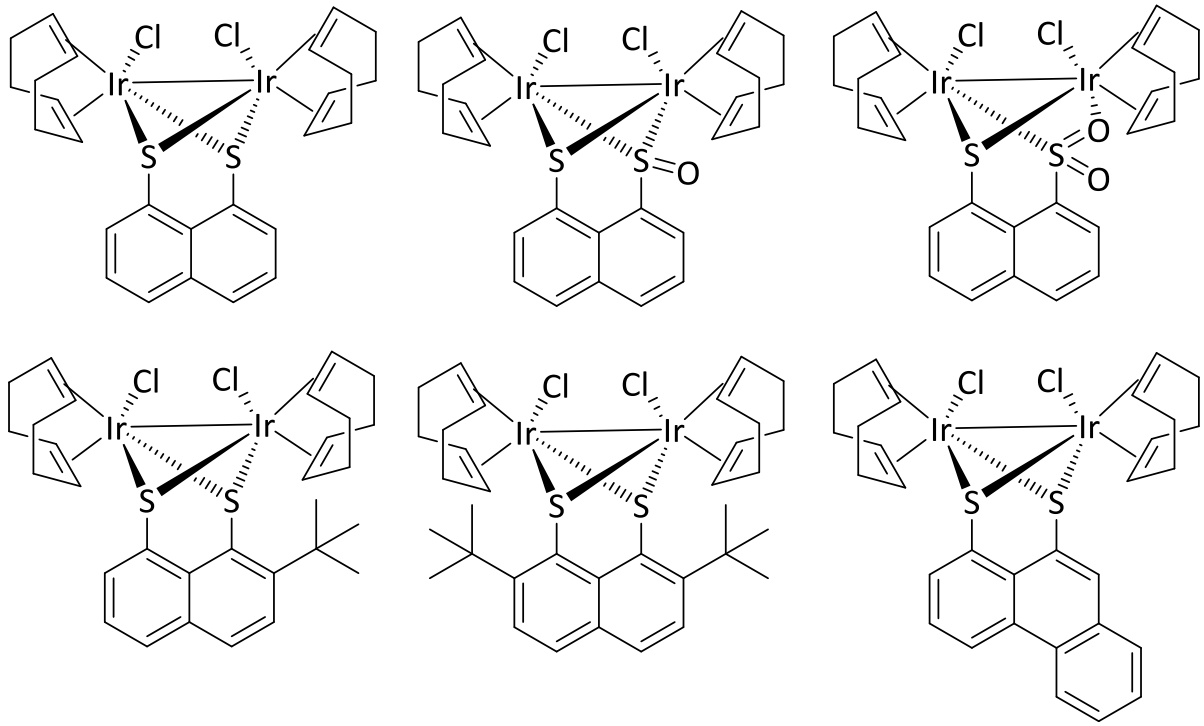

Figure 53: Dinuclear iridium(II) complexes using a variety of naphthalene motifs.

Vahrenkamp has reported a series of oligomeric, dimeric and monomeric zinc complexes using the sterically crowded ditertbutyl naphthalene dithiole and the electron poor naphthoic anhydride dithiole. The products were presumed to be polymeric in structure and subsequent reaction with amine donors resulted in a dimeric complex when pyridine was used and a monomeric structure when 2,9-dimethylphenanthroline was used.[124]

Complexes formed between sulfur ligands and titanocene are often used as sulfur transfer reagents due to the stability of the titanocene unit towards nucleophiles.[192] A number of titanocene based complexes using naphthalene based sulfur ligands have been published. The dinculear TCTTN titanocene complex was synthesised by Fanghaenel and co-workers in 1995. More recently, the Woollins group have reacted a series of related naphthalene dithioles and their oxides with the titanocene precursor $[Cp_2Ti(CO)_2]$.[165] An interesting observation was an oxygen elimination reaction, which only affected the S=O fragments but not the $S(=O)_2$ groups. Thus, the same product was observed when using the parent dithiole or dithiole monoxide and the dithiole dioxide or dithiole trioxide (Scheme 23). The Woollins group further extended the series of metallocene complexes by *in situ* reduction of the naphthalene dithiole with lithium triethylborohydride and reacting it with a series of precursors $[Cp^*_2MCl_2]$ (where M = Ti, Zr, Hf).[193] A detailed review covering both the preparation of these ligand systems and their coordination chemistry was published by Kilian, Knight and Woollins in 2011.[46]

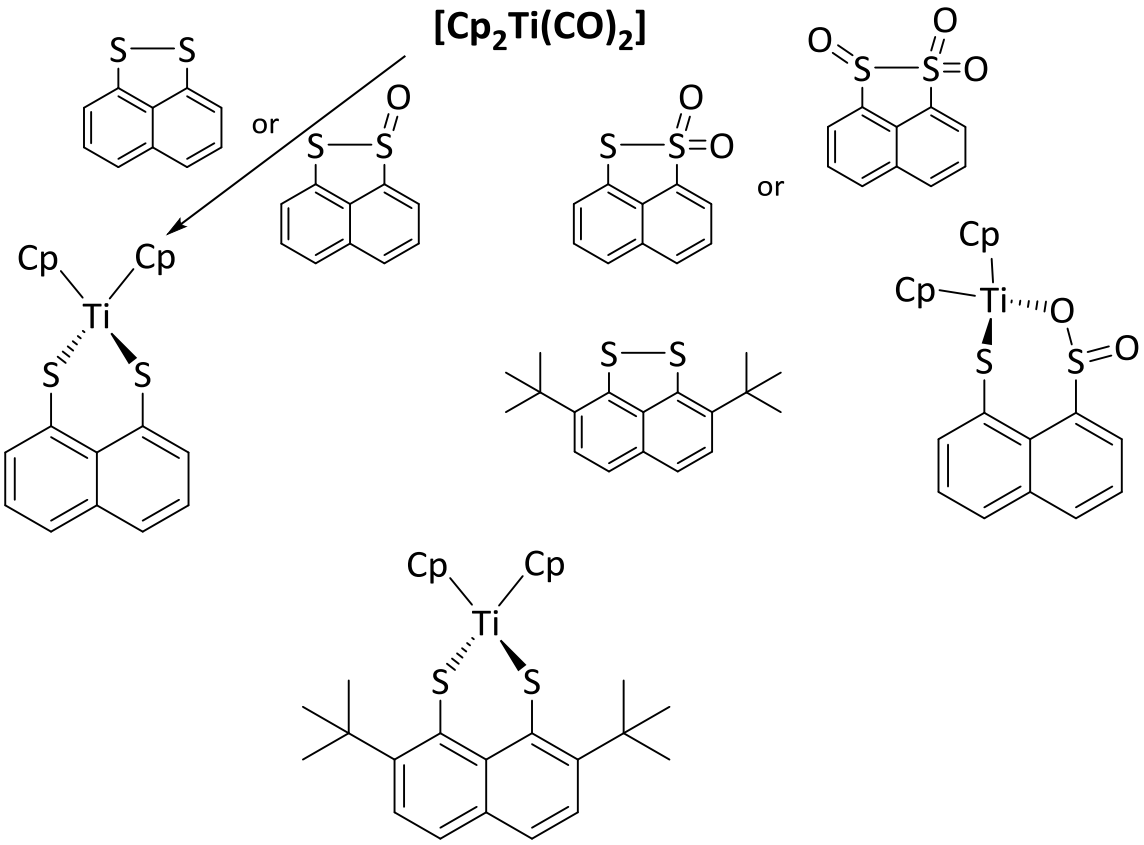

Scheme 23: Synthesis of titanocene complexes with a variety of naphthalene based sulfur ligands.

3.4.2.3 – Biphenyl dithiolate based transition metal complexes

As mentioned previously, the coordination chemistry of biphenyl dithiolate has seen very little investigation outside of the iron hydrogenase mimics. A crystal structure of $[(AuPPh_3)_2BiphenS_2]$ was published by Larkin and co-workers in 2004.[194] The Woollins group have investigated the oxidative addition of biphenyl dithiine and its related oxides to $[Cp_2Ti(CO)_2]$.[165] As with the naphthalene examples, the oxygen elimination reaction only affects the S=O fragments. The reaction of the same ligand set was also studied with the zero-valent platinum starting material $[Pt(PPh_3)_4]$ (Scheme 24).[166] These oxidative addition reactions resulted in a series of complexes which were structurally characterised by single crystal X-ray diffraction.

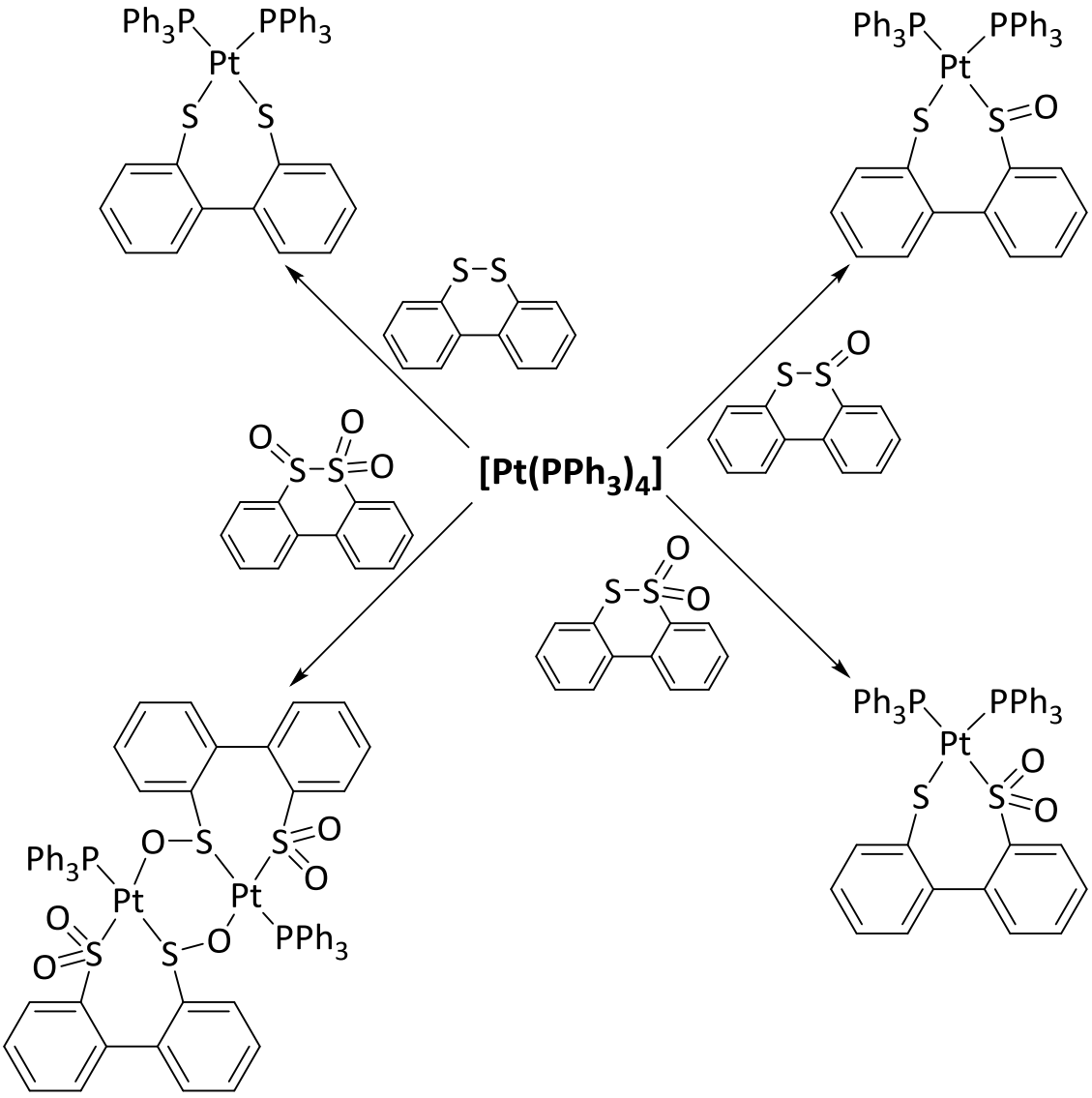

Scheme 24: Platinum complexes with a variety of biphenyl based sulfur ligands.

A derivatised version of the biphenyl dithiine backbone has been used as a tetravalent ligand bound to copper.[195] A molybdenum complex containing two biphenyl dithiolate ligands in a distorted square planar like geometry with a molybdenum–oxygen triple bond is also reported.[196] Some mono- and di-nuclear nickel complexes are also known.[197] Rauchfuss and co-workers have reported the synthesis of a titanocene complex by ring opening of dibenzothiophene with lithium followed by the addition of sulfur and titanocene dichloride. The final product was obtained from a salt elimination reaction.[198]

3.4.2.4 – Acenaphthene dithiolate based transition metal complexes

All but one of the complexes published using the acenaphthene based ligand come from the Woollins research group. Rather unsurprisingly, the other example relates to an [FeFe] hydrogenase

mimic reported by Topf and co-workers in 2012.[164] They used the acenaphthene backbone to create a ligand with functional prerequisites for visible light absorption, photoinduced electron transfer and catalytic proton reduction. This was done by the addition of a 1,2-diimine based π-acceptor site being added to the ethylene bridge on the parent acenaphthene dithiole. The reaction of this ligand with $[Fe_3(CO)_{12}]$ led to a complex (Figure 54, left) which was active in redox chemistry.

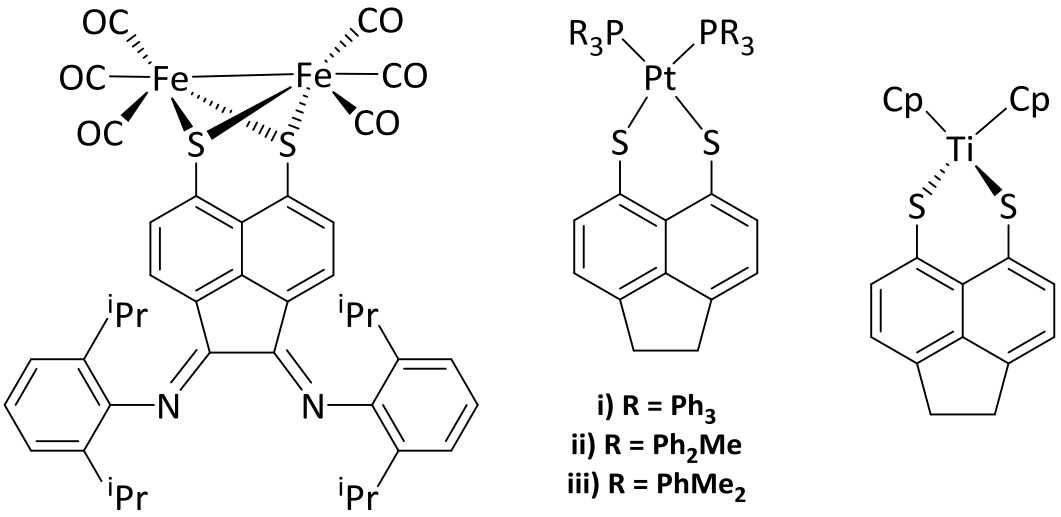

Figure 54: Complexes formed using the acenaphthene dithiolate ligand.

The Woollins group have studied the coordination of the acenaphthene dithiole to platinum resulting in complexes of the type $[Pt(PR_3)_2(AcenapS_2)]$ (Figure 54, centre). Two strategies were employed, the first of which involved the oxidative addition of the parent dithiole to the zero-valent platinum species $[Pt(PPh_3)_4]$ mentioned previously.[190] The second involved the reduction of the dithiole *in situ* using lithium triethylborohydride and reaction with a platinum(II) species ($[PtCl_2(PR_3)_2]$).[199] The related ligand backbone acenaphthylene was studied in a similar manner in 2015.[200] A titanocene complex has also been reported through an oxidative addition process with $[Cp_2Ti(CO)_2]$ (Figure 54, right).[165]

3.4.2.5 – Binaphthalene dithiolate based transition metal complexes

In section 3.4.2 we saw that only two complexes using the 2,2'-binaphthalene dithiolate backbone had been prepared. The structurally related and more common ligand, 1,1'-binaphthalene dithiolate has seen slightly more investigation with regards to its complexation chemistry. During the 1990s, Claver and co-workers published a series of papers on the use of rhodium [1,1'-binaphthalene]-2,2'-dithiolate ($BinapS_2$) based complexes in asymmetric hydroformylation.[201-203] Ruiz and co-workers also used a similar system in the formation of palladium complexes which actively catalysed the alkoxycarbonylation of styrene.[204] An [FeFe] hydrogenase mimic using the $BinapS_2$ ligand was also

recently reported by Wang.[205] The two complexes reported by the Woollins group using the 2,2'-BinapS_2 ligand (Figure 55) involved reaction with a platinum and titanium metal precursor.[165,166]

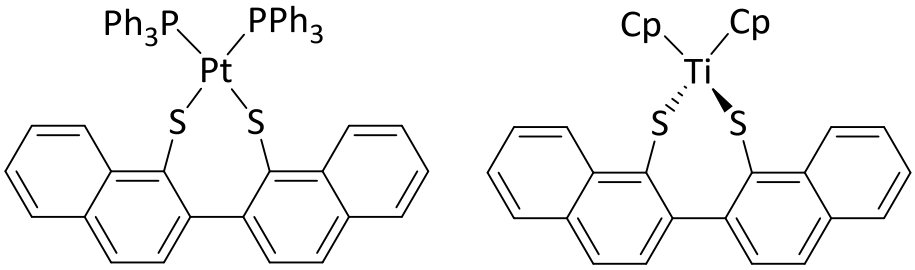

Figure 55: Platinum and Titanium complexes involving the [2,2'-BinapS_2] ligand.

Chapter 4 – Structural Diversity in Bimetallic Rhodium and Iridium Dithiolato Complexes

4.1 – Introduction to Bimetallic Dithiolato Complexes

Bimetallic transition metal complexes are of particular interest due to their potential catalytic activity. The presence of a second metal in close proximity to the first can be used to modify the reactivity and electronic properties of the overall system thus tailoring it for specific catalytic applications.[46] Complexes of this type have also been shown to exhibit interesting electrochemical properties and be active in redox chemistry.[206] Several examples of bimetallic complexes using dithiolato bridging ligands have been shown in sections 3.4.4.1 and 3.4.4.2 (Figure 56).

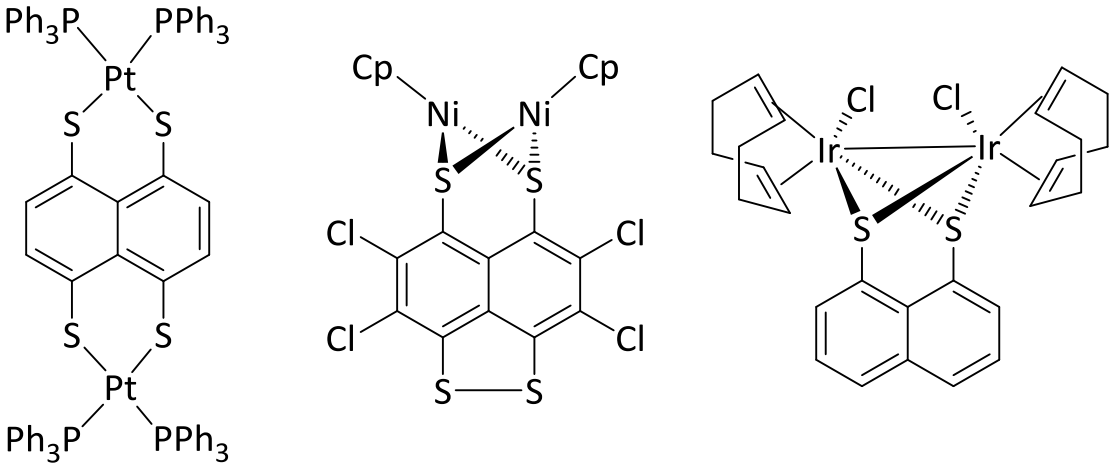

Figure 56: Previously mentioned bimetallic transition metal complexes.

Transition metal complexes containing chalcogen rich ligands have received a large amount of attention in the synthesis of molecular electrical conductors. The discovery of the first organic metal TTF–TCNQ (Figure 57, top) in 1973[207] has led to a number of transition metal systems designed to "mimic" this structure and result in potentially superconducting properties. One of the most widely studied ligands to date is 2-thioxo-1,3-dithiole-4,5-dithiolate (dmit) with a series of nickel, palladium and platinum complexes prepared. The superconducting properties of these complexes have all been examined with superconductance achieved at temperatures of less than 5 K.[206] Pullen and co-workers have made use of this dmit ligand in conjunction with tetrathiooxalate (tto) to form

bimetallic nickel(II) complexes whose electrical conducting properties were investigated (Figure 57, centre). Several other research groups have made use of the tto ligand to form bimetallic systems; Dahl reported the first crystallographically characterised tto nickel complex in 1982 (Figure 57, bottom left),[208] with similar work conducted by Rauchfuss[209]. Another set of intriguing bimetallic nickel complexes were prepared by Moutloali and co-workers. They used a series of dithiolato Schiff base ligands to synthesis bimetallic nickel complexes (Figure 57, bottom right) and investigated their electrochemistry.[210] They determined that there was electronic communication between the two nickel centres by means of cyclic voltammetry. As with so much sulfur chemistry, an interest in bimetallic systems present in nature has also been established in the literature. One such example is the work by Harrop and co-workers.[211] They prepared two Ni–Ni models which exhibited structural features and chemical properties similar to those of the binuclear active site of ACS/CODH. These were the first examples of sulfur bridged bimetallic nickel complexes that bind CO at the bridged Ni(I) centre in a similar fashion to that proposed in the mechanism of acetyl coenzyme A synthesis.[212]

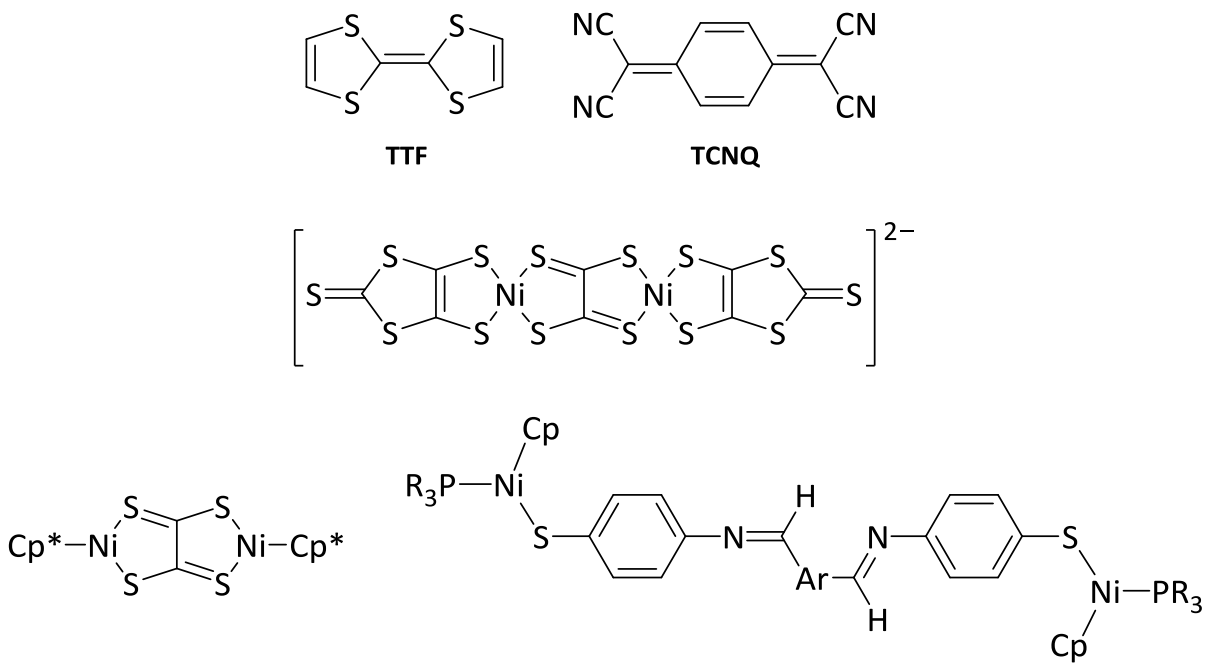

Figure 57: Structures of TTF and TCNQ with examples of homobimetallic Ni complexes.

4.1.1 – Bimetallic complexes using alkyl dithiolato ligands

A number of heterobimetallic complexes have been synthesised by Claver and co-workers using a range of alkyl dithiolato ligands (Figure 58, left).[156] They prepared a series of palladium and platinum dithiolato precursor complexes bearing both mono- and bi-dentate phosphine ligands. The

mononuclear rhodium complex $[Rh(cod)_2]ClO_4$ was then added resulting in a bimetallic system as the sulfur lone pairs displaced one of the cod ligands. A number of the obtained complexes were characterised by single crystal X-ray diffraction which confirmed the μ^2 nature of the two sulfur atoms. They later went on to test these systems as catalyst precursors in the hydroformylation of styrene.[213] By performing high pressure NMR studies they concluded that the mononulcear species observed most likely gave rise to the catalytic activity. Additionally, half sandwich [Pt(II)–M(III)] (M = Ir, Rh) complexes containing a bridging edt ligand have also been reported (Figure 58, centre).[214]

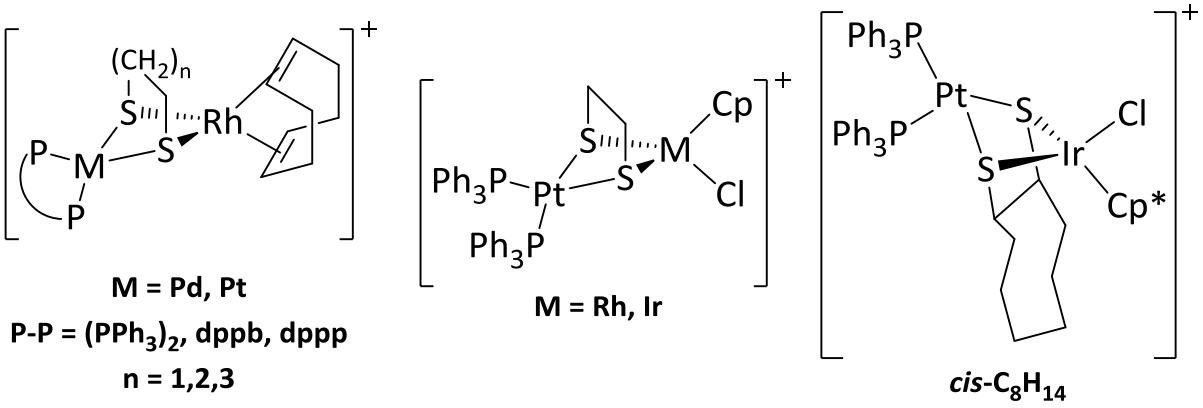

Figure 58: Heterobimetallic examples using alkyl dithiolato ligands.

Further research into these systems has been conducted by Ishii and co-workers. They studied the synthesis of [Pt(II)–Ir(III)] heterobimetallic complexes using both *trans*- and *cis*-cyclooctane-1,2-dithiolato ligands (Figure 58, right).[215] A modified synthetic approach was used to add the iridium centre to the preformed platinum complex. Metal exchange reactions with a cationic dithiolato [Pt(II)–Ag(I)] complex were carried out using the dimeric iridium source $[Cp^*IrCl_2]_2$. The molecular structures of the complexes were examined by single crystal X-ray diffraction with the iridium centre identified as adopting a distorted tetrahedral geometry. The catalytic activity of the [Pt(II)–Ir(III)] complexes in the hydrosilylation of alkynes was examined. The *trans*-derivative showed a lower activity than the *cis*-derivative and in all cases the *Z*-isomer of the vinylsilane represented the majority of the products observed, with some examples of it being the only product.

Two other noteworthy examples of a bimetallic dithiolato complex are the ruthenium porphyrins bridged by a range of alkyl dithiolates reported by Richter-Addo.[152] In this paper, they prepared the first examples of bimetallic metal porphyrins utilising μ^2-dithiolato ligands. The other was a publication by Seidel in 2010[216] where they synthesised a [Co(I)–Pt(II)] complex bridged by the

acetylenedithiolato ligand. The structures were examined by single crystal X-ray diffraction alongside examination of the spectroscopic properties and electronic structures of these complexes.

4.1.2 – Bimetallic complexes using aromatic dithiolato ligands

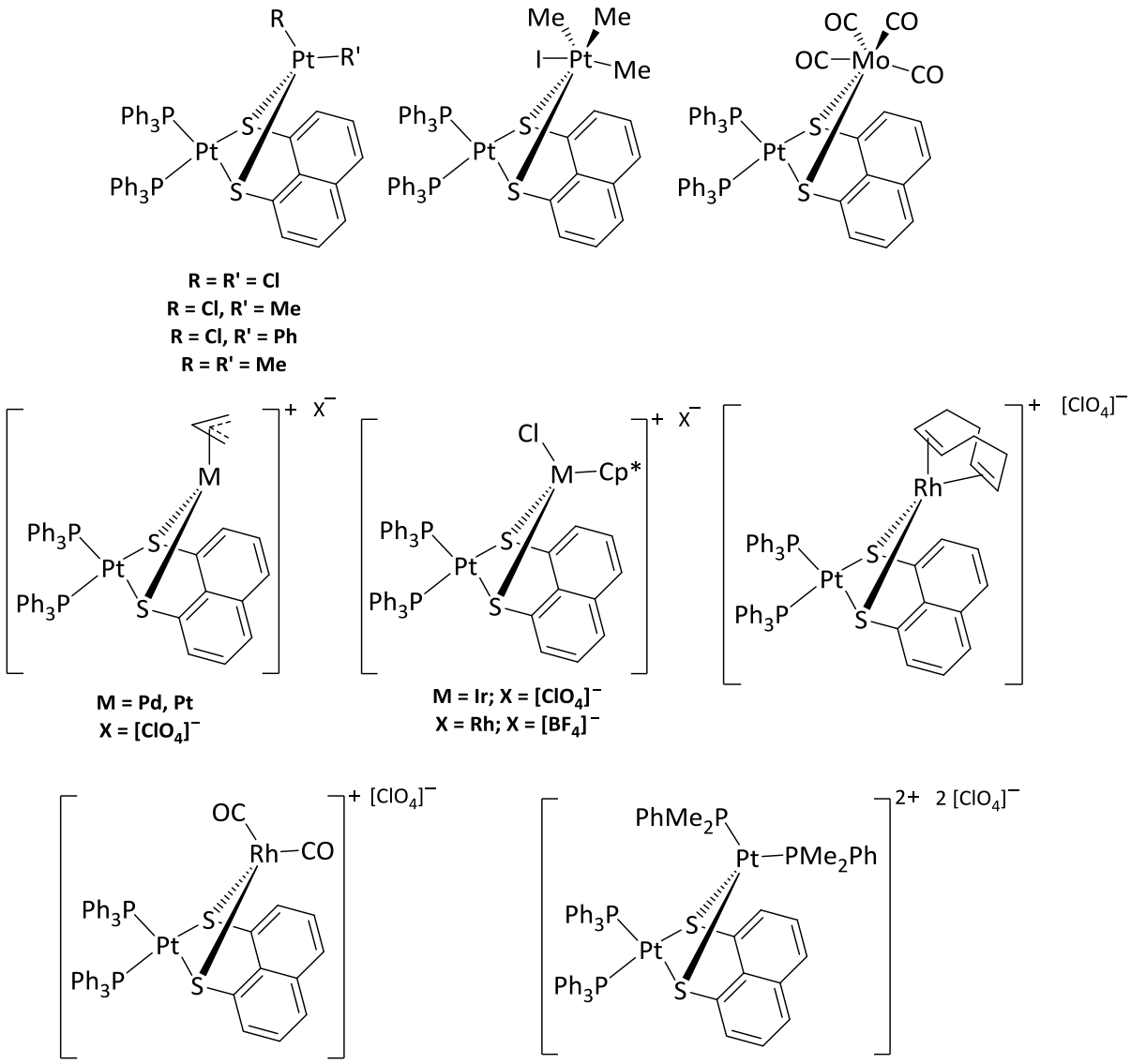

Figure 59: Naphthalene dithiolate bimetallic complexes from a platinum precursor.

The work conducted on both homo- and hetero-bimetallic systems using an aromatic dithiolate ligand is incredibly limited. The work discussed previously on the [FeFe] hydrogenase mimics makes up a large portion of the results encountered when searching using Scifinder®. The Woollins group have published two papers investigating the use of the $NapS_2$ ligand in the formation of bimetallic systems.[217,218] This involved following a similar approach to that used by Claver and co-workers, firstly forming a monometallic complex then adding a second reactive metal centre to allow

coordination through the sulfur lone pairs. The initial metal complex formed was $[Pt(NapS_2)(PPh_3)_2]$ which was then reacted to form a series of homo- and hetero-bimetallic complexes using platinum, palladium, molybdenum, iridium and rhodium with examples of neutral, monocationic and dicationic complexes reported (Figure 59).

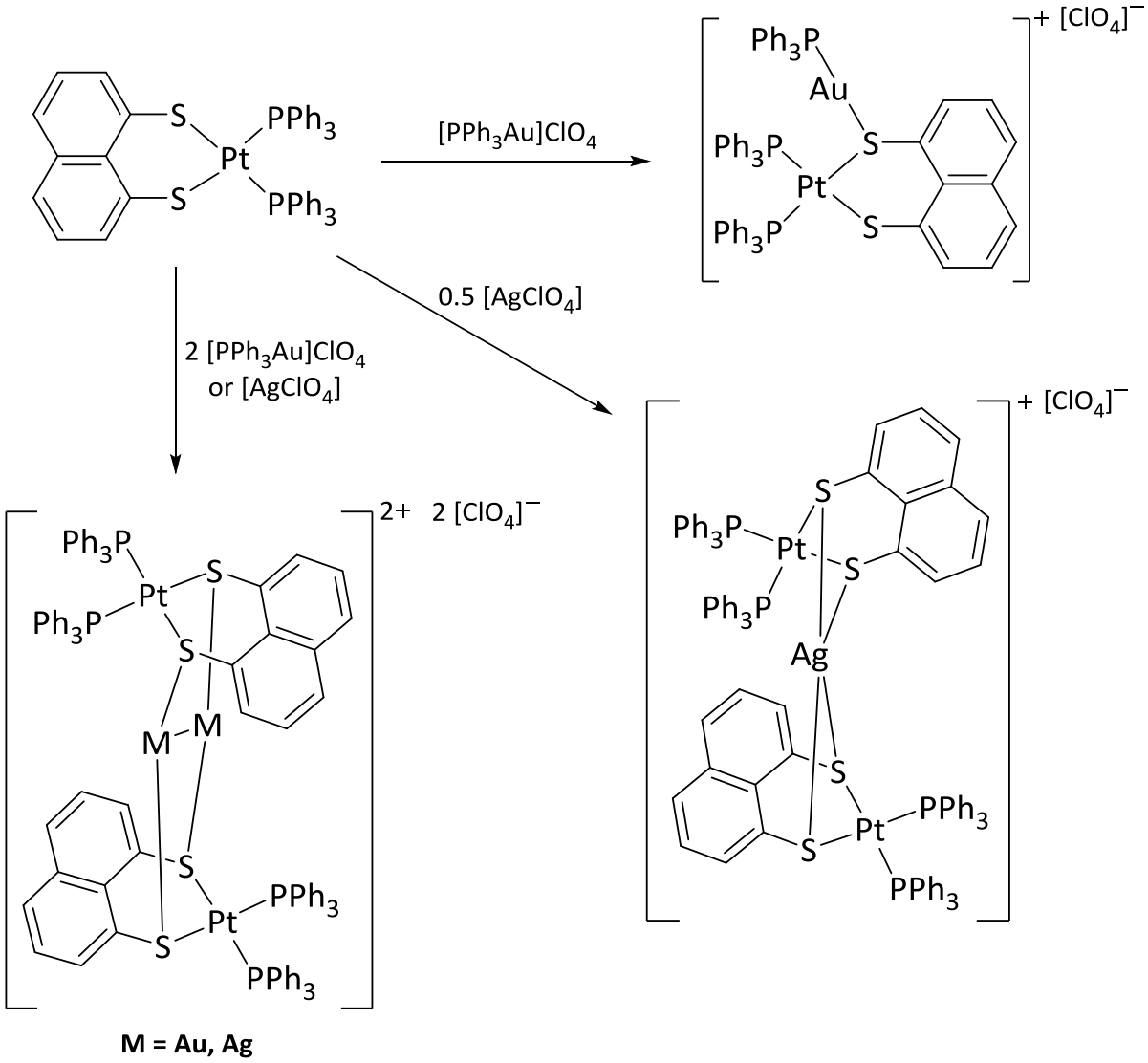

Scheme 25: Synthesis of $NapS_2$ dithiolate bimetallic systems containing platinum and gold or silver.

Using the same platinum precursor, the Woollins group also prepared bimetallic complexes containing a group 11 metal.[218] When reacted with a suitable gold precursor $[AuPPh_3]ClO_4$, a simple bimetallic system was formed (Scheme 25). Interestingly, the analogous silver complex was not prepared as instead the silver centre coordinated two of the platinum complex moieties resulting in a trimetallic complex (Scheme 25). The fluxional nature of the gold metal centre was established by

means of ^{31}P NMR spectroscopy. Two multimetallic complexes were also formed when the stoichiometry of the gold and silver source was altered (Scheme 25).

Other examples of multimetallic dithiolate complexes have been reported in the literature. Tetranuclear and pentanuclear copper(I) dithiolate complexes have been synthesised from the reaction of [$NapS_2$] with $[Cu_2(\mu_2\text{-dppm})_2(MeCN)_2](PF_6)_2$.[219] The tetranuclear complex has a square planar Cu_4 core capped by a 5-coordinate sulfur atom, whilst the pentanuclear complex has a Cu centred square planar Cu_5 core.

4.2 – Constructing a Bimetallic System: Building Blocks

The requirements for the construction of a bimetallic system have been well examined in the previous sections. This includes a ligand with the ability to bind, in part at least, in a bridging fashion and metal centres capable of forming covalent and or dative bonds. As discussed, we have investigated several bimetallic systems using the $NapS_2$ ligand.[191,217,218] In order to further investigate the effect of size and flexibility of the ligand in these types of complexes, a series of aromatic based dithiolate ligands were selected (Figure 60). A large amount of the previous work within the Woollins group involved the use of a platinum based complex precursor. In an attempt to further expand the complexation chemistry of **A**-**D**, a search for other potential metals was conducted.

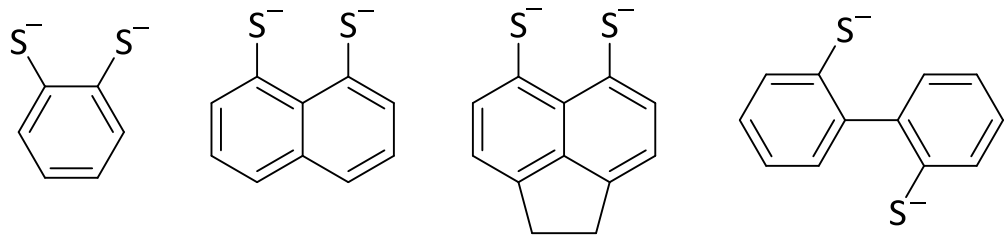

Figure 60: Dithiolato ligands (**A**-**D**) selected for investigation into bimetallic complexes.

Looking outside of examples from the Woollins group using ligand **B**, the most widely studied ligand of the series was **A**. A paper by Suzuki and co-workers from 1997 seemed to provide an excellent starting point for our renewed investigations.[162] They reported the reaction of **A** with a rhodium precursor to form a homobimetallic rhodium(III) dithiolato complex. The solution ^1H NMR spectrum of the isolated complex showed it to exist in both a bimetallic and monometallic form, the latter being a $16e^-$ species. The solid state structure obtained by single crystal X-ray diffraction confirmed

the existence of the bimetallic form $[Cp^*Rh(BenzS_2)]_2$ (Figure 61) where one of the sulfurs acts as a μ^2-bridging atom. Another interesting result presented was the corresponding iridium analogue was only obtained in the form of the stable $16e^-$ monomer $[Cp^*Ir(BenzS_2)]$ (Figure 61).

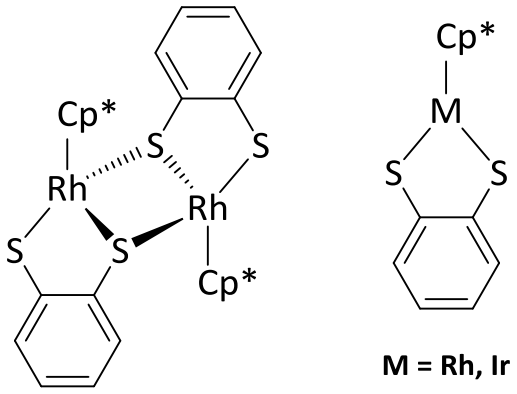

Figure 61: Bi- and mono-metallic Rh/Ir complexes obtained by Suzuki and co-workers.

The bimetallic rhodium complex arises from the need to comply with Langmuir's law, with one sulfur atom donating a lone pair to another metal.[220] In these systems the Cp* ligand acts as a cap to one half of the metal atom leaving the second half open for coordination. We decided to use our series of dithiolate ligands to investigate how the size and flexibility of the ligand affects the formation of homobimetallic rhodium complexes of the type reported by Suzuki. We also wanted to see if the stable $16e^-$ species observed for the iridium complex would still be the major product when other ligands were used. This type of complex is potentially interesting as a number of catalytic cycles proceed *via* $16e^-$ species such as hydrogenations and hydroformylations. Given the planar nature of **A**-**C** we proposed that the new ligands would be placed perpendicular to the plane of the Cp* ring in a similar fashion to that observed by Suzuki. With regards to ligand **D**, the rotation about the biphenyl ring link would most likely result in a staggered configuration. Complexes synthesised would be characterised by multinuclear NMR spectroscopy, mass spectrometry, IR and Raman spectroscopy and, where possible, single crystal X-ray diffraction to determine unambiguously the structure of the products.

4.2.1 – Starting material preparation and new structural characterisation

Synthetic routes to the dithiol compounds of **A**, **B**, and **D** have been reported in the literature. Ligand **A** was found to be commercially available but can be easily synthesised from thiophenol.[221] Reacting thiophenol with n-BuLi followed by the addition of sulfur and then an acidic work up afforded crude benzene-1,2-dithiol (**H_2A**) with purification performed by vacuum distillation. The compound was obtained as a colourless liquid with a strong thiol odour. For ligands **B** and **D** the

synthesis of the dithiol compounds required a two-step process starting from naphthalene and biphenyl respectively. The first being a double lithiation using n-BuLi followed by the addition of sulfur and an aqueous work up to form naphtho[1,8-*cd*]-1,2-dithiole[222,223] (**S_2B**) and dibenzo-[*c*,*e*]-1,2-dithiine[224,225] (**S_2D**). The acenaphthene based dithiole compound could not be formed directly from acenaphthene; instead a further step to prepare **AcenapBr$_2$** was needed.[99,226] The synthesis of **AcenapBr$_2$** has been discussed previously in section 2.2. Using this compound, 5,6-dihydroacenaphtho-[5,6-*cd*]-1,2-dithiole (**S_2C**) was synthesised according to the literature procedure.[199] Purification of **S_2B**-**D** was performed by column chromatography using silica gel and hexane or petroleum ether. Isolated yields after purification were low to moderate, **S_2B**; 43%, **S_2C**; 21% and **S_2D**; 36%. Both **S_2B** and **S_2C** were obtained as red solids whilst **S_2D** was a bright yellow solid.

The reduction of disulfides **S_2B**-**D** was achieved following a procedure reported by Yui and co-workers for the formation of naphthalene-1,8-dithiol (**H_2B**).[227] This involved the use of sodium borohydride to reduce the S–S bond followed by an acidic work up after which all three pro-ligands were isolated as near colourless solids, each possessing only a mild thiol odour. The full synthetic outline to the pro-ligands is shown in Scheme 26. The characterisation data obtained (^{1}H & ^{13}C{^{1}H} NMR, IR and Raman) for the known compounds **AcenapBr$_2$**, **H_2A**, **S_2B**, **H_2B**, **S_2C**, **S_2D** and [1,1'-biphenyl]-2,2'-dithiol (**H_2D**) were in good agreement to that previously reported.[99,199,221-228]

Acenaphthene-5,6-dithiol (**H_2C**) represents a newly isolated compound and was fully characterised by ^{1}H and ^{13}C{^{1}H} NMR spectroscopy, mass spectrometry alongside IR and Raman spectroscopy. The compound was found to be air stable with no decomposition observed over several months whilst storing in air. For our purposes the compound did not require further purification, however analytically pure colourless crystalline material was obtained after recrystallisation from boiling hexane; the homogeneity was verified by elemental analysis. The ^{1}H NMR spectrum of **H_2C** shows the distinctive thiol peak at δ_H = 4.16 ppm and the aromatic protons as a set of partially overlapping doublets centred at δ_H = 7.47 and 7.09 ppm, while the signal from the alkyl bridge can be seen as a broad singlet at δ_H = 3.31 ppm. The ^{13}C{^{1}H} NMR spectrum showed the expected signals including all the quaternary carbons. A medium intensity band at 2546 cm^{-1} in the Raman spectra and a weak band at 2510 cm^{-1} in the IR correspond to ν(S–H) vibrations. The mass spectrum (ES$^-$) shows the parent ion at *m/z* 217.01 corresponding to the loss of H$^+$.

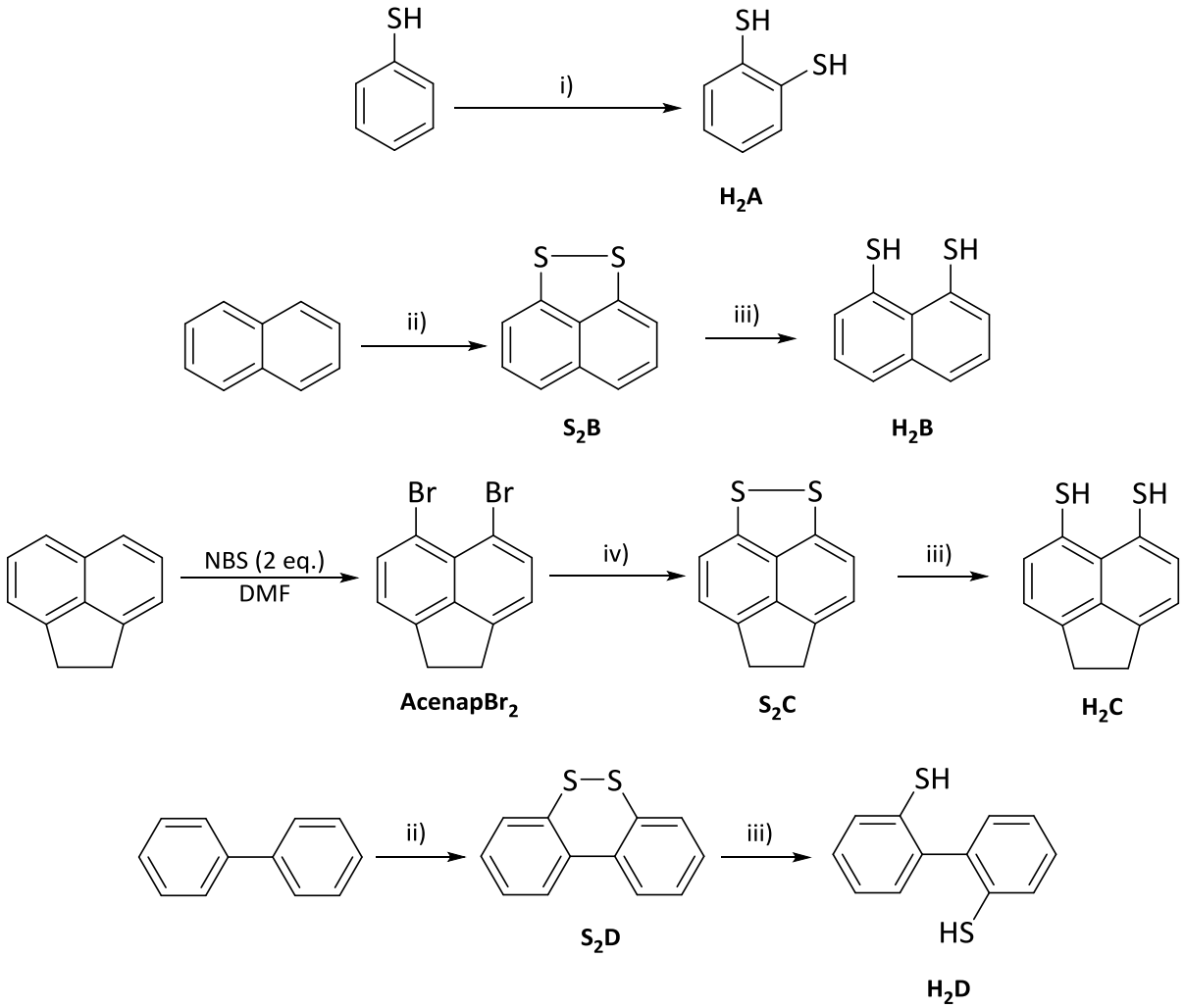

Scheme 26: Synthetic routes to pro-ligands **H_2A**-**D**. Conditions: i) 1. n-BuLi, TMEDA, hexane, 0 °C. 2. Sulfur flowers, −20 °C. 3. $HCl_{(aq)}$. ii) 1. n-BuLi, TMEDA, hexane, 60 °C. 2. Sulfur flowers, THF, −78 °C. iii) 1. $NaBH_4$, EtOH/THF. 2. $HCl_{(aq)}$. iv) 1. n-BuLi, TMEDA, ether, −78 °C. 2. S_8, −40 °C.

The rhodium and iridium precursors pentamethylcyclopentadienylrhodium(III) chloride dimer, $[Cp^*RhCl_2]_2$, (**SM**-**1**) and pentamethylcyclopentadienyliridium(III) chloride dimer, $[Cp^*IrCl_2]_2$, (**SM**-**2**) were prepared following the literature procedure reported by Maitlis and co-workers (Scheme 27).[229] These complexes were prepared with excellent yields of 92% (**SM**-**1**) and 82% (**SM**-**2**). The characterisation data obtained were in good agreement to that reported previously with analytical purity confirmed by elemental analysis.[229]

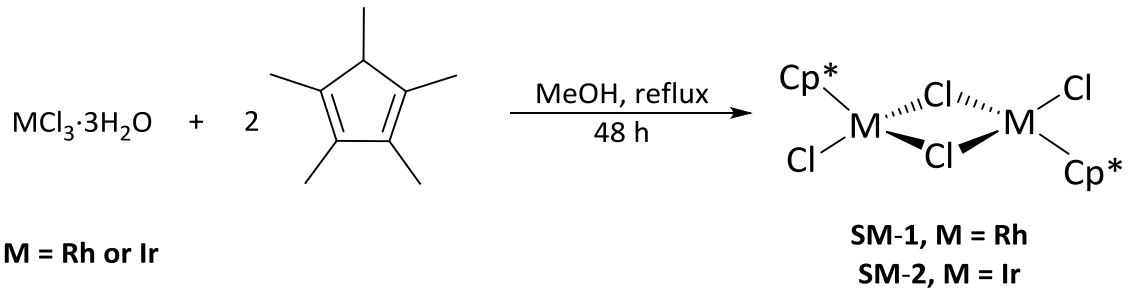

Scheme 27: Synthetic route to the rhodium and iridium precursors.

4.2.1.1 – Crystallographic characterisation of H_2A-D

Despite **H_2A**/**B**/**D** being reported and spectroscopically characterised previously no X-ray crystal data had been published. In order to examine changes in the structure of the ligand upon binding to a metal, crystals of the dithiols suitable for X-ray work were grown. For **H_2B**-**D** these were obtained from boiling hexane followed by cooling in the fridge (**H_2C**/**D**) or freezer (**H_2B**). In the case of **H_2A** the compound crystallised upon standing when stored in the fridge following distillation.[i] The crystal structures of **H_2A**-**D** are shown in Figure 62 with selected structural parameters in Table 7 (**H_2A**/**D**) and Table 8 (**H_2B**/**C**).

Table 7: Selected bond lengths [Å], angles [°], torsion angles [°] and displacements [Å] for **H_2A** and **H_2D**.

	H_2A		**H_2D**[a]
S1–C1	1.776(4) [1.773(3)]	S1–C1	1.764(8)–1.783(8)
S2–C2	1.771(3) [1.777(4)]	S8–C8	1.760(8)–1.785(8)
S1···S2	3.068(1) [3.072(1)]	S2···S8	3.716–4.335(3)
S1–C1···C2–S2	1.1(4) [2.3(4)]	C2–C1–C7–C8	79.8–102.1(9)
Splay angle[b]	−3.4(4) [−3.5(4)]		
Out of plane displacements			
S1	0.025 [0.041]	S2	0.007–0.065
S2	0.030 [0.036]	S8	0.012–0.137

[a] ranges quoted from all four molecules within the asymmetric unit.

[] denotes data from second molecule in asymmetric unit.

[b] calculated as [(S1–C1–C2 + C1–C2–S2)−240].

[i] single crystal X-ray diffraction data provided by Mr Nicholas Black, PhD student, Woollins Research Group.

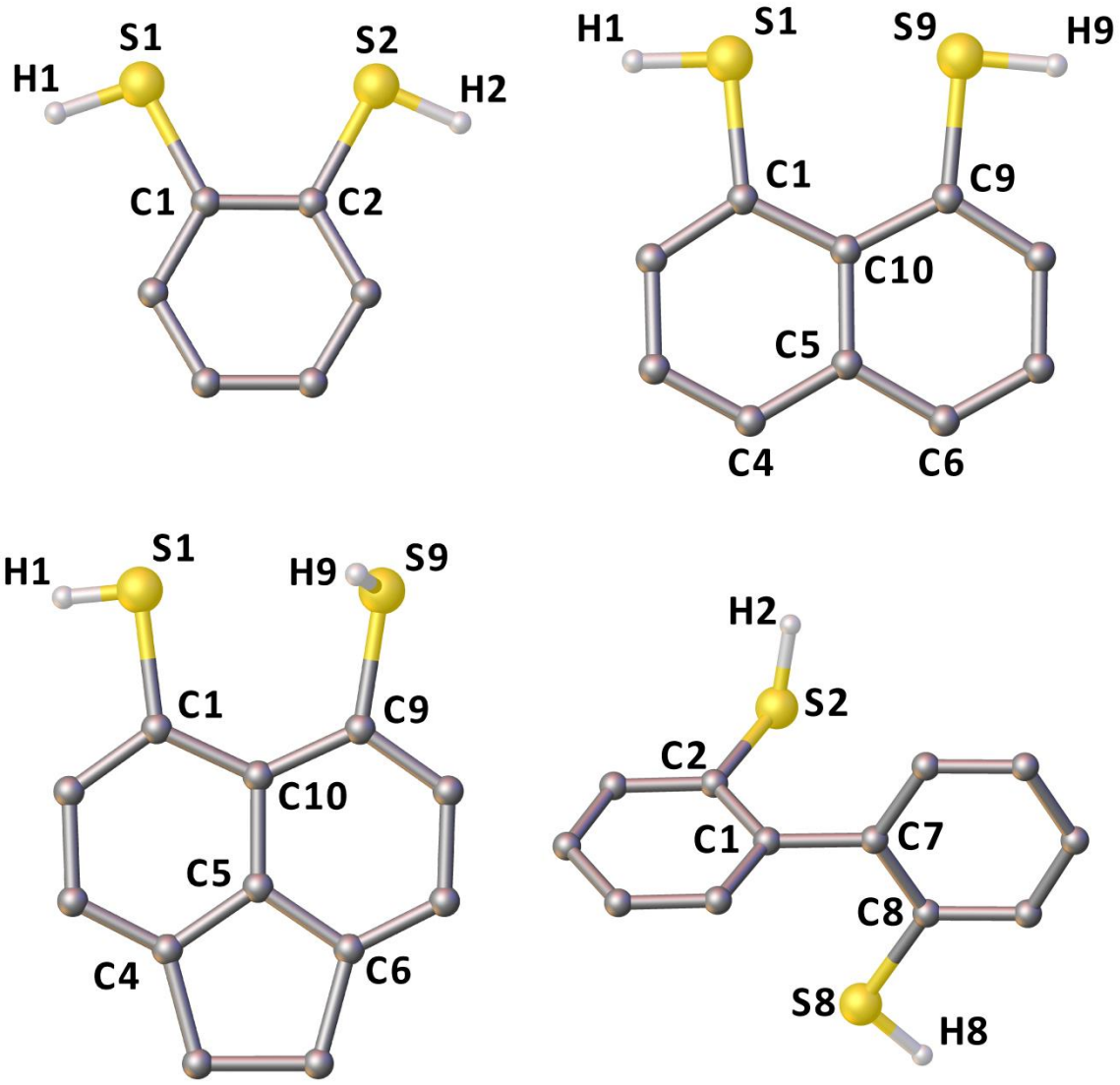

Figure 62: Crystal structures of **H_2A** (top left), **H_2B** (top right), **H_2C** (bottom left) and **H_2D** (bottom right). Carbon bound hydrogens are omitted for clarity, only one of the two (**H_2A**-**C**) / four (**H_2D**) molecules from the asymmetric unit are shown. Hydrogen atoms were placed in idealised geometries.

There are two molecules within the asymmetric unit for **H_2A**-**C** with four present in **H_2D**. When compared to the respective disulfides, the S···S distances have increased for both **H_2B** and **H_2C** by *ca.* 0.8–0.9 Å and 1.0–1.2 Å respectively as the bonding interaction is replaced by a repulsive force.[230,231] Interestingly, the S···S distance (3.068(1) Å) in **H_2A** is between that seen in the other two planar ligands despite being *ortho* substituted. The increase in the S···S distance when comparing the disulfide to the dithiol is largest in **H_2D** (1.65–2.67 Å) as the rotation around the aryl–aryl bond allows the sulfur atoms to move further apart. The splay angles for **H_2B**/**C** are positive with values of 10.4(9)–11.8(9)° and 15.9(9)–20.5(9)° for **H_2B** and **H_2C** respectively, providing further evidence of the

repulsive interaction now present between the sulfur atoms. In contrast to this the splay angle in **H_2A** has a small negative value indicating a slight attractive force between the two sulfur atoms. The larger S···S distance and splay angle observed for **H_2C** over **H_2B** is most likely due to the ethylene bridge in the acenaphthene backbone which acts to angle the *peri*-atoms away from each other.

The torsion angle S1–C1···C9–S9 has increased in both **H_2B** and **H_2C** by 5.2–6.1° and 1.1–2.6° respectively compared to their corresponding disulfides, indicating a mild but noticeable out-of-plane displacement. The equivalent torsion angle in **H_2A** ranges from 1.1(4)–2.3(4)° which is the lowest value for the planar ligands. In this case, the larger torsion angle observed in **H_2B** over **H_2C** is because the sulfur atoms can't move apart in the plane of the ring enough to relieve the strain so are forced to move in another direction. The torsion angle between the phenyl rings in **H_2D** varies at 79.8°, 82.7° and 102.1°, which suggests the ideal position for the rings to sit, is approximately 10–12° off perpendicular. The buckling of the central naphthalene ring system, which is examined by looking at the C1–C10–C5–C6 and C9–C10–C5–C4 torsion angles, is more noticeable in **H_2B** over **H_2C**. The out-of-plane displacements in **H_2A**/**C** are less than those observed in **H_2B**/**D** with **H_2B** having the largest of all the displacements observed.

Table 8: Selected bond lengths [Å], angles [°], torsion angles [°] and displacements [Å] for **H_2B** and **H_2C**.

	H_2B	**H_2C**
S1–C1	1.788(3) [1.786(5)]	1.785(4) [1.782(4)]
S9–C9	1.784(3) [1.789(5)]	1.788(4) [1.788(4)]
S1···S9	2.919(2) [2.951(2)]	3.104(1) [3.264(2)]
C1–C10–C5–C6	176.8(3) [176.9(4)]	178.9(3) [179.4(3)]
C9–C10–C5–C4	178.3(3) [178.4(4)]	178.0(3) [177.0(3)]
S1–C1···C9–S9	5.4(2) [6.3(2)]	3.0(2) [1.5(2)]
Splay angle[a]	11.8(9) [10.4(9)]	15.9(9) [20.5(9)]
Out of plane displacements		
S1	0.092 [0.152]	0.099 [0.018]
S9	0.146 [0.147]	0.063 [0.103]

[] denotes data from second molecule in the asymmetric unit.

[a] calculated as [(S1–C1–C10 + C1–C10–C9 + C10–C9–S9)−360].

The single crystal X-ray structures of **SM**-**1** and **SM**-**2** have been reported previously by Churchill and co-workers.[232,233] Any comparison made between our new complexes and these starting materials will be done so using the data they obtained.

4.3 – Constructing a Bimetallic System: The Assembly

In the work by Suzuki and co-workers, they prepared **C4-3a** and **C4-4a** by the addition of a methanol solution of the metal precursor to a methanol solution of **H_2A** and sodium methoxide with the reaction stirred for six hours (Rh) or fifteen hours (Ir) at room temperature.[162] The by-products of the reaction are sodium chloride and methanol both of which are easily removed during the work up.

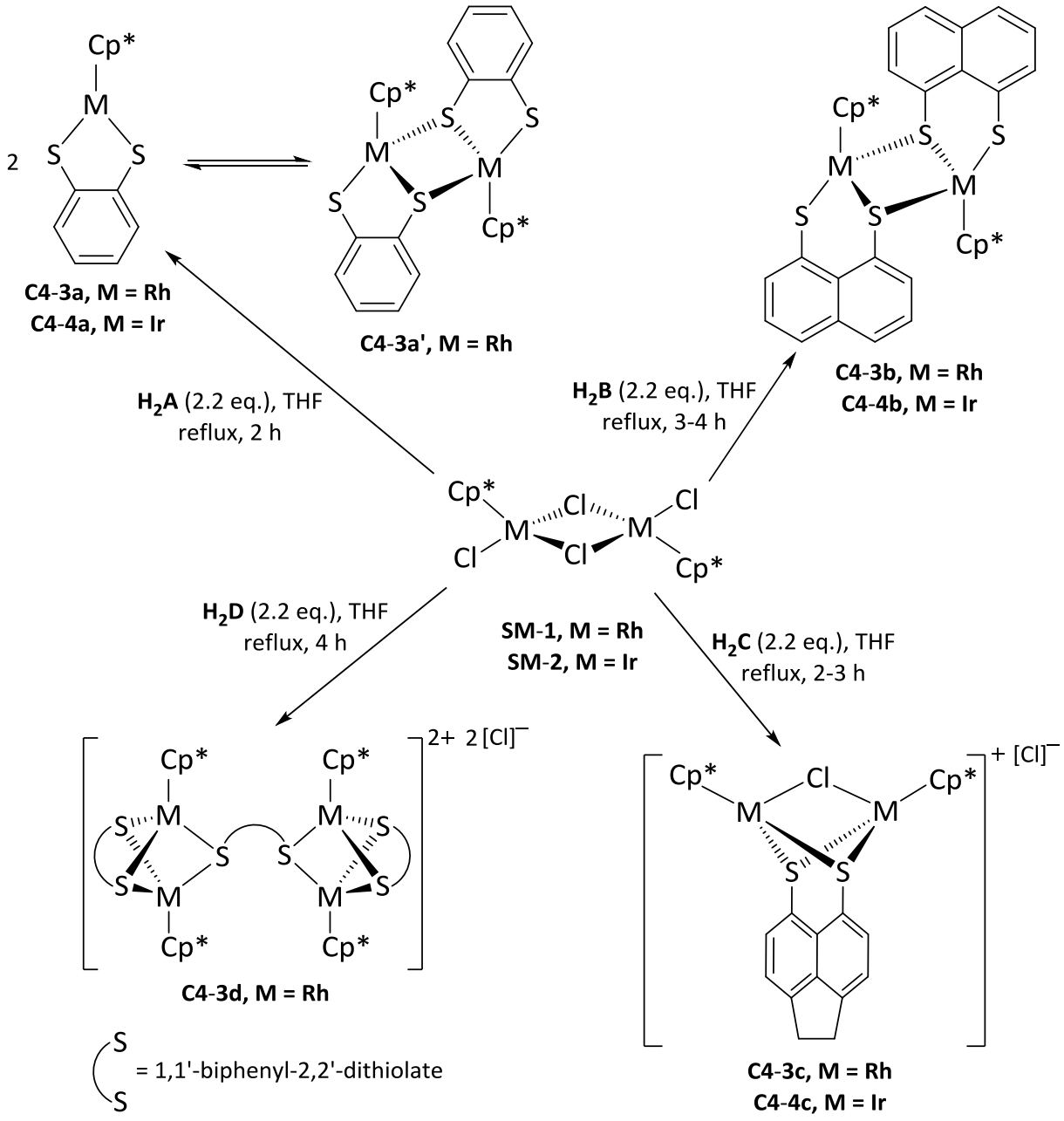

Scheme 28: Synthetic routes to multimetallic rhodium and iridium dithiolato complexes.

Previous work within the Woollins research group has shown the ability of the thiol pro-ligands to react directly with metal chloride centres, without the need for base, resulting in HCl as the by-product. The synthetic route followed to this series of rhodium and iridium dithiolato complexes is outlined in Scheme 28. The presence of the Cp* group allowed for easy monitoring of the reaction by ^{1}H NMR spectroscopy. The metathesis of the chloride ligands in **SM**-**1** and **SM**-**2** with the dithiolato ligands **A**-**D** proceeds smoothly in refluxing THF with the elimination of HCl. No trapping agent was required for the HCl by-product. Novel complexes **C4**-**3b**/**3c**/**3d** and **C4**-**4b** were isolated in 40–84% yields after purification. However, the iridium complex **C4**-**4c** was obtained in only a 2% yield using this synthetic protocol. An improved synthesis of **C4**-**4c** and **C4**-**3c** will be discussed in section 4.3.2. In all cases, the products were purified by column chromatography using silica gel and either DCM or a DCM/alcohol (methanol or ethanol) mixture as the eluent. Our synthetic procedure to **C4**-**3a**/**4a** provided yields (**C4**-**3a** = 84%; **C4**-**4a** = 84%) comparable to those reported previously by Suzuki.[162] By removing the base and refluxing, the reaction the time taken for the reactions were substantially reduced. During the reaction itself it was observed that upon addition of **H_2A** to the suspension of **SM**-**1** or **SM**-**2** an instantaneous colour change to dark purple was observed. This implies an initial instant reaction between these two materials; no such observation was made for the other ligands.

4.3.1 – Neutral bimetallic complexes

The characterisation data obtained for **C4**-**3a** and **C4**-**4a** matched that previously reported,[162] with the purity of our samples confirmed by elemental analysis. The ^{1}H NMR spectrum of the dark purple compound obtained after purification displayed three major peaks, two in the aromatic region and one in the alkyl region. The aromatic signals appear as multiplets with ranges of δ_H 7.88–7.84 and 7.11–7.07 ppm with similar line shapes to those seen for the starting material **H_2A**. The methyl protons from the Cp* ring appear at δ_H 2.04 ppm. Based on the observations made by Suzuki these were assumed to be from the monomeric form **C4**-**3a**.[162] The NMR sample was left for several hours then re-examined; four new peaks in the aromatic region were observed as well as one in the alkyl region. A doublet centred at δ_H 7.46 ppm with a coupling constant of 7.6 Hz, one multiplet ranging from δ_H 7.13–7.07 ppm and two triplets centred at δ_H = 6.83 and 6.64 ppm with coupling constants of 7.6 Hz arising from the phenyl ring. These new signals were assigned to the dimeric form **C4**-**3a'** as the dative bond formed from one of the sulfurs atoms removes the symmetry within the phenyl ring. The peak at δ_H 1.27 ppm from the methyl protons of the Cp* rings is shifted significantly upfield compared to the monomeric form. Figure 63 shows the aromatic region of the two ^{1}H NMR spectra showing both **C4**-**3a** initially isolated then conversion to a mixture of both **C4**-**3a** and **C4**-**3a'**.

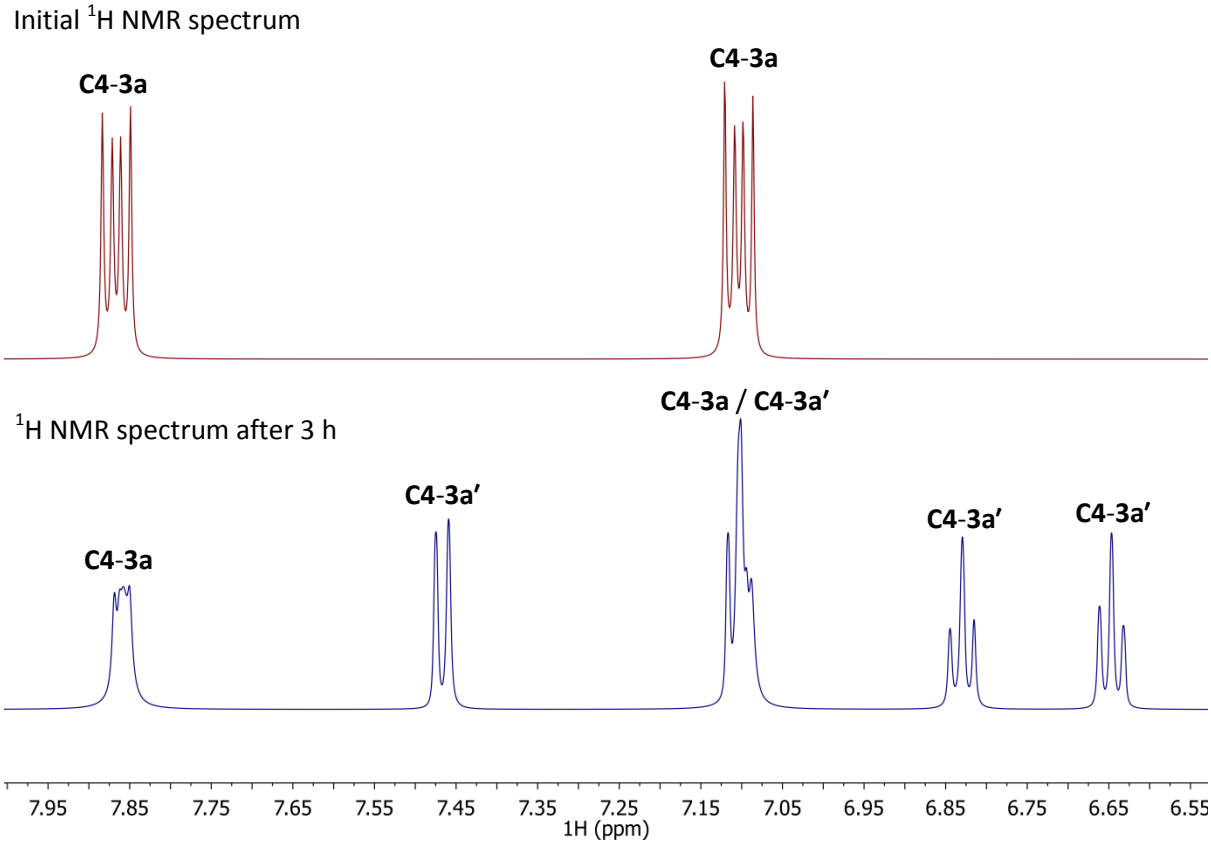

Figure 63: Aromatic region of the ^{1}H NMR spectrum ($CDCl_3$, 500 MHz) of **C4-3a** after purification (top) then 3 hours later (bottom). Small impurity peaks (**H_2A**) and solvent ($CDCl_3$) have been removed for clarity.

The $^{13}C\{^1H\}$ NMR spectra mirrored the observations made from the ^{1}H NMR data for **C4-3a**. The initial spectrum obtained displayed three aromatic carbon peaks in the range of δ_C 157.2–120.2 ppm with the quaternary carbon from the Cp* ring appearing as a doublet due to $^1J_{CRh}$ coupling ($^1J_{CRh}$ 7.1 Hz) centred at δ_C 96.6 ppm. Rhodium has one isotope, ^{103}Rh, which is NMR active with a spin of ½; coupling to protons of the pentamethylcyclopentadienyl group were not observed in any of the work presented in this thesis. The methyl carbons from the Cp* rings appear as a singlet at δ_C 8.1 ppm. The second spectrum run after several hours showed the appearance of signals from **C4-3a'**. Three aromatic carbon peaks were present (δ_C 152.5–122.5 ppm) with the coupling constant for the quaternary Cp* carbon smaller than before ($^1J_{CRh}$ 5.7 Hz). The methyl carbons from the Cp* rings are shifted slightly downfield to δ_C 10.7 ppm. The IR and Raman spectra displayed signals which supported the formation of the complex. The mass spectrum displayed the base peak at *m/z* 378.00 which corresponds to $[½M]^+$ with smaller peaks corresponding to $[M+Na]^+$ *m/z* 400.99 and $[M]^+$ *m/z* 755.99 also present.

The iridium analogue **C4**-**4a** was fully characterised with the ^{1}H NMR spectrum being similar to that of the equivalent rhodium complex. Two multiplet peaks in the aromatic region at δ_H 8.08–8.04 and 7.05–7.01 ppm alongside the methyl proton from the Cp* ring at δ_H 2.16 ppm were seen. The spectrum obtained of the same sample several hours later showed no evidence for the formation of a dimeric species; this was still the case after three days. One possible explanation for this is based upon observations made by Sellmann and co-workers. They proposed that in order for the metal centre to achieve the 18e$^-$ configuration the thiolate donates its p electrons to the metal, thus the metal–thiolate bonds have a bond character of 1.5.[234] The ^{13}C{^{1}H} NMR spectrum supported the monomeric form with the quaternary Cp* carbon appearing as a singlet since iridium has no spin ½ isotopes. The mass spectrum of the complex displayed a base peak at *m/z* 468.05 which corresponds to $[M]^+$ with a smaller peak at *m/z* 491.04 which was assigned as $[M+Na]^+$. No higher mass signals were observed providing further support to the purely monomeric nature of the complex.

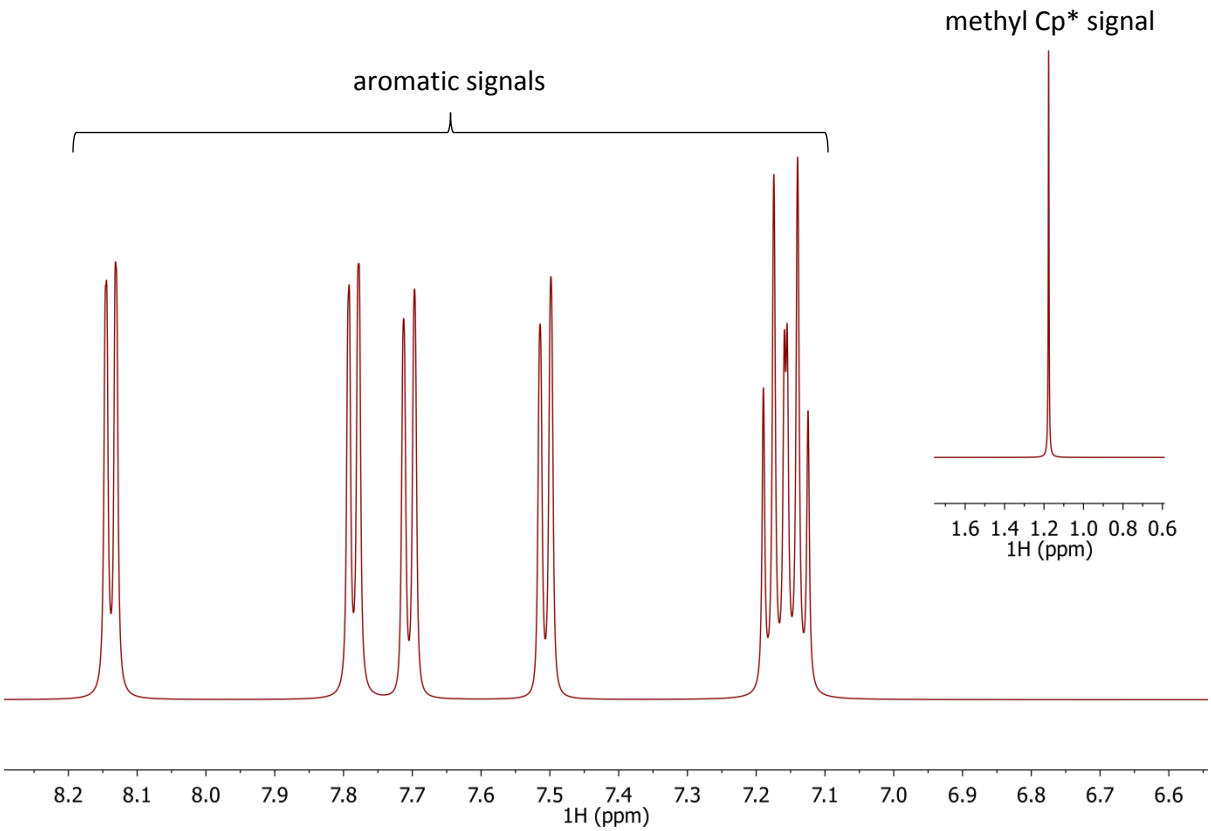

Figure 64: ^{1}H NMR spectrum ($CDCl_3$, 500 MHz) of **C4**-**3b** aromatic region with an overlay of the methyl Cp* signal. Small impurity peaks (**H_2B**) and solvent ($CDCl_3$) have been removed for clarity.

The products from the reaction between **SM**-**1** or **SM**-**2** and **H_2B** were first analysed by ^{1}H NMR spectroscopy. The data for **C4**-**3b** displayed six distinct aromatic signals consisting of four doublets (δ_H 8.14, 7.78, 7.70 & 7.50 ppm) and two triplets (δ_H 7.17 & 7.14 ppm) (Figure 64). With a singlet

present in the alkyl region (δ_H 1.17 ppm) from the methyl protons of the Cp* ring (Figure 64), which is shifted upfield by 0.45 ppm when compared to **SM**-**1**. The presence of six aromatic signals indicated the most likely form of this complex was dimeric like **C4**-**3a'**; the NMR sample was left for several hours and re-examined. There was no evidence of any other product after this time, even after three days this was still the case. The ^{1}H NMR data obtained for **C4**-**4b** was analogous to that of **C4**-**3b** indicating that in this case the rhodium and iridium complexes behave in the same way. The signal from the methyl protons of the Cp* ring in **C4**-**4b** was again shifted upfield compared to **SM**-**2** ($\Delta\delta$ 0.36 ppm). As with the rhodium complex the NMR sample was analysed later but no additional peaks were observed. This indicates both of these dimeric complexes proved to be stable in solution over a period of several days. The two triplet signals observed seem strange given that all six of the naphthalene protons are inequivalent. These two signals come from the *meta* protons which each couple to their *ortho* and *para* neighbours. Both of these result in $^3J_{HH}$ coupling constants with magnitudes that are almost identical. Thus, what should appear as a doublet of doublets is observed as a *pseudo*-triplet.

The ^{13}C{^{1}H} NMR spectra of both **C4**-**3b** and **C4**-**4b** mirrored that of the ^{1}H NMR data with ten signals from the naphthalene backbone observed. The quaternary Cp* carbon in the rhodium complex is again split into a doublet with a coupling constant of 5.7 Hz. The IR and Raman spectra displayed peaks which supported the successful formation of the complexes. APCI$^+$ mass spectra show both the [M+H]$^+$ (**C4**-**3b** *m/z* 857.04; **C4**-**4b** *m/z* 1035.15) and [½M+H]$^+$ (**C4**-**3b** *m/z* 429.02; **C4**-**4b** *m/z* 519.08) peaks, in both cases the [½M+H]$^+$ signal is the base peak. The analytical purity of the complexes **C4**-**3a**/**b** and **C4**-**4a**/**b** was determined by elemental analysis.

4.3.1.1 – Crystallographic characterisation of C4-3a'/b and C4-4a/b

The crystal structures of **C4**-**3a'** and **C4**-**4a** have already been reported; our own data was obtained in order to further confirm the structure of the complex formed using our synthetic method. For completeness, the structures are examined from the data already published with comparisons made between the free (**H_2A**) and bound ligand.[162] The crystal structures of **C4**-**3a'** and **C4**-**4a** are shown in Figure 65 with selected structural parameters in Table 9. The fact that the only crystal structure obtained by Suzuki or during this work was that of **C4**-**3a'** is easily explained. As we saw in the ^{1}H NMR spectra above, initially only the monomeric form is seen after purification the last step of which is removing the solvent using a rotary evaporator. This is a quick process when compared to growing a crystal by slow evaporation. Given that the dimeric form takes time to appear and eventually dominates the ^{1}H NMR spectrum, it makes sense that this form would be most likely to crystallise over a long period of time. The only way to obtained a crystal structure of **C4**-**3a** would be

by a rapid crystallisation process; attempts at this proved unsuccessful with the crystals being of to poor a quality to utilise.

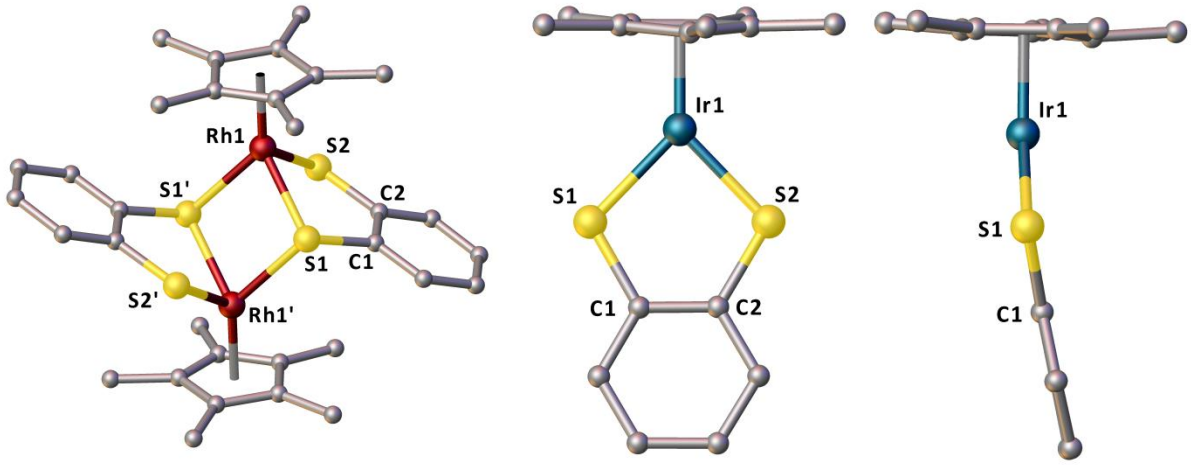

Figure 65: Crystal structures of **C4-3a'** (left), **C4-4a** (centre & right). Hydrogen atoms are omitted for clarity.

Table 9: Selected bond lengths [Å], angles [°], torsion angles [°] and displacements [Å] for **C4-3a'** and **C4-4a**.

	C4-3a'	**C4-4a**
M1···M1'	3.5307(8)	-
S1···S2	3.182(2)	3.111(6)
M1–S1	2.356(1)	2.253(4)
M1–S2	2.358(1)	2.244(4)
M1–S1'	2.401(1)	-
S1–M1–S2	84.90(4)	87.6(1)
S1–M1–S1'	84.15(4)	-
S2–M1–S1'	84.59(4)	-
S1–C1···C9–S9	0.59(3)	2.8(9)
Splay angle[a]	1.0(3)	0(2)
Out of plane displacements		
S1	0.090	0.021
S2	0.039	0.010
M1	0.815	0.209

[a] calculated as [(S1–C1–C2 + C1–C2–S2)−240].

The Rh1···Rh1' distance of 3.5307(8) Å indicates there is no bonding interaction between the two metal centres and is 0.20 Å less than that seen in **SM-1**.[232] The distance between S1···S2 has increased in both complexes by 0.11 Å in **C4-3a'** and 0.04 Å in **C4-4a**. The similarity in these distances

may at first seem surprising given that iridium is one row below rhodium in the periodic table and should therefore be larger. The lanthanide contraction, which is caused by inefficient shielding of the nuclear charge by the 4f electrons, results in the period six elements displaying almost identical radii to those in the fifth period.[235] Both rhodium and iridium have the same metallic radii of 5.78 Å and almost the same single bond radii of 1.25 Å and 1.26 Å respectively.[236] An increase in the splay angle for both complexes accompanies this as the metal centre forces the sulfur atoms further apart.

The bond lengths between the rhodium and sulfur atoms give a clear indication of the elongated dative bond formed in the dimerisation process. The rhodium complex adopts a piano stool geometry meaning the ideal angle around the metal centre is 90°. All the angles around the metal are distinctly less than this due to the restriction of the sulfur atoms imposed by the aromatic backbone. The out-of-plane displacement of the sulfur atoms shows minimal change in both complexes. The rhodium atom sits well above the plane of the benzene ring as you would expect for the piano stool type structure, interestingly the iridium atom is much closer at a distance of only 0.209 Å. If we consider Sellmann's explanation again, if the p electrons from the sulfur are being donated in **C4**-**4a** then we would expect the metallocycle to be planar. The small out-of-plane displacement of the iridium atom supports this theory. Further evidence lies in the Ir–S bond lengths which are significantly shorter than the normal Ir–S bond lengths seen previously (2.35 Å),[237] implying a stronger interaction than normal. This near linearity between Ir1–S1–C1 can be seen in Figure 65 (right).

Further reasoning for the purely monomeric form of the iridium complex **C4**-**4a** can be proposed by examining the packing within the crystal structure. There is evidence of π–π interactions between the Cp* ligand and the benzene ring of the dithiolate (Figure 66). The average C···C distance between the Cp* and the benzene ring is 3.66 Å whilst the centroid to centroid distance is just 3.59 Å. Normal π–π interactions range between 3.3–3.8 Å which is well within the distances measured here.[238]

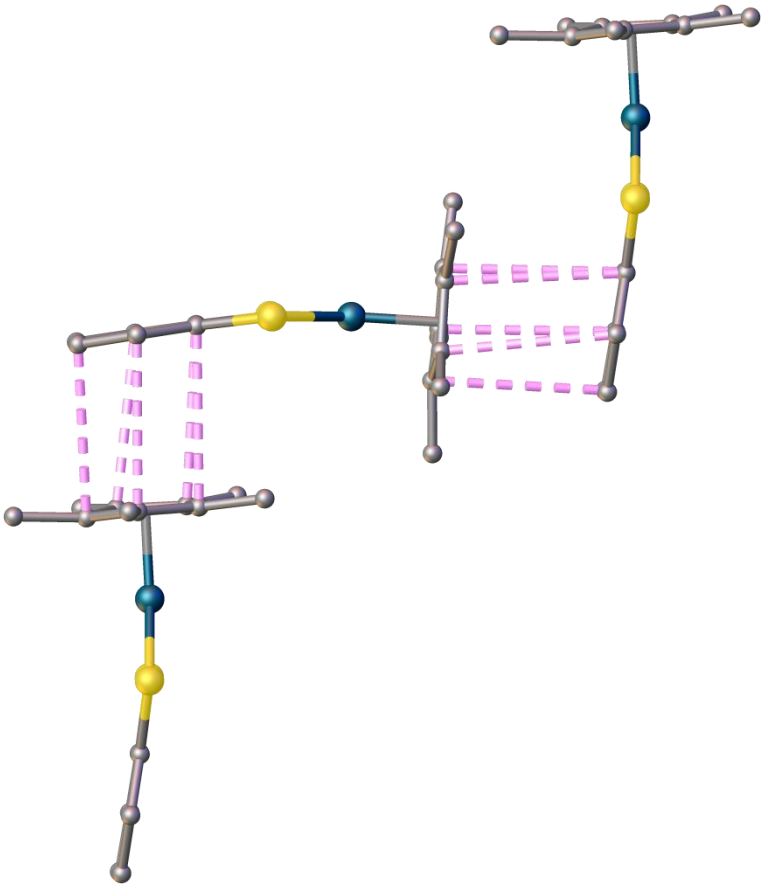

Figure 66: Packing within the crystal structure of **C4**-**4a** showing the π–π interactions.

The crystal structures of **C4**-**3b** and **C4**-**4b** are shown in Figure 67 with selected structural parameters in Table 10. From the data already obtained we proposed the structures to be similar to that already seen for **C4**-**3a'**. This was indeed the case with the complexes being isostructural forming dimeric structures and adopting a piano stool geometry. The distance between the metal atoms has decreased in both cases by 0.14 Å and 0.15 Å in **C4**-**3b** and **C4**-**4b** compared to their respective starting materials.[232,233] In addition the S1···S2 distance has increased in both complexes by similar amounts (0.70–0.72 Å). This is accompanied by the expected increase in the splay angle of 9.0° for **C4**-**3b** and 9.6° for **C4**-**4b** compared to the pro-ligand **H_2B**. The M1–S1 are both slightly shorter than the M1–S9 bonds in both cases with the dative M1–S1' bond being 0.05–0.07 Å longer than the other M–S bonds. In both complexes the angles around the metal centre are all less than 90° showing a definite tightening of the structure. This is most likely due to the naphthalene backbone restricting the ability of the sulfur donor atoms to adopt more idealised positions.

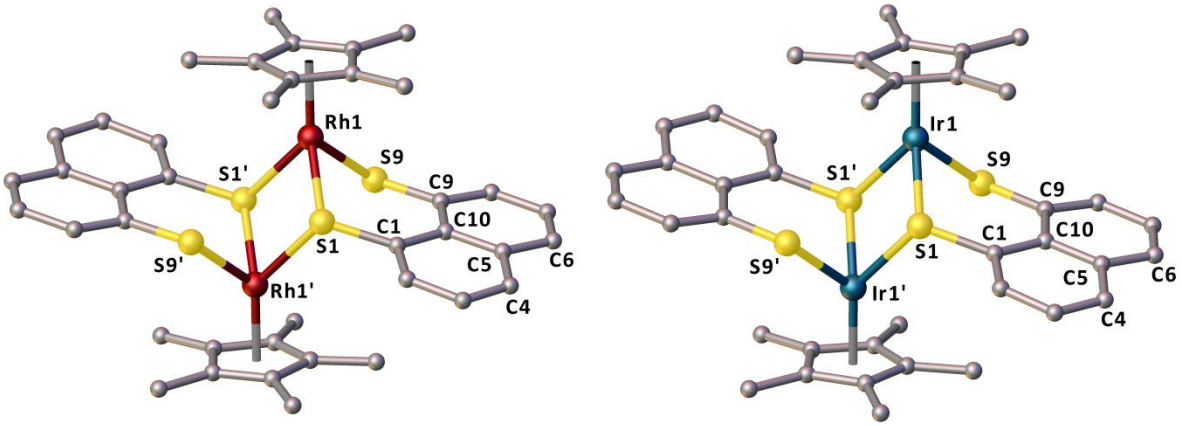

Figure 67: Crystal structures of **C4**-**3b** (left) and **C4**-**4b** (right). Hydrogen atoms are omitted for clarity.

Table 10: Selected bond lengths [Å], angles [°], torsion angles [°] and displacements [Å] for **C4**-**3b** and **C4**-**4b**.

	C4-3b	**C4-4b**
M1···M1′	3.5749(8)	3.6204(4)
S1···S9	3.235(2)	3.250(1)
M1–S1	2.321(1)	2.323(1)
M1–S9	2.349(1)	2.355(1)
M1–S1′	2.406(1)	2.392(1)
S1–M1–S9	87.69(4)	88.02(4)
S1–M1–S1′	81.72(4)	79.68(4)
S9–M1–S1′	79.30(4)	78.94(4)
S1–C1···C9–S9	11.17(3)	11.1(3)
C1–C10–C5–C6	175.25(3)	179.1(4)
C9–C10–C5–C4	179.76(4)	175.0(4)
Splay Angle[a]	20.8(9)	21.4(7)
Out of plane displacements		
S1	0.245	0.194
S9	0.175	0.208
M1	1.172	1.181

[a] calculated as (S1–C1–C10 + C1–C10–C9 + C10–C9–S9) − 360.

The restrictive nature of the backbone is further evidenced by an increase of 5.7° in the S1–C1···C9–S9 torsion angle compared to **H_2B** as the sulfur atoms move apart to accommodate the metal. The out-of-plane displacement of the sulfur atoms is larger than we have seen before, mirroring the larger torsion angles. The least energetically demanding conformation that allows the metal to insert between the sulfur atoms is by moving the atoms out of the plane, hence the observed increase in

these values. There is also a pronounced buckling of the central naphthalene ring system as shown by the C1–C10–C5–C6 and C9–C10–C5–C4 torsion angles.

4.3.2 – Cationic bimetallic complexes

In previous work where the Woollins group have used both **H_2B** and **H_2C** there has been little difference in the structure of the complex formed.[165,190] It was surprising then when the reaction yields using **H_2C** were far lower than those seen for **H_2B**. In the case of the **C4**-**4c** the yield was only 2% which provided enough material to analyse by ^{1}H NMR spectroscopy. The yield of 52% obtained for **C4**-**3c** allowed for a more thorough analysis to be conducted.

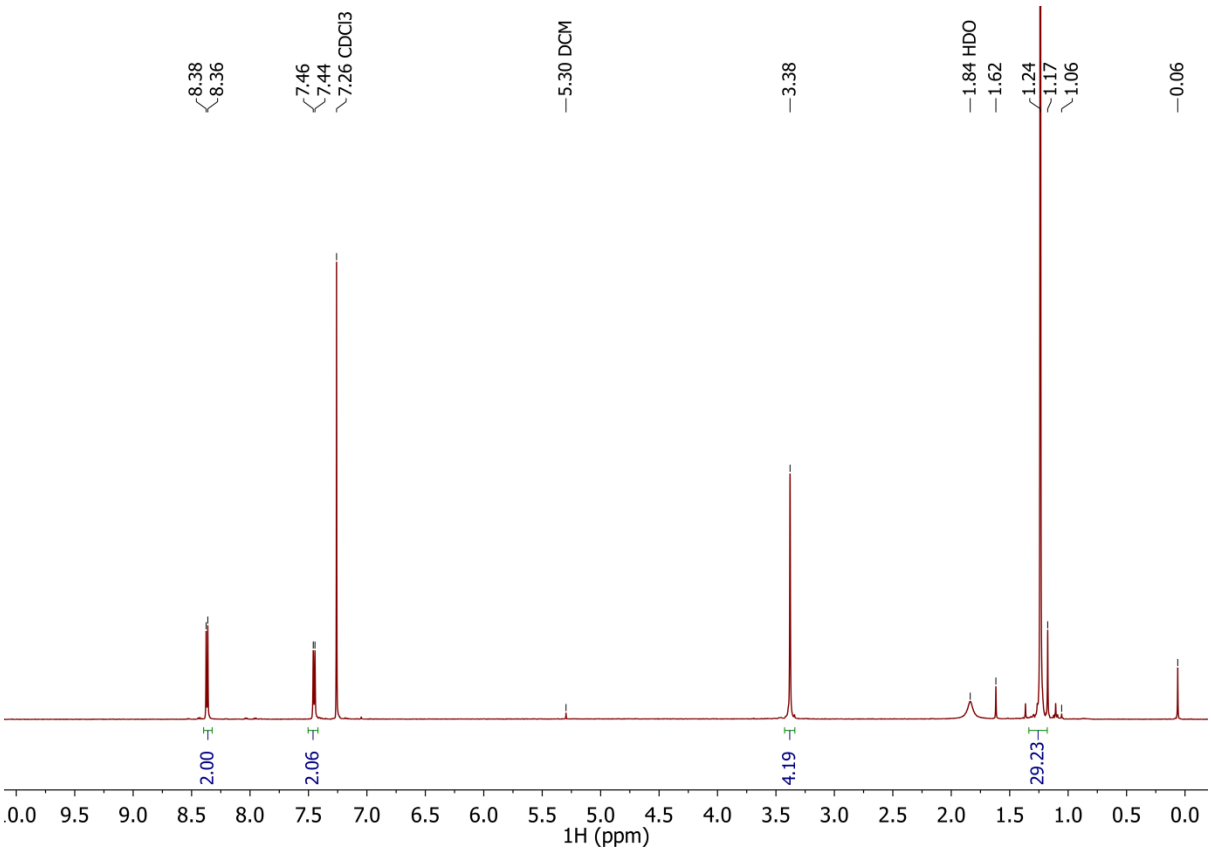

Figure 68: ^{1}H NMR spectrum ($CDCl_3$, 500 MHz) of the product obtained when using **H_2C**.

The ^{1}H NMR spectrum of the product obtained when using **H_2C** in the reaction is shown in Figure 68. Two things immediately stood out when examining the spectrum. Firstly, the presence of only two signals in the aromatic region suggested that in this case the complex had not formed the dimeric structure seen previously. Secondly, by examining the integrals from the aromatic and methyl Cp* protons we could see a 1:2 ratio of dithiolate to Cp*; this observation ruled out the possibility that a stable 16e$^-$ species may have formed in a similar fashion to **C4**-**4a**. In our previous work with ligand **B** we have seen the formation of bimetallic complexes where the dithiolate bridges two metal centres

(this was discussed in section 3.4.4.2 and shown in Figure 53).[191] A similar structure was proposed here with the dithiolate ligand displacing two of the chlorides with the sulfur lone pairs then donating to each of the metal centres to fill the vacant coordination site (Figure 69, left). The ^{1}H NMR spectrum obtained from the iridium complex supported this as the same features were seen.

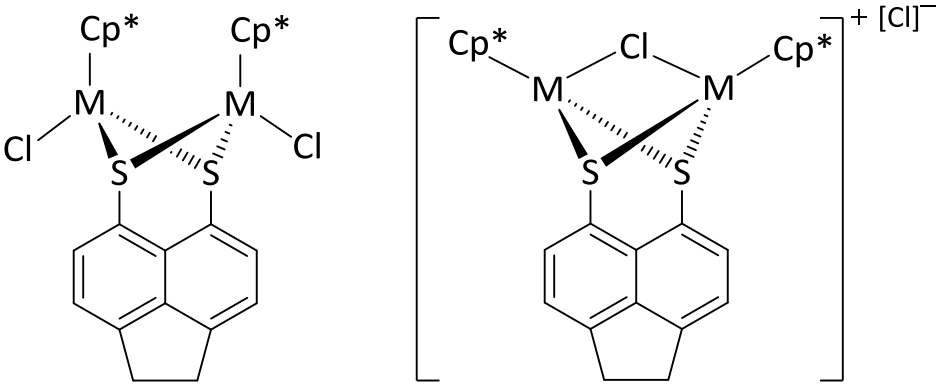

Figure 69: Possible structure for **C4**-**3c** and **C4**-**4c**, proposed (left) and actual (right).

Further characterisation of **C4**-**3c** was carried out with the ^{13}C{^{1}H} NMR spectrum showing the expected signals with all the quaternary carbon atoms clearly visible. The coupling between the quaternary Cp* carbon and rhodium is higher than that seen previously at 7.4 Hz. The IR and Raman spectra showed the expected peaks with one peak in the Raman spectrum being in the region for a Rh–Cl bond. The mass spectrum of the complex showed one distinct peak at *m/z* 727.02 which corresponds to $[M]^{+}$. Elemental analysis was also obtained matching the proposed formula. Crystals suitable for X-ray work were obtained from a diffusion of diethyl ether into a DCM solution containing the complex. The structure obtained is shown in Figure 69 (right) the similarity between the proposed and actual complex is clear with the obtained data fitting both structure types. This structure could represent an intermediate complex formed on the way to the neutral dimeric form already seen in **C4**-**3b** and **C4**-**4b**. If **H_2C** is reacting slower this would explain the low yield obtained and possibly the isolation of this intermediate. Initial attempts at driving the reaction forwards involved increasing the reaction time however this did not result in improved yields or any evidence of the neutral dimeric structure.

Further attempts at synthesising the neutral dimeric structure type using ligand **C** were made by following the procedure employed by Suzuki.[162] It was hoped that by forming the dithiolate through deprotonation using sodium methoxide this would be a more reactive species and the expected product would form. Several attempts using this method were made with conditions that included refluxing the reaction for between seven and forty-eight hours. However, in all cases only the

cationic complexes **C4**-**3c** and **C4**-**4c** were isolated as the products. Greatly improved yields were observed using this method (**C4**-**3c** 83% and **C4**-**4c** 98%) with Scheme 29 detailing the best conditions.

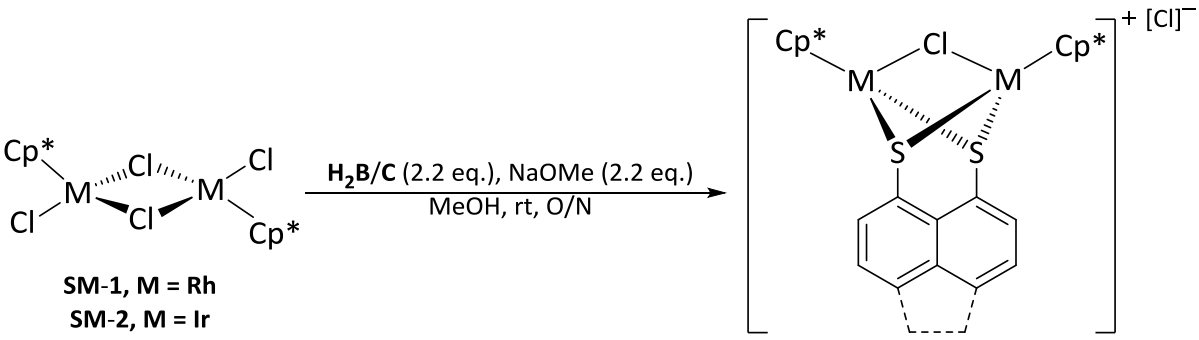

SM-1, M = Rh
SM-2, M = Ir

acenaphthene	naphthalene
C4-3c, M = Rh	**C4-5b, M = Rh**
C4-4c, M = Ir	**C4-6b, M = Ir**

Scheme 29: Improved synthetic route to **C4**-**3c** and **C4**-**4c** and the synthesis of **C4**-**5b** and **C4**-**6b**.

Since attempts at trying to form the neutral complex with the acenaphthene ligand were unsuccessful we chose to try and prepare the naphthalene analogue of the cationic complex. This was easily done using the conditions shown in Scheme 29. Complexes **C4**-**5b** and **C4**-**6b** were isolated in yields of 58% and 75% respectively after purification by column chromatography with small amounts of the neutral dimeric complexes **C4**-**3b** and **C4**-**4b** also isolated.

The ^{1}H NMR spectrum of **C4**-**5b** and **C4**-**6b** displayed three distinct signals in the aromatic region corresponding to the naphthalene backbone. The methyl Cp* signals were both shifted upfield compared to their respective starting materials. As in the acenaphthene examples, the structure of the complex was alluded to by the 1:2 ratio observed between the ligand and Cp* signals. The ^{13}C{^{1}H} NMR spectra of the complexes were consistent with the formation of the cationic complex. The coupling between the quaternary Cp* carbon and rhodium in **C4**-**5b** was similar to that observed in **C4**-**3b** at 7.6 Hz. Both **C4**-**5b** and **C4**-**6b** displayed base peaks in their mass spectra which corresponded to $[M]^{+}$ (**C4**-**5b** *m/z* 701.00, **C4**-**6b** *m/z* 880.99). Analytical purity of **C4**-**4c**, **C4**-**5b** and **C4**-**6b** was determined by elemental analysis.

4.3.2.1 – Crystallographic characterisation of C4-3c/4c and C4-5b/6b

For all of these cationic complexes, crystals suitable for X-ray work were obtained by slow diffusion of ether into a solution of the complex in DCM. The crystal Structures of **C4**-**3c**/**4c** and **C4**-**5b**/**6b** are

shown in Figure 70 with selected structural parameters in Table 11. The complexes were found to be isostructural all adopting the same piano stool structure seen previously.

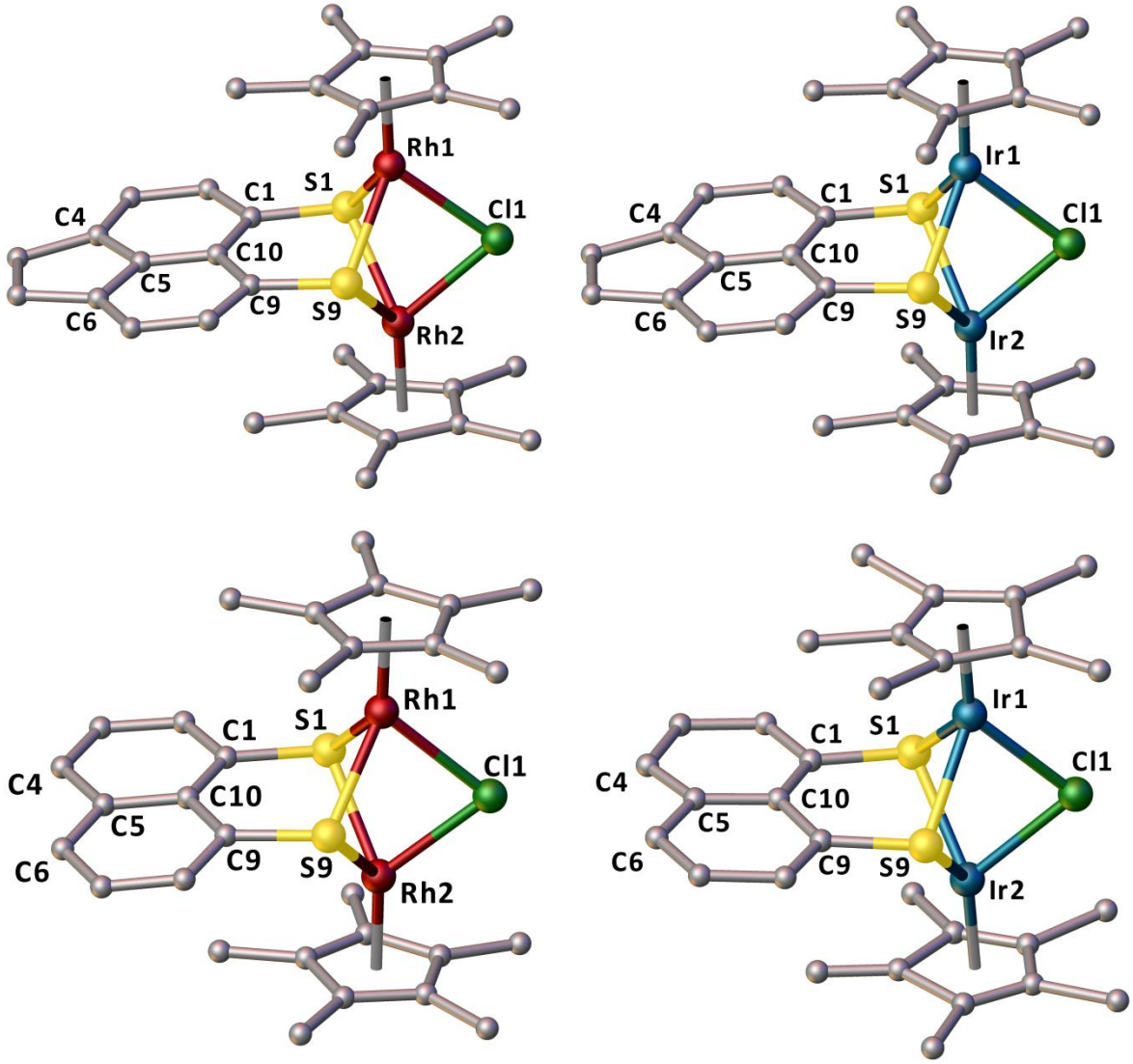

Figure 70: Crystal structures of **C4**-**3c** (top left), **C4**-**4c** (top right), **C4**-**5b** (bottom left) and **C4**-**6b** (bottom right). Hydrogen atoms and chloride counterions are omitted for clarity. Co-crystallised solvent molecules (**C4**-**3c** (H_2O), **C4**-**5b** (Et_2O) & **C4**-**6b** ($CHCl_3$)) are also omitted for clarity.

In these structures both the sulfur atoms are acting as μ^2-bridges between the two metal Cp* centres with one of the bridging chlorine atoms retained from the starting material. The M···M distance in **C4**-**3c** and **C4**-**4c** is much shorter than those observed in the neutral dimeric complexes. A direct comparison between the two structure types is possible for the naphthalene examples. In **C4**-**5b** the M···M distance is 0.36 Å shorter compared to **C4**-**3b** whilst in the iridium analogues it is 0.31 Å shorter. The S···S distance has decreased by 0.13 Å and 0.16 Å in **C4**-**3c** and **C4**-**4c** respectively; this is

the first time a decrease in this value has been observed in our complexes with the rigid backbone *cf.* the free ligand. We also see that the S···S distance is shorter in **C4**-**5b** and **C4**-**6b** *cf.* the dimeric examples and are comparable to the distance seen in the pro-ligand indicating there is little change upon complexation to the metal. The M–S bond lengths in all of the complexes are similar to those observed throughout the previous examples with M–Cl bond lengths comparable to the starting materials.

Table 11: Selected bond lengths [Å], angles [°], torsion angles [°] and displacements [Å] for **C4**-**3c**/**4c** and **C4**-**5b**/**6b**.

	C4-**3c**	**C4**-**4c**	**C4**-**5b**	**C4**-**6b**
M1···M2	3.2045(5)	3.3024(5)	3.216(2)	3.307(1)
S1···S9	3.058(2)	3.027(2)	3.004(6)	2.975(5)
M1–S1	2.3739(6)	2.387(2)	2.375(5)	2.382(4)
M1–S9	2.3708(7)	2.386(2)	2.358(4)	2.382(4)
M1–Cl1	2.4754(6)	2.476(2)	2.471(5)	2.458(6)
S1–M1–S9	80.08(2)	78.72(6)	78.8(1)	77.3(1)
S1–M1–Cl1	80.81(2)	78.50(6)	81.0(2)	77.9(1)
S9–M1–Cl1	80.96(2)	78.26(6)	80.9(2)	77.9(1)
S1–C1···C9–S9	2.72(1)	2.5(4)	3.4(9)	0.0(7)
C1–C10–C5–C6	178.4(2)	178.7(7)	177.9(2)	176.3(2)
C9–C10–C5–C4	179.1(2)	179.8(7)	173.6(2)	−176.3(2)
Splay Angle[a]	15.69(6)	14.14(7)	14.7(4)	13.4(4)
Out of plane displacements				
S1	0.044	0.052	0.017	0.018
S9	0.168	0.174	0.225	0.018
M1	1.499	1.547	1.494	1.690
M2	1.700	1.747	1.713	1.616

[a] calculated as [(S1–C1–C10 + C1–C10–C9 + C10–C9–S9)–360].

The angles around the metal centre within each complex are all similar and represent the most consistent set of values observed throughout this series of complexes. In all cases they are well below the ideal angle of 90° as the rigid backbones limit the movement of the sulfur donor atoms. This symmetrical tightening of the structure supports the decrease in the S···S distance observed in **C4**-**3c** and **C4**-**4c**. In addition, the splay angle has decreased to 15.69(6)° and 14.14(7)° in **C4**-**3c** and **C4**-**4c** respectively. Whilst in the naphthalene examples we see an increase in the splay angle, due to the more restrictive nature of the naphthalene backbone of the pro-ligand compared to the acenaphthene. There is a decrease in the S1–C1···C9–S9 torsion angle in **C4**-**3c** and **C4**-**4c** compared to the pro-ligand as the strain on the sulfur atoms is slightly reduced due to the low coordination

angles around the metal. The buckling of the acenaphthene backbone is comparable to the pro-ligand as is the out-of-plane displacement of the sulfur atoms. For **C4**-**5b** and **C4**-**6b** we see two very different splay angles; the rhodium complex has a value similar to that of the pro-ligand whilst the iridium value is zero. This is due to a crystallographically imposed centre of symmetry that runs through the centre of the iridium structure. Looking at the central C1–C10–C5–C6 and C9–C10–C5–C4 torsion angles we can see less strain within the acenaphthene complexes than the naphthalene derivatives. The distance that the metal centres sit away from the plane of the backbones are larger in the cationic complexes compared to the neutral dimeric ones. This is a consequence of the change in binding modes of the second sulfur atom of the ligand on going between the two structure types.

4.3.3 – Dicationic multimetallic complexes

Only the reaction using **SM**-**1** proved to be successful when using **H_2D** as when **SM**-**2** was used an insoluble sticky solid was obtained as the product which could not be identified. The reaction utilising **H_2D** resulted, at first, in an intriguing ^{1}H NMR spectrum following purification by column chromatography (Figure 71). The purification process itself required a DCM/ethanol mixture to elute what was believed to be the product band. This was also the case for **C4**-**3c**/**4c** and **C4**-**5b**/**6b** which immediately implied that an ionic complex may have formed. The aromatic region of the ^{1}H NMR spectrum mainly consisted of overlapping multiplets with a few more distinct signals shifted downfield. Two signals that could be assigned as methyl Cp* protons were also present, shifted upfield compared to the starting material. Examining the integrals provided interesting results with a rough 3:4 ratio of dithiolate to Cp* observed. The appearance of two distinct Cp* signals was also puzzling as this suggested two different rhodium environments. The ^{13}C{^{1}H} NMR spectrum also contained more signals than there should be if one of the previously seen structural types had been formed.

In order to aid the analysis the NMR sample ($CDCl_3$) was layered with ether to see if crystals suitable for X-ray work could be obtained. The multimetallic structure of **C4**-**3d** shown in section 4.3, Scheme 28 (page 96), was obtained. Re-examining both the ^{1}H and ^{13}C{^{1}H} NMR data led to the conclusion that this structure could indeed be representative of the bulk material. The observed ligand to Cp* ratio (^{1}H NMR spectrum) would be correct for this complex and the number of carbon signals (^{13}C{^{1}H} NMR spectrum) also matched this proposed structure. The mass spectra obtained showed a base peak that could be assigned to one of the dinuclear fragments and one ligand breaking off *m/z* 909.06. The peak corresponding to $[M]^{2+}$ which appears at *m/z* 800.05 was less than 5% intensity

showing the ease at which the complex fragments. Unfortunately several attempts at obtaining elemental analysis proved to be unsuccessful.

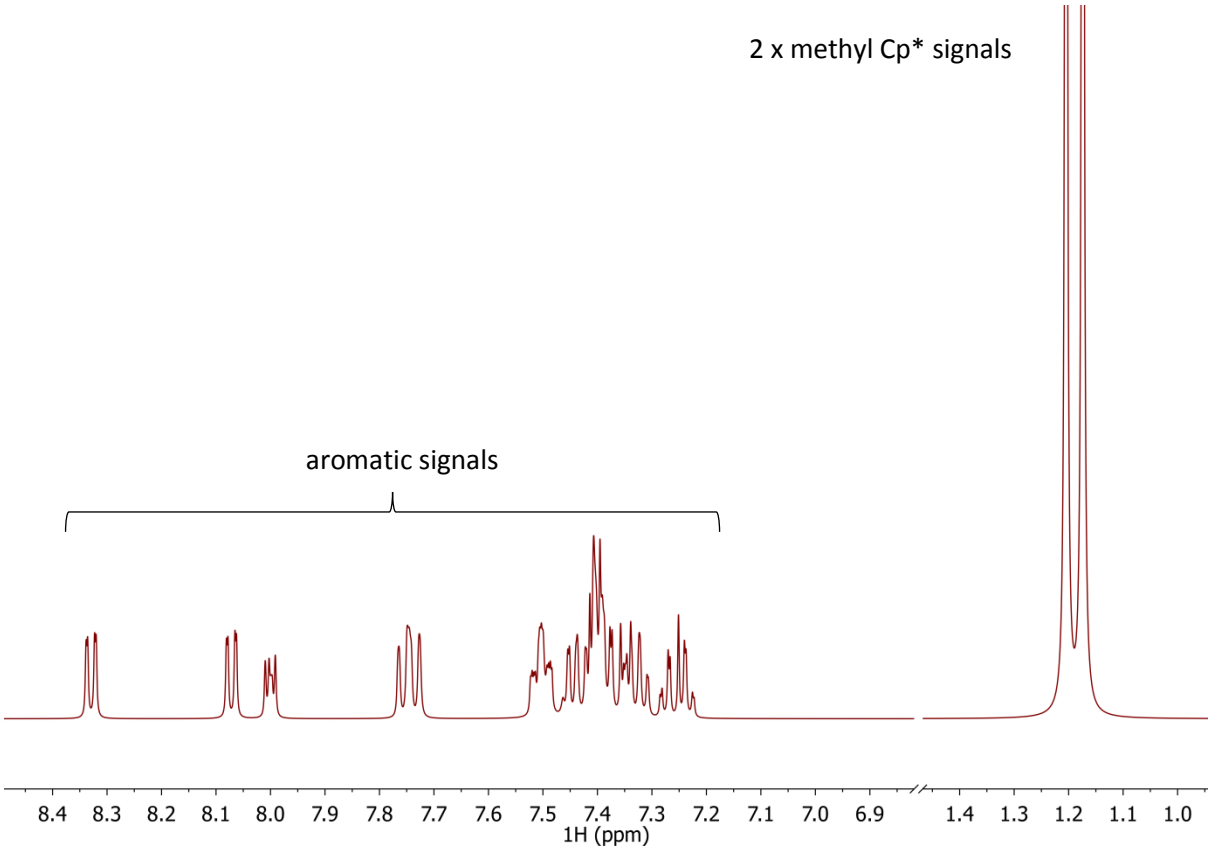

Figure 71: ^{1}H NMR spectrum ($CDCl_3$, 500 MHz) of **C4**-**3d** after purification. Small impurity peaks (**S_2D**, **H_2D**) and solvent ($CDCl_3$) have been removed for clarity.

4.3.3.1 – Crystallographic characterisation of C4-3d

The crystal structure of **C4**-**3d** is shown in Figure 72 with selected structural parameters in Table 12. Crystals suitable for X-ray work were obtained *via* two methods; the first was described above in section 4.3.3, the second method involved slow diffusion of ether into a DCM solution containing the complex, these crystals provided the best data. At first glance the structure looks quite different to anything observed previously. However, if one imagines the μ^4-bridging dithiolate ligand as linking two bimetallic moieties we can see that the sulfur atom has merely replaced the chlorine present in the structures of **C4**-**3c**/**4c** and **C4**-**5b**/**6b**. This multimetallic complex forms due to the rotational freedom present between the two aryl rings of the biphenyl dithiolate ligand. Within the complex two different binding modes of the dithiolate ligand were observed, with two terminal chelating ligands and one bridging ligand. The dicationic charge comes from the presence of four rhodium(III) centres being coordinated to only six thiolate sulfur atoms and four Cp* ligands with two chloride counterions balancing this 2+ charge.

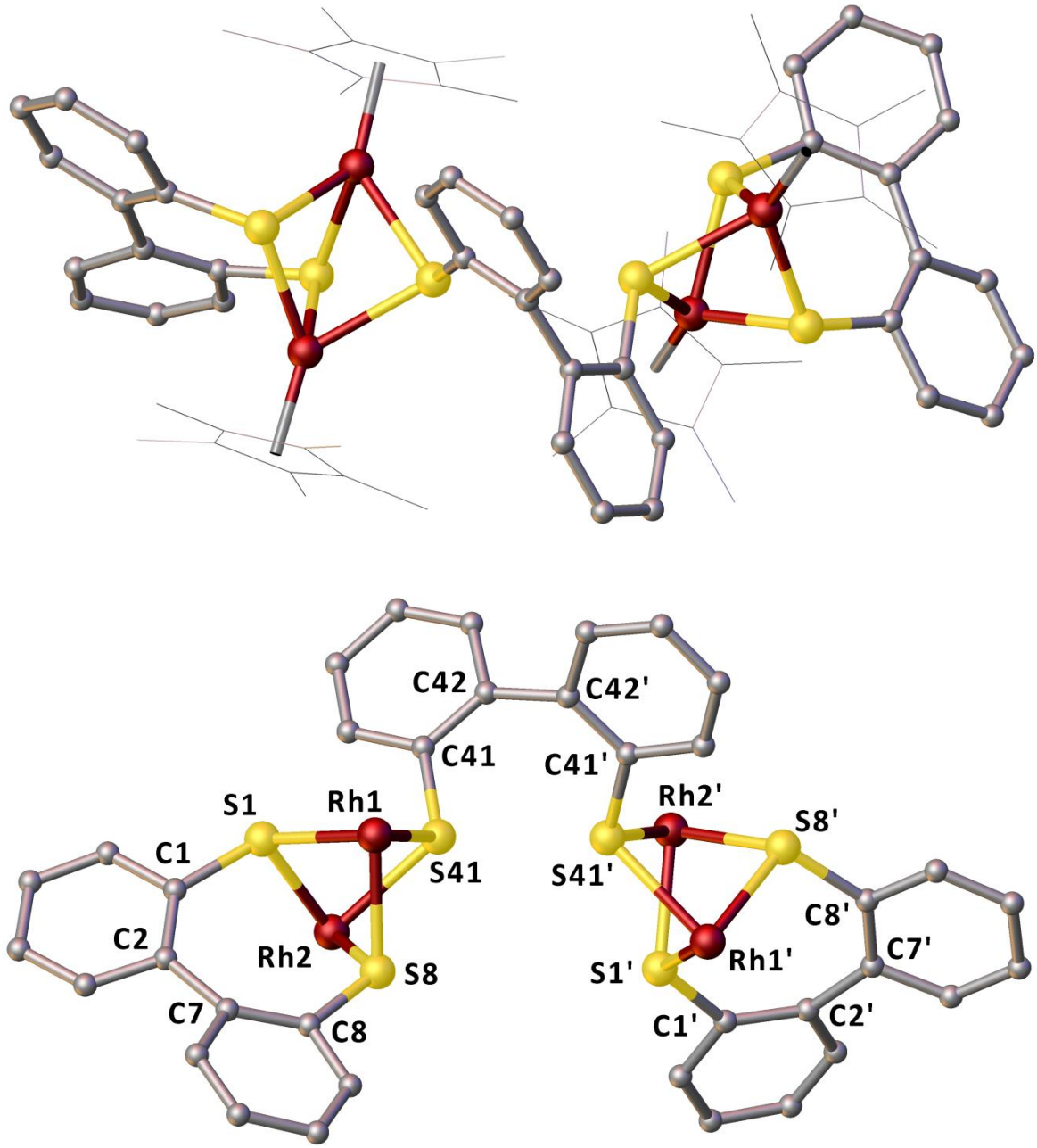

Figure 72: Crystal structure of **C4**-**3d** with Cp* ligands wire framed (top) and removed (bottom). Hydrogen atoms and chloride counterions are omitted for clarity. Co-crystallised solvent molecules (DCM) are also omitted for clarity.

A crystallographically imposed centre of symmetry running through the aryl–aryl bond of the bridging dithiolate ligand is present within the structure. The S···S distance in the μ^2-bridging ligands are shorter by 0.84 Å compared to the pro-ligand. With the Rh···Rh distance (3.283(1) Å) being similar to those previously seen for the ionic rhodium complexes **C4**-**3c** and **C4**-**5b**. Two distinct Rh–S bond lengths from the μ^2- and μ^4-bridging ligands are seen within the structure. The μ^2-bridging

ligand has Rh–S bond lengths ranging from 2.336(2)–2.383(2) Å which are similar to those we have previously observed in **C4**-**3c** and **C4**-**5b**. However the μ^4-bridging ligand shows Rh–S bond lengths in the range of 2.449(2)–2.466(2) Å which are similar to lengths observed in **C4**-**3b**. Unlike the other charged complexes presented here, the non-Cp* angles around the metal centre show a wide range (74.67(5)°–80.09(5)°). This is likely due to the steric demands of the biphenyl backbone preventing the sulfur atom (S41) from adopting a more idealised position. The aryl-aryl torsion on the μ^4-bridging ligand is 69.2(9)° which is similar to that observed for the pro-ligand whilst the μ^2-bridging ligand shows a significant decrease to 28(1)° upon binding to the two rhodium centres. The out-of-plane displacements of the sulfur atoms have increased compared to the pro-ligand for the μ^2-bridging ligand but decreased in the case of the μ^4-bridging ligand.

Table 12: Selected bond lengths [Å], angles [°], torsion angles [°] and displacements [Å] for **C4**-**3d**.

	3d		
Rh1···Rh2	3.283(1)	S1···S8	3.026(3)
Rh1–S1	2.366(2)	Rh2–S1	2.343(2)
Rh1–S8	2.336(2)	Rh2–S8	2.383(2)
Rh1–S41	2.466(2)	Rh2–S41	2.449(2)
S1–Rh2–S41	75.41(5)	S8–Rh2–S41	78.61(5)
S8–Rh1–S41	79.16(5)		
C1–C2–C7–C8	28(1)	C41–C42–C42'–C41'	69.2(9)
Out of plane displacements			
S1	0.141	S41	0.035
S2	0.301		

4.4 – Conclusions

We have prepared and characterised a series of Rh(III) and Ir(III) η^5-Cp* half sandwich complexes by chloride ligand replacement reactions of $[Cp^*RhCl_2]_2$ and $[Cp^*IrCl_2]_2$ with a series of dithiols attached to aromatic backbones. This work demonstrates the utility and versatility of these sulfur ligands in organometallic complexes. The ligands have shown remarkable variety in the type of complexes formed. A subtle change in the organic backbone (naphthalene to acenaphthene) resulted in a profound difference in the structure of the complex formed. In addition, the introduction of rotationally free backbone produced yet another type of structure. Single crystal X-ray diffraction confirmed these three distinct complex classes; such a variety is achieved through the utilisation of κ^1 and κ^2 bonding of the sulfur donor atoms and *via* chelating and bridging coordination modes of the dithiolate ligands. Additionally, a structural characterisation of the pro-ligands benzene-1,2-

dithiol, naphthalene-1,8-dithiol, acenaphthene-5,6-dithiol and [1,1'-biphenyl]-2,2'-dithiol has been conducted using single crystal X-ray diffraction. This allowed comparisons to be made between the free and bound ligand in the solid state demonstrating the varying levels of strain experienced by each ligand type.

The work presented in this chapter has contributed to the following publications:

Structural diversity of bimetallic rhodium and iridium half sandwich dithiolato complexes: Phillip S. Nejman, Brian Morton-Fernandez, David J. Moulding, Kasun S. Athukorala Arachchige, David B. Cordes, Alexandra M. Z. Slawin, Petr Kilian, J. Derek Woollins, *Dalton Trans.*, **2015**, *44*, 16758–16766.

The preparation and characterisation of rhodium(III) and iridium(III) half sandwich complexes with naphthalene-1,8-dithiolate, acenaphthene-5,6-dithiolate and biphenyl-2,2'-dithiolate: Phillip S. Nejman, Brian Morton-Fernandez, Nicholas Black, David B. Cordes, Alexandra M. Z. Slawin, Petr Kilian, J. Derek Woollins, *J. Organomet. Chem.*, **2015**, *776*, 7–16.

Chapter 5 – Monomeric Rhodium and Iridium Dithiolato Complexes with Neutral Phosphine/Phosphite Donors

5.1 – Introduction to Monomeric Dithiolato Complexes

As we saw in chapter 4 the bimetallic complexes are formed through the need to comply with Langmuir's Law. This results in a lone pair from one or both of the sulfur atoms being used to form a dative bond to fill a vacant coordination site around the metal. If another atom capable of donating a lone pair was incorporated into the system, then monometallic complexes should be isolated. Phosphines, and to a lesser extent phosphites, are widely utilised in transition metal chemistry. They are neutral donor ligands capable of binding to a wide range of metals in various oxidation states.[239] Metal phosphine complexes have many uses in the field of homogeneous catalysis with several prominent examples known such as Wilkinson's catalyst, Grubbs' catalyst and *tetrakis*(triphenylphosphine)palladium(0), $[Pd(PPh_3)_4]$ (Figure 73).

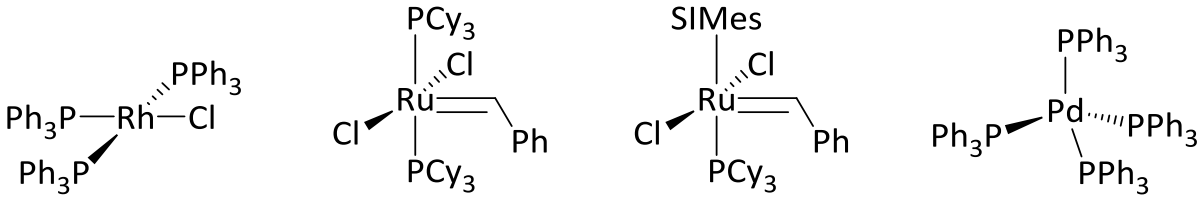

Figure 73: Transition metal phosphine complexes used in catalysis.

Wilkinson's catalyst has been extensively used in the hydrogenation of alkenes[240] with other uses including hydroboration of alkenes[241] and the selective 1,4-reduction of α,β-unsaturated carbonyl compounds in conjunction with triethylsilane.[242] Grubbs' catalysts are active in olefin metathesis; their success is due to their tolerance of functional groups on the alkene, compatibility with a wide range of solvents and air stability.[243] There have been several generations of the Grubbs' catalyst, the first generation involved the use of two tricyclohexylphosphine ligands with the second generations having one of these ligands replaced with an NHC. The palladium complex, $[Pd(PPh_3)_4]$,

is widely used as a catalyst in coupling reactions such as the Heck reaction and Suzuki coupling.[244] Phosphites ($P(OR)_3$) also have uses in catalysis with nickel complexes catalysing the hydrocyanation of alkenes.[244]

5.1.1 – Dithiolato rhodium and iridium complexes with phosphorus ligands

Given the relatively small amount of literature available on the aromatic dithiolato ligands studied in this work thus far, it should be of no surprise that examples of complexes with additional phosphorus ligands are even rarer. Searches for rhodium and iridium complexes with aromatic dithiolate and phosphorus ligands provided only a few results, most of which have been discussed previously in chapter 3. The HCDTN ligand has been used to form a rhodium complex with one chloride and two triphenylphosphine ligands.[188] Iridium complexes of this type are also scarce with the only examples prepared by Teo and co-workers during their work on bimetallic systems.[184,185] There were no examples of biphenyl dithiolate rhodium or iridium complexes with phosphorus ligands. Only complexes using related dithiolates based on the 1,1'-binaphthalene and 4,4'-biphenanthrene backbone are known.[202,203] Rhodium complexes of this type have been reported utilising the $BenzS_2$ ligand by Herberhold,[245] Ghilardi[246] and Sellmann.[247] To the best of our knowledge no iridium versions of these complexes have yet been reported.

Expanding the search to include any dithiolate ligand provided some more literature examples of monometallic rhodium and iridium complexes. Several research groups have reported the synthesis of rhodium and iridium complexes bearing both polysulfur and phosphine ligands. Wakatsuki and co-workers were one of the first groups to prepare a series of half sandwich rhodium complexes containing polysulfur ligands (RhS_X, X = 4, 5, 6) and a triphenylphosphine ligand.[248] They reacted $[CpRh(PPh_3)_2]$ with excess elemental sulfur in benzene at room temperature overnight. Purification by column chromatography on alumina resulted in three distinct bands. The complexes shown in Figure 74 (top row) were isolated with the RhS_5 and RhS_6 complexes characterised using single crystal X-ray diffraction. Further examples were prepared using modified Cp ligands resulting in more RhS_4 and RhS_5 complexes in addition to an interesting bimetallic structure (Figure 74, bottom row). Herberhold and co-workers published a series of analogous iridium complexes this time using a trimethylphosphine ligand and Cp* resulting in IrS_4, IrS_5 and IrS_6 rings.[249] In the same paper they also prepared the polyselenium versions of the complexes with examples of both types characterised using single crystal X-ray diffraction. Finally, Shaver and co-workers prepared the same iridium complex with an IrS_4 ring, Cp* and trimethylphosphine ligand by reacting $[Cp^*Ir(SH)_2PMe_3]$ with excess SO_2 in either benzene or DCM at room temperature.[250]

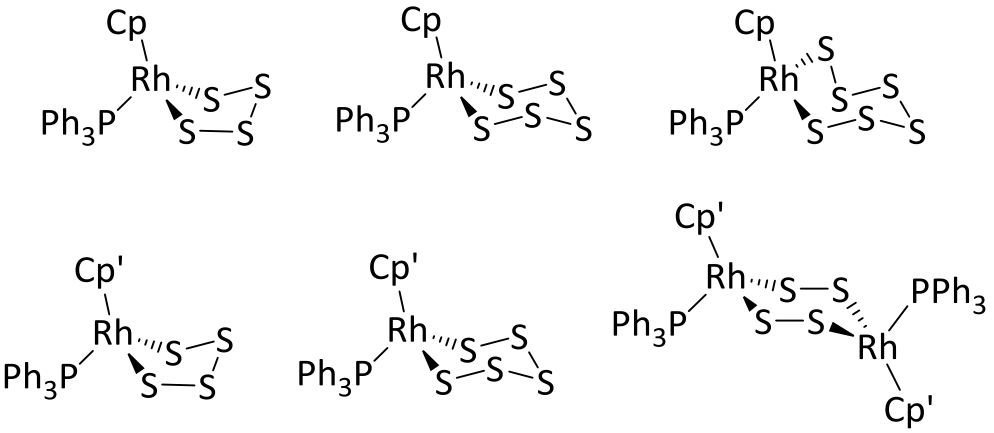

Figure 74: Rhodium complexes incorporating polysulfur, Cp and phosphine ligands.

Another ligand which has seen investigation is methanedithiolate and its structural derivatives. Bergman and co-workers reported a series of monomeric Cp* iridium *bis*(thiolate), *bis*(hydridosulfide), hydrido thiolate and dithiolate complexes. They structurally characterised several of the complexes using single crystal X-ray diffraction and examined their reactivity. During the reactivity study they observed that their metalla dithiol complex reacts with solvent acetone in the presence of catalytic acid to form the dithiolate complex as shown in Scheme 30. The reaction was shown to be reversible with the metalla thiol complex reformed upon reaction of the dithiolate complex with H_2S at 80 °C for twenty four hours (Scheme 30).[251] A rhodium example was reported by Jones and co-workers, they prepared it by reacting the dihydride complex [Cp*RhH_2PMe_3] with CS_2 at 25 °C. They conducted detailed mechanistic studies of the formation of the complex and investigated its reactivity towards CO_2 and OCS.[252]

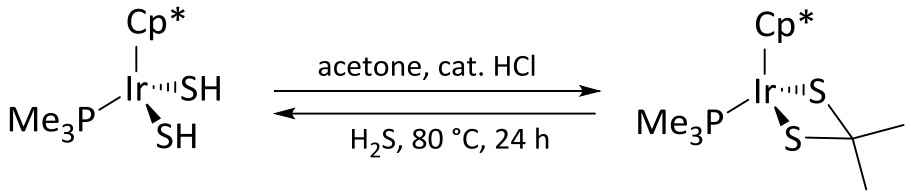

Scheme 30: Reversible formation of an iridium dithiolate complex from a metalla dithiol.

As part of their investigation into the use of iridium complexes to activate unreactive C–F bonds, Hughes and co-workers prepared two dithiolato complexes. They were both obtained from the same reaction and structurally characterised using single crystal X-ray diffraction.[253] One of the complexes contained a methanedithiolate ligand substituted with a CF_3 group (Figure 75, left); the second was similar with a thioether bridging two methanethiolate moieties (Figure 75, right).

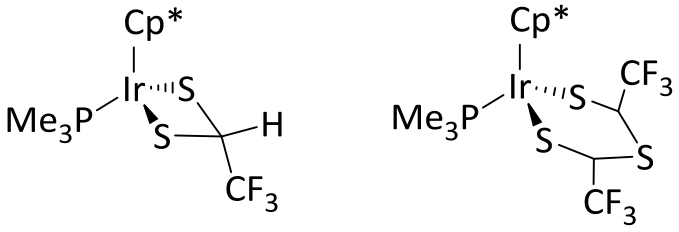

Figure 75: Dithiolate containing complexes prepared by Hughes and co-workers.

The Claus process is widely used to convert H_2S, obtained from the hydrodesulfurisation of petroleum, to sulfur and water. This reaction requires harsh conditions of 200-300 °C and an alumina catalyst. During investigations into the use of iridium based catalysts for this process, Shaver and co-workers prepared two interesting dithiolato complexes (Figure 76). The first was simply prepared by reacting [Cp*Ir(SH)$_2$PMe$_3$] with *N*-sulfinylaniline resulting in the formation of an IrS_3 metalla cycle with the central S atom being mono-oxidised. Secondly, reacting the same starting material with carbon disulfide formed the analogous complex with the S=O fragment replaced with C=S. Both of the complexes were investigated using single crystal X-ray diffraction.[254]

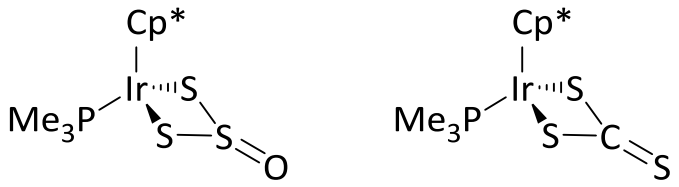

Figure 76: Iridium based catalysts for hydrodesulfurisation of petroleum synthesised by Shaver and co-workers.

In 1992 Herberhold and co-workers prepared a series of rhodium and iridium half sandwich complexes using 1,1'-ferrocene dichalcogenate ligands (Figure 77).[255] They found the iridium complexes to be more stable than the rhodium ones and the tellurium analogues displaying a strong tendency to decompose in air. By reacting these monomeric iridium complexes with elemental sulfur, the phosphine group could be removed resulting in complexes analogous to our neutral bimetallic systems seen in chapter 4. Reaction of these complexes with a different phosphine donor regenerated the monomeric complex. The same dichloro iridium starting materials were also used by Yang in 1995 to prepare monomeric dithiolene complexes. They studied the electrochemical properties and determined the HOMO and LUMO of the complexes.[256]

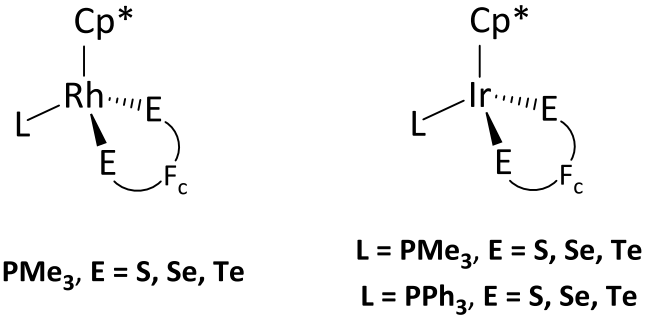

L = PMe_3, E = S, Se, Te

L = PMe_3, E = S, Se, Te
L = PPh_3, E = S, Se, Te

Figure 77: Monomeric rhodium and iridium complexes using 1,1'-ferrocene dichalcogenate ligands.

5.2 – Synthetic Routes to Monomeric Dithiolato Complexes

Having investigated the reaction of the ligands in the formation of bimetallic systems, it was decided to see how these ligands would act in monometallic complexes. There are two synthetic routes which could be considered when preparing monomeric dithiolato complexes. Route 1 involves the formation of our neutral bimetallic system which is then reacted with a suitable phosphorus ligand to break the dimer apart and form the monometallic species. Route 2 is similar but instead of forming a dimeric dithiolato complex, the metal starting materials, which themselves are dimeric, can be reacted with a phosphorus ligand and broken apart to form monomeric starting materials. Both of these routes are outline in Scheme 31.

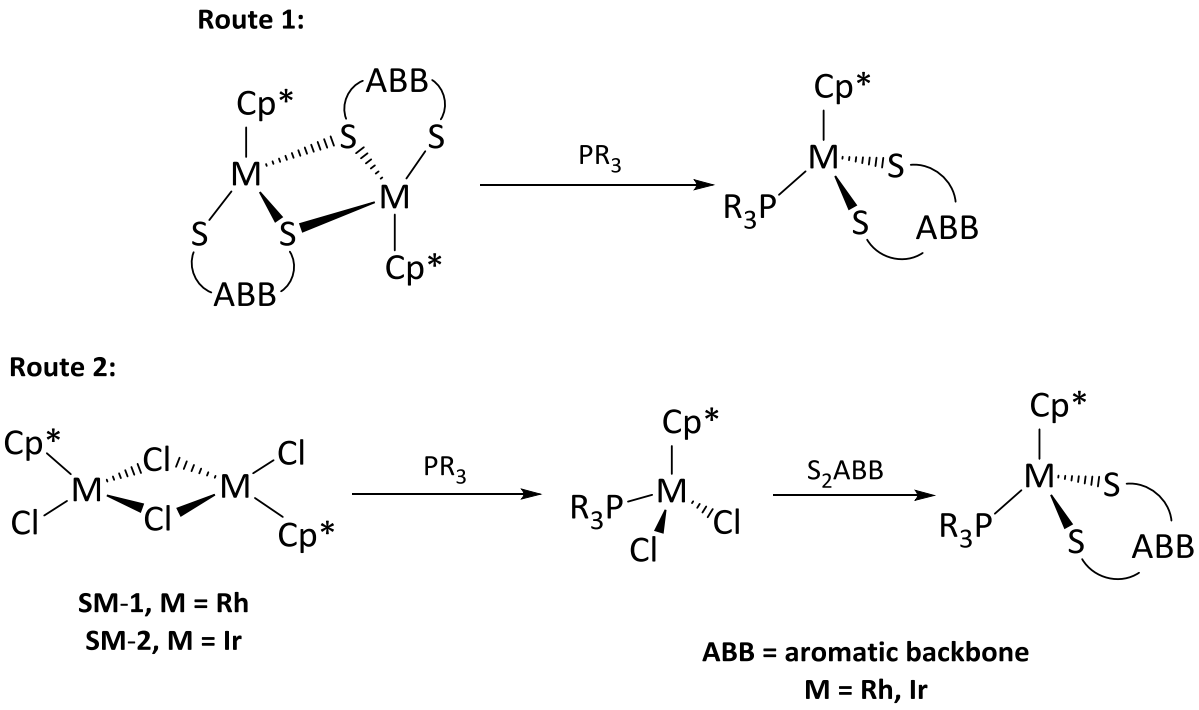

Scheme 31: Two synthetic routes to the formation of monomeric dithiolato complexes.

Route 1 has been successfully used before within the literature,[255] however in the current study only two out of the four ligands resulted in appropriate neutral dimeric complexes that might react with a phosphorus donor atom. The yields for the formation of these complexes are not consistently high for all the ligands. Rhodium and iridium starting materials are not cheap so the highest yielding route would be the most favourable. Route 2 has the advantage of providing high literature yields for the formation of a wide range of complexes with phosphorus ligands. We would expect the addition of our ligands to also result in high yields given the simplicity of the reaction. Taking this into account, along with the ability to test our entire ligand range, route 2 was selected.

5.2.1 – Starting material preparation and new structural characterisation

Having chosen route 2 as the synthetic approach to our monomeric complexes, a series of rhodium and iridium dichloro starting materials were prepared. Previously within the Woollins group the dibromo rhodium complex [Cp*$RhBr_2PMe_3$] had been synthesised. The complex was prepared *via* a two-step method reported in the literature.[257] In order to investigate both structural and spectroscopic changes in our dithiolato complexes with various phosphorus donor ligands, a set of four phosphorus donors were selected; triethylphosphine, triethyl phosphite, triphenylphosphine and triphenyl phosphite. These represented differences in the steric interactions of the phosphorus donor as well as the electronics and were reacted with the $[Cp^*MCl_2]_2$ (M = Rh, Ir) starting materials.

Several of the dichloro complexes of the type [Cp*MCl_2PR_3] required for this study have been previously reported in the literature. The complexes [Cp*MCl_2PPh_3] (M = Rh, Ir) were first reported by Maitlis in 1969,[258] with Ara and co-workers reporting using a similar procedure to prepare [Cp*MCl_2PEt_3] (M = Rh, Ir).[259] The rhodium analogue of [Cp*$MCl_2P(OEt)_3$] was reported by Isobe in 1994[260], however to the best of our knowledge no iridium analogue of this complex has yet been reported. In addition, no synthetic procedures to the rhodium or iridium dichloro complex using triphenyl phosphite have been reported. A search using the SciFinder® web portal did result in one paper for the [Cp*$IrCl_2P(OPh)_3$] complex but no synthetic method was provided.[261] The synthetic routes to the starting materials are outlined in Scheme 32.

The monomeric dichloro complexes were easily obtained with isolated yields ranging from 69–99% following the appropriate work up. For **C5**-**3**–**C5**-**8** this involved removal of the solvent and drying under vacuum; in the case of **C5**-**9** and **C5**-**10**, the complexes were washed with petroleum ether 40-60 then dried under vacuum. The rhodium complexes were all isolated as red or dark red solids with

the iridium versions being yellow or orange/yellow. All of the complexes were characterised by ^{1}H, $^{13}C\{^{1}H\}$, ^{31}P NMR spectroscopy, mass spectrometry and IR/Raman spectroscopy.

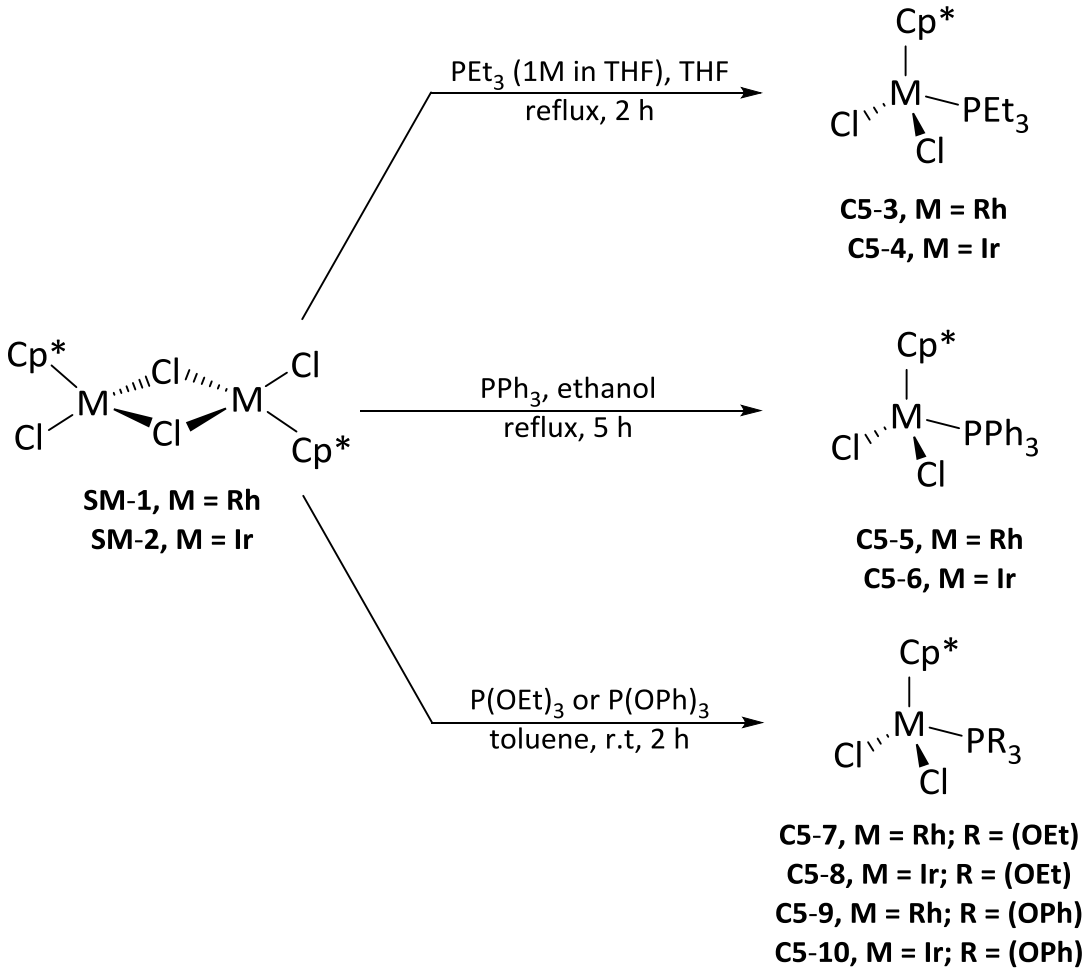

Scheme 32: Synthetic routes to dichloro rhodium and iridium starting materials.

The $^{31}P\{^{1}H\}$ NMR spectra of the complexes are shown in Figure 78. The rhodium examples all appear as doublets as the phosphorus nuclei couples to the NMR active spin ½ rhodium nuclei. The coupling constants ranged from 137.5–240.0 Hz, with the two phosphine donor complexes being at the lower end of the range and the phosphites being at the higher end. In all cases the rhodium complexes displayed signals shifted downfield compared to the iridium analogues which are all singlets.

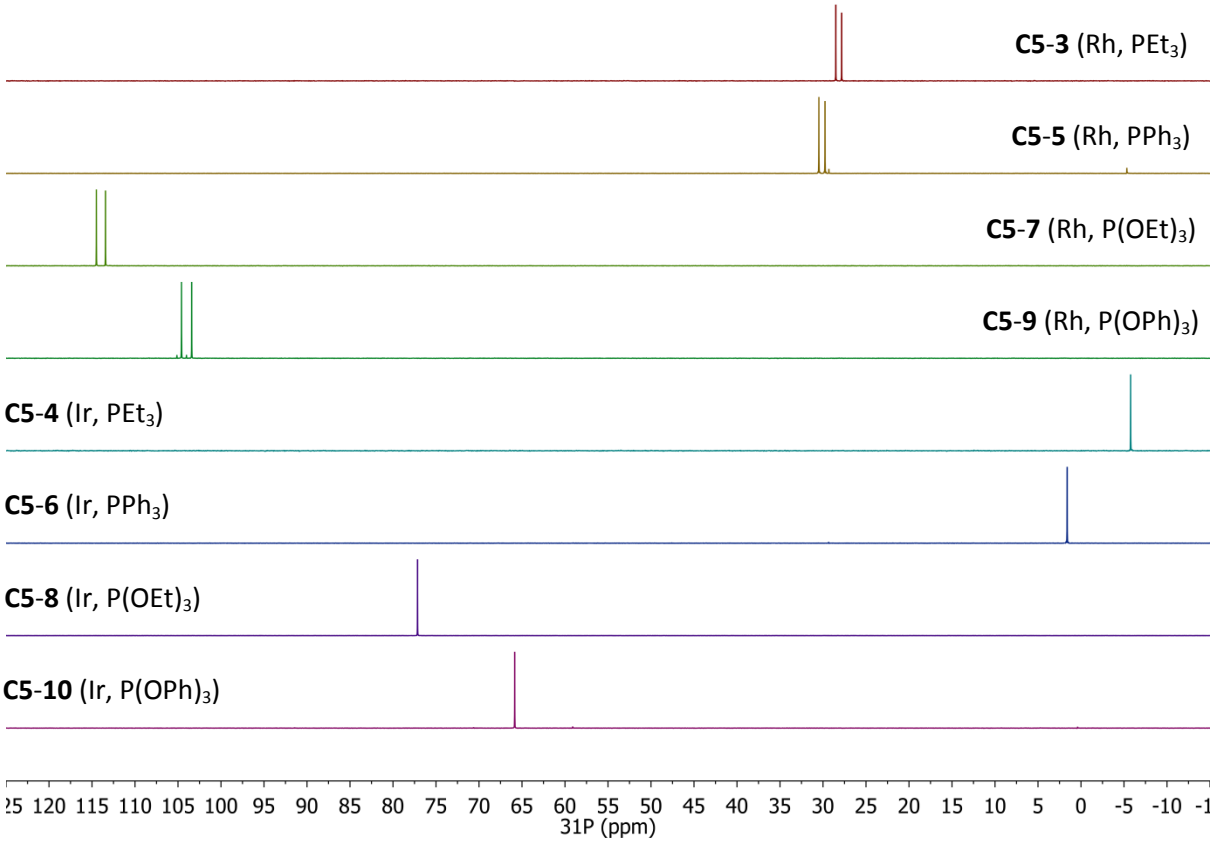

Figure 78: $^{31}P\{^{1}H\}$ NMR spectra ($CDCl_3$, 202 MHz) of the rhodium and iridium dichloro starting materials.

The ^{1}H NMR spectra of all the complexes displayed the expected signals following the addition of the phosphorus donor ligand. In all the spectra, the signal from the methyl protons of the Cp* ligand are split into doublets by long range $^{4}J_{HP}$ coupling. For the rhodium complexes this ranged from 3.1–5.9 Hz whilst the iridium versions showed slightly smaller values ranging from 1.7–3.6 Hz. The signals appear in a similar position to the starting materials **SM-1** and **SM-2** except for **C5-5** and **C5-6** which are shifted slightly upfield. The triethylphosphine compound **C5-3** shows the expected doublet of quartets for the CH_2 part of the ethyl chain due to coupling to both the phosphorus atom and the CH_3 protons of the ethyl chain. However, for the iridium derivative **C5-4** the analogous signal appears as a multiplet. For compounds **C5-7/8** the CH_2 signals appear as *pseudo*-pentets due to the similar magnitudes of the $^{3}J_{HP}$ and $^{3}J_{HH}$ coupling constants. In **C5-7** and **C5-8** the signals are shifted downfield compared to **C5-3** and **C5-4** respectively due to the presence of the oxygen atom. For **C5-3** and **C5-4** the CH_3 protons of the ethyl chain appear as a doublet of triplets with coupling to both the phosphorus atom and CH_2 protons. For **C5-7** and **C5-8** these signals appear as triplets with no coupling to the phosphorus atom observed. Again, the signals in the triethyl phosphite example are shifted slightly downfield due to the presence of the oxygen atom compared to the triethylphosphine derivative. The complexes bearing the triphenylphosph-ine/ite ligands displayed

mostly multiplet signals for the protons on the phenyl rings. In **C5**-**5** and **C5**-**6** two multiplet signals were observed with the highest shifted arising from the *ortho* protons and the *meta* and *para* protons resulting in overlapping signals. The presence of the oxygen atom resulted in the highest shifted signal being assigned to the *ortho* and *meta* protons in **C5**-**9** and **C5**-**10**. The *para* protons in these complexes resulted in the expected triplet signal shifted upfield. All of the multiplet signals observed from the four complexes were very broad with poorly defined lineshapes. This was a consequence of the free rotation that was able to occur within the phosphorus donor ligand.

The $^{13}C\{^{1}H\}$ NMR spectra of all the complexes displayed the expected signals. For all of the rhodium complexes the quaternary Cp* carbon appears as a doublet of doublets with coupling to both the rhodium and phosphorus nuclei. The analogous signal in the iridium derivatives appeared as a doublet with coupling only to the phosphorus nuclei. Complexes with the ethyl fragment afforded signals with coupling to the phosphorus nuclei with the phosphite examples being shifted downfield compared to the phosphines. For the phenyl derivatives, the carbon atoms in the phosphine complexes were shifted downfield compared to those of the phosphites. In the case of **C5**-**5** and **C5**-**6**, the quaternary carbons of the phenyl rings could not be observed within the $^{13}C\{^{1}H\}$ spectra. The IR and Raman spectra of the complexes were as expected with M–Cl (M = Rh, Ir) stretches observed between 258–299 cm^{-1} in the Raman spectra. All of the mass spectra (ES^{+} or NSI^{+}) displayed peaks corresponding to $[M-Cl]^{+}$ except **C5**-**10** which had a peak at *m/z* 697.17 which matched $[M-Cl_2+OAc]^{+}$. The homogeneity of the complexes was established using elemental analysis. The characterisation data obtained (^{1}H, $^{13}C\{^{1}H\}$, ^{31}P NMR, IR, Raman and Mass spectra) were in good agreement with that previously reported for the known complexes.[257-260]

5.2.1.1 – Crystallographic Characterisation of C5-3/4 and C5-8–C5-11

Despite the majority of the prepared dichloro/dibromo starting materials (**C5**-**3**–**11**) being reported in the literature, only three had been characterised structurally using single crystal X-ray diffraction. Both **C5**-**5** and **C5**-**6** have had crystal structures reported[262,263] along with **C5**-**7**.[264] To the best of our knowledge, the remaining dichloro complexes and the dibromo complex ($[Cp^*RhBr_2PMe_3]$, **C5**-**11**) have not been crystallographically characterised and as such the structures were obtained. Crystals suitable for X-ray work were obtained by slow evaporation from either diethyl ether (**C5**-**3**/**4** & **C5**-**9**–**C5**-**11**) or deuterated chloroform (**C5**-**8**, grown from the NMR sample). The crystal structures of **C5**-**3**/**4** and **C5**-**8**–**C5**-**11** are shown in Figure 79 with selected structural parameters in Table 13 (**C5**-**3**/**4**/**8**) and Table 14 (**C5**-**9**/**10**/**11**). All of the complexes crystallised with one molecule within the asymmetric unit except for **C5**-**10** which had two.

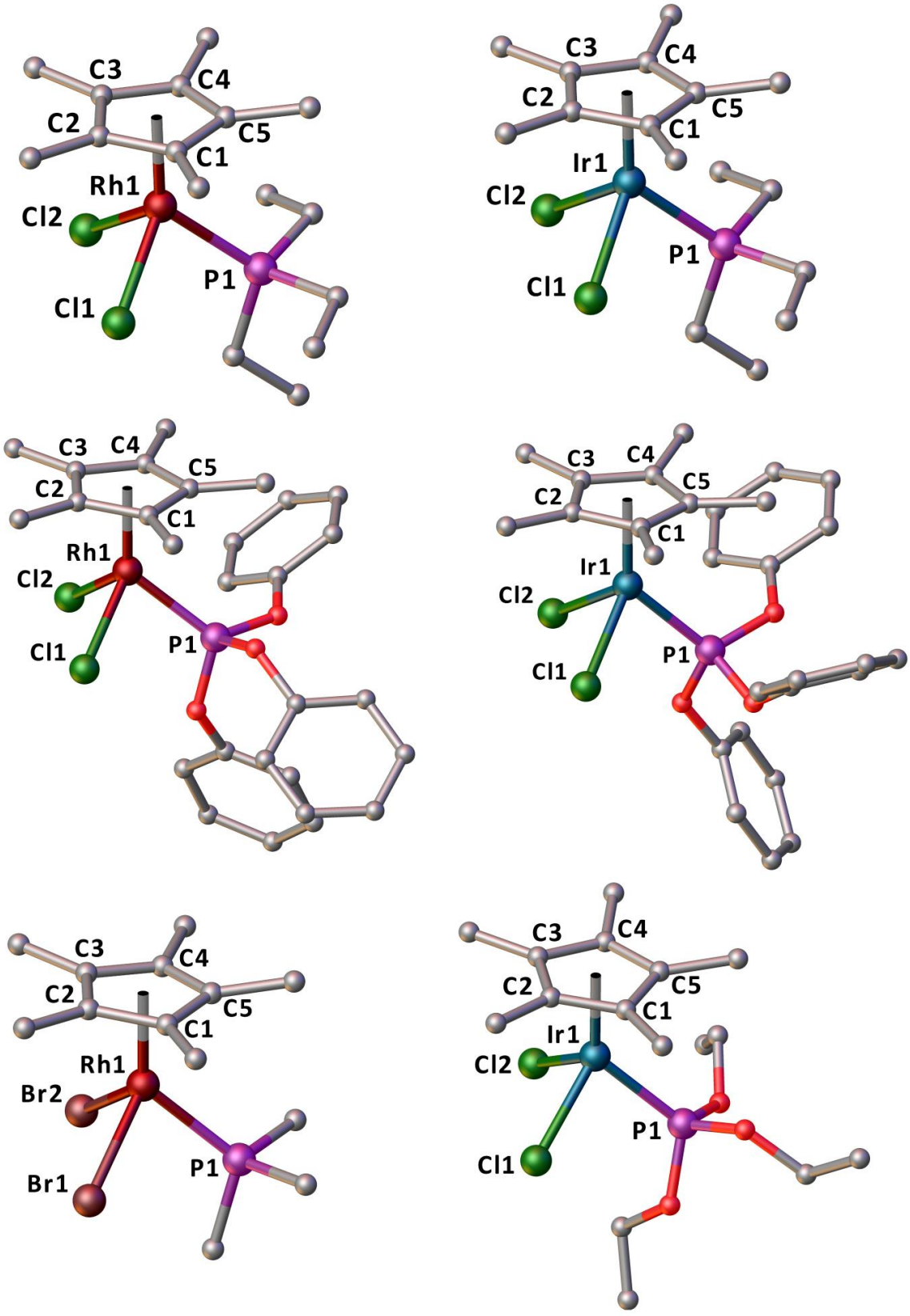

Figure 79: Crystal structures of **C5-3** (top left), **C5-4** (top right), **C5-9** (centre left), **C5-10** (centre right), **C5-11** (bottom left) and **C5-8** (bottom right). Hydrogen atoms are omitted for clarity. Co-crystallised solvent molecules (**C5-3/4** (H_2O), **C5-10** (Toluene)) are also omitted for clarity.

Table 13: Selected bond lengths [Å] and angles [°] for **C5-3/4** and **C5-8**.

	C5-3	**C5-4**	**C5-8**
M1–Cl1	2.4124(8)	2.425(1)	2.382(2)
M1–Cl2	2.4072(7)	2.423(1)	2.408(2)
M1–P1	2.3102(7)	2.320(1)	2.243(2)
M1–C1	2.155(3)	2.185(5)	2.173(6)
M1–C2	2.222(3)	2.255(5)	2.252(6)
M1–C3	2.230(3)	2.255(5)	2.248(6)
M1–C4	2.155(3)	2.172(5)	2.158(6)
M1–C5	2.175(3)	2.177(5)	2.168(6)
Cl1–M1–Cl2	90.95(3)	88.36(4)	88.96(7)
Cl1–M1–P1	89.63(3)	89.41(4)	88.27(6)
Cl2–M1–P1	89.33(2)	89.10(4)	91.22(7)

The complexes are all isostructural adopting the same piano stool structure seen previously in chapter 4. The Cp* ring is slightly tilted as the M–C bond lengths vary depending on whether the bond is *trans* to the strongly bound phosphorus ligand or the chloride ligands. The M–X (X = Cl , Br) bond lengths are fairly typical for this type of complex and comparable to those reported within the Cambridge Structural Database.[25,26] The angles around the metal centre are all close to the ideal angle of 90° with the greatest deviation from this in **C5-11**.

Table 14: Selected bond lengths [Å] and angles [°] for **C5-9/10/11**.

	C5-9	**C5-10**	**C5-11**
M1–X1	2.3960(6)	2.413(1) [2.407(1)]	2.529(1)
M1–X2	2.4007(8)	2.413(1) [2.430(1)]	2.550(1)
M1–P1	2.2312(7)	2.251(1) [2.246(1)]	2.284(2)
M1–C1	2.144(2)	2.197(4) [2.189(5)]	2.141(4)
M1–C2	2.224(2)	2.227(5) [2.262(5)]	2.225(4)
M1–C3	2.227(2)	2.249(5) [2.262(4)]	2.252(4)
M1–C4	2.155(3)	2.203(4) [2.181(4)]	2.169(4)
M1–C5	2.162(2)	2217(4) [2.199(4)]	2.179(4)
X1–M1–X2	92.72(2)	87.33(4) [89.44(4)]	94.82(2)
X1–M1–P1	93.37(2)	87.85(4) [85.39(4)]	87.14(3)
X2–M1–P1	83.99(2)	89.70(4) [90.76(4)]	86.91(3)

[] denotes data from the second molecule within the asymmetric unit.

The Tolman cone angle is often used to describe phosphine and phosphite ligands in terms of the space they occupy around the metal centre. Values are determined based on the ligand adopting a conformation that requires the least amount of space.[265] As such, using this parameter as a hard

indicator of the steric influence of phosphine and phosphite ligands should be avoided. If we take triphenyl phosphite as an example, the Tolman cone angle is 128°; however work by Darensbourg and co-workers has shown that the calculated cone angle based on solid state data can range from 140−160°.[266] During discussions of the sterics of the phosphorus donor ligands reported herein, the Tolman cone angle value will be used for consistency.

The M–P bond lengths vary similarly across both the rhodium and iridium series of complexes. For the rhodium complexes, the M–P bond lengths are 2.2312(7) Å (**C5**-**9**), 2.267(3) Å (**C5**-**7**),[264] 2.284(2) Å (**C5**-**11**), 2.3102(7) Å (**C5**-**3**) and 2.341(2) Å (**C5**-**5**)[267] with the iridium derivatives at 2.243(2) Å (**C5**-**8**), 2.251(1) Å (**C5**-**10**), 2.318(1) Å (**C5**-**6**)[263] and 2.320(1) Å (**C5**-**4**). Clearly the phosphite donors have smaller M–P bond lengths than the phosphine derivatives. The Tolman cone angles of the ligands are 109° ($P(OEt)_3$), 118° (PMe_3), 128° ($P(OPh)_3$), 132° (PEt_3) and 145° (PPh_3).[265] Our observed order of M–P bond lengths across the series does not match that which would be predicted using this parameter. To explain the trend, the electronic parameters of each ligand much also be considered. The Tolman electronic parameter is a measure of electron donating or withdrawing ability of a ligand. It is determined by measuring the frequency of the A_1 C≡O stretch of the nickel complex, $[LNi(CO)_3]$.[13] If ligand L is a good π-acceptor then it will compete with the CO ligands and ν(CO) will increase owing to the strengthening of the C≡O bond *cf* $[Ni(CO)_4]$. Conversely, if L increases the π density on the metal then the C≡O bond will weaken and appear at a lower frequency. If we order the ligands by their Lewis basicity, $P(OPh)_3 < P(OEt)_3 < PPh_3 < PMe_3 < PEt_3$, we see that phosphites are the weakest σ donors. In contrast to this, the phosphite ligands are better at accepting π back donation from the metal d-orbitals. The Tolman electronic parameter for $P(OEt)_3$ is 2076.3 cm^{-1} whilst the value for PEt_3 is 2061.7 cm^{-1}.[265] This is because the π back donation goes into the phosphorus–oxygen σ^*-orbital rather than the phosphorus–carbon σ^*-orbital. This acts to increase the interaction between the metal and the phosphorus atoms resulting in shorter bond lengths. Thus, in these complexes it appears as though the electronics of the ligands are over-riding any steric constraints.

5.3 – Varying the Size and Flexibility of the Aromatic Backbone

With the dibromo starting material **C5**-**11** already available, a small series of complexes with our dithiol pro-ligands was proposed. In the previous work (chapter 4) there were several structure types isolated with the different ligands. One reason for this was the ability of the ligands to fill the vacant coordination site in different ways (naphthalene versus biphenyl). With the phosphorus ligand occupying the remaining coordination site within the starting material, it was expected that all the ligands would form simple monomeric complexes with the dithiolate ligands acting in a chelating fashion. In order to see if the size and flexibility of the backbone had any effect on the complex formed, four potential dithiolato ligands were selected (pre-cursors shown in Figure 80).

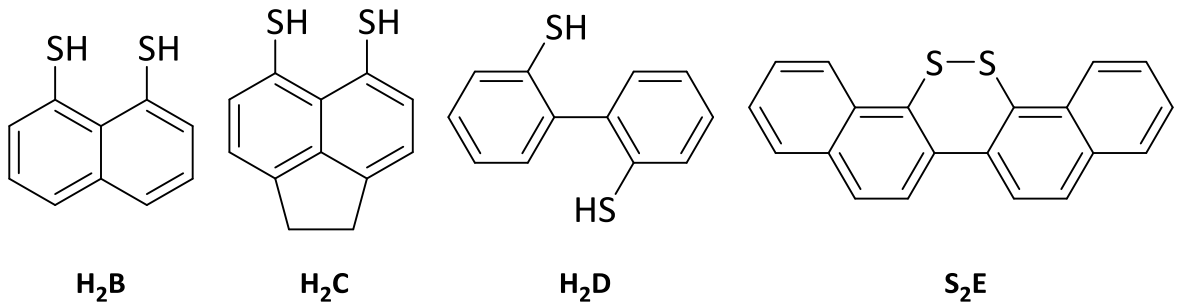

Figure 80: Ligand pre-cursor compounds selected for this study.

For this investigation the $BenzS_2$ ligand was replaced with 2,2'-$BinapS_2$, the precursor of which, dinaphtho[1,2-*c*:2',1'-*e*][1,2]dithiine (**S_2E**), had been previously prepared within the group following a literature procedure.[268] In the case of **S_2E**, the reduction to the dithiol was not attempted as the amount of disulfide available was not sufficient. For this reason the reduction to the reactive dithiolate was performed *in situ* using lithium triethylborohydride, a procedure performed previously.[190]

5.3.1 – Monomeric rhodium dithiolato complexes with a PMe_3 ligand

The synthesis of [Cp*Rh($NaphthS_2$)PMe_3] (**C5**-**11b**), [Cp*Rh($AcenapS_2$)PMe_3] (**C5**-**11c**), [Cp*Rh($BiphenS_2$)PMe_3] (**C5**-**11d**) and [Cp*Rh(2,2'-$BinapS_2$)PMe_3] (**C5**-**11e**) is shown in Scheme 33. The metathesis of the bromide ligands with dithiolates **B**–**E** proceeds smoothly at room temperature. The presence of the phosphine group allowed the reaction progress to be monitored by ^{31}P NMR spectroscopy. In the case of **C5**-**11b**–**d** this meant the loss of the signal from the starting material **C5**-**11**, whilst for **C5**-**11e**, both it and **C5**-**11** are soluble in THF so the conversion could be

observed directly. Upon completion of the reaction, for **C5-11b–d** filtration of the precipitate followed by washing with methanol was sufficient to afford pure compound. For **C5-11e** purification by column chromatography was required. Excellent isolated yields of between 82–91% were obtained after purification.

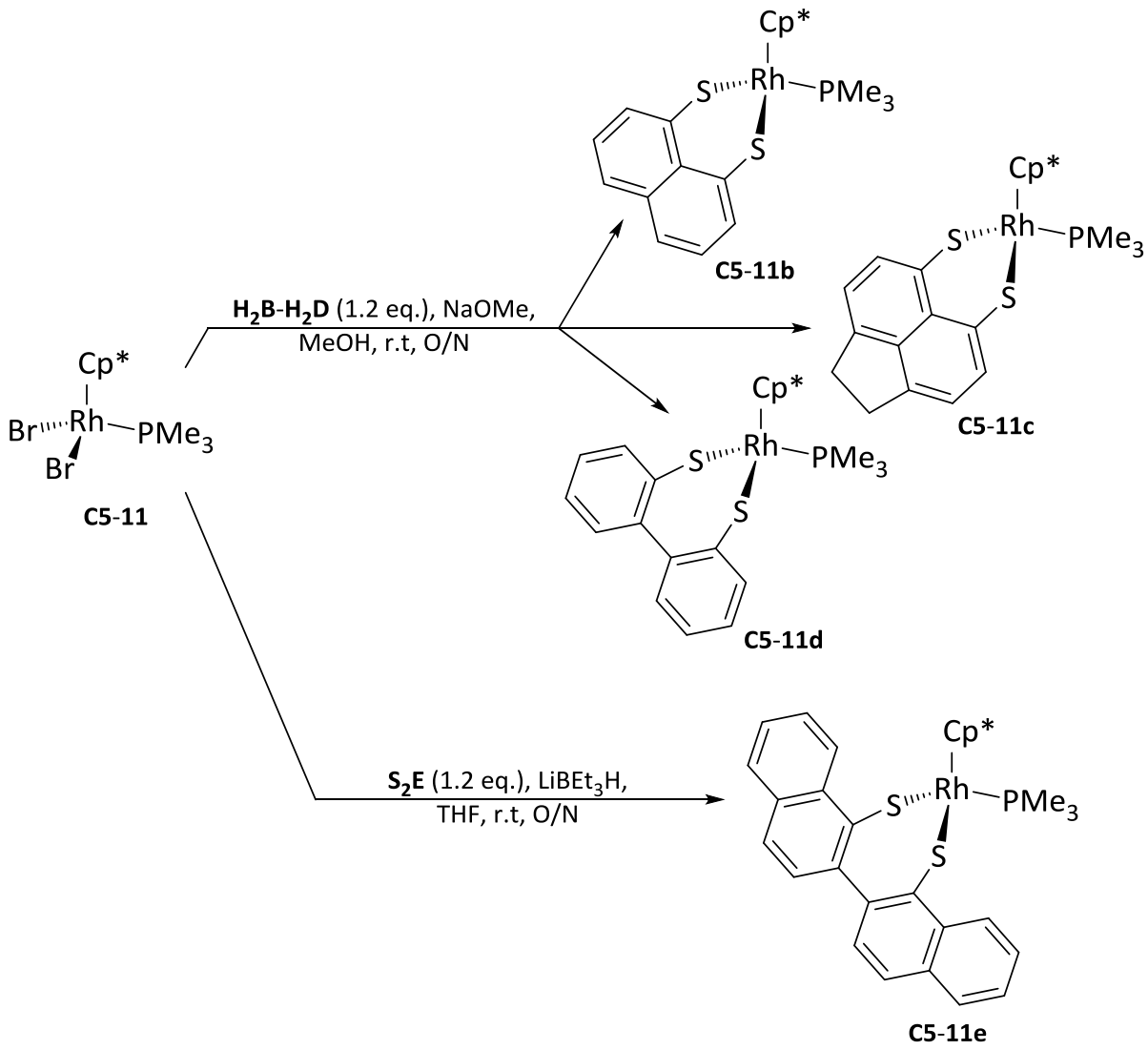

Scheme 33: Synthetic routes to monomeric rhodium dithiolato complexes with a PMe_3 ligand.

The ^{1}H NMR spectra for **C5-11b/c** show the expected signals, with splitting, from the aromatic backbones in the range of δ_H 7.88–6.91 ppm. In the case of **C5-11d** and **C5-11e** we observe 8 and 10 signals respectively as the two joined aryl ring systems are inequivalent. This is due to the inability of the ligand backbones to rotate around the aryl–aryl bond. Four of the aromatic signals observed for **C5-11d** appear as a *pseudo*-triplet of doublets instead of the expected doublet of doublet of doublets. This is due to the $^3J_{HH}$ coupling constants observed between H_b and H_a as well as H_b and H_c (Figure 81) being almost identical. For **C5-11e** this signal is not observed as the equivalent positions

from each of the two naphthalene ring systems overlap resulting in multiplets. The η^5–Cp* methyl signals range from δ_H 1.58–1.42 ppm and are split into doublets by long range phosphorus coupling ($^4J_{HP}$ = 3.0–3.2 Hz). The signals from the methyl groups attached to the phosphorus atom appear as a doublet of doublets for **C5-11b–d**, with $^2J_{HP}$ coupling ($^2J_{HP}$ = 10.3–10.5 Hz) and long range $^3J_{HRh}$ coupling ($^3J_{HRh}$ = 0.6–0.7 Hz). Only a doublet is observed for this signal in **C5-11e** with a similar $^2J_{HP}$ coupling to that seen in the other complexes.

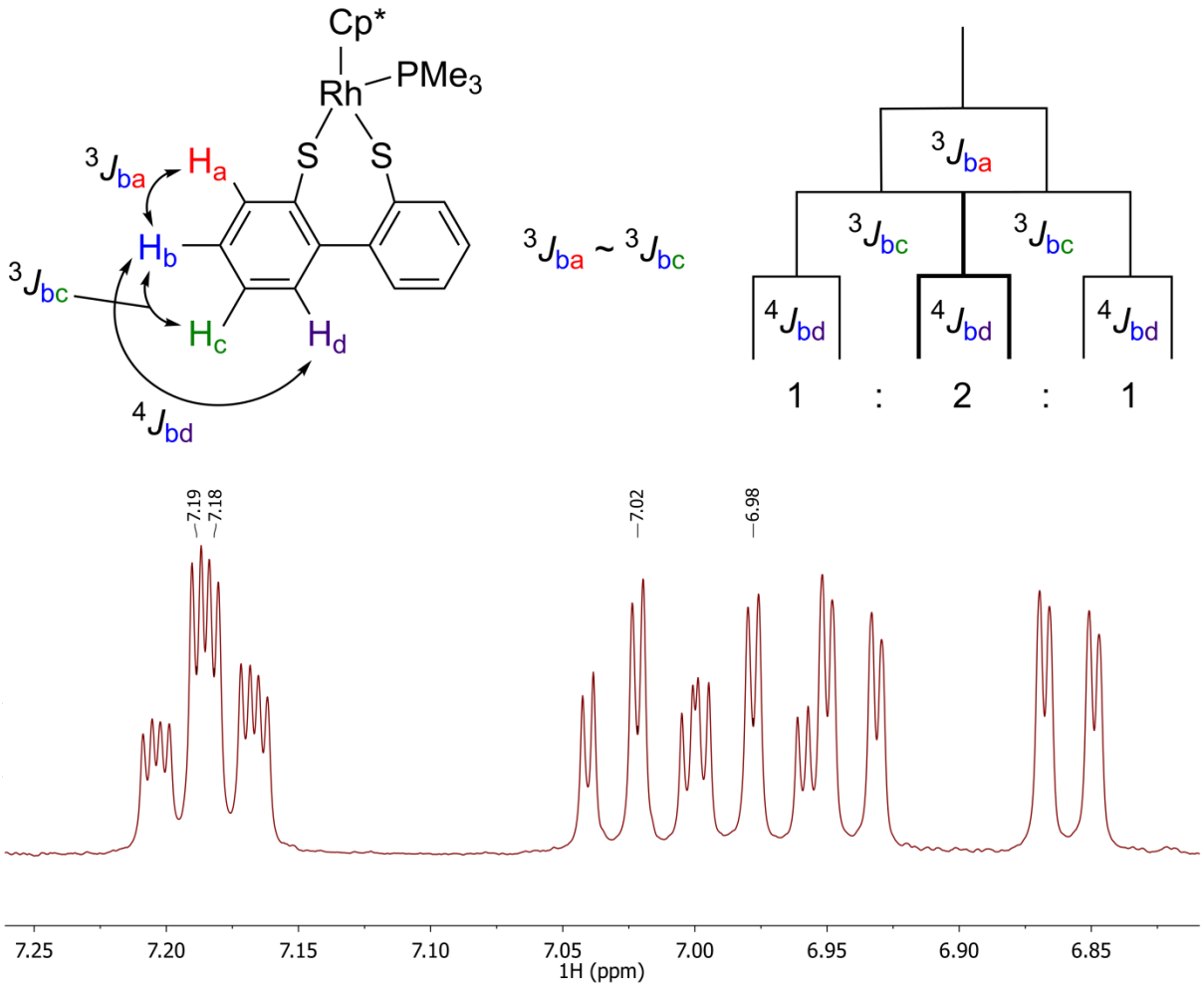

Figure 81: The formation of the *pseudo*-triplet of doublets in **C5-11d** (^{1}H NMR spectrum, $CDCl_3$, 400 MHz).

The $^{31}P\{^1H\}$ NMR resonances for **C5-11** and **C5-11b–e** are shown in Table 15. The complexes all display an upfield shift in the $^{31}P\{^1H\}$ NMR spectra compared to the starting material **C5-11** ($\Delta\delta$ = 0.7–3.3 ppm). The coordination of the dithiolate ligand is also accompanied by a small increase in the $^1J_{PRh}$ coupling (Δ^1J_{PRh} = 11–15 Hz) in **C5-11b–e** when compared to **C5-11**.

Table 15: $^{31}P\{^{1}H\}$ NMR data ($CDCl_3$, 162 MHZ (**C5**-**11**, **C5**-**11b**–**d**), 202 MHz (**C5**-**11e**)) for **C5**-**11** and **C5**-**11b**–**e**. All δ values are in ppm and *J* values are in Hertz.

	C5-**11**[+]	**C5**-**11b**	**C5**-**11c**	**C5**-**11d**	**C5**-**11e**
δ_P	3.6	1.7	2.9	0.3	2.2
$^{1}J_{PRh}$	137	150	148	153	152

[+] values obtained from a sample run on a Bruker Avance II 400 NMR spectrometer (162 Hz).

As expected, the $^{13}C\{^{1}H\}$ NMR spectra of **C5**-**11b**–**e** mirrors that of the ^{1}H NMR spectra, with signals for all carbons observed arising from the aromatic backbone. Interestingly, only one of the quaternary carbons bound to the sulfur atoms is split into a doublet ($^{3}J_{CP}$ = 6.5 Hz (**C5**-**11d**) and 6.7 Hz (**C5**-**11e**)) by the phosphorus atom in the biphenyl and binaphthyl complexes. This provides further support of the difference between the two sides of the aryl–aryl bond. The mass spectra of **C5**-**11b**–**e** each showed a peak corresponding to $[M-PMe_3+H]^+$ ions at *m/z* 429.02, 455.03, 455.03 and 555.07 respectively. Additionally, homogeneity of the complexes was confirmed by elemental analysis.

5.3.1.1 – Crystallographic characterisation of C5-11b–e

Crystals suitable for X-ray work were obtained for all the complexes by slow evaporation from a DCM solution. The single crystal X-ray structures of **C5**-**11b**–**e** are shown in Figure 82 with selected structural parameters shown in Table 16. All of the complexes adopt a piano stool geometry around the rhodium centre.

The Rh–S bond lengths of **C5**-**11b** and **C5**-**11c** were almost identical (**C5**-**11b**; 2.331(1) and 2.332(1) Å, **C5**-**11c**; 2.330(2) Å) whilst in **C5**-**11d** and **C5**-**11e** there was more variation and they were slightly longer (**C5**-**11d**; 2.3691(8) and 2.3705(8) Å, **C5**-**11e**; 2.3677(7) and 2.3994(8) Å). These are comparable to other half sandwich complexes with Rh–S bonds reported by Jin and co-workers ranging from 2.340 to 2.386 Å.[269-271] The Rh–P bond lengths show no appreciable change compared to **C5**-**11** with little variation across the series.

All of the non-Cp* angles around the rhodium centre are reduced to less than 90° for **C5**-**11b** and **C5**-**11c**. This is a consequence of the rigid ligand backbone preventing the sulfur atoms from adopting a more ideal geometry. The effect is most obvious for the naphthalene system as the *peri*-positions are restricted to a slightly shorter distance than those in the acenaphthene system. For both **C5**-**11b** and **C5**-**11c** the splay angles are large and positive (**C5**-**11b**; 19.2(5)°, **C5**-**11c**; 21.0(3)°) as the rhodium

centre forces the sulfur atoms apart. The S1–C1···C9–S9 torsion angle is larger in the naphthalene derivative compared to the acenaphthene, again as a consequence of the more limited movement of the sulfur atoms imposed by the backbone. The central C–C–C–C torsion angles are similar in both complexes showing limited buckling of the ring system. The out-of-plane displacements of the sulfur atoms are slightly greater in **C5**-**11b** than **C5**-**11c**.

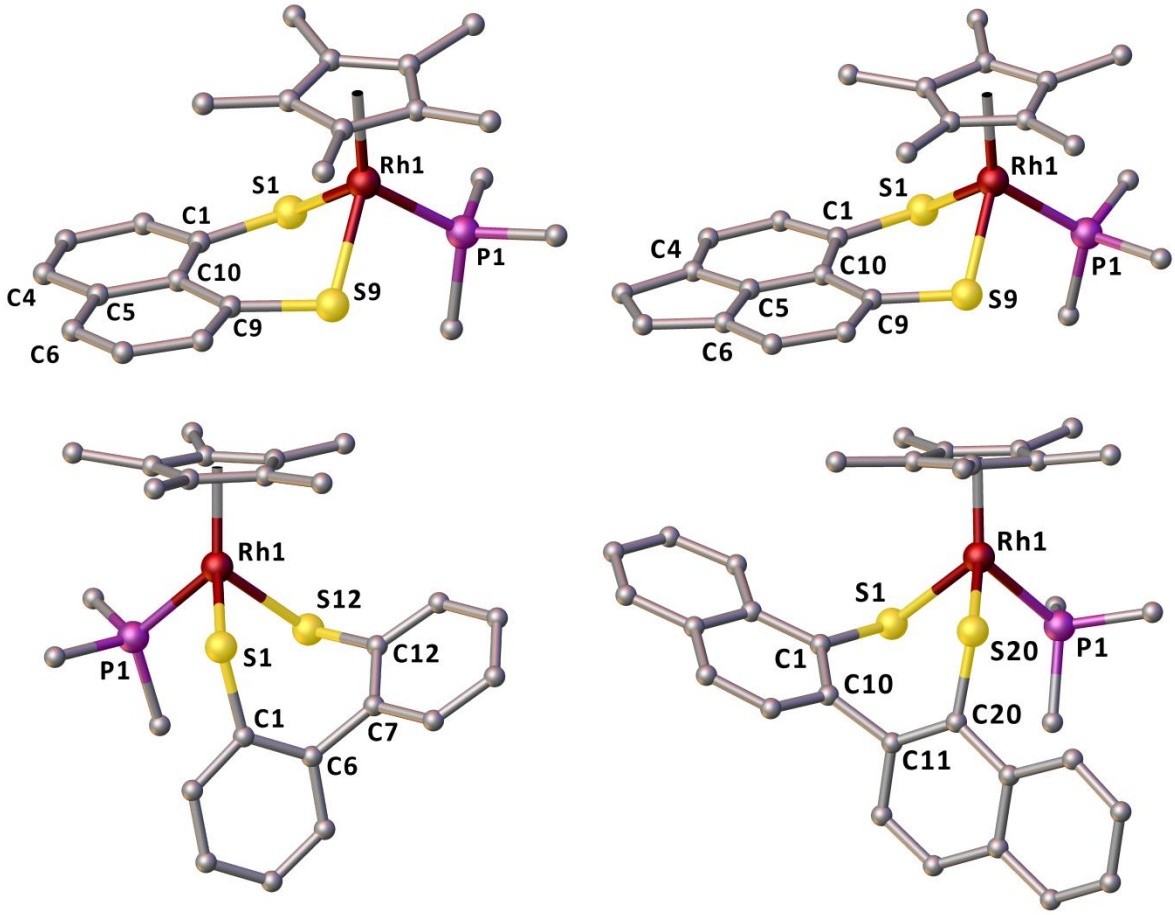

Figure 82: Crystal structures of **C5**-**11b** (top left), **C5**-**11c** (top right), **C5**-**11d** (bottom left) and **C5**-**11e** (bottom right). Hydrogen atoms are omitted for clarity.

In complexes **C5**-**11d** and **C5**-**11e** the non-Cp* angles show a broader range than in naphthalene and acenaphthene examples ranging from 88.79(3)–93.94(3)° and 84.11(3)–96.29(3)° respectively. The ability of the backbone to twist around the aryl–aryl bond allows the sulfur atoms to adopt a more idealised geometry. The torsion angle between the two aryl rings is larger in **C5**-**11e** (79.0(4)°) than **C5**-**11d** (68.0(4)°) most likely due to the added steric bulk of having a binaphthyl instead of biphenyl based system. In both the biphenyl and binaphthyl derivatives, the out-of-plane displacements of the sulfur atoms are similar.

Table 16: Selected bond lengths [Å], angles [°], torsion angles [°] and displacements [Å] for **C5-11b–e**.

	C5-11b	**C5-11c**	**C5-11d**	**C5-11e**
Rh1–P1	2.284(1)	2.272(2)	2.2773(9)	2.2851(8)
Rh1–S1	2.331(1)	2.330(2)	2.3691(8)	2.3677(7)
Rh1–S9	2.332(1)	2.330(2)	-	-
Rh1–S12	-	-	2.3705(8)	-
Rh1–S20	-	-	-	2.3994(8)
P1–Rh1–S1	89.85(5)	87.02(3)	88.79(3)	96.29(3)
P1–Rh1–S9	84.87(5)	87.37(4)	-	-
P1–Rh1–S12	-	-	91.27(3)	-
P1–Rh1–S20	-	-	-	84.11(3)
S1–Rh1–S9	85.41(5)	87.78(3)	-	-
S1–Rh1–S12	-	-	93.94(3)	-
S1–Rh1–S20	-	-	-	95.00(3)
splay angle[a]	19.2(5)	21.0(3)	-	-
S1–C1···C9–S9	8.9(3)	5.2(2)	-	-
C1–C10–C5–c6	177.5(6)	178.5(3)	-	-
C9–C10–C5–C4	178.1(6)	177.3(3)	-	-
C1–C6–C7–C12	-	-	68.0(4)	-
C1–C10–C11–C20	-	-	-	79.0(4)
Out of plane displacements				
S1	0.149	0.121	0.184	0.189
S9	0.213	0.117	-	-
S12	-	-	0.003	-
S20	-	-	-	0.086

[a] calculated as [(S1–C1–C10)+(C1–C10–C9)+(C10–C9–S9)−360].

5.4 – Examining the Role of the Phosphorus Ligand in Monomeric Rhodium and Iridium Dithiolato Complexes

In the previous section (5.3) it was confirmed that in the monomeric dithiolato complexes, changes to the ligand backbone has little effect on the structure formed. Another variable to change is the phosphorus ligand used to create these monomeric species. By changing the size and electronic properties of the phosphorus donor atom we can investigate how this affects the formation of the complex as well as the structure. Looking at the previous work it can be seen that the acenaphthene and naphthalene complexes are very similar as are the biphenyl and binaphthalene derivatives. Due to the difficulty in synthesising **S_2E** it was removed for this investigation. After synthesising and characterisation the complexes (**C5**-**3b**–**d** & **C5**-**4b**–**d**) it was obvious that the acenaphthene and naphthalene ligands were behaving identically thus we chose to remove the acenaphthene ligand as well. This decision was made as the acenaphthene ligand represented the hardest to synthesise of the two with lower yields for the formation of **S_2C** over **S_2B**. This left both a rigid planar aromatic (**B**) and a flexible aromatic (**D**) ligand to examine.

As before, the reaction to form the triethylphosphine derivatives could be easily followed by ^{31}P NMR spectroscopy. The metathesis of the chloride ligands with the dithiolate proceeds smoothly in refluxing THF (Scheme 34) with isolated yields after purification of 75–83%. Attempts at using the same synthesis method for the triphenylphosphine analogues resulted in reaction times of 2–3 days. For these complexes, and the phosphite versions, the method using a more reactive ligand by deprotonation of the thiol prior to reaction was utilised (Scheme 34). Using this method, the remaining complexes were isolated with a wide range of yields observed after purification (8–79%).

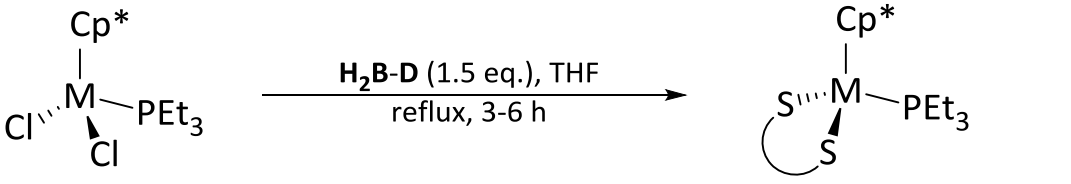

C5-3, M = Rh
C5-4, M = Ir

C5-3b, M = Rh **C5-4b, M = Ir**
C5-3c, M = Rh **C5-4c, M = Ir**
C5-3d, M = Rh **C5-4d, M = Ir**

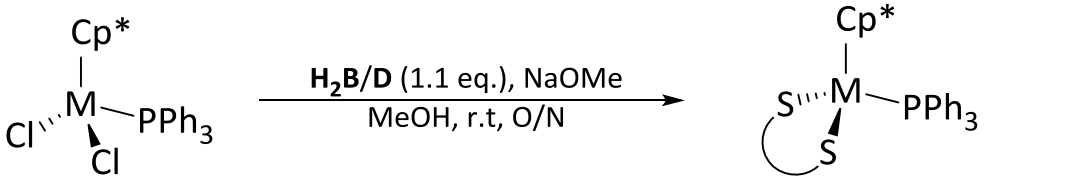

C5-5, M = Rh
C5-6, M = Ir

C5-5b, M = Rh **C5-6b, M = Ir**
C5-5d, M = Rh **C5-6d, M = Ir**

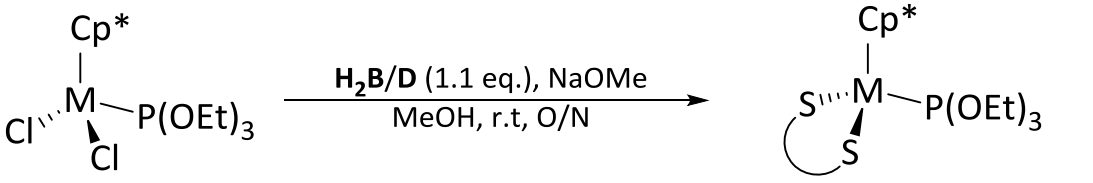

C5-7, M = Rh
C5-8, M = Ir

C5-7b, M = Rh **C5-8b, M = Ir**
C5-7d, M = Rh **C5-8d, M = Ir**

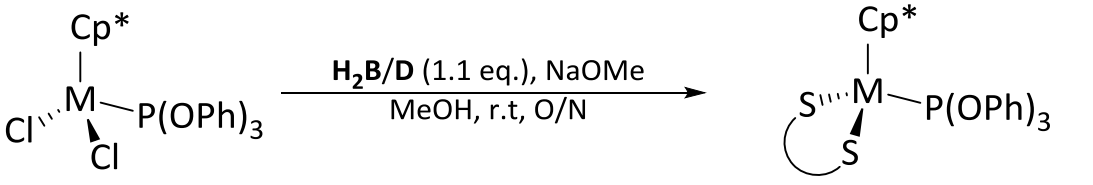

C5-9, M = Rh
C5-10, M = Ir

C5-9b, M = Rh **C5-10b, M = Ir**
C5-9d, M = Rh **C5-10d, M = Ir**

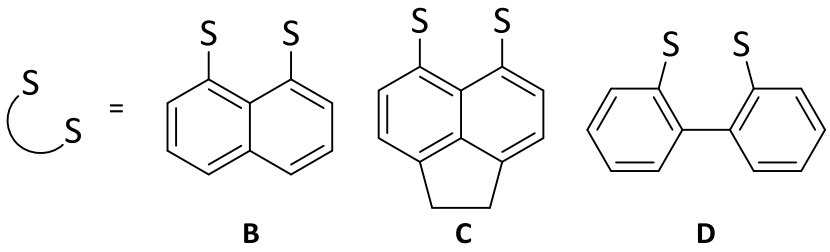

B **C** **D**

Scheme 34: Synthetic routes to monomeric rhodium and iridium dithiolato complexes containing various phosphorus donor ligands.

5.4.1 – Spectroscopic and structural analysis of triethylphosphine containing complexes

The ^{1}H NMR spectra of **C5**-**3b**–**d** and **C5**-**4b**–**d** show the expected aromatic ligand backbone signals in the range of δ_H 7.86–6.68 ppm and δ_H 7.84–6.73 ppm respectively. Just like in the biphenyl example from section 5.3.1, the two aryl rings are inequivalent. The *pseudo*-triplet of doublets observed in the biphenyl containing complex seen previously have become multiplets as the signals from the two sides of the aryl–aryl bond overlap. With the presence of the phosphorus atom, the η^5–Cp* signals all appear as doublets with $^{4}J_{HP}$ coupling constants ranging from 1.8–2.9 Hz.

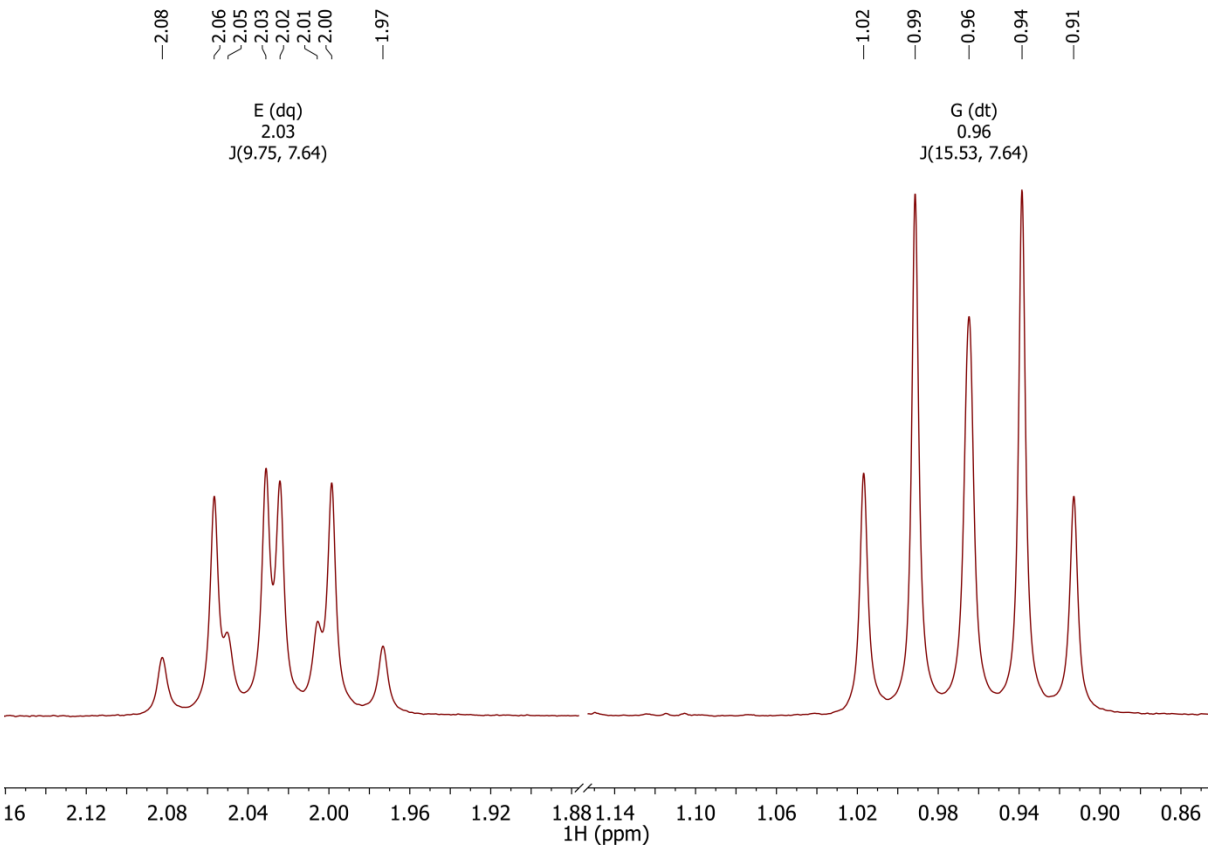

Figure 83: ^{1}H NMR spectrum ($CDCl_3$, 300 MHz) of the ethyl signals in **C5**-**4b**.

In both the rhodium and iridium naphthalene/acenaphthene complexes, the signals arising from the ethyl chain attached to the phosphorus atoms are as expected. For the CH_2 fragment, a doublet of quartets is observed with the signal for the terminal CH_3 group appearing as a doublet of triplets (Figure 83). In both signals the larger coupling constant arises from coupling to the phosphorus atom with the second from $^{3}J_{HH}$ coupling.

Interestingly, the two CH_2 hydrogen atoms in **C5**-**3d** and **C5**-**4d** are anisochronous, displaying two distinct complex multiplets (**C5**-**3d** δ_H 2.04–1.86 (m, 3H) and 1.73–1.58 (m, 3H); **C5**-**4d** δ_H 2.05–1.89 (m, 3H), 1.73–1.57 (m, 3H)) (Figure 84). There are two possible explanations for this, firstly, the

biphenyl dithiolate ligand takes up more space around the metals coordination sphere than the naphthalene and acenaphthene based ligands. This could cause some restricted rotation in the phosphorus–carbon bond of the triethylphosphine ligand resulting in inequivalent CH_2 protons. Secondly, the biphenyl dithiolate aryl–aryl bond may be introducing an axis of chirality thus making the CH_2 protons diastereotopic. This would seem to be the more likely explanation given the observed difference between the two sides of the biphenyl aryl rings.

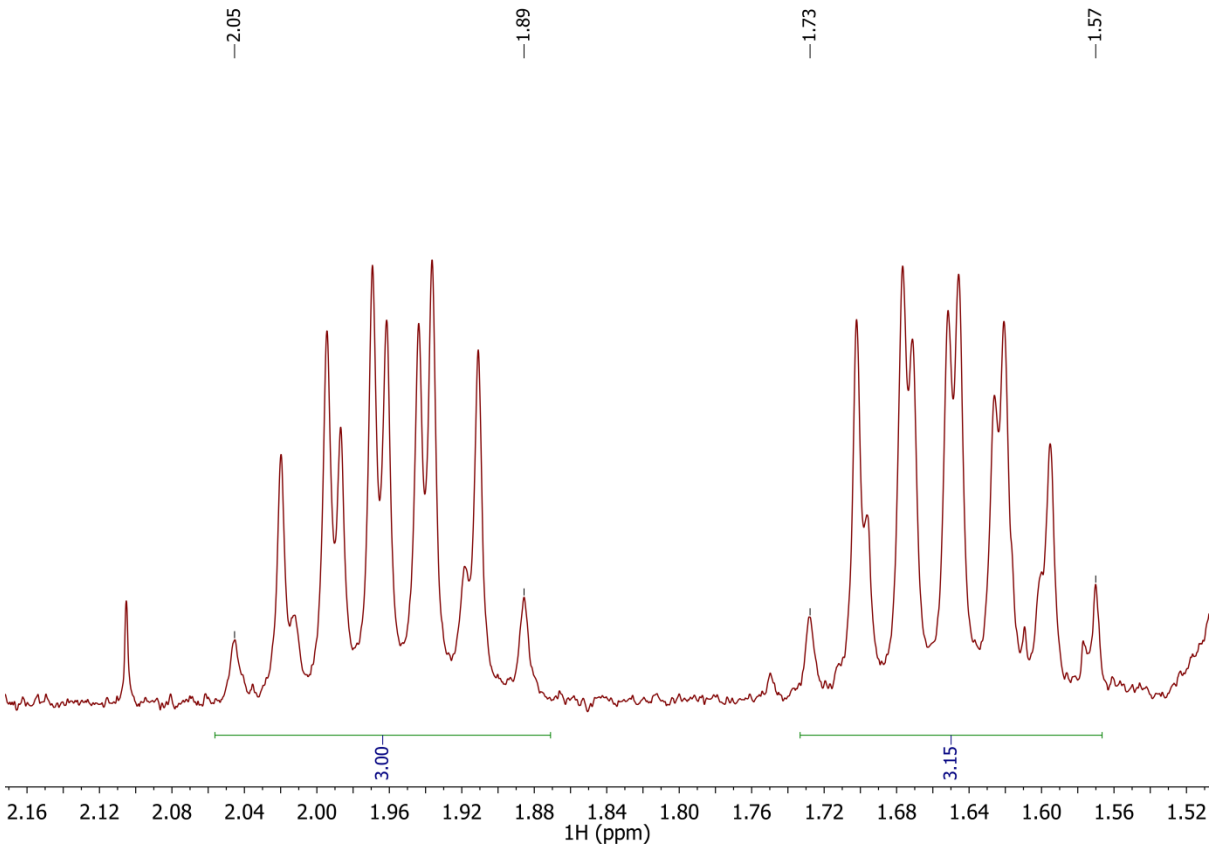

Figure 84: ^{1}H NMR spectrum ($CDCl_3$, 300 MHz) of the CH_2 fragments of the ethyl signals in **C5**-**4d**.

The $^{31}P\{^{1}H\}$ NMR data for complexes **C5**-**3b**–**d** and **C5**-**4b**–**d** are summarised in Table 17. For both the rhodium and iridium series there is a slight upfield shift in the ^{31}P NMR spectra compared to their respective starting materials (**Rh**, $\Delta\delta_P$ = 3.3 to 6.3 ppm; **Ir**, $\Delta\delta_P$ = 8.1 to 9.7 ppm). Whilst this upfield shift is larger in the iridium series compared to the rhodium analogues, less variation is observed between the complexes **C5**-**4b**–**d**. As we have seen previously, the coordination of the dithiolate ligand results in a small increase in the $^{1}J_{PRh}$ coupling in **C5**-**3b**–**d** compared to **C5**-**3**.

Table 17: $^{31}P\{^{1}H\}$ NMR data ($CDCl_3$, 121 MHz (**C5**-**3b**–**d**, **C5**-**4b**–**d**), 202 MHz (**C5**-**3**/**4**)) for **C5**-**3**/**4**, **C5**-**3b**–**d** and **C5**-**4b**–**d**. All δ values are in ppm and *J* values are in Hertz.

	C5-3	**C5-3b**	**C5-3c**	**C5-3d**
δ_P	28.2	24.6	24.9	21.9
$^{1}J_{PRh}$	137.5	146.7	145.9	150.8
	C5-4	**C5-4b**	**C5-4c**	**C5-4d**
δ_P	−5.8	−13.9	−14.4	−15.5

The $^{13}C\{^{1}H\}$ NMR spectra of all the complexes display the expected signals from the aromatic backbone and phosphorus ligand. Coupling between the quaternary Cp* carbon and the rhodium and phosphorus nuclei is observed as is long range coupling between the methyl Cp* groups and the phosphorus nuclei. As expected, only one signal corresponding to the ethyl CH_2 carbons in each of the complexes **C5**-**3b–d** and **C5**-**4b**–**d** is present. Only one of the quaternary carbon atoms bound to a sulfur is split into a doublet by the phosphorus nuclei ($^{3}J_{CP}$ = 6.5 Hz). The mass spectra (ES^+ for **C5**-**3b**/**c**, $APCI^+$ for **C5**-**3d**) show the $[M+H]^+$ ions at *m/z* 547.11, 573.13 and 573.13 respectively. For the iridium derivatives (ES^+ for **C5**-**4b**/**c**, $APCI^+$ for **C5**-**4d**), the $[M+H]^+$ ion is also observed at *m/z* 637.17, 663.19 and 663.19 respectively. Peaks corresponding to $[M-PEt_3+H]^+$ are also present and in the case of **C5**-**4b** and **C5**-**4c** these are base peaks. The analytical purity of the six new complexes was verified using elemental analysis.

5.4.1.1 – Crystallographic characterisation of C5-3b–d and C5-4b–d

Crystals suitable for X-ray work were obtained for all the complexes by slow evaporation from a DCM solution. The crystal structures are shown in Figure 85 with selected structural parameters of **C5**-**3b**/**c** and **C5**-**4b**/**c** in Table 18 with **C5**-**3d** and **C5**-**4d** summarised in Table 19. Once again the complexes all adopt the same piano stool structure with the rhodium and iridium series being isostructural.

The Rh–S bonds lengthen going through the series, varying from 2.3371(9) and 2.3307(7) Å in **C5**-**3b**, 2.342(2) and 2.344(2) Å in **C5**-**3c** to 2.3840(8) and 2.3821(9) Å in **C5**-**3d**. These are comparable to other half sandwich complexes with Rh–S bond lengths reported by Jin and co-workers ranging from 2.340–2.386 Å.[269-271] The Rh–P bonds are slightly shortened in all the complexes: **C5**-**3b** 2.2914(8) Å, **C5**-**3c** 2.299(2) Å and **C5**-**3d** 2.2939(8) Å compared to **C5**-**3**. These Rh–P bond lengths are similar to those previously reported for half sandwich rhodium complexes with neutral phosphine ligands ranging from 2.274–2.295 Å.[272] The distance between the two sulfur atoms increases through the series. Comparing the S···S distance between the free and bound ligands, an increase is observed

from 2.951(2) Å to 3.173(1) Å for **H_2B** and 3.1038(13) Å to 3.231(2) Å for **H_2C** as the rhodium centre bridges the *peri*-positions. Complex **C5**-**3d** has the largest distance between the sulfur atoms (3.448(1) Å) as they are attached to a much more flexible backbone. This represents a decrease compared to the pro-ligand as the sulfur atoms are held closer together within the coordination sphere.

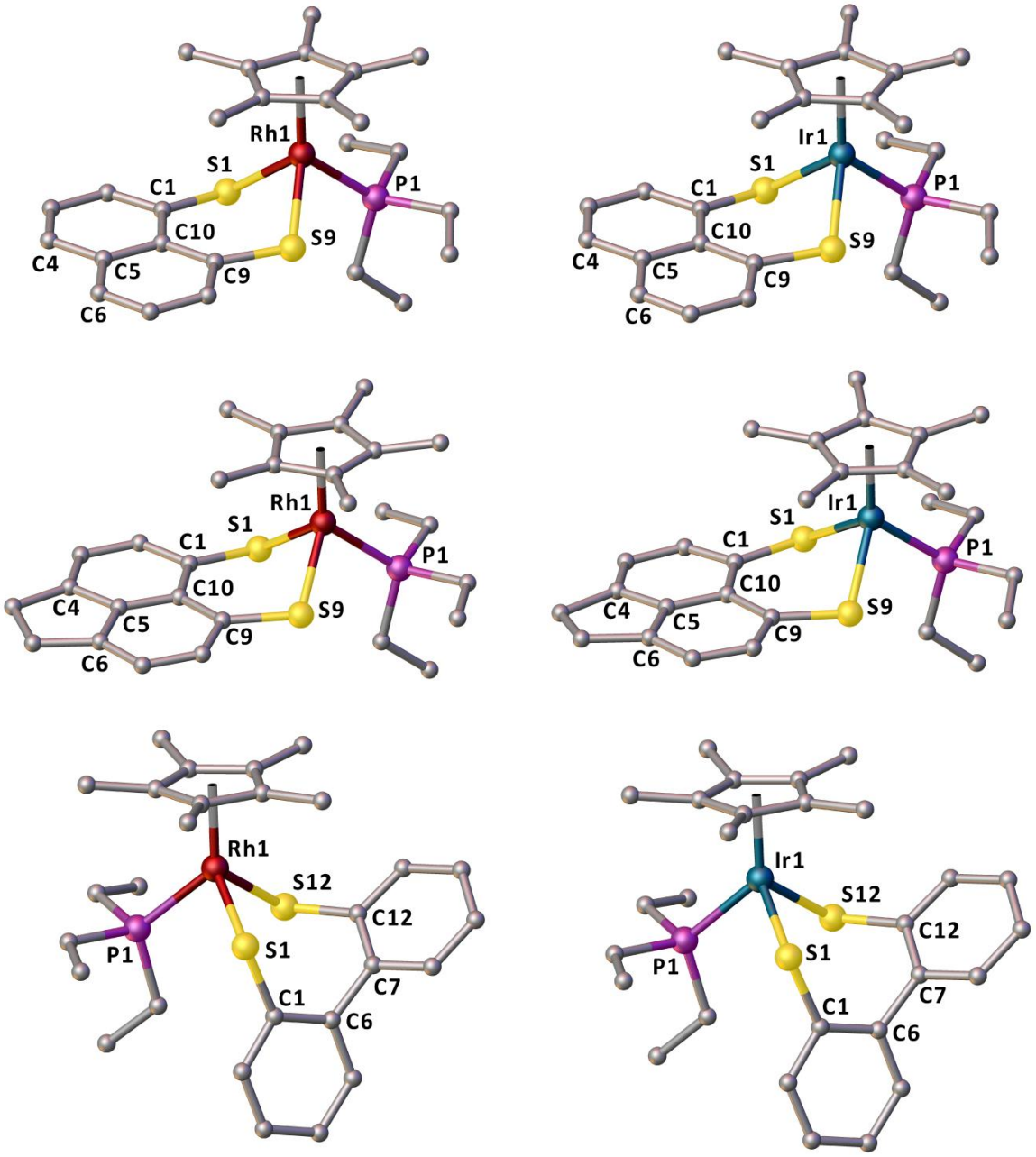

Figure 85: Crystal structures of **C5**-**3b** (top left), **C5**-**4b** (top right), **C5**-**3c** (centre left), **C5**-**4c** (centre right), **C5**-**3d** (bottom left) and **C5**-**4d** (bottom right). Hydrogen atoms are omitted for clarity. Co-crystallised solvent molecules (**C5**-**3c**, DCM) are also omitted for clarity.

Table 18: Selected bond lengths [Å], angles [°], torsion angles [°] and displacements [Å] for **C5**-**3b/c** and **C5**-**4b/c**.

	C5-**3b**	**C5**-**3c**	**C5**-**4b**	**C5**-**4c**
M1–P1	2.2914(8)	2.299(2)	2.276(1)	2.2801(9)
M1–S1	2.3371(9)	2.342(2)	2.348(1)	2.3509(9)
M1–S9	2.3307(7)	2.344(2)	2.339(1)	2.3579(9)
S1···S9	3.173(1)	3.231(2)	3.185(2)	3.262(2)
S1–C1	1.765(3)	1.764(8)	1.763(5)	1.775(3)
S9–C9	1.763(3)	1.769(8)	1.765(4)	1.765(3)
S1–M1–S9	85.64(3)	87.19(6)	85.60(4)	87.70(3)
S1–M1–P1	89.40(3)	88.72(7)	89.38(4)	88.87(3)
S9–M1–P1	88.33(3)	88.18(7)	88.27(4)	88.23(3)
splay angle[a]	19.7	20.5	20.5	21.4
S1–C1···C9–S9	6.63(2)	4.12(5)	6.92(3)	4.47(5)
C1–C10–C5–C6	177.70(3)	176.72(8)	176.64(5)	178.91(3)
C9–C10–C5–C4	178.10(3)	178.99(8)	179.60(5)	177.41(3)
Out of plane displacements				
S1	0.211	0.181	0.195	0.073
S9	0.067	0.028	0.082	0.131

[a] calculated as [(S1–C1–C10)+(C1–C10–C9)+(C10–C9–S9)−360].

All the non-Cp* angles around the rhodium centre are slightly reduced to less than 90° for complexes **C5**-**3b/c**. This can be explained by the rigid ligand backbone preventing the sulfur atoms from moving further apart to adopt a more relaxed geometry. The effect is most marked for the naphthalene system as the sulfur atoms in the *peri*-position are restricted to a slightly shorter distance than those in the acenaphthene system. The splay angles are almost identical at 19.7° (**C5**-**3b**) and 20.5° (**C5**-**3c**), respectively. Both of these values are increased compared to the pro-ligands as the rhodium metal pushes the sulfur atoms apart. The torsion angle S1–C1···C9–S9 is slightly bigger in **C5**-**3b** than in **C5**-**3c**, as is the out-of-plane displacements of the sulfur atoms from the backbone. Both complexes show comparable buckling of the central ring system with the central C–C–C–C torsions ranging 176.7−178.9°.

Complex **C5**-**3d** shows a more relaxed dithiol ligand geometry, resulting in two of the angles around the rhodium being slightly above 90° (92.69(3)°, 93.16(3)°). The ability of the backbone to twist along the central C–C bond removes the restrictions on the sulfur atoms observed in **C5**-**3b** and **C5**-**3c**. The torsion angle between the two aromatic rings is 68.0(4)°, a smaller value than that observed in the pro-ligand. The out-of-plane displacements of the sulfur atoms are smaller than in the naphthalene and acenaphthene containing complexes.

Table 19: Selected bond lengths [Å], angles [°], torsion angles [°] and displacements [Å] for **C5**-**3d** and **C5**-**4d**.

	C5-**3d**	**C5**-**4d**
M1–P1	2.2939(8)	2.2993(9)
M1–S1	2.3840(8)	2.409(1)
M1–S12	2.3821(9)	2.4031(9)
S1···S12	3.448(1)	3.463(1)
S1–C1	1.772(3)	1.785(4)
S12–C12	1.790(3)	1.801(3)
S1–M1–S12	92.69(3)	92.08(3)
S1–M1–P1	93.16(3)	92.64(3)
S12–M1–P1	89.60(3)	89.45(3)
C1–C6–C7–C12	68.0(4)	66.83(5)
Out of plane displacements		
S1	0.114	0.124
S12	0.002	0.005

There is a drop in the observed tilt of the Cp* ligand in the iridium series compared to the rhodium complexes. The Ir–S bond lengthens going from **C5**-**4b–d** ranging from 2.339(1) Å in **C5**-**4b** to 2.409(9) Å in **C5**-**4d** and are comparable to other Ir–S bonds.[191] The Ir–P bond length increases going from **C5**-**4b** to **C5**-**4d** with all the complexes showing a shortened Ir–P bond compared to the dichloro starting material. The S···S distance increases across the series as before. The non-Cp* angles around the iridium centre for **C5**-**4b** and **C5**-**4c** are all less than 90°, with **C5**-**4d** having two greater than 90° (92.08(3)°, 92.64(3)°). The S···S distance, splay angle and torsion S1–C1···C9–S9 all increase in the iridium complexes compared to their rhodium analogues. The out-of-plane displacements of the sulfur atoms from the central ring systems are comparable to the rhodium analogues. Additionally, the torsion angle between the two aryl rings in **C5**-**4d** is similar to that seen in the rhodium derivative.

5.4.2 – Spectroscopic and structural analysis of triphenylphosphine containing complexes

The yields for the triphenylphosphine derivatives were similar to those obtained for the triethylphosphine complexes ranging from 75−79%. The increased size of the phosphine ligand could be partly responsible for the slower reaction when the same conditions are used. In the case of the biphenyl complexes, a stability issue in deuterated chloroform resulted in a peak appearing for the dichloro starting complex if the sample was left for too long (> 4 h). As a result, the NMR spectra were run in either deuterated benzene or DCM; the use of benzene obscured the aromatic signals

and so it was avoided. Due to stability problems these complexes could not be purified by column chromatography so instead the isolated solid was washed with methanol.

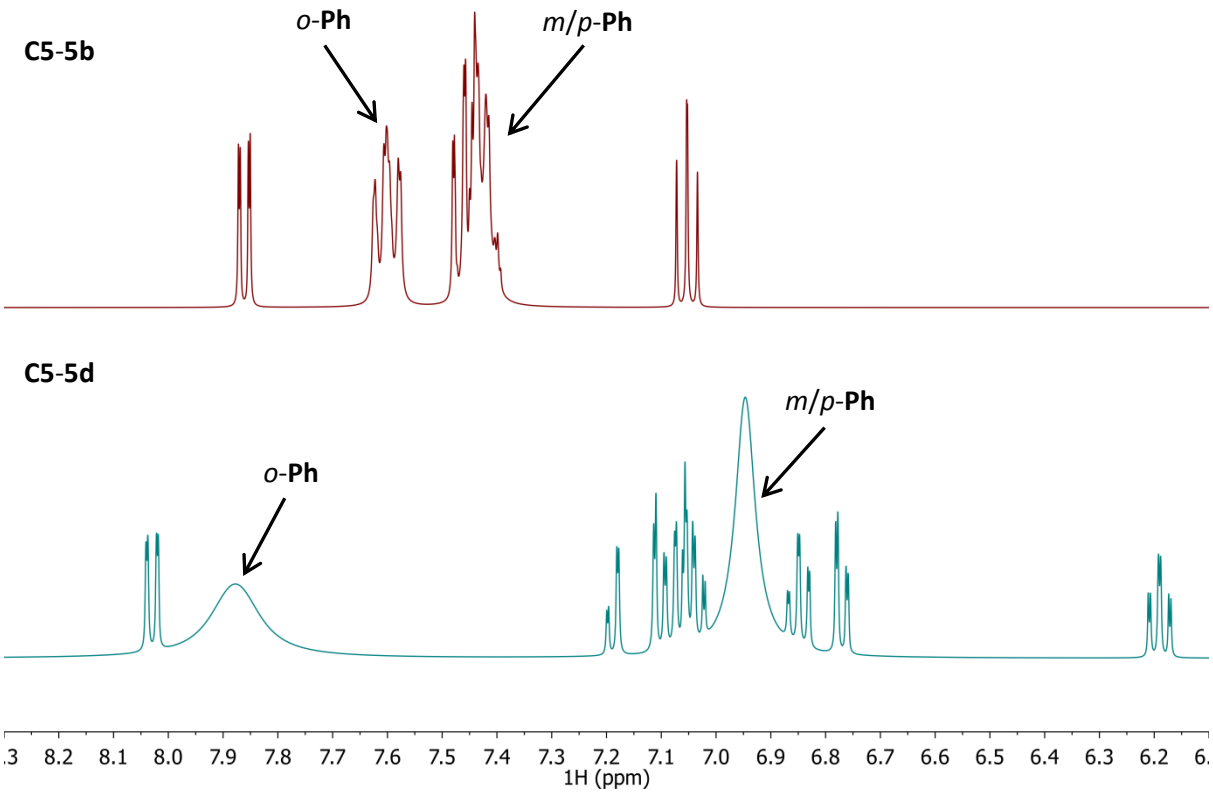

Figure 86: ^{1}H NMR spectrum (CD_2Cl_2, 400 MHz (**C5-5b**), 500 MHz, (**C5-5d**)) of the aromatic region in **C5-5b** (top) and **C5-5d** (bottom). Small impurity peaks (**S_2B** (**C5-5b**), **S_2D** (**C5-5d**)) have been removed for clarity.

As expected, the ^{1}H NMR spectra of **C5-5b/d** and **C5-6b/d** show the signals from the aromatic backbone as we have seen before. The naphthalene derivatives display three peaks from the dithiolate ligand and two broad multiplets from the phenyl rings with no difference between the rhodium and iridium versions. The biphenyl containing complexes display complex aromatic regions as the eight signals arising from the dithiolate ligand overlap, and in some cases are covered by, the very broad signals from the phenyl rings. Unlike in the naphthalene examples, the phenyl ring signals have no distinct line shape. The aromatic regions of the **C5-5b** and **C5-5d** are shown in Figure 86. In all cases, the η^5–Cp* ligand signal appears as a doublet with similar coupling constants to those seen previously.

The ^{31}P{^{1}H} NMR data for **C5-5b/d** and **C5-6b/d** are summarised in Table 20. The biphenyl analogues both display an upfield shift compared to the starting material with the iridium version displaying

the biggest change ($\Delta\delta_P$ = 10.9 ppm). Interestingly, **C5**-**5b** is shifted downfield compared to the starting material with the **C5**-**6b** shifted slightly upfield as before. The coordination of the dithiolate ligand again results in an increase in the $^1J_{PRh}$ coupling constant.

Table 20: $^{31}P\{^1H\}$ NMR data ($CDCl_3$ (**C5**-**5**/**6**), CD_2Cl_2 (**C5**-**5b**/**d** & **C5**-**6b**), C_6D_6 (**C5**-**6d**), 162 MHz (**C5**-**5b**/**6b**), 202 MHz (**C5**-**5**/**6**, **C5**-**5d**/**6d**)) for **C5**-**5**/**6**, **C5**-**5b**/**d** and **C5**-**6b**/**d**. All δ values are in ppm and *J* values are in Hertz.

	C5-**5**	**C5**-**5b**	**C5**-**5d**
δ_P	30.1	36.6	28.6
$^1J_{PRh}$	144.1	153.0	157.5
	C5-**6**	**C5**-**6b**	**C5**-**6d**
δ_P	1.6	0.6	−9.3

The $^{13}C\{^1H\}$ NMR spectra of the complexes mirrored the ^1H NMR data with the expected signals from the ligand backbone observed. In the naphthalene derivative, the quaternary carbon bound to the sulfur atom is split into a doublet by long range coupling to the phosphorus nuclei. As before, only one of the analogous carbon atoms in the biphenyl version appears as a doublet. The quaternary carbon from the phosphine ligand is not visible in the biphenyl complexes but can be seen in the naphthalene examples with $^1J_{CP}$ coupling constants of 45.3 Hz (**C5**-**5b**) and 54.9 Hz (**C5**-**6b**). In the proton spectra of the biphenyl complex broad phenyl signals were observed, broadening of this carbon signal would result in it disappearing into the baseline. The remaining phenyl carbon signals are present for all the complexes. The expected splitting due to coupling with the phosphorus nuclei are observed in the naphthalene complexes. However, broadening of the signals in the biphenyl derivatives means this coupling could not be observed. The mass spectra of the complexes all show peaks corresponding to $[PPh_3+H]^+$ at *m/z* 263.11 and in all cases this is the base peak. Peaks which corresponding to $[M-PPh_3+H]^+$ are also observed but only **C5**-**5d**/**6d** have this peak with an intensity greater than 5%. The bulk purity of the complexes was assessed using elemental analysis.

5.4.2.1 – Crystallographic characterisation of C5-5b/d and C5-6b/d

Crystals suitable for X-ray work were obtained by slow evaporation from benzene (**C5**-**5b**/**6b**) or diethyl ether (**C5**-**5d**/**6d**). The crystal structures are shown in Figure 87 with selected structural parameters in Table 21. Two molecules crystallised within the asymmetric unit for **C5**-**5b** and **C5**-**6b**/**6d** with two co-crystallised solvent molecules also present within **C5**-**6d**.

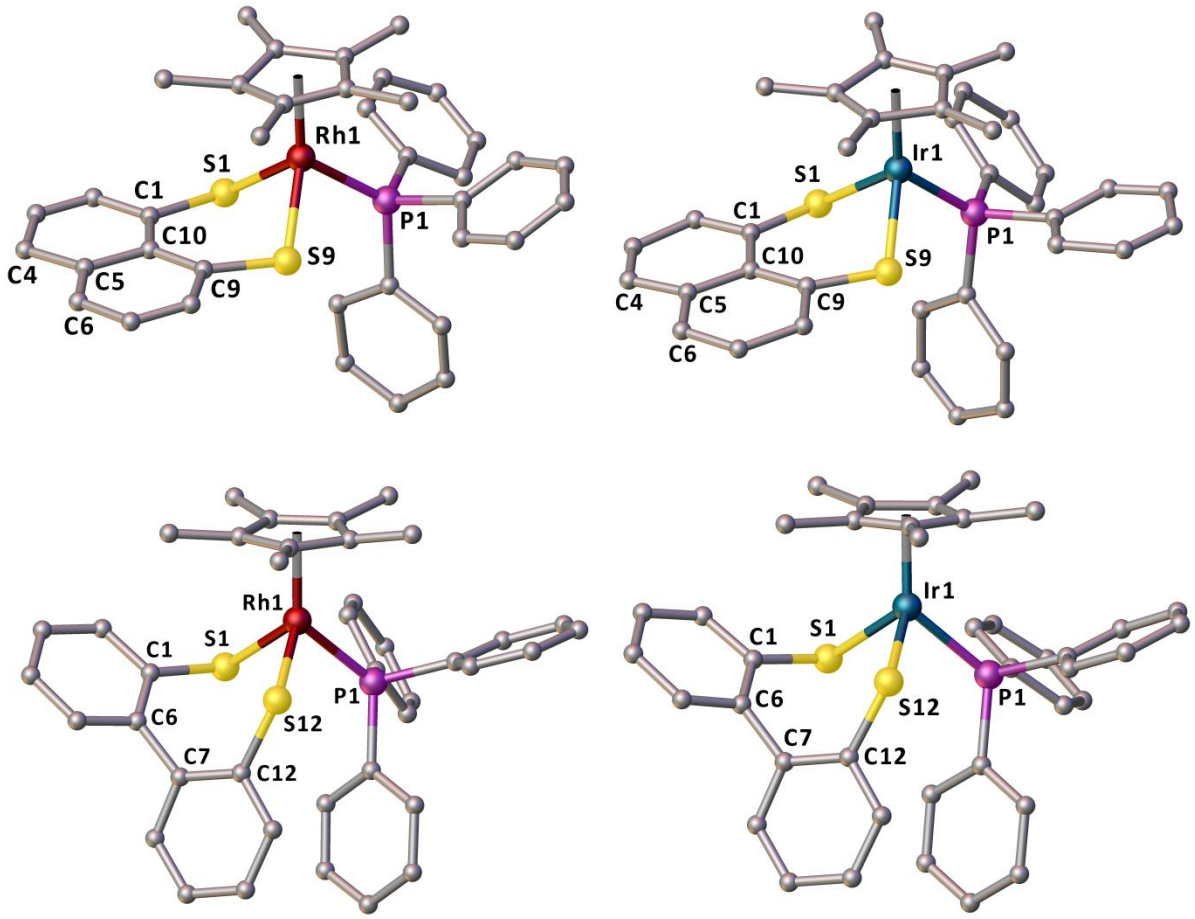

Figure 87: Crystal structures of **C5**-**5b** (top left), **C5**-**6b** (top right), **C5**-**5d** (bottom left) and **C5**-**6d** (bottom right). Only one of the two molecules within the asymmetric unit is shown for **C5**-**5b**/**6b**/**6d**. Hydrogen atoms and co-crystallised solvent molecules (**C5**-**6d**, Benzene) are omitted for clarity.

The M–S bond lengths are similar to those seen in our previous complexes with the iridium analogues being slightly longer than the equivalent rhodium complex. There is little change in this distance between the triethyl/triphenylphosphine derivatives. Again, the M–P bond lengths are shortened upon complexation of the dithiolate ligand compared to their respective dichloro starting materials.[263,267] The distance between the two sulfur atoms increases for the naphthalene examples compared to the free ligand, whilst the biphenyl containing complexes display a decreased value compared to the pro-ligand.

All of the non-Cp* angles in **C5**-**5b**/**6b** are close to, or less than, the ideal angle of 90° as the restrictive backbone prevents the sulfur atoms attaining a more ideal geometry. In **C5**-**5d**/**6d**, the greater rotational freedom within the backbone of the ligand allows the sulfur atoms to sit further apart and we see a corresponding increase in two of the angles around the metal centre. The splay angle in **C5**-**5b** is distinctly smaller ($\Delta_{splay\ angle} \approx 5.0°$) than the one seen in **C5**-**6b** and the

triethylphosphine derivatives **C5**-**3b** and **C5**-**4b**. The smaller splay in **C5**-**5b** is countered by it having a larger S1–C1···C9–S9 torsion angle than **C5**-**6b**. Interestingly, both of these values are smaller than those seen in **C5**-**3b** and **C5**-**4b** indicating a less strained system. The buckling of the central naphthalene ring system is similar between all the phosphine containing complexes. Within **C5**-**5d** and **C5**-**6d** the torsion angle between the two aryl rings is similar and comparable to our previous complexes. The out-of-plane displacements of the sulfur atoms are within the expected range based upon the values we have seen previously.

Table 21: Selected bond lengths [Å], angles [°], torsion angles [°] and displacements [Å] for **C5**-**5b**/**d** and **C5**-**6b**/**d**.

	C5-**5b**[b]	**C5**-**6b**[b]		**C5**-**5d**	**C5**-**6d**[b]
M1–P1	2.335(9)	2.303(10)	M1–P1	2.2981(8)	2.285(2)
M1–S1	2.336(9)	2.368(10)	M1–S1	2.3727(8)	2.375(2)
M1–S9	2.333(9)	2.339(10)	M1–S12	2.3552(9)	2.385(2)
S1···S9	3.168(10)	3.173(10)	S1···S12	3.451(1)	3.467(3)
S1–C1	1.76(3)	1.77(4)	S1–C1	1.773(3)	1.758(8)
S9–C9	1.78(3)	1.78(4)	S12–C12	1.777(3)	1.762(10)
S1–M1–S9	85.5(3)	85.4(3)	S1–M1–S12	93.78(3)	93.86(7)
S1–M1–P1	86.0(3)	87.2(4)	S1–M1–P1	93.56(3)	91.03(7)
S9–M1–P1	90.0(3)	89.0(3)	S12–M1–P1	84.25(3)	89.26(8)
splay angle[a]	15.58(6)	20.56(9)	-	-	-
S1–C1···C9–S9	4.0(2)	0.5(2)	-	-	-
C1–C10–C5–C6	178(3)	178(4)	C1–C6–C7–C12	67.6(4)	67.7(12)
C9–C10–C5–C4	176(4)	178(3)	-	-	-
Out of plane displacements					
S1	0.171	0.124	S1	0.171	0.135
S9	0.075	0.126	S12	0.034	0.027

[a] calculated as [(S1–C1–C10)+(C1–C10–C9)+(C10–C9–S9)−360].

[b] data shown for only one molecule within the asymmetric unit.

5.4.3 – Spectroscopic and structural analysis of triethyl phosphite containing complexes

The synthesis of complexes **C5**-**7b**/**7d** and **C5**-**8b**/**8d** were easily performed and resulted in isolated yields after purification of 55−77%. No stability issues were observed when purifying by column chromatography for **C5**-**7b**/**7d** and **C5**-**8b** whereas **C5**-**8d** did not require purification after isolation from the reaction mixture. The stability of the complexes in chloroform was greater than the triphenylphosphine complexes with no visible decomposition after twenty four hours. For consistency, the NMR analysis was performed using either deuterated benzene or DCM.

In both **C5-7b** and **C5-8b** the three expected aromatic signals are present in the ^{1}H NMR spectra between δ_H 7.92−6.98 ppm. For the biphenyl complexes **C5-7d** and **C5-8d**, the aromatic region consists of the previously seen doublet of doublet and triplet of doublet signals with some overlapping to form multiplets. The presence of the oxygen atom next to the ethyl chain results in these signals being shifted downfield with the CH_2 fragment most affected. In both **C5-7b** and **C5-8b** the signal arising from the CH_2 part of the ethyl chain was expected to be the same doublet of quartets seen previously in **C5-3b** and **C5-4b**. However, due to the now $^{3}J_{HP}$ coupling constant being almost identical to the $^{3}J_{HH}$ coupling constant, the signal appears as a pentet. Unlike in the triethylphosphine complexes, the CH_3 fragment in **C5-7b** and **C5-8b** results in a triplet as the $^{4}J_{HP}$ coupling is too small to be observed. The signal from the η^5-Cp* ligand still appears as a doublet but with larger $^{4}J_{HP}$ coupling constants than those seen in the phosphine derivatives.

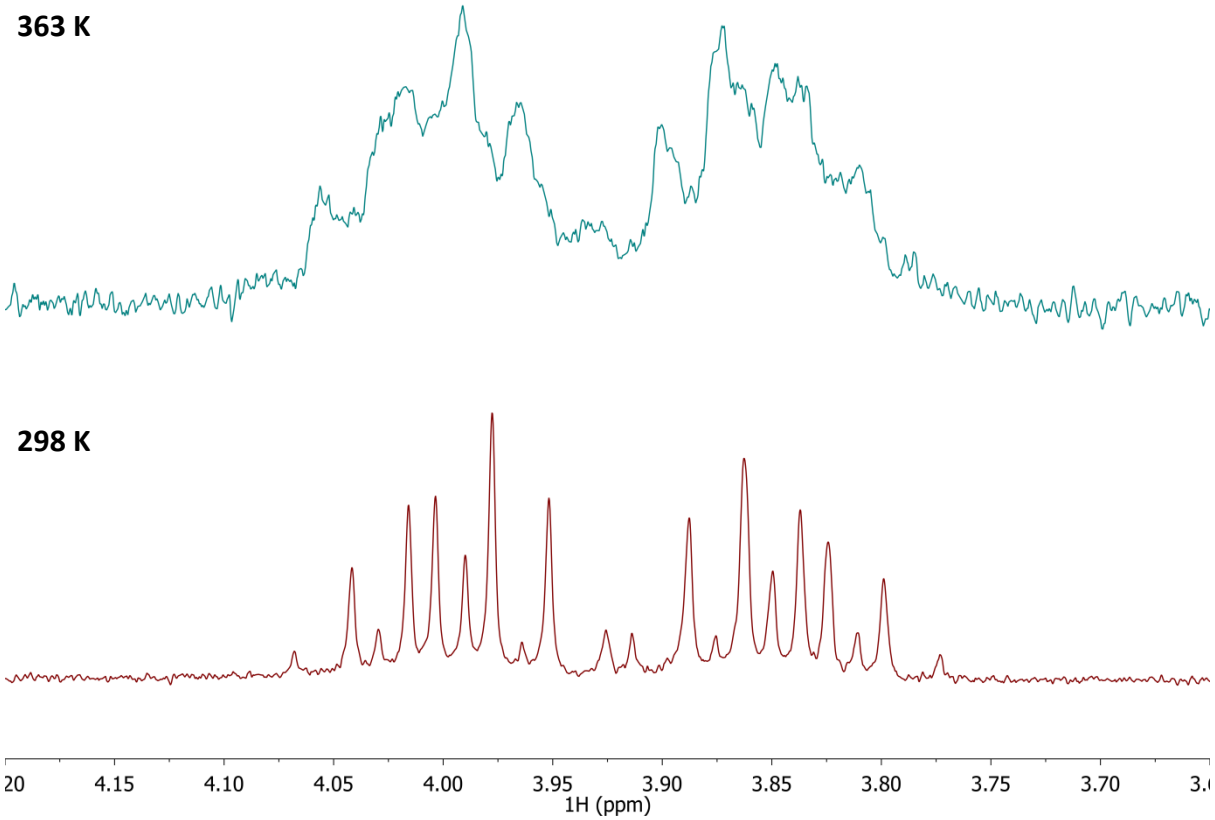

Figure 88: ^{1}H NMR spectra (C_6D_6, 270 MHz) of the methylene protons in **C5-7d** at 363 K (top) and 298 K (bottom).

As was observed in **C5-3d** and **C5-4d**, the two CH_2 protons in **C5-7d** and **C5-8d** have become inequivalent upon complexation of the biphenyl dithiolate ligand. Two distinct multiplets are observed between δ_H 4.02−3.95 & 3.88−3.80 ppm (**C5-7d**) and δ_H 4.07−4.00 & 3.85−3.77 (**C5-8d**). In order to investigate whether or not restricted rotation could be the cause for this observation, a

second ^{1}H NMR spectrum was obtained at 363 K (Figure 88). Two signals are still clearly visible despite the expected broadening of each due to the higher temperature at which the spectra was obtained. This supports our previous assertion that there is an axis of chirality introduced by the biphenyl ligand which results in the two CH_2 protons becoming diastereotopic.

Table 22: $^{31}P\{^{1}H\}$ NMR data ($CDCl_3$ (**C5**-**7**/**8**), CD_2Cl_2 (**C5**-**7b**/**8b**), C_6D_6 (**C5**-**7d**/**8d**), 162 MHz (**C5**-**7b**/**8b**), 202 MHz (**C5**-**7**/**8** & **C5**-**7d**/**8d**)) for **C5**-**7**/**8**, **C5**-**7b**/**d** and **C5**-**8b**/**d**. All δ values are in ppm and *J* values are in Hertz.

	C5-7	**C5-7b**	**C5-7d**
δ_P	114.0	123.5	120.0
$^{1}J_{PRh}$	215.1	235.0	243.0
	C5-8	**C5-8b**	**C5-8d**
δ_P	77.2	74.2	74.6

The $^{31}P\{^{1}H\}$ NMR data for **C5**-**7b**/**d** and **C5**-**8b**/**d** are summarised in Table 22. Both of the rhodium complexes result in a downfield shift upon complexation of the dithiolate whilst the iridium versions shift slightly upfield. There is a large increase in the $^{1}J_{PRh}$ coupling constant between both the naphthalene complexes **C5**-**3b** and **C5**-**7b** as well as the biphenyl containing complexes **C5**-**3d** and **C5**-**7d**. The distance between the two coupling nuclei can be a factor when the magnitude of the coupling is considered. However, the data in section 5.4.3.1 shows the Rh–P distances to be very similar. Previously we discussed the importance of electronic effects when comparing the phosphine and phosphite ligands (section 5.2.1.1). The improved π back donation occurring within **C5**-**7b**/**7d** results in a more efficient transfer of magnetic information leading to larger coupling constants.

The signals arising from the aromatic backbone and η^5-Cp* ligands in the $^{13}C\{^{1}H\}$ NMR spectra of **C5**-**7b**/**7d** and **C5**-**8d**/**8d** were analogous to their respective phosphine derivatives. Both of the ethyl carbon signals are split into doublets with the CH_2 fragment having $^{2}J_{CP}$ coupling constants between 5.6−6.7 Hz, whilst the CH_3 fragment ranged from 6.0−7.2 Hz. They are also shifted downfield compared to the phosphine versions as expected due to the presence of the oxygen atom. The mass spectra ($APCI^+$) of the complexes all showed a peak corresponding to $[M+H]^+$ at *m/z* 595.09 (**C5**-**7b**), 621.11 (**C5**-**7d**), 685.16 (**C5**-**8b**) and 711.17 (**C5**-**8d**); for **C5**-**8d** this was the base peak. The analytical purity of complexes **C5**-**7b**/**d** and **C5**-**8b**/**d** was confirmed by elemental analysis.

5.4.3.1 – Crystallographic characterisation of C5-7b/7d and C5-8b/8d

Crystals suitable for X-ray work were obtained by slow evaporation from either benzene (**C5**-**7b**/**8b**) or diethyl ether (**C5**-**7d**). A co-crystallised benzene solvent molecule was present within the structure of **C5**-**7b** and in the case of **C5**-**8d** two molecules of the complex crystallised within the asymmetric unit. The crystal structures are shown in Figure 89 with selected structural parameters in Table 23.

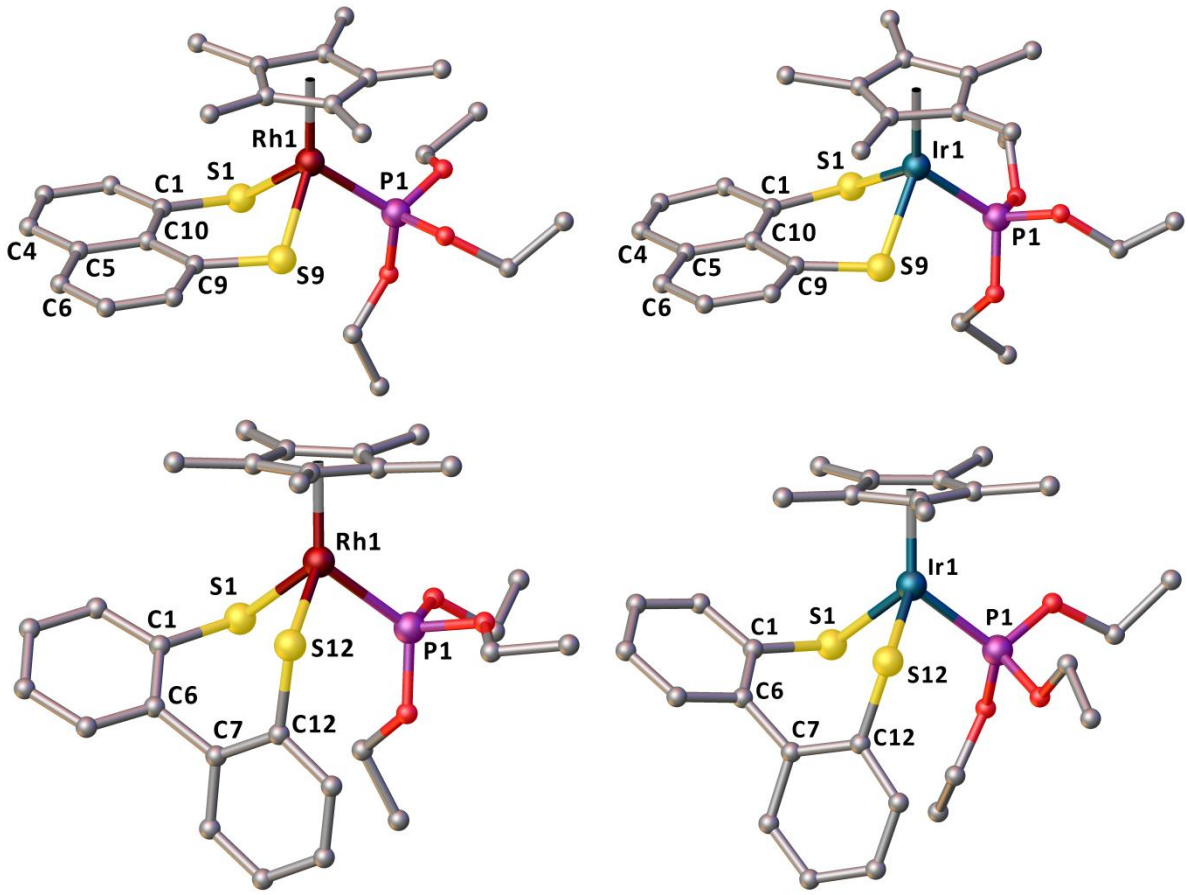

Figure 89: Crystal structures of **C5**-**7b** (top left), **C5**-**8b** (top right), **C5**-**7d** (bottom left) and **C5**-**8d** (bottom right). Only one of the two molecules within the asymmetric unit is shown for **C5**-**8d**. Hydrogen atoms and co-crystallised solvent molecules (**C5**-**7b**, Benzene) are omitted for clarity.

The M–P bond lengths in **C5**-**7b**/**8b** are comparable to those seen in the triethylphosphine containing complexes. This suggests that the steric effect of the phosphorus ligand, based on their respective Tolman cone angles, has little influence on the coordination of the dithiolate ligand. The same observation is made for **C5**-**7d**/**8d** when compared to the other biphenyl dithiolate triethylphosphine complexes. The M–S and S–C bond lengths were all within the expected range for complexes of this type as was the S···S distance.

Table 23: Selected bond lengths [Å], angles [°], torsion angles [°] and displacements [Å] for **C5-7b/d** and **C5-8b/d**.

	C5-7b	**C5-8b**		**C5-7d**	**C5-8d**
M1–P1	2.2291(8)	2.216(6)	M1–P1	2.241(1)	2.221(5)
M1–S1	2.335(1)	2.352(5)	M1–S1	2.367(2)	2.356(5)
M1–S9	2.3281(9)	2.345(6)	M1–S12	2.373(2)	2.365(6)
S1···S9	3.179(1)	3.172(8)	S1···S12	3.420(3)	3.400(7)
S1–C1	1.765(4)	1.79(2)	S1–C1	1.772(4)	1.77(2)
S9–C9	1.767(4)	1.77(2)	S12–C12	1.771(3)	1.80(2)
S1–M1–S9	85.96(3)	84.9(2)	S1–M1–S12	92.35(3)	92.1(2)
S1–M1–P1	89.58(3)	87.4(2)	S1–M1–P1	88.94(3)	95.2(2)
S9–M1–P1	90.96(3)	89.4(2)	S12–M1–P1	94.43(3)	88.5(2)
splay angle[a]	19.9(7)	19.8(5)	-	-	-
S1–C1···C9–S9	6.5(2)	6.8(6)	-	-	-
C1–C10–C5–C6	178.4(3)	178(2)	C1–C6–C7–C12	64.0(4)	68(3)
C9–C10–C5–C4	178.3(3)	178(2)	-	-	-
Out of plane displacements					
S1	0.227	0.019	S1	0.152	0.046
S9	0.043	0.277	S12	0.102	0.063

[a] calculated as [(S1–C1–C10)+(C1–C10–C9)+(C10–C9–S9)−360].

[b] data shown for only one molecule within the asymmetric unit.

The angles around the metal centres within all the complexes are comparable to those seen previously. The splay angles in **C5-7b/8b** are approximately 20° which is similar to the other naphthalene dithiolate complexes. Both **C5-7b/8b** have comparable buckling of the central naphthalene ring system and the torsion between the two aryl rings in **C5-7d/8d** are within the expected range. Finally, the out-of-plane displacements of the sulfur atoms are consistent with those from the other complexes **C5-3b/d** and **C5-4b/d**.

5.4.4 – Spectroscopic and structural analysis of triphenyl phosphite containing complexes

The synthesis of **C5-9b/d** and **C5-10b/d** proved to be harder than the previous complexes. For the biphenyl derivatives the yields obtained were 22% for **C5-9d** and 44% for **C5-10d**, with both being well below what was expected. Complexes **C5-9b** and **C5-10b** were even lower at 8% and 19% respectively. At first it was believed that the variable size of the triphenyl phosphite ligand based on cone angles calculated by Darensbourg[266] was causing the reaction to proceed slowly. As such, the following reaction conditions were tested for **C5-9b**; a) stirring at room temperature for two days, b) stirring at reflux overnight and c) stirring at reflux for two days. In all cases there was none of the previously isolated product formed after the reaction. Examination of the unlocked $^{31}P\{^{1}H\}$ NMR

spectrum of the reaction solution began to explain what was happening as a doublet was seen at approximately δ_P 130 ppm (J 239.3 Hz). This didn't correspond to any of the starting materials used and so must be a new compound formed during a side reaction. The solvent was removed and the unknown compound dissolved in DCM and filtered through celite to remove the salt by-product. With material now pure enough for analysis both the ^{1}H and $^{31}P\{^{1}H\}$ NMR spectrum were obtained.

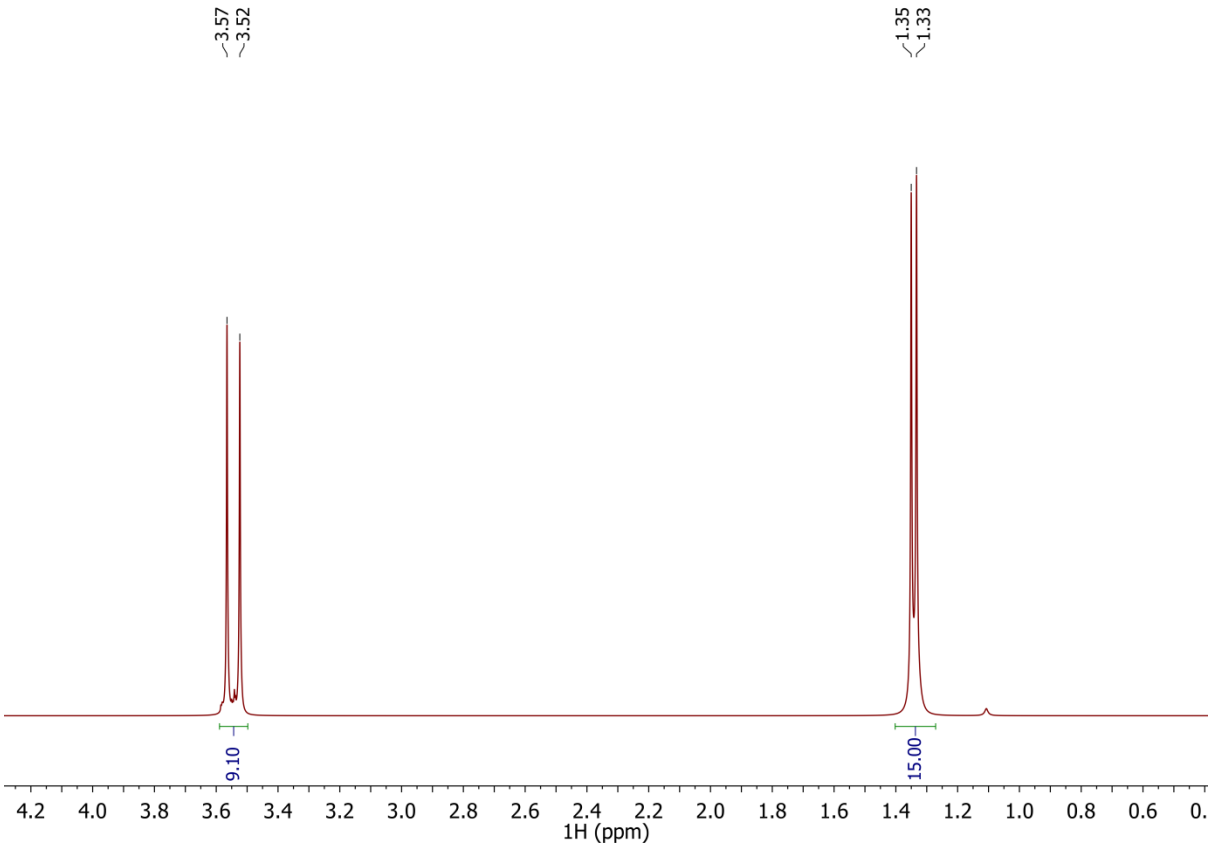

Figure 90: Alkyl region of the ^{1}H NMR spectrum (CD_2Cl_2, 270 MHz) of the product from the side reaction (**C5**-**12b**). Impurity peak (H_2O) has been removed for clarity.

The ^{1}H NMR spectrum showed only three signals in the aromatic region which could be assigned to the naphthalene backbone, a doublet centred at δ_H 3.54 (J = 11.2 Hz) and the expected doublet from the η^5-Cp* ligand around δ_H 1.34 ppm along with other impurities. The ratio between the signal at δ_H 3.54 and 1.34 ppm was found to be 9:15 (Figure 90). One possible way for this ratio to arise would be if three equivalent methyl groups were present within the compound. The $^{31}P\{^{1}H\}$ NMR spectrum indicates the phosphorus ligand is still a phosphite. Coupling this with the ^{1}H NMR spectrum suggests that during the reaction the triphenyl phosphite ligand had become trimethyl phosphite. Crystals suitable for X-ray work were obtained by slow evaporation from the NMR sample. The structure obtained confirmed the presence of a trimethyl phosphite ligand (Figure 91). The sulfur donor atoms

have also undergone minor oxidation with the oxygen atom present having 25% occupancy at each position.

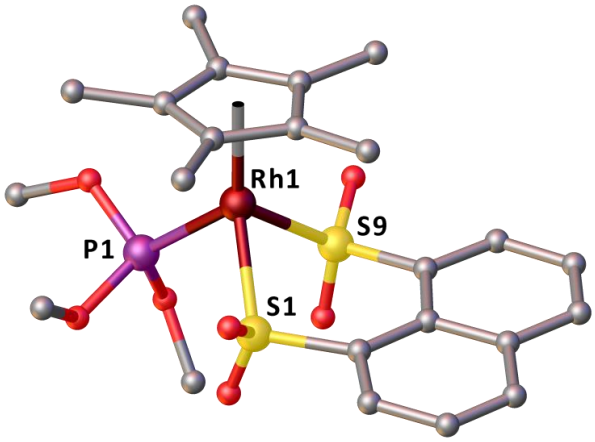

Figure 91: Crystal structure of the side reaction product (**C5**-**12b**). Hydrogen atoms are omitted for clarity.

A possible explanation for this occurrence is related to the electronics within the target compound. As the phosphorus ligand is donating its lone pair to the metal centre, the phosphorus itself becomes relatively δ^+, making it susceptible to nucleophilic attack. In the reaction excess sodium methoxide is used which could act as a nucleophile to displace the OPh group (Scheme 35). Given that total conversion to this product was observed, it is likely that the methanol is also participating in this exchange reaction. There could also be a steric factor as the $P(OPh)_3$ is a larger ligand than $P(OMe)_3$, substitution of the OPh with OMe may be releasing strain within the complex. The occurrence of this displacement reaction was also supported with observations made during the reaction. In the $P(OEt)_3$ derivatives (**C5**-**7b** and **C5**-**8b**) the reaction mixture is a solution and in other examples where we have used the bulkier aryl phosphine and phosphite ligands, the product precipitates out of the reaction mixture. Only a small amount of solid was obtained by filtration during the synthesis of **C5**-**9b** as the side product **C5**-**12b** is soluble in methanol.

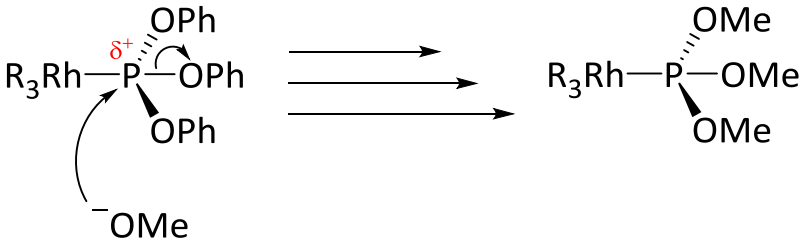

Scheme 35: Possible exchange reaction occurring to form **C5**-**12b**.

In order to test this theory, additional experiments were carried out. The first involved taking triphenyl phosphite and heating it overnight in the presence of sodium methoxide in methanol, replicating the conditions of the previous experiments. In the $^{31}P\{^{1}H\}$ NMR spectrum, triphenyl phosphite appears at δ_P 129.6 ppm whilst the product from the reaction showed a signal at δ_P 142.1 ppm. This new signal correlates to the literature value for trimethyl phosphite which appears at δ_P 140 ppm.[273] An additional peak appearing further upfield was also seen, corresponding to trimethyl phosphate. This demonstrates that the proposed exchange reaction is favourable, even in the free ligand in which the phosphorus would be considerably less δ^+.

In order to optimise the reaction for the desired product (**C5**-**9b**) a small scale experiment was carried out using sodium hydroxide in place of sodium methoxide. The yield for this reaction was improved at 49% however evidence of **C5**-**12b** was still present within the reaction solvent confirming that the methanol itself can participate in the exchange reaction. Replacement of methanol with THF as outlined in Scheme 36 resulted in greatly improved yields for both **C5**-**9b** (88%) and **C5**-**10b** (83%) with no appreciable amount of the trimethylphosphite analogues obtained.

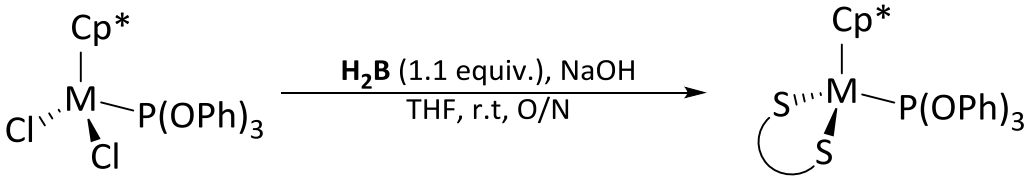

C5-**9, M = Rh**
C5-**10, M = Ir**

C5-**9b, M = Rh**
C5-**10b, M = Ir**

Scheme 36: Alternative reaction conditions for the synthesis of **C5**-**9b**/**10b**.

In the case of **C5**-**10d** the complex was found to be stable to purification *via* column chromatography; attempts at purifying the other complexes this way were not attempted due to low yields. The ^{1}H NMR spectra of all the complexes showed the same signals arising from both the dithiolate ligand backbone and η^5-Cp* ligand as before with the phenyl ring signals clearly visible. Unlike in the triphenylphosphine complexes, three distinct signals corresponding to the *ortho*, *meta* and *para* hydrogen atoms were observed. The $^{13}C\{^{1}H\}$ NMR spectra mirrored that of the ^{1}H NMR spectra with the expected signals with appropriate splitting present. The $APCI^+$ (**C5**-**9b** and **C5**-**10b**/**d**) and NSI^+ (**C5**-**9d**) mass spectra all showed peaks corresponding to the $[M+H]^+$ ion at *m/z* 739.0974 (**C5**-**9b**), 765.11 (**C5**-**9d**), 829.16 (**C5**-**10b**) and 855.17 (**C5**-**10d**). Other peaks for the $[P(OPh)_3+H]^+$ ion were also seen in the two iridium complexes and in both cases were the base peaks. As before the homogeneity of the complexes was confirmed by elemental analysis.

The $^{31}P\{^{1}H\}$ NMR data obtained for complexes **C5**-**9b**/**d** and **C5**-**10b**/**d** are summarised in Table 24. As before, the signals for the iridium complexes have shifted upfield whilst the rhodium complexes have shifted downfield compared to their respective starting materials. The $^{1}J_{PRh}$ coupling in **C5**-**9b**/**d** is the largest we have seen thus far. An increase of over 100 Hz is observed when comparing the triphenylphosphine to the triphenyl phosphite containing complexes. The Rh–P bond lengths in **C5**-**9b**/**d** are slightly shorter than those in **C5**-**5b**/**d**, however this would not account for such a large increase in the coupling. For the same reason as those discussed in section 5.4.3, the change in the electronic properties of the ligand is the primary cause for this increase. Interestingly, this value is higher than the triethyl phosphite derivatives providing further evidence that the steric factors are of little importance since the Tolman cone angle of triphenyl phosphite (128°) is much larger than triethyl phosphite (109°).

Table 24: $^{31}P\{^{1}H\}$ NMR data ($CDCl_3$ (**C5**-**9**/**10**), CD_2Cl_2 (**C5**-**9b**/**9d** & **C5**-**10b**), C_6D_6 (**C5**-**10d**), 162 MHz (**C5**-**9b**/**10b**), 202 MHz (**C5**-**9**/**10** & **C5**-**9d**/**10d**)) for **C5**-**9**/**10**, **C5**-**9b**/**d** and **C5**-**10b**/**d**. All δ values are in ppm and *J* values are in Hertz

	C5-9	**C5-9b**	**C5-9d**
δ_P	104.0	112.4	110.6
$^{1}J_{PRh}$	240.0	263.7	269.9
	C5-10	**C5-10b**	**C5-10d**
δ_P	65.8	60.6	62.9

5.4.4.1 – Crystallographic characterisation of C5-9b/d and C5-10d

Crystals suitable for X-ray work were obtained for **C5**-**9b**, **C5**-**9d** and **C5**-**10d** by slow evaporation from a DCM, benzene or diethyl ether solution respectively. Both **C5**-**9b** and **C5**-**10d** crystallised with two molecules within the asymmetric unit. The structure obtained from the crystals of **C5**-**10b** was of a poor quality and was only adequate for obtaining distances around the coordination sphere of the metal. For this reason, it is not included within the discussion.

As with all the other complexes, the structure adopts a piano stool geometry. The M–S, S–C and S···S distances are all comparable to those we have seen previously. Some of the M–P bond lengths are the shortest seen through the series, due to the improved π back donation discussed in section 5.2.1.1 earlier. The angles around the metal centre follow similar patterns to our previous complexes with larger angles for the biphenyl analogue than the naphthalene derivative. The splay angle in **C5**-**9b** is within the expected range as are the out-of-plane displacements of the sulfur atoms and the buckling of the central naphthalene ring system. For both **C5**-**9d** and **C5**-**10d**, the torsion between

the two aryl rings is similar to that seen before as are the out-of-plane displacements of the sulfur atoms.

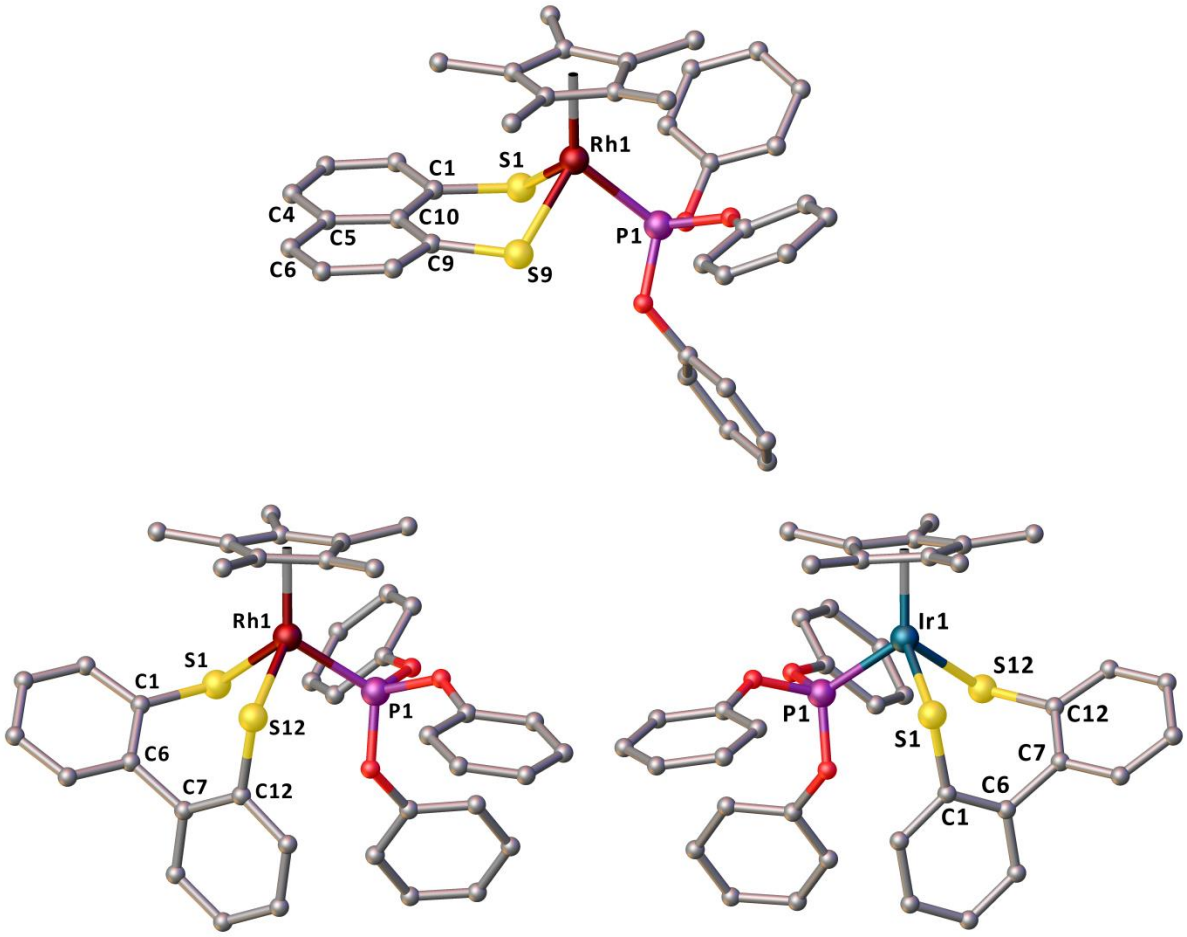

Figure 92: Crystal structures of **C5**-**9b** (top), **C5**-**9d** (bottom left) and **C5**-**10d** (bottom right). Only one of the two molecules within the asymmetric unit is shown for **C5**-**9b** and **C5**-**10d**. Hydrogen atoms are omitted for clarity.

Table 25: Selected bond lengths [Å], angles [°], torsion angles [°] and displacements [Å] for **C5-9b/d** and **C5-10d**.

	C5-9b[b]		**C5-9d**	**C5-10d**[b]
M1–P1	2.223(2)	M1–P1	2.2108(8)	2.199(2)
M1–S1	2.340(2)	M1–S1	2.3821(8)	2.407(2)
M1–S9	2.332(2)	M1–S12	2.3987(8)	2.397(2)
S1···S9	3.175(3)	S1···S12	3.420(3)	3.400(7)
S1–C1	1.764(9)	S1–C1	1.772(4)	1.80(2)
S9–C9	1.770(8)	S12–C12	1.771(3)	1.77(2)
S1–M1–S9	85.22(8)	S1–M1–S12	90.15(3)	89.44(7)
S1–M1–P1	85.01(8)	S1–M1–P1	95.15(3)	95.49(8)
S9–M1–P1	90.87(8)	S12–M1–P1	94.69(3)	95.03(8)
splay angle[a]	18.2(7)	-	-	-
S1–C1···C9–S9	8.6(5)	-	-	-
C1–C10–C5–C6	176.6(9)	C1–C6–C7–C12	63.8(4)	64(1)
C9–c10–C5–C4	176.1(9)	-	-	-
Out of plane displacements				
S1	0.109	S1	0.102	0.063
S9	0.283	S12	0.152	0.046

[a] calculated as [(S1–C1–C10)+(C1–C10–C9)+(C10–C9–S9)−360].

[b] data shown for only one molecule within the asymmetric unit.

5.5 – Conclusions

Synthetic routes towards monomeric half sandwich rhodium and iridium complexes containing both dithiolato and phosphorus ligands have been investigated. The two routes available were compared and one selected based on the highest predicted overall yield due to the high cost of the starting materials. This required the synthesis of several dichloro rhodium and iridium starting materials which were fully characterised principally using multinuclear NMR spectroscopy and single crystal X-ray diffraction. The majority of the single crystal X-ray diffraction data presented in this chapter was collected and solved personally.

A series of ligands were chosen to examine whether the same change in structure between rigid and rotationally free dithiolato ligands would be seen in the monomeric complexes. Four complexes were prepared in high yields and fully characterised to confirm their identity and structure. Single crystal X-ray diffraction was used to examine the solid state structure and it was found that all the complexes adopted the same piano stool geometry. The presence of the phosphorus ligand

occupying the vacant coordination site resulted in no difference between the two types of ligand backbone used.

Finally, the importance of the phosphorus ligand was investigated to see if changes to the size and electronic factors would have any effect on the synthesis and structure of the complex. It was found that two different synthetic routes were required depending on both the size and electronics of the phosphorus ligand. No changes in the solid state structure were found when using the series of phosphine and phosphites ligands selected. One interesting observation was the lack of correlation between the size of the ligand, based upon its Tolman cone angle, and the M–P bond length. In some cases larger ligands actually had shorter M–P bond lengths. By examining the $^{1}J_{PRh}$ coupling constants across the series, the reason was identified. Greater π back donation in the phosphite containing complexes leads to a shorter M–P bond length and thus a larger coupling constant than in the phosphine derivatives. Hence, in this case, the electronic properties of the phosphorus ligands are overcoming any negative steric effects.

The work presented in this chapter has contributed to the following publications:

Varying the flexibility of the aromatic backbone in half sandwich rhodium(III) dithiolato complexes: A synthetic, spectroscopic and structural investigation: Phillip S. Nejman, Alexandra M. Z. Slawin, Petr Kilian, J. Derek Woollins, *Cogent Chemistry*, **2016**, *2(1)*, 1–14, Article number 1245900.

The preparation and characterisation of rhodium(III) and iridium(III) half sandwich complexes with naphthalene-1,8-dithiolate, acenaphthene-5,6-dithiolate and biphenyl-2,2'-dithiolate: Phillip S. Nejman, Brian Morton-Fernandez, Nicholas Black, David B. Cordes, Alexandra M. Z. Slawin, Petr Kilian, J. Derek Woollins, *J. Organomet. Chem.*, **2015**, *776*, 7–16.

Part 3 – Synthetic Protocols

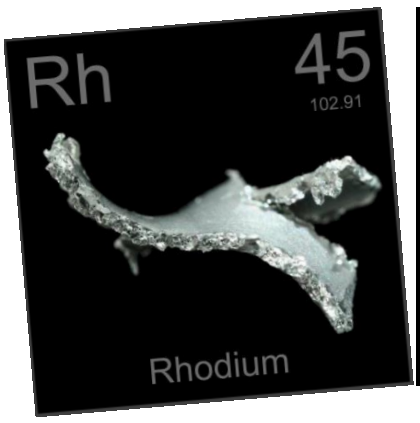

Chapter 6 – Experimental

General Considerations

All synthetic manipulations were performed under an atmosphere of dry nitrogen using standard Schlenk-line techniques or under an argon atmosphere in a *Saffron glovebox* unless stated otherwise. Dry solvents were either collected from an *MBraun Solvent Purification System* and stored over molecular sieves, or were dried and stored according to common procedures.[274] Water used in experiments was deoxygenated by prolonged bubbling of nitrogen gas through it. Chemicals were purchased from Sigma Aldrich, Acros Organics, Fluorochem, Alfa Aesar, Strem Chemicals Ltd., Apollo Scientific or were taken from the laboratory inventory and used without further purification.

NMR Spectroscopy

All NMR spectra were recorded using a *JEOL GSX Delta 270, Bruker Avance 300, Bruker Avance II 400, Bruker Avance 500* or *Bruker Avance III 500* (MHz) spectrometer at 25 °C. Assignments of ^{1}H and $^{13}C\{^{1}H\}$ NMR spectra were made in conjunction with H–H DQF-COSY, H–C HSQC, H–C HMBC and H–P HMBC two-dimensional experiments. $^{13}C\{^{1}H\}$ NMR spectra were recorded using the DEPT-Q–135 (**D**istortionless **E**nhancement by **P**olarisation **T**ransfer with retention of **Q**uaternaries) pulse sequence with broadband proton decoupling. For ^{31}P NMR, 85% H_3PO_4 in D_2O was used as an external standard. For ^{1}H and $^{13}C\{^{1}H\}$ NMR, tetramethylsilane was used as an external standard. Residual solvent peaks were also used for calibration ($CDCl_3$ δ_H 7.26, δ_C 77.2 ppm; CD_2Cl_2 δ_H 5.32, δ_C 53.8 ppm; C_6D_6 δ_H 7.16, δ_C 128.1 ppm). Pictures of NMR spectra were created using *MestReNova*. Chemical shifts (δ) are given in parts per million (ppm) relative to the solvent peaks. Coupling constants (J) are given in Hertz (Hz).

Mass Spectrometry

Mass Spectrometry at the University of St Andrews was performed using a *Micromass LCT* (Electrospray Ionisation) from solutions of the analyte in methanol or acetonitrile by Mrs Caroline Horsburgh. Spectra acquired at the EPSRC UK National Mass Spectrometry Facility in Swansea were done so using a *Thermofisher LTQ Orbitrap XL* (APCI and NSI).

Infrared and Raman Spectroscopy

Infrared spectra were recorded as KBr discs in the range of 4000–400 cm^{-1} using a *Perkin-Elmer System 2000 NIR Fourier Transform* Spectrometer. Raman Spectra were recorded as solid samples using a *Perkin-Elmer System 2000 NIR Fourier Transform* Spectrometer with a dipole pumped NdYAG laser ranging between 30–600 mW power with a scanning range of 3500–150 cm^{-1}.

Elemental Analysis and Melting Points

Elemental Analysis (C, H and N) was performed by the Elemental Analysis Service of London Metropolitan University by Mr Stephen Boyer with the determined values give in percent (%). Melting and decomposition points are uncorrected and were determined by heating solid samples in sealed glass capillaries using a *Stuart SMP 30 melting point apparatus*.

X-ray Crystallography

The crystallographic data were collected using either: *Rigaku SCX-Mini diffractometer* (Mercury 2CCD) at –148(1) or –100(1) °C with SHINE optic using Mo-Kα radiation; *Rigaku Mo MM007* (dual port) high brilliance generator with Saturn 70 and Mercury CCD detectors, rotating anode/confocal optics and two XStream LT accessories at –180(1) °C using Mo-Kα radiation; *Rigaku FRX/Dectris P200 diffractometer* with confocal optics Mo-Kα radiation at –100(1) °C; *Rigaku MM007HF/Dectris P200/P100 diffractometers* with confocal optics Cu-Kα radiation at –180(1) or –100(1) °C (Mo-Kα = λ = 0.71073 Å and Cu-Kα = 1.5418 Å). Intensity data were collected using ω steps accumulating area detector frames spanning at least a hemisphere of reciprocal space for all structures. All data were corrected for Lorentz polarisation, and long-term intensity fluctuations. Absorption effects were corrected on the basis of multiple equivalent reflections. The data for all compounds were collected and processed using *CrystalClear (Rigaku)*. The crystal structures were solved using direct methods and refined by full-matrix least-squares against F^2 (SHELXL) or heavy–atom Patterson methods and expanded using Fourier techniques. All calculations were performed using the *CrystalStructure* crystallographic software package except for refinement which was performed using *SHELXL–97/2013*. The non-hydrogen atoms were refined anisotropically, hydrogen atoms were assigned riding isotropic displacement parameters and constrained to idealised geometries. Searches of the Cambridge Structure Database (CSD) were performed using either *ConQuest*[275] or the *WebCSD*.[25] Images of crystal structures displayed in this thesis were obtained using *OLEX–2 v1.2.8*[276] with all other manipulations carried out using *Mercury v3.7*.[26] The crystallographic files (.cif) presented in this thesis are available on the attached CD.

6.1 – Chapter 2 Experimental Procedures

6.1.1 – Triphenylbismuth ($BiPh_3$)

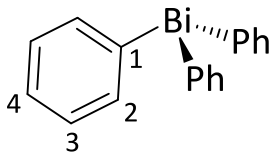

$BiPh_3$ was prepared according to the literature procedure.[101,102] A 250 mL 3-necked round bottom flask was equipped with a pressure equalising dropping funnel and a reflux condenser connected to a Schlenk line. Magnesium turnings (1.27 g, 52.30 mmol) were added to diethyl ether (20 mL) in the flask and a solution of bromobenzene (7.47 g, 5.0 mL, 47.60 mmol) in diethyl ether (40 mL) added to the dropping funnel. A small amount of the PhBr/diethyl ether solution was added to start the reaction (if necessary, a small amount of I_2 can be added to initiate the reaction). Once the initial reaction subsided, the remaining PhBr/diethyl ether solution was added dropwise over 1 h. The mixture was then heated at reflux for 1 h and left to cool to room temperature. A suspension of $BiCl_3$ (5.0 g, 15.92 mmol) in diethyl ether (20 mL) was added *via* syringe in portions over 30 mins at 0 °C. The reaction was refluxed for 1 h then cooled to room temperature. A 10% ammonium chloride solution (30 mL) was added cautiously to the reaction followed by a few drops of 3M HCl. The diethyl ether layer was removed and the aqueous layer extracted with more diethyl ether (20 mL). The combined organic layers were dried over magnesium sulfate and filtered. Removal of the solvent afforded the crude product was an off white/green solid. This was dissolved in hot ethanol then left to cool. Upon addition of water (dropwise) the product precipitated out as a white crystalline solid (5.32 g, 12.08 mmol, 76%) m.p 77.5−78.4 °C (lit. 77−78 °C).[101] Analytical data obtained were in good agreement with that previously reported.[101]

Anal. calcd. for $C_{18}H_{15}Bi$ (440.29 g mol^{-1}): C, 49.10; H, 3.44. Found: C, 49.05; H, 3.39.

^{1}H NMR (500 MHz, $CDCl_3$): δ 7.76−7.73 (m, 6 H, H2), 7.40−7.36 (m, 6 H, H3), 7.32 (tt, $^3J_{HH}$ = 7.3, $^2J_{HH}$ = 2.3 Hz, 3 H, H4).

^{13}C{^{1}H} NMR (125 MHz, $CDCl_3$): δ 151.9 (C_q, C1), 137.8 (CH, C2), 130.7 (CH, C3), 128.1 (CH, C4).

HRMS (APCI$^+$): *m/z* (%) 457.0998 (50) $[M+OH]^+$, 363.0579 (100) $[M-Ph]^+$.

IR (KBr): **ν_{max}/cm^{-1}** 3056s (ν_{Ar-H}), 1566m, 1425s, 1057m, 996m, 728s, 694s, 449m.

Raman (glass capillary): ν_{max}/cm^{-1} 3040m (ν_{Ar-H}), 1570m, 1016m, 1000s, 646m, 221m, 208m.

6.1.2 – Diphenylbismuth chloride ($BiPh_2Cl$)

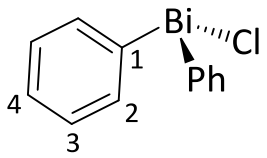

$BiPh_2Cl$ was prepared according to the literature procedure.[101] To a solution of $BiPh_3$ (1.0 g, 2.27 mmol) in diethyl ether (30 mL) at 0 °C (ice bath) was added $BiCl_3$ (358 mg, 1.13 mmol) in one portion. The reaction was left to stir for 4 h at this temperature then warmed to room temperature and stirred O/N. The reaction was filtered and washed with diethyl ether then the white solid obtained dried under vacuum for 3 h. The product was obtained as a white powder (1.20 g, 3.02 mmol, 89%) m.p 185.1−187.0 °C (lit. 184−185 °C).[101] Analytical data obtained were in good agreement with that previously reported.[101]

^{1}H NMR (500 MHz, d_6-acetone): δ 8.35−8.31 (m, 4 H, H2), 7.66−7.60 (m, 4 H, H3), 7.39−7.32 (tt, $^3J_{HH}$ = 7.5, $^4J_{HH}$ = 1.4 Hz, 2 H, H4).

^{13}C{^{1}H} NMR (125 MHz, d_6-acetone): δ 184.4 (C_q, C1), 137.0 (CH, C2), 131.4 (CH, C3), 127.9 (CH, C4).

HRMS (APCI$^+$): *m/z* (%) 363.0579 (100) $[M-Cl]^+$.

IR (KBr): **ν_{max}/cm^{-1}** 3060m (ν_{Ar-H}), 3047m (ν_{Ar-H}), 1568m, 1474s, 1429s, 1055m, 996s, 752s, 691s, 438m.

Raman (glass capillary): ν_{max}/cm^{-1} 3049m (ν_{Ar-H}), 1571m, 999s, 211s, 175w.

6.1.3 – Dichloro(phenyl)bismuth ($BiPhCl_2$)

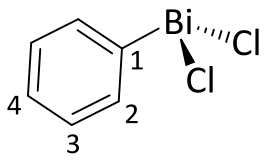

$BiPhCl_2$ was prepared according to the literature procedure.[100] To a solution of $BiPh_3$ (1.0 g, 2.27 mmol) in diethyl ether (30 mL) was added slowly over 1 h a suspension of $BiCl_3$ (1.44 g, 4.57 mmol) in diethyl ether (50 mL) at room temperature. During this time a pale yellow precipitate formed. The suspension was filtered and washed with diethyl ether (2 × 10 mL) then dried under vacuum for 4 h. The product was obtained as an off white solid (1.70 g, ≈70%). Analytical data obtained were in good agreement with that previously reported.[100]

Yield is approximate due to contamination with [$BiPh_2Cl$] and is calculated based on the ^{1}H NMR spectrum. This impurity meant m.p and elemental analysis could not be obtained.

^{1}H NMR (400 MHz, d_6-acetone): δ 9.02−8.99 (m, 2 H, H2), 8.00−7.94 (m, 2 H, H3), 7.45 (tt, $^3J_{HH}$ = 7.4, $^4J_{HH}$ = 1.4 Hz, 1 H, H4).

^{13}C{^{1}H} NMR (100 MHz, d_6-acetone): δ 220.8 (C_q, C1), 137.7 (CH, C2), 132.9 (CH, C3), 128.3 (CH, C4).

HRMS (APCI$^+$): *m/z* (%) 278.9189 (50) $[M-Ph]^+$, 243.9497 (100) $[BiCl]^+$.

IR (KBr): **ν_{max}/cm^{-1}** 3047w (ν_{Ar-H}), 1610br, 1429m, 1052w, 995m, 726s, 691m, 438m.

6.1.4 – 5,6-dibromoacenaphthene (AcenapBr$_2$)

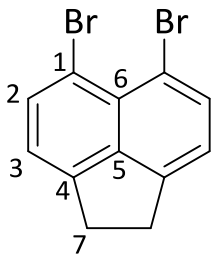

AcenapBr$_2$ was prepared according to the literature procedure.[99] A solution of N-bromosuccinimide (251.6 g, 1.41 mol) in DMF (750 ml) was added drop wise over 4 h to a rapidly stirring solution of acenaphthene (109.0 g, 0.71 mol) in DMF (180 ml), cooled to 0°C using an ice bath. Once the addition was complete the solution was warmed to room temperature and left to stir for a further 24 h. After this time, the solid precipitate was filtered and washed with ethanol (3 x 150 ml) to leave the crude product as a pale brown powder. The crude product was purified by rapidly stirring in refluxing ethanol (400 ml) for 12 h. The solution was cooled in an ice bath and filtered to yield the pure product which was dried *in vacuo* for 3–4 h (42.9 g, 20%). Analytical data obtained were in good agreement with that previously reported.[99,226]

Anal. calcd. for $C_{12}H_8Br_2$ (311.99 g mol^{-1}): C, 46.20; H, 2.58. Found: C, 46.12; H, 2.52.

^{1}H NMR (500 MHz, $CDCl_3$): δ 7.81 (d, 2 H, $^3J_{HH}$ = 7.4 Hz, H2), 7.11 (d, 2 H, $^3J_{HH}$ = 7.4 Hz, H3), 3.32 (s, 4 H, H7).

^{13}C{^{1}H} NMR (125 MHz, $CDCl_3$): δ 147.1 (C_q, C4), 142.0 (C_q, C5), 135.9 (CH, C2), 127.8 (C_q, C6), 121.0 (CH, C3), 114.4 (C_q, C1), 30.1 (CH_2, C7).

IR (KBr): ν_{max}/cm^{-1} 2944m (ν_{C-H}), 2366m, 1597s, 1409s, 1322s, 1225s, 1105s, 1021s, 836vs, 808s, 600s, 498m.

Raman (glass capillary): ν_{max}/cm^{-1} 3067s (ν_{Ar-H}), 2932s (ν_{C-H}), 1564s, 1435s, 1323vs, 1222m, 812m, 709m, 575s, 500m, 468w, 306vs.

6.1.5 – (^{i}Pr)$_2$P-Acenap-Br (C2-1)

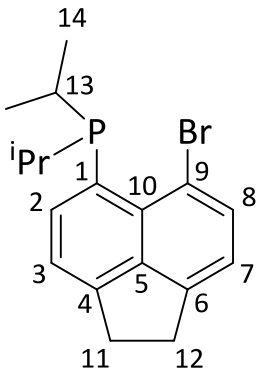

Compound **C2**-**1** was prepared according to the literature procedure.[24] To a cooled (−78 °C) rapidly stirring solution of AcenapBr$_2$ (16.0 g, 51.30 mmol) in THF (180 mL), n-BuLi (20.5 mL, 2.5 M sol^{n} in hexanes, 51.30 mmol) was added drop wise over 1 h and the mixture left to stir for a further 2 h at the same temperature. A solution of chlorodiisopropylphosphine (8.20 mL, 7.83 g, 51.30 mmol) in THF (18 mL) was then added using a syringe over 2 h. The solution was allowed to warm up to room temperature O/N. The volatiles were removed *in vacuo* and the solvent replaced with diethyl ether (200 mL) and washed with degassed water (75 mL). The organic layer was removed and dried over magnesium sulfate then filtered and the solvent removed *in vacuo* to reveal a yellow solid. The compound was recrystallised from hot ethanol to afford **C2**-**1** as a yellow crystalline solid (16.30 g, 46.68 mmol, 91%, m.p 83–85 °C (lit. 83−86 °C)[24]).

Anal. calcd. for $C_{18}H_{22}PBr$ (349.25 g mol^{-1}): C, 61.90; H 6.35. Found: C, 62.01; H 6.30.

^{1}H NMR (500 MHz, $CDCl_3$): δ 7.68 (d, $^{3}J_{HH}$ = 7.4 Hz, 1 H, H8), 7.60 (d, $^{3}J_{HH}$ = 7.4 Hz, 1 H, H2), 7.21 (d, $^{3}J_{HH}$ = 7.4 Hz, 1 H, H7), 7.00 (d, $^{3}J_{HH}$ = 7.4 Hz, 1 H, H3), 3.28–3.26 (m, 2 H, H11), 3.22–3.19 (m, 2 H, H12) 2.15 (d sept., $^{3}J_{HH}$ = 7.0 Hz, $^{2}J_{HP}$ = 1.9 Hz, 2 H, H13), 1.10 (dd, $^{3}J_{HP}$ = 12.8, $^{3}J_{HH}$ = 7.0 Hz, 6 H, H14, 2 × CH_3), 0.98 (dd, $^{3}J_{HP}$ = 13.4, $^{3}J_{HH}$ = 7.1 Hz, 6 H, H14, 2 × CH_3).

^{13}C{^{1}H} NMR (125 MHz, $CDCl_3$): δ 147.9 (C_q, C6), 146.9 (C_q, C4), 141.6 (d, $^{3}J_{CP}$ = 4.4 Hz, C_q, C5), 135.3 (CH, C2), 134.9 (CH, C8), 134.0 (d, $^{2}J_{CP}$ = 18.5 Hz, C_q, C10), 130.3 (d, $^{1}J_{CP}$ = 34.6 Hz, C_q, C1), 120.2 (CH, C3), 119.6 (CH, C7), 115.6 (C_q C9), 30.4 (CH_2, C11/12), 29.8 (CH_2, C11/12), 25.6 (d, $^{1}J_{CP}$ = 17.8 Hz, CH, C13), 20.6 (d, $^{2}J_{CP}$ = 15.5 Hz, CH_3, C14, 2 × CH_3), 19.3 (d, $^{2}J_{CP}$ = 16.4 Hz, CH_3, C14, 2 × CH_3).

^{31}P{^{1}H} NMR (109 MHz, $CDCl_3$): δ −2.1 (s).

MS (ES$^+$): *m/z* (%) 350.89 (^{81}Br) (98) [M$^+$], 348.89 (^{79}Br) (100) [M$^+$].

IR (KBr): **ν_{max}/cm^{-1}** 3071w (ν_{Ar-H}), 2921s (ν_{C-H}), 1603s, 1358s, 1249m, 1051m, 838s, 660m.

Raman (glass capillary): ν_{max}/cm^{-1} 3070s (ν_{Ar-H}), 2953s, 2925s (ν_{C-H}), 2898s, 1607m, 1564s, 1442s, 1414m, 1347m, 1328m, 959w (ν_{P-Ar}), 580s, 295s (ν_{C-Br}), 222s.

6.1.6 – ((^{i}Pr)$_2$P-Acenap-)$_3$Bi (C2-2)

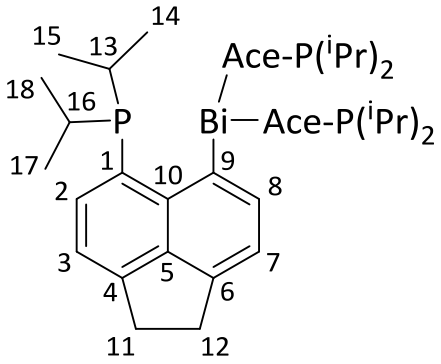

To a stirred solution of (^{i}Pr)$_2$P-Acenap-Br (1.00 g, 2.86 mmol) in ether (25 mL) at −78 °C was added n-BuLi (1.2 mL, 2.5 M sol^n in hexanes, 2.95 mmol) over 30 mins. The yellow suspension was stirred for 3 h at this temperature. A suspension of $BiCl_3$ (296 mg, 0.94 mmol) in ether (30 mL) was stirred rapidly at −78 °C. The lithiated suspension was added *via* cannula and the mixture stirred for 1.5 h at this temperature. The reaction was allowed to warm to room temperature and stirred O/N resulting in a white solid. The suspension was filtered, washed with ether (10 mL) then degassed water (10 mL) and dried for 4 h under vacuum. The product was obtained as a white powder (300 mg, 0.29 mmol, 32%) m.p 202.7−203.6 °C (decomp.). Crystals suitable for X-ray work were obtained from a saturated solution in DCM at 0 °C.

Anal. calcd. for $C_{54}H_{66}P_3Bi$ (1017.00 g mol^{-1}): C, 63.77; H, 6.46. Found: C, 63.64; H, 6.46.

^{1}H NMR (500 MHz, $CDCl_3$): δ 8.60 (dd, $^3J_{HH}$ = 6.9, $^{7ts}J_{HP}$ = 2.4 Hz, 3 H, H8), 7.60 (dd, $^3J_{HH}$ = 7.2, $^3J_{HP}$ = 2.8 Hz, 3 H, H2), 7.27 (d, $^3J_{HH}$ = 7.1 Hz, 3 H, H3), 6.85 (d, $^3J_{HH}$ = 6.8 Hz, 3 H, H7), 3.38−3.19 (m, 12 H, H11/12), 2.10 (h, $^3J_{HH}$ = 6.9 Hz, 3 H, H16), 1.89 (h, $^3J_{HH}$ = 6.8 Hz, 3 H, H13), 1.25−1.18 (m, 9 H, H17), 1.15−1.09 (m, 9 H, H18), 0.66−0.58 (m, 9 H, H15), 0.20−0.13 (m, 9 H, H14).

$^{13}C\{^{1}H\}$ NMR (125 MHz, $CDCl_3$): δ 176.6 (C_q, C9), 148.8 (C_q, C4), 146.6 (CH, C8), 145.3−144.9 (m, C_q, C10), 144.0 (C_q, C6), 141.5−141.3 (m, C_q, C5), 132.7 (CH, C2), 132.6−132.4 (m, C_q, C1), 123.5 (CH, C7), 117.9 (CH, C3), 130.2 (CH_2, C11/12), 130.1 (CH_2, C11/12), 27.0−26.7 (m, CH, C16), 25.5−25.3 (m, CH, C13), 21.5−21.2 (m, CH_3, C17), 20.3−20.1 (m, CH_3, C18), 19.9−19.5 (m, CH_3, C14/15).

^{31}P NMR (202 MHz, $CDCl_3$): δ −21.3 (br s).

$^{31}P\{^{1}H\}$ NMR (202 MHz, $CDCl_3$): δ −21.3 (s).

HRMS (APCI$^+$): *m/z* (%) 1017.42 (2) $[M]^+$, 747.27 (100) $[M-C_{18}H_{22}P]^+$.

IR (KBr): **ν_{max}/cm^{-1}** 3022w (ν_{Ar-H}), 2948s (ν_{C-H}), 1631br, 1460s, 1322s, 1245s, 843s, 608m.

Raman (glass capillary): ν_{max}/cm^{-1} 3048m (ν_{Ar-H}), 1570m, 999s, 648m, 240w, 211s, 176m.

6.1.7 – (^{i}Pr)$_2$P-Acenap-BiPh$_2$ (C2-5)

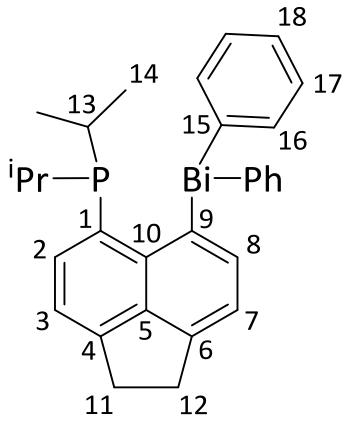

To a stirred solution of (^{i}Pr)$_2$P-Acenap-Br (1.00 g, 2.86 mmol) in THF (30 mL) at −78 °C was added n-BuLi (1.14 mL, 2.5 M sol^{n} in hexanes, 2.86 mmol) over 30 mins. The reaction was stirred for 3 h at this temperature. A suspension of $BiPh_2Cl$ (1.14 g, 2.86 mmol) in THF (30 mL) was added in portions over 1 h. The reaction was warmed to room temperature and stirred O/N. The THF was removed under vacuum and diethyl ether (70 mL) added then the organic layer washed with degassed water. The aqueous layer was extracted further with diethyl ether (2 x 15 mL) and the combined organic fractions dried over magnesium sulfate. The ether was removed to afford a sticky solid. Addition of MeCN caused the product to solidify, this was collected by filtration. Recrystallisation from hot

MeCN affords the product as an off white solid (1.09 g, 1.72 mmol, 60%) m.p 144.6−146.1 °C (decomp.). Crystals suitable for X-ray work were obtained from hot MeCN.

Anal. calcd. for $C_{30}H_{32}BiP{\cdot}CH_3CN$ (673.58 g mol^{-1}): C, 57.04; H, 5.24; N, 2.07. Found C, 56.95; H, 5.30; N 1.97.

^{1}H NMR (400 MHz, $CDCl_3$): δ 8.22 (d, $^3J_{HH}$ = 7.0 Hz, 1 H, H8), 7.85−7.81 (m, 4 H, H16), 7.63 (dd, $^3J_{HH}$ = 7.1, $^2J_{HP}$ = 3.8 Hz, 1 H, H2), 7.37−7.31 (m, 5 H, H3/17), 7.29−7.24 (m, 2 H, H18), 7.18 (d, $^3J_{HH}$ = 7.0 Hz, 1 H, H7), 3.44−3.35 (m, 4 H, H11/12), 2.13−2.00 (m, 2 H, H13), 1.07 (dd, $^3J_{HP}$ = 15.3, $^3J_{HH}$ = 6.9 Hz, 6 H, H14, 2 × CH_3), 0.61 (dd, $^3J_{HP}$ = 12.2, $^3J_{HH}$ = 7.0 Hz, 6 H, H14, 2 × CH_3).

^{13}C{^{1}H} NMR (100 MHz, $CDCl_3$): δ 167.3 (d, $^{5ts}J_{CP}$ = 42.2 Hz, C_q, C15), 153.4 (C_q, C9), 149.3 (C_q, C4), 146.5 (d, $^4J_{CP}$ = 1.4 Hz, C_q, C6), 143.7 (C_q, C10), 142.8 (CH, C8), 141.4 (C_q, C5), 138.3 (CH, C16), 133.9 (d, $^2J_{CP}$ = 2.8 Hz, CH, C2), 131.3 (d, $^1J_{CP}$ = 14.8 Hz, C_q, C1), 130.2 (CH, C17), 126.7 (CH, C18), 123.0 (CH, C7), 118.9 (CH, C3), 30.2 (CH_2, C11/12), 25.9 (d, $^1J_{CP}$ = 12.0 Hz, CH, C13), 20.4 (d, $^2J_{CP}$ = 17.7 Hz, CH_3, C14, 2 × CH_3), 19.2 (d, $^2J_{CP}$ = 8.9 Hz, CH_3, C14, 2 × CH_3).

^{31}P NMR (162 MHz, $CDCl_3$): δ −23.7 (br s).

^{31}P{^{1}H} NMR (162 MHz, $CDCl_3$): δ −23.7 (s).

HRMS (APCI$^+$): *m/z* (%) 555.16 (100) $[M-Ph]^+$, 271.16 (70).

IR (KBr): ν_{max}/cm^{-1} 3053w (ν_{Ar-H}), 2921m (ν_{C-H}), 1425m, 1248w, 841m, 724s, 696s, 447m.

Raman (glass capillary): ν_{max}/cm^{-1} 3034w (ν_{Ar-H}), 2924w (ν_{C-H}), 1328m, 999s, 641m, 208m, 177s.

6.1.8 – ((^{i}Pr)$_2$P-Acenap-)$_2$BiPh (C2-6)

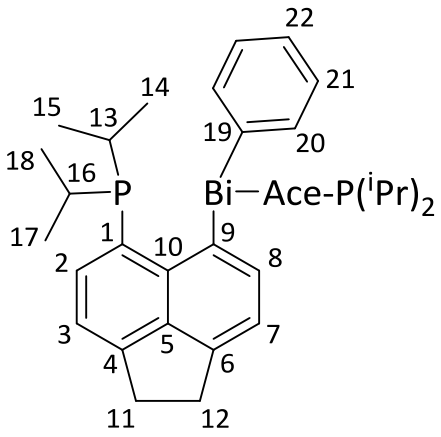

Method 1

To a stirred solution of (^{i}Pr)$_2$P-Acenap-Br (1.09 g, 3.15 mmol) in THF (30 mL) at −78 °C was added n-BuLi (1.25 mL, 2.5 M sol^{n} in hexanes, 3.15 mmol) over 30 mins. The reaction was stirred for 3 h at this temperature. A suspension of $BiPhCl_2$ (0.56 g, 1.57 mmol) in THF (35 mL) was added in portions over 1 h. The reaction was warmed to room temperature and stirred O/N. The THF was removed under vacuum and diethyl ether (70 mL) added and the organic layer washed with degassed water. The aqueous layer was extracted further with diethyl ether (2 x 15 mL) and the combined organic fractions dried over magnesium sulfate. The ether was removed to afford a sticky solid. Addition of MeCN caused the compound to solidify. Compound **C2-6** was obtained as an off white solid (1.23 g). *No yield is reported due to contamination with **C2-2** and **C2-5***. Crystals suitable for X-ray work were obtained from hot MeCN.

Method 2

To a stirred solution of (^{i}Pr)$_2$P-Acenap-Br (1.18 g, 3.34 mmol) in THF (70 mL) at −78 °C was added n-BuLi (1.40 mL, 2.5 M sol^{n} in hexanes, 3.34 mmol) over 15 mins. The reaction was left to stir at this temperature for 2 h. To this was added a suspension of (^{i}Pr)$_2$P-Acenap-BiPhCl (2.00 g, 3.34 mmol) in THF (30 mL) portionwise over 0.5 h. The reaction was left stirring at room temperature O/N. The THF was removed and diethyl ether added (120 mL), the suspension was filtered through celite which was then washed with more diethyl ether (30 mL). The solvent was removed and the product recrystallised from hot MeCN to afford the final compound as an off white solid (1.69 g, 2.06 mmol, 62%) m.p 169.5−171.9 °C. Crystals suitable for X-ray work were obtained from MeCN.

Anal. calcd. for $C_{42}H_{49}BiP_2$ (824.31 g mol^{-1}): C, 61.14; H, 5.99. Found: C, 61.21;H, 6.06.

^{1}H NMR (500 MHz, $CDCl_3$): δ 8.30 (d, $^{3}J_{HH}$ = 6.8 Hz, 2 H, H8), 7.89 (d, $^{3}J_{HH}$ = 7.3 Hz, 2H, H20), 7.65 (dd, $^{3}J_{HH}$ = 7.2, $^{2}J_{HP}$ = 2.8 Hz, 2 H, H2), 7.34 (d, $^{3}J_{HH}$ = 7.2 Hz, 2 H, H3), 7.28 (*p*t, $^{3}J_{HH}$ = 7.4 Hz, 2 H, H21), 7.21 (t, $^{3}J_{HH}$ = 7.1 Hz, 1 H, H22), 7.02 (d, $^{3}J_{HH}$ = 7.0 Hz, 2 H, H7), 3.44−3.38 (m, 4 H, 2 × CH_2, H11), 3.37−3.29 (m, 4 H, 2 × CH_2, H12), 2.15−1.99 (m, 4 H, 4 × CH, H13/16), 1.06 (dd, $^{3}J_{HP}$ = 14.6, $^{3}J_{HH}$ = 6.8 Hz, 6 H, 2 × CH_3, H14/15/17/18), 1.03−0.95 (br m, 6 H, 2 × CH_3, H14/15/17/18), 0.69 (br s, 6 H, 2 × CH_3, H14/15/17/18), 0.58 (br s, 6 H, 2 × CH_3, H14/15/17/18).

^{13}C{^{1}H} NMR (125 MHz, $CDCl_3$): δ 175.5 (t, $^{5ts}J_{CP}$ = 34.7 Hz, C_q, C19), 149.3 (C_q, C4), 145.5 (C_q, C5), 144.3 (CH, C8), 144.0 (C_q, C10), 141.2 (d, $^{3}J_{CP}$ = 9.3 Hz C_q, C5), 139.2 (CH, C20), 133.5 (CH, C2), 131.8 (d, $^{1}J_{CP}$ = 16.4 Hz, C_q, C1), 129.8 (CH, C21), 125.9 (CH, C22), 123.1 (CH, C7), 118.5 (CH, C3), 30.1 (2 × CH_2, C11), 30.0 (2 × CH_2, C12), 26.2 (d, $^{1}J_{CP}$ = 13.0 Hz, 2 × CH, C13/16), 25.8 (d, $^{1}J_{CP}$ = 12.3 Hz, 2 × CH, C13/16), 20.6−20.1 (m, 4 × CH_3, C14/15/17/18), 19.6 (d, $^{2}J_{CP}$ = 8.7 Hz, 2 × CH_3, C14/15/17/18), 18.9 (d, $^{2}J_{CP}$ = 8.0 Hz, 2 × CH_3, C14/15/17/18).

^{31}P NMR (202 MHz, $CDCl_3$): δ −22.9 (br s).

^{31}P{^{1}H} NMR (202 MHz, $CDCl_3$): δ −22.9 (br s).

HRMS (APCI^{+}): *m/z* (%) 825.3192 (17) $[M+H]^+$, 747.2752 (100) $[M-Ph]^+$, 556.1728 (80) $[M-C_{18}H_{21}P]^+$.

IR (KBr): ν_{max}/cm^{-1} 3048w (ν_{Ar-H}), 2926m (ν_{C-H}), 1424m, 1251w, 841m, 723s, 695s, 444m.

6.1.9 – $[(^{i}Pr)_2P\text{-Acenap-BiPh}]^+ [BF_4]^-$ (C2-7)

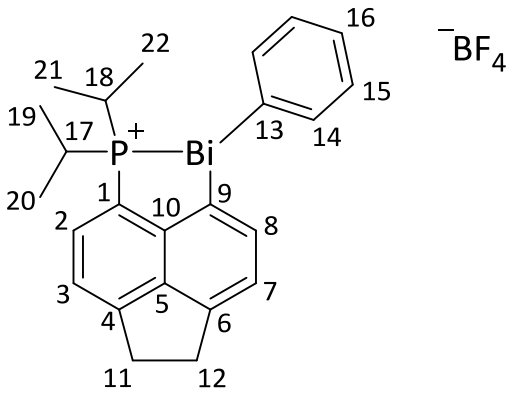

($^{i}Pr)_2$P-Acenap-$BiPh_2$ (0.50 g, 0.79 mmol) was dissolved in diethyl ether (20 mL) and cooled to 0 °C. To this was added $BF_3{\cdot}Et_2O$ (0.15 mL, 1.18 mmol), immediately a white precipitate formed. The reaction was warmed to room temperature and stirred for 3 h. The solid was collected by filtration and washed with diethyl ether. Compound **C2**-**7** was obtained as a white powder (326 mg, 0.51 mmol, 65%) m.p 218.9−220.2 °C (decomp.). Crystals suitable for X-ray work were obtained by diffusion of diethyl ether into a DCM solution of **C2**-**7**.

Anal. calcd. for $C_{24}H_{27}BBiF_4P$ (642.24 g mol^{-1}): C, 44.88; H, 4.24. Found: C, 44.97; H, 4.19.

^{1}H NMR (500 MHz, $CDCl_3$): δ 8.28 (d, $^{3}J_{HH}$ = 7.0 Hz, 1 H, H8), 7.96−7.93 (m, 2 H, H14), 7.79 (d, $^{3}J_{HH}$ = 7.0 Hz, 1 H, H7), 7.70 (dd, $^{3}J_{HP}$ = 8.5, $^{3}J_{HH}$ = 7.3 Hz, 1 H, H2), 7.48 (d, $^{3}J_{HH}$ = &.3 Hz, 1 H, H3), 7.37 (*p*t, $^{3}J_{HH}$ = 7.6 Hz, 2 H, H15), 7.27−7.23 (m, 1 H, H16), 3.64−3.45 (m, 4 H, H11/12), 3.12−3.01 (m, 1 H, H17), 3.00−2.91 (m, 1 H, H20), 1.28−1.19 (m, 6 H, H18/19), 1.12 (dd, $^{3}J_{HP}$ = 20.1, $^{3}J_{HH}$ = 7.0 Hz, 3 H, H21), 0.53 (dd, $^{3}J_{HP}$ = 18.3, $^{3}J_{HH}$ = 7.2 Hz, 3 H, H22).

^{13}C{^{1}H} NMR (125 MHz, $CDCl_3$): δ 165.7 (C_q, C9), 154.3 (d, $^{4}J_{CP}$ = 2.0 Hz, C_q, C4), 154.2 (d, $^{2}J_{CP}$ = 12.8 Hz, C_q, C13), 152.9 (d, $^{2}J_{CP}$ = 21.5 Hz, C_q, C10), 147.5 (C_q, C6), 144.5 (d, $^{3}J_{CP}$ = 11.2, C_q, C5), 139.5 (CH, C14), 139.0 (d, $^{3}J_{CP}$ = 5.2 Hz, CH, C8), 136.5 (CH, C2), 131.4 (d, $^{4}J_{CP}$ = 1.5 Hz, CH, C15), 129.2 (CH, C16), 127.2 (d, $^{1}J_{CP}$ = 36.7 Hz, C_q, C1), 124.4 (CH, C7), 121.4 (d, $^{3}J_{CP}$ = 7.5 Hz, CH, C3), 30.8 (CH_2, C11), 30.7 (CH_2, C12), 27.8 (d, $^{1}J_{CP}$ = 17.4 Hz, CH, C17), 25.3 (d, $^{1}J_{CP}$ = 20.4 Hz, CH, C18), 19.9 (CH_3, C19), 18.1 (CH_3, C20), 17.7 (CH_3, C21), 17.1 (d, $^{2}J_{CP}$ = 5.4 Hz, CH_3, C22).

^{31}P NMR (202 MHz, $CDCl_3$): δ 56.6 (br s).

$^{31}P\{^{1}H\}$ NMR (202 MHz, $CDCl_3$): δ 56.6 (s).

HRMS (ASAP$^+$): *m/z* (%) 555.1661 (100) $[M]^+$.

IR (KBr): ν_{max}/cm^{-1} 3042w (ν_{Ar-H}), 2927w (ν_{C-H}), 1592w, 1084s, 1056s, 1008s, 852m, 731m, 519w.

6.1.10 – ($^{i}Pr)_2$P-Acenap-BiPhCl (C2-8)

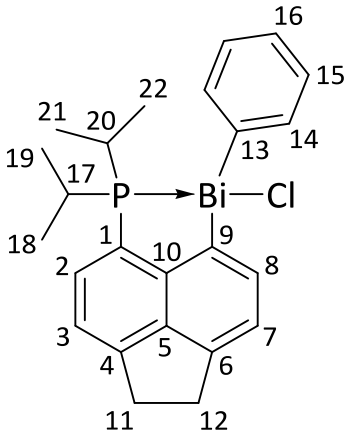

$[(^{i}Pr)_2$P-Acenap-BiPh$]^+$ $[BF_4]^-$ (326 mg, 0.51 mmol) was dissolved in DCM (15 mL), to this was added NaCl (0.29 g, 5.0 mmol) in degassed water (10 mL). The reaction was stirred vigorously for 15 mins. The DCM layer was removed and the aqueous layer extracted again with DCM (15 mL). The combined organic fractions were dried over magnesium sulfate and filtered. Removal of the solvent afforded the product as an off white solid (259 mg, 0.44 mmol, 86%) m.p 210.4−211.8 °C (decomp.). Crystals suitable for X-ray work were obtained by diffusion of diethyl ether into a DCM solution of **C2-8**.

Anal. calcd. for $C_{24}H_{27}BiClP$ (590.87 g mol^{-1}): C, 48.78; H, 4.60. Found: C, 48.71; H, 4.59.

^{1}H NMR (500 MHz, $CDCl_3$): δ 9.32 (d, $^{3}J_{HH}$ = 7.0 Hz, 1 H, H8), 7.98 (d, $^{3}J_{HH}$ = 7.3 Hz, 2 H, H14), 7.69 (d, $^{3}J_{HH}$ = 7.0 Hz, 1 H, H7), 7.53 (*p*t, ^{3}J = 7.0 Hz, 1 H, H2), 7.36−7.30 (m, 3 H, H3/15), 7.17 (t, $^{3}J_{HH}$ = 7.3 Hz, 1 H, H16), 3.50−3.38 (m, 4 H, H11/12), 2.50−2.31 (m, 2 H, H17/20), 1.11 (dd, $^{3}J_{HP}$ = 17.7, $^{3}J_{HH}$ = 7.0 Hz, 3 H, H19), 1.06 (dd, $^{3}J_{HP}$ = 13.7, $^{3}J_{HH}$ = 7.0 Hz, 3 H, H18), 0.95 (dd, $^{3}J_{HP}$ = 18.3, $^{3}J_{HH}$ = 6.7 Hz, 3 H, H21), 0.35 (dd, $^{3}J_{HP}$ = 16.1, $^{3}J_{HH}$ = 6.7 Hz, 3 H, H22).

$^{13}C\{^1H\}$ NMR (125 MHz, $CDCl_3$): δ 165.1 (C_q, C9), 160.7 (d, $^{5ts}J_{CP}$ = 8.4 Hz, C_q, C13), 152.5 (C_q, C4), 150.4 (d, $^3J_{HH}$ = 28.1 Hz, C_q, C10), 147.0 (C_q, C6), 143.7 (d, $^3J_{HH}$ = 11.4 Hz, C_q, C5), 141.0 (CH, C8), 138.8 (CH, C14), 134.7 (d, $^2J_{CP}$ = 3.2 Hz, CH, C2), 131.0 (CH, C15), 128.1 (d, $^1J_{CP}$ = 21.0 Hz, C_q, C1), 128.0 (CH, C16), 124.5 (CH, C7), 120.0 (d, $^3J_{CP}$ = 4.7 Hz, CH, C3), 30.7 (CH_2, C11/12), 30.5 (CH_2, C11/12), 26.0 (d, $^1J_{CP}$ = 5.8 Hz, CH, C17), 24.7 (d, $^1J_{CP}$ = 10.9 Hz, CH, C20), 20.3 (d, $^2J_{CP}$ = 6.2 Hz, CH_3, C19), 18.5 (d, $^2J_{CP}$ = 8.0 Hz, CH_3, C18), 18.0 (CH_3, C21), 17.6 (CH_3, C22).

^{31}P NMR (202 MHz, $CDCl_3$): δ 18.8 (br s).

$^{31}P\{^1H\}$ NMR (202 MHz, $CDCl_3$): δ 18.8 (s).

HRMS ($APCI^+$): *m/z* (%) 555.1661 (100) $[M-Cl]^+$.

IR (KBr): ν_{max}/cm^{-1} 3044w (ν_{Ar-H}), 2925s (ν_{C-H}), 1591s, 1443s, 1254s, 847vs, 739s, 443m.

6.1.11 – (^{i}Pr)$_2$P-Acenap-BiPhBr (C2-9)

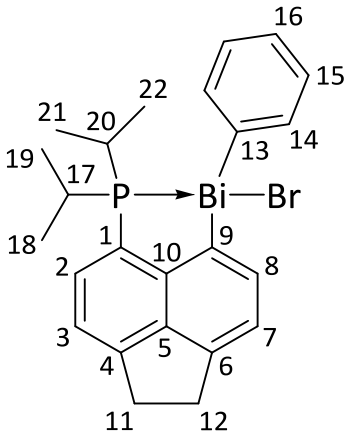

$[(^iPr)_2P\text{-Acenap-BiPh}]^+ [BF_4]^-$ (294 mg, 0.45 mmol) was dissolved in DCM (30 mL), to this was added a saturated $KBr_{(aq)}$ solution (25 mL). The reaction was stirred vigorously for 50 mins. The DCM layer was removed and the aqueous layer extracted again with DCM (15 mL). The combined organic fractions were dried over magnesium sulfate and filtered. Removal of the solvent afforded the product as a white solid (241 mg, 0.38 mmol, 83%) m.p 215.6–217.0 °C (decomp.). Crystals suitable for X-ray work were obtained by slow evaporation from MeCN.

Anal. calcd. for $C_{24}H_{27}BiBrP$ (635.34 g mol^{-1}): C, 45.37; H, 4.28. Found: C, 45.50; H, 4.35.

^{1}H NMR (500 MHz, $CDCl_3$): δ 9.47 (d, $^{3}J_{HH}$ = 7.2 Hz, 1 H, H8), 7.99 (d, $^{3}J_{HH}$ = 7.7 Hz, 2 H, H14), 7.68 (d, $^{3}J_{HH}$ = 7.2 Hz, 1 H, H7), 7.54 (*p*t, ^{3}J = 6.9 Hz, 1 H, H2), 7.34 (d, $^{3}J_{HH}$ = 6.9 Hz, 1 H, H3), 7.31 (*p*t, $^{3}J_{HH}$ = 7.7 Hz, 2 H, H15), 7.17 (*p*t, $^{3}J_{HH}$ = 7.4 Hz, 1 H, H16), 3.51−3.42 (m, 4 H, H11/12), 2.49−2.34 (m, 2 H, H17/20), 1.13 (dd, $^{3}J_{HP}$ = 17.7, $^{3}J_{HH}$ = 7.0 Hz, 3 H, H19), 1.07 (dd, $^{3}J_{HP}$ = 13.6, $^{3}J_{HH}$ = 7.0 Hz, 3 H, H18), 0.97 (dd, $^{3}J_{HP}$ = 17.9, $^{3}J_{HH}$ = 7.0 Hz, 3 H, H21), 0.36 (dd, $^{3}J_{HP}$ = 15.9, $^{3}J_{HH}$ = 7.0 Hz, 3 H, H22).

^{13}C{^{1}H} NMR (125 MHz, $CDCl_3$): δ 162.8 (C_q, C9), 158.6 (d, $^{5ts}J_{CP}$ = 7.3 Hz, C_q, C13), 152.5 (d, $^{4}J_{CP}$ = 1.7 Hz, C_q, C4), 150.5 (d, $^{2}J_{CP}$ = 27.6 Hz, C_q, C10), 147.0 (C_q, C6), 143.5 (d, $^{3}J_{CP}$ = 11.1 Hz, C_q, C5), 142.9 (CH, C8), 139.0 (CH, C14), 134.5 (d, $^{2}J_{CP}$ = 3.4 Hz, CH, C2), 131.0 (CH, C15), 128.0 (CH, C16), 127.7 (d $^{1}J_{CP}$ = 19.9 Hz, C_q, C1), 124.9 (CH, C7), 120.1 (d, $^{3}J_{CP}$ = 5.0 Hz, CH, C3), 30.7 (CH_2, C11/12), 30.6 (CH_2, C11/12), 26.1 (d, $^{1}J_{CP}$ = 5.7 Hz, CH, C17), 24.8 (d, $^{1}J_{CP}$ = 10.8, CH, C20), 20.2 (d, $^{2}J_{CP}$ = 6.6 Hz, CH_3, C19), 18.6 (d, $^{2}J_{CP}$ = 7.5 Hz, CH_3, C18), 18.0 (CH_3, C21), 17.7 (CH_3, C22).

^{31}P NMR (202 MHz, $CDCl_3$): δ 15.4 (br s).

^{31}P{^{1}H} NMR (202 MHz, $CDCl_3$): δ 15.4 (s).

HRMS (APCI^{+}): *m/z* (%) 635.0916 (^{79}Br) $[M+H]^+$ (<1%), 637.0898 (^{81}Br) (<1%) $[M+H]^+$, 555.1789 (100) $[M-Br]^+$.

IR (KBr): ν_{max}/cm^{-1} 3042w (ν_{Ar-H}), 2958s (ν_{C-H}), 1592s, 1443s, 1254s, 847vs, 735s, 443m.

6.1.12 – (^{i}Pr)$_2$P-Acenap-BiPhI (C2-10)

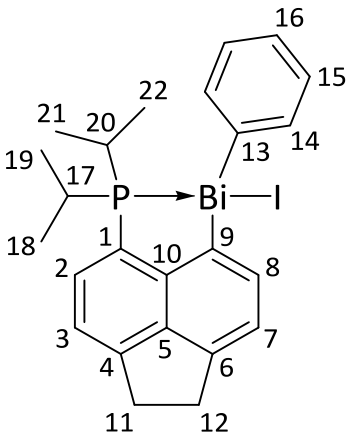

[(^{i}Pr)$_2$P-Acenap-BiPh]$^{+}$ [BF_4]$^{-}$ (323 mg, 0.51 mmol) was dissolved in DCM (25 mL), to this was added a saturated $NaI_{(aq)}$ solution (25 mL). The reaction was stirred vigorously for 50 mins. The DCM layer was removed and the aqueous layer extracted again with DCM (15 mL). The combined organic fractions were dried over magnesium sulfate and filtered. Removal of the solvent afforded the product as a yellow solid (265 mg, 0.39 mmol, 77%) m.p 221.6−223.1 °C (decomp.). Crystals suitable for X-ray work were obtained by slow evaporation from MeCN.

Anal. calcd. for $C_{24}H_{27}BiPI$ (682.33 g mol^{-1}): C, 42.25; H, 3.99. Found: C, 42.25; H, 3.89.

^{1}H NMR (500 MHz, $CDCl_3$): δ 9.61 (d, $^{3}J_{HH}$ = 7.2 Hz, 1 H, H8), 8.01 (d, $^{3}J_{HH}$ = 7.8 Hz, 2 H, H14), 7.63 (d, $^{3}J_{HH}$ = 7.2 Hz, 1 H, H7), 7.56 (*p*t, ^{3}J = 7.2 Hz, 1 H, H2), 7.36 (d, $^{3}J_{HH}$ = 7.2 Hz, 1 H, H3), 7.29 (*p*t, $^{3}J_{HH}$ = 7.7 Hz, 2 H, H15), 7.18 (*p*t, $^{3}J_{HH}$ = 7.6 Hz, 1 H, H16), 3.52−3.44 (m, 4 H, H11/12), 2.49−2.37 (m, 2 H, H17/20), 1.11 (dd, $^{3}J_{HP}$ = 17.8, $^{3}J_{HH}$ = 7.1 Hz, 3 H, H19), 1.08 (dd, $^{3}J_{HP}$ = 13.6, $^{3}J_{HH}$ = 7.0 Hz, 3 H, H18), 1.00 (dd, $^{3}J_{HP}$ = 18.1, $^{3}J_{HH}$ = 7.0 Hz, 3 H, H21), 0.3 (dd, $^{3}J_{HP}$ = 16.0, $^{3}J_{HH}$ = 7.0 Hz, 3 H, H22).

^{13}C{^{1}H} NMR (125 MHz, $CDCl_3$): δ 159.5 (C_q, C9), 155.1 (d, $^{5ts}J_{CP}$ = 6.2 Hz, C_q, C13), 152.7 (C_q, C4), 150.9 (d, $^{2}J_{CP}$ = 28.0 Hz, C_q, C10), 147.2 (C_q, C6), 146.1 (CH, C8), 143.2 (d, $^{3}J_{CP}$ = 11.3 Hz, C_q, C5), 139.6 (CH, C14), 134.4 (d, $^{2}J_{CP}$ = 3.7 Hz, CH, C2), 131.0 (CH, C15), 128.0 (CH, C16), 127.7 (d $^{1}J_{CP}$ = 20.4 Hz, C_q, C1), 125.4 (CH, C7), 120.2 (d, $^{3}J_{CP}$ = 5.1 Hz, CH, C3), 30.7 (CH_2, C11/12), 30.7 (CH_2, C11/12), 26.1 (d, $^{1}J_{CP}$ = 5.2 Hz, CH, C17), 24.8 (d, $^{1}J_{CP}$ = 11.0 Hz, CH, C20), 20.3 (d, $^{2}J_{CP}$ = 5.8 Hz, CH_3, C19), 18.6 (d, $^{2}J_{CP}$ = 7.2 Hz, CH_3, C18), 17.9 (CH_3, C21), 17.7 (CH_3, C22).

^{31}P NMR (202 MHz, $CDCl_3$): δ 12.9 (br s).

$^{31}P\{^{1}H\}$ NMR (202 MHz, $CDCl_3$): δ 12.9 (s).

HRMS (APCI$^+$): *m/z* (%) 555.1758 (100) $[M-I]^+$.

IR (KBr): ν_{max}/cm^{-1} 3034w (ν_{Ar-H}), 2924s (ν_{C-H}), 1591s, 1442s, 1252s, 844vs, 735s, 444m.

6.1.13 – $[(^{i}Pr)_2P$-Acenap-$BiPh_3]^+$ $[BiPh_2Cl_2]^-$ (C2-12)

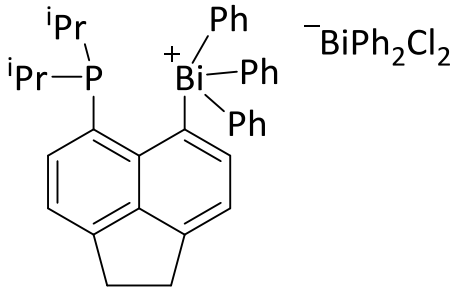

To a stirred solution of $(^{i}Pr)_2$P-Acenap-Br (1.50 g, 4.29 mmol) in diethyl ether (35 ml) at −78 °C was added n-BuLi (1.70 mL, 2.5 M sol^n in hexanes, 4.29 mmol) dropwise over 0.5 h. The reaction was then stirred for 3 h at this temperature. Separately $BiPh_3Cl_2$ (2.19 g, 4.29 mmol) was added to ether 75 mL and cooled to –40 °C. Over 2 h the lithiated species was added to this solution then the reaction left to warm to room temperature and stir O/N. A precipitate formed which was collected by filtration and washed with diethyl ether. The product was obtained as a beige solid (3.38 g, 2.96 mmol, 69%). Crystals suitable for X-ray work were obtained by diffusion of diethyl ether into a DCM solution of **C2-12**.

^{1}H NMR (400 MHz, $CDCl_3$): δ 8.72−8.63 (m, 6 H, ArH), 8.54 (d, $^{3}J_{HH}$ = 7.4 Hz, 1 H, ArH), 7.98 (d, $^{3}J_{HH}$ = 7.4 Hz, 1 H, ArH), 7.87−7.82 (m, 6 H, ArH), 7.78−7.26 (m, 2 H, ArH), 7.62−7.49 (m, 8 H, ArH), 7.43−7.37 (m, 6 H, ArH), 7.17−7.11 (m, 3 H, ArH), 3.54−3.43 (m, 4 H, 2 × CH_2), 2.07−1.96 (m, 2 H, 2 × CH), 0.81 (dd, $^{3}J_{HP}$ = 15.6, $^{3}J_{HH}$ = 6.9 Hz, 6 H, 2 × CH_3), 0.51 (dd, $^{3}J_{HP}$ = 13.2, $^{3}J_{HH}$ = 7.2 Hz, 6 H, 2 × CH_3).

$^{13}C\{^{1}H\}$ NMR (100 MHz, $CDCl_3$): δ 183.9 (C_q, ArC), 152.9 (C_q, ArC), 151.1 (C_q, ArC), 148.4 (C_q, ArC), 148.1 (C_q, ArC), 142.2 (d, *J* = 6.3 Hz, Cq, ArC), 138.2 (CH, ArC), 137.6 (CH, ArC), 135.9 (CH, ArC), 132.0 (CH, ArC), 131.4 (CH, ArC), 130.9 (CH, ArC), 130.5 (CH, ArC), 126.6 (CH, ArC), 122.5 (C_q, ArC), 122.2 (CH, ArC), 121.4 (CH, ArC), 30.8 (CH_2), 30.4 (CH_2), 24.9 (d, $^{1}J_{CP}$ = 4.2 Hz, 2 × CH), 19.3 (d, $^{3}J_{CP}$ = 11.4 Hz, 2 × CH_3), 18.1 (d, $^{3}J_{CP}$ = 4.8 Hz, 2 × CH_3).

$^{31}P\{^{1}H\}$ NMR (162 MHz, $CDCl_3$): δ −46.3 (br s).

HRMS (NSI$^+$): *m/z* (%) 709.2426 (80) $[M]^+$, 555.1642 (100) $[C_{24}H_{27}PBi]^+$, 347.1928 (17) $[C_{24}H_{28}P]^+$.

IR (KBr): ν_{max}/cm^{-1} 3042m (ν_{Ar-H}), 2923m (ν_{C-H}), 1638s, 1433s, 992m, 729s, 692m, 447m.

6.2 – Chapter 4 Experimental Procedures

6.2.1 – Benzene-1,2-dithiol (H_2A)

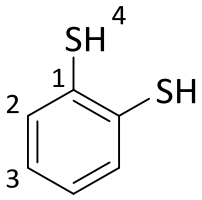

H_2A was prepared according to the literature procedure.[228] A solution of TMEDA (6.60 mL, 43.81 mmol) and n-BuLi (32.0 mL, 2.5 M sol^n in hexanes, 80.0 mmol) in hexane (20 mL) was cooled to 0 °C and thiophenol (4.0 mL, 39.13 mmol) added slowly over 30 mins. The solution was stirred for 1 h then warmed to room temperature and stirred O/N resulting in a white suspension. This was cooled to −20 °C then sulfur added (1.45 g, 45.34 mmol) and the reaction stirred for 2 h before warming to room temperature and stirring O/N. The solution was acidified with 2 M HCl then extracted with diethyl ether and dried over magnesium sulfate, removal of the solvent resulted in a yellow oil. This was purified by vacuum distillation to provide the compound as a pale yellow oil which crystallises upon storage at 4 °C (1.62 g, 11.4 mmol, 30%), b.p 73−76 °C at 1.3 mbar (lit. 75 °C at 1 mm Hg).[228] Analytical data obtained were in good agreement with that previously reported.[228] Crystals suitable for X-ray work were obtained by storing the compound in a fridge (4 °C) for several days.

^{1}H NMR (500MHz, $CDCl_3$): δ 7.36 (dd, $^3J_{HH}$ = 5.8 Hz, $^4J_{HH}$ = 3.3 Hz, 2 H, H2), 7.07 (dd, $^3J_{HH}$ = 5.8 Hz, $^4J_{HH}$ = 3.3 Hz, 2 H, H3), 3.72 (s, 2 H, H4).

$^{13}C\{^{1}H\}$ NMR (125 MHz, $CDCl_3$): δ 131.2 (C_q, C1), 131.1 (CH, C2), 126.8 (CH, C3).

IR (KBr): ν_{max}/cm^{-1} 3055s (ν_{Ar-H}), 2538s (ν_{S-H}), 1571s, 1428s, 1266s, 1114m, 1042s, 927m, 742s, 657m.

Raman (glass capillary): ν_{max}/cm^{-1} 3054s (ν_{Ar-H}), 2544m (ν_{S-H}), 1571s, 1040s, 660m (ν_{C-S}), 474m.

6.2.2 – Naphtho[1,8-*cd*]-1,2-dithiole (S_2B)

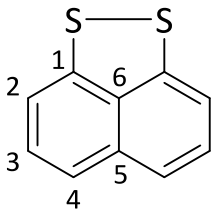

S_2B was prepared according to the literature procedure.[223] To a stirred solution of naphthalene (4.0 g, 31.27 mmol) in hexane (20 mL) was added TMEDA (18.8 mL, 124.84 mmol) and n-BuLi (49.9 mL, 2.5 M sol^{n} in hexanes, 124.84 mmol). The solution was heated to 60 °C for 3 h resulting in a brown suspension. The reaction was cooled to −78 °C and diluted with THF (60 mL), sulfur (8.3 g, 259.7 mmol) was added with vigorous stirring and the reaction left O/N at room temperature. The resulting orange/yellow solution was washed with water until the water layer remained colourless. The organic layer was dried over magnesium sulfate and the solvent removed to yield a red oil. Purification by flash column chromatography (silica gel/hexane) resulted in red/orange solid (2.57 g, 13.51 mmol, 43%), m.p 115−118 °C (lit. 116 °C).[222] Analytical data obtained were in good agreement with that previously reported.[222,223]

^{1}H NMR (500MHz, $CDCl_3$): δ 7.35 (d, $^{3}J_{HH}$ = 8.1 Hz, 2 H, H4), 7.27 (pt, $^{3}J_{HH}$ = 7.9 Hz, 2 H, H3), 7.15 (d, $^{3}J_{HH}$ = 7.6 Hz, 2 H, H2).

^{13}C{^{1}H} NMR (125 MHz, $CDCl_3$): δ 144.1 (C_q, C5), 135.7 (C_q, C1), 134.7 (C_q, C6), 127.9 (CH, C3), 121.6 (CH, C4), 115.9 (CH, C2).

IR (KBr): ν_{max}/cm^{-1} 1601m, 1542s, 1485m, 1349s, 1207s, 897m, 796s, 755s.

Raman (glass capillary): ν_{max}/cm^{-1} 3060m (ν_{Ar-H}), 1548m, 1386s, 900m, 571s (ν_{C-S}), 513s (ν_{S-S}), 392s, 346m.

6.2.3 – 5,6-dihydroacenaphtho-[5,6-*cd*]-1,2-dithiole (S_2C)

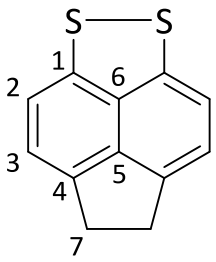

S_2C was prepared according to the literature procedure.[199] To a stirred solution of $AcenapBr_2$ (5.0 g, 16.03 mmol) and TMEDA (4.8 mL, 32.06 mmol) in diethyl ether (200 mL) was slowly added n-BuLi (6.4 mL, 2.5 M sol^n in hexanes, 16.03 mmol) at −78 °C. Upon completion this mixture was stirred for 15 min at this temperature, sulfur (0.51 g, 16.03 mmol) was added and stirring continued for 2 h at −40 °C. The mixture was cooled to −78 °C, then n-BuLi (6.4 mL, 2.5M sol^n in hexanes, 16.03 mmol) added slowly and the reaction stirred at this temperature for 15 min. Sulfur (0.51 g, 16.03 mmol) was added and the reaction stirred for another 2 h at −40 °C. The mixture was quenched with acetic acid (2−3 mL) and exposed to an air stream overnight. The solvent was removed and water added then the suspension was extracted with DCM (3 × 75 mL) then dried over magnesium sulfate. After the solvent was removed *in vacuo* the solid was purified by column chromatography (silica gel/hexane) to yield the product as red crystals (721 mg, 3.30 mmol, 21%), m.p 178−181 °C (lit. 178−182 °C).[199] Analytical data obtained were in good agreement with that previously reported.[199]

^{1}H NMR (400MHz, $CDCl_3$): δ 7.06 (d, $^3J_{HH}$ = 7.4 Hz, 2 H, H3), 7.03 (d, $^3J_{HH}$ = 7.4 Hz, 2 H, H2), 3.31 (s, 4 H, H7).

^{13}C{^{1}H} NMR (100 MHz, $CDCl_3$): δ 141.4 (C_q, C4), 140.3 (C_q, C6), 138.3 (C_q, C5), 134.3 (C_q, C1) 121.1 (CH, C2), 116 (CH, C3), 30.7 (CH_2, C7).

IR (KBr): ν_{max}/cm^{-1} 2920m (ν_{C-H}), 1561s, 1421m, 1396s, 1228m, 1035m, 829s, 804s, 608m.

Raman (glass capillary): ν_{max}/cm^{-1} 3063m (ν_{Ar-H}), 2919m (ν_{C-H}), 1617m, 1411s, 598s (ν_{C-S}), 462m (ν_{S-S}), 388s.

6.2.4 – Dibenzo-[*c*,*e*]-1,2-dithiine (S_2D)

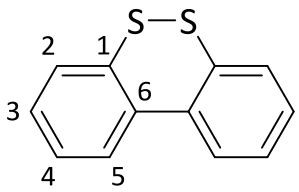

S_2D was prepared following the procedure published for **S_2B** using biphenyl in place of naphthalene.[223] To a stirred solution of biphenyl (5.0 g, 32.4 mmol) in hexane (25 mL) was added TMEDA (9.7 mL, 64.82 mmol) and n-BuLi (25.9 mL, 2.5 M sol^n in hexanes, 64.82 mmol). The solution was heated to 60 °C for 3 h resulting in a dark red suspension. The reaction was cooled to −78 °C and diluted with THF (30 mL), sulfur (3.01 g, 93.8 mmol) was added with vigorous stirring and the reaction left stirring O/N at room temperature. The resulting dark red solution was washed with water until the water layer remained colourless. The organic layer was dried over magnesium sulfate and the solvent removed to yield a yellow solid. Purification by flash column chromatography (silica gel/hexane) resulted in a bright yellow solid (2.49 g, 11.52 mmol, 36%), m.p 111−113 °C (lit. 113 °C).[225] Analytical data obtained were in good agreement with that previously reported.[224,225]

^{1}H NMR (500MHz, $CDCl_3$): δ 7.70 (dd, $^3J_{HH}$ = 7.8, $^4J_{HH}$ = 1.3 Hz, 2 H, H5), 7.51 (dd, $^3J_{HH}$ = 7.7, $^4J_{HH}$ = 1.2 Hz, 2 H, H2), 7.38 (ddd, $^3J_{HH}$ = 7.7, $^4J_{HH}$ = 1.3 Hz, 2 H, H4), 7.28 (ddd, $^3J_{HH}$ = 7.5, $^4J_{HH}$ = 1.3 Hz, 2 H, H3).

^{13}C{^{1}H} NMR (125 MHz, $CDCl_3$): δ 138.0 (C_q, C6), 136.1 (C_q, C1), 128.9 (CH, C2), 128.5 (CH, C4), 127.9 (C2,3).

IR (KBr): ν_{max}/cm^{-1} 3058w (ν_{Ar-H}), 1455m, 1419m, 865m, 751s.

Raman (glass capillary): ν_{max}/cm^{-1} 3061m (ν_{Ar-H}), 1583s, 1299m, 1042s, 525s (ν_{C-S}), 438m (ν_{S-S}), 184s.

6.2.5 – Naphthalene-1,8-dithiol (H_2B)

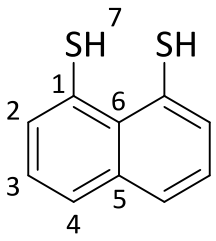

H_2B was prepared according to the literature procedure.[227] A solution of **S_2B** (2.15 g, 11.25 mmol) in THF (30 mL) was added dropwise to an ethanol (35 mL) suspension of $NaBH_4$ (1.15 g, 30.63 mmol) at 0 °C. Upon complete addition the reaction was stirred for 15 mins at this temperature then poured into water (30 mL). The solution was acidified using 3 M HCl then extracted with diethyl ether (3 × 30 mL) and the combined organic layers dried over magnesium sulfate. Removal of the solvent resulted in an off white waxy solid (1.72 g, 8.93 mmol, 79%), m.p 120−123 °C (lit. 122 °C).[277] Analytical data obtained were in good agreement with that previously reported.[227,277] Crystals suitable for X-ray work were obtained from recrystallising in boiling hexane and cooling in the freezer.

^{1}H NMR (500MHz, $CDCl_3$): δ 7.63 (d, $^3J_{HH}$ = 8.1 Hz, 2 H, H4), 7.51 (d, $^3J_{HH}$ = 7.4 Hz, 2 H, H2), 7.24 (*p*t, $^3J_{HH}$ = 7.6 Hz, 2 H, H3), 4.14 (s, 2 H, H7).

^{13}C{^{1}H} NMR (125 MHz, $CDCl_3$): δ 136.4 (C_q, C5) 132.1 (CH, C2), 131.7 (C_q, C6), 129.1 (C_q, C1), 128.2 (CH, C4), 125.7 (CH, C3).

IR (KBr): ν_{max}/cm^{-1} 2520w (ν_{S-H}), 1459s, 1196s, 810s, 756s.

Raman (glass capillary): ν_{max}/cm^{-1} 3055w (ν_{Ar-H}), 2539m (ν_{S-H}), 1552s, 1421m, 1336s, 1146m, 1101m, 868m, 542s (ν_{C-S}).

6.2.6 – Acenaphthene-5,6-dithiol (H_2C)

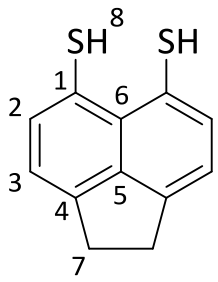

A solution of **S_2C** (100 mg, 0.46 mmol) in THF (30 mL) was added dropwise to an ethanol (10 mL) suspension of $NaBH_4$ (80 mg, 2.11 mmol) at 0 °C. Upon complete addition the reaction was stirred for 15 mins at this temperature then water (30 mL) added. The solution was acidified using 3 M HCl then extracted with diethyl ether (3 × 30 mL) and the combined organic layers dried over magnesium sulfate. Removal of the solvent under vacuum yielded a very pale brown solid (98 mg, 0.45 mmol, 97%), m.p 125−127 °C. Crystals suitable for X-ray work were obtained from recrystallising in boiling hexane.

Anal. calcd. for $C_{12}H_{10}S_2$ (218.33 g mol^{-1}): C, 66.04; H, 4.62. Found: C, 65.91; H, 4.62

^{1}H NMR (500MHz, $CDCl_3$): δ 7.47 (d, $^3J_{HH}$ = 7.2 Hz, 2 H, H3), 7.09 (d, $^3J_{HH}$ = 7.2 Hz, 2 H, H2), 4.16 (s, 2 H, H8), 3.31 (s, 4 H, H7).

^{13}C{^{1}H} NMR (125 MHz, $CDCl_3$): δ 145.8 (C_q, C4), 141.3 (C_q, C6), 133.4 (CH, C3), 130.4 (C_q, C5), 123.2 (C_q, C1), 120.1 (CH, C2), 30.0 (CH_2, C7).

MS (ES^-): *m/z* (%) 217.01 (75) $[M-H]^-$, 185.99 (65) $[M-S]^-$, 96.96 (100) $[HSO_4]^-$.

IR (KBr): ν_{max}/cm^{-1} 2921w (ν_{C-H}), 2510w (ν_{S-H}), 1459s, 1197m, 833s, 810m.

Raman (glass capillary): ν_{max}/cm^{-1} 3059m (ν_{Ar-H}), 2931m, (ν_{C-H}), 2546s (ν_{S-H}), 2514s (ν_{S-H}), 1599s, 1566s, 1440s, 1412s, 1336s, 580s (ν_{C-S}), 567m, 243m.

6.2.7 – [1,1'-biphenyl]-2,2'-dithiol (H_2D)

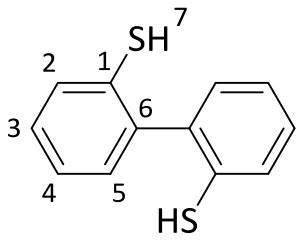

H_2D was prepared following the procedure published for **H_2B** using **S_2D** in place of **S_2B**.[227] A solution of **S_2D** (2.0 g, 9.21 mmol) in THF (30 mL) was added dropwise to an ethanol (35 mL) suspension of $NaBH_4$ (1.39 g, 36.74 mmol) at 0 °C. Upon complete addition the reaction was stirred for 15 mins at this temperature then poured into water (30 mL). The solution was acidified using 3 M HCl then extracted with diethyl ether (3 × 30 mL) and the combined organic layers dried over magnesium sulfate. Removal of the solvent resulted in a white solid (1.988 g, 9.10 mmol, 99%), m.p 76−79 °C (lit. 78−79 °C).[225] Analytical data obtained were in good agreement with that previously reported.[224,225] Crystals suitable for X-ray work were obtained from recrystallising in boiling hexane.

^{1}H NMR (500MHz, $CDCl_3$): δ 7.44 (dd, $^3J_{HH}$ = 7.70, $^4J_{HH}$ = 1.30 Hz, 2 H, H5), 7.27 (ddd, $^3J_{HH}$ = 7.4, $^4J_{HH}$ = 1.6 Hz, 2 H, H4), 7.23 (ddd, $^3J_{HH}$ = 7.4, $^4J_{HH}$ = 1.5 Hz, 2 H, H3), 7.17 (dd, $^3J_{HH}$ = 7.4, $^4J_{HH}$ = 1.6 Hz, 2 H, H2), 3.29 (s, 2 H, H7).

^{13}C{^{1}H} NMR (125 MHz, $CDCl_3$): δ 138.9 (C_q, C6), 131.8 (C_q, C1), 130.2 (CH, C2), 129.3 (CH, C5), 128.7 (CH, C4), 125.8 (CH, C3).

IR (KBr): ν_{max}/cm^{-1} 3047w (ν_{Ar-H}), 2558m (ν_{S-H}), 1455s, 1426s, 1071m, 1038m, 916m, 753s, 731m, 461m.

Raman (glass capillary): ν_{max}/cm^{-1} 3056m (ν_{Ar-H}), 2561s (ν_{S-H}), 1591m, 1296m, 1246m, 1038s, 670m (ν_{C-S}).

6.2.8 – Pentamethylcyclopentadienylrhodium(III) chloride (SM-1)

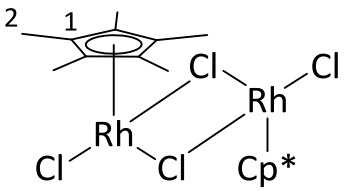

SM-1 was prepared according to the literature procedure.[229] To a solution of $RhCl_3 \cdot 3H_2O$ (5.00 g, 18.94 mmol) in MeOH (50 mL) was added Cp* (3.22g, 23.78 mmol) and the reaction refluxed for 48 h. A red precipitate was filtered and the filtrate put on ice for 1 hr to allow more compound to be collected. The combined filtrands were washed with EtOH (100 mL) then diethyl ether (100 mL) and dried under vacuum (5.36 g, 8.67 mmol, 92%). Analytical data obtained were in good agreement with that previously reported.[229]

Anal. calcd. for $C_{20}H_{30}Cl_4Rh_2$ (615.92 g mol^{-1}): C, 38.96; H, 4.90. Found: C, 38.89; H, 4.90.

^{1}H NMR (270 MHz, $CDCl_3$): δ 1.62 (s, 15 H, H2).

$^{13}C\{^1H\}$ NMR (125 MHz, $CDCl_3$): δ 94.1 (d, $^1J_{CRh}$ = 9.5 Hz, C_q, C1), 9.4 (CH_3, C2).

IR (KBr): ν_{max}/cm^{-1} 2972w (ν_{Ar-H}), 2918m (ν_{C-H}), 1466s, 1371s, 1027s.

Raman (glass capillary): ν_{max}/cm^{-1} 2968w (ν_{Ar-H}), 2912s (ν_{C-H}), 593s, 452s, 270m (ν_{Rh-Cl}), 196m (ν_{Rh-Cl}).

6.2.9 – Pentamethylcyclopentadienyliridium(III) chloride (SM-2)

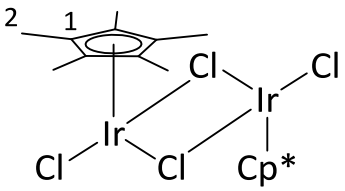

SM-1 was prepared according to the literature procedure.[229] To a solution of $IrCl_3 \cdot 3H_2O$ (5.00 g, 14.21 mmol) in MeOH (50 mL) was added Cp* (2.91 g, 21.32 mmol) and the reaction heated to reflux for 48 h. An orange precipitate formed which was collected by filtration and washed with EtOH (100

mL) then diethyl ether (100 mL) and the solid dried under vacuum (4.64 g, 5.82 mmol, 82%). Analytical data obtained were in good agreement with that previously reported.[229]

Anal. calcd. for $C_{20}H_{30}Cl_4Ir_2$ (796.03 g mol^{-1}): C, 30.14; H, 3.78. Found: C, 30.11; H, 3.82.

^{1}H NMR (270 MHz, $CDCl_3$): δ 1.58 (s, 15 H, H2).

$^{13}C\{^1H\}$ NMR (125 MHz, $CDCl_3$): δ 86.2 (C_q, C1), 9.3 (CH_3, C2).

IR (KBr): ν_{max}/cm^{-1} 2987m (ν_{Ar-H}), 2916m (ν_{C-H}), 1450s, 1373s, 1033s.

Raman (glass capillary): ν_{max}/cm^{-1} 2970m (ν_{Ar-H}), 2917s (ν_{C-H}), 1424m, 590s, 542m, 461m, 449s, 286m (ν_{Ir-Cl}), 189m (ν_{Ir-Cl}).

6.2.10 – $[Cp^*Rh(BenzS_2)]_n$ (n = 1 or 2) (C4-3a)

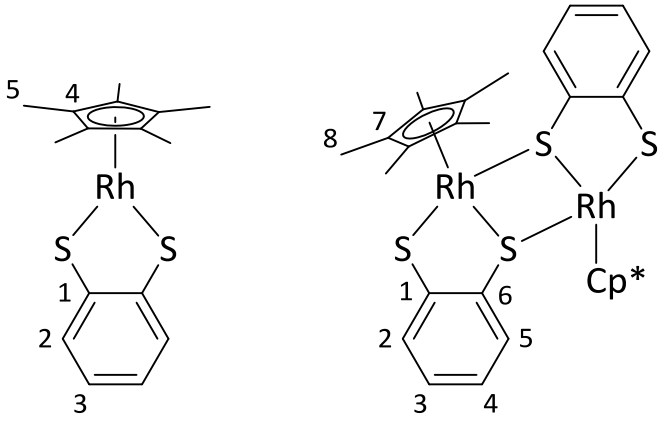

SM-1 (100 mg, 0.16 mmol) was added to THF (25 mL) followed by **H_2A** (75 mg, 0.52 mmol) and the reaction refluxed for 2 h during which time the solution turned purple. The solvent was removed under vacuum and the crude product heated to 60 °C under vacuum to remove excess ligand. The purple solid was purified by column chromatography (silica gel/DCM) resulting in a purple solid (101 mg, 0.13 mmol, 84%). Analytical data obtained were in good agreement with that previously reported.[162] Crystals suitable for X-ray work were obtained by slow evaporation from a DCM solution.

Anal. calcd. for $C_{32}H_{38}Rh_2S_4$ (756.70 g mol^{-1}): C, 50.79; H, 5.06. Found: C, 50.70; H, 5.13.

Monomeric complex (n =1)

^{1}H NMR (500 MHz, $CDCl_3$): δ 7.85 (dd, $^3J_{HH}$ = 6.1, $^4J_{HH}$ = 3.3 Hz, 2 H, H2), 7.08 (dd, $^3J_{HH}$ = 6.1, $^4J_{HH}$ = 3.2 Hz, 2 H, H3), 2.04 (s, 15 H, H5).

^{13}C{^{1}H} NMR (125 MHz, $CDCl_3$): δ 152.5 (C_q, C1), 130.0 (CH, C2), 122.5 (CH, C3), 98.4 (d, C_q, $^1J_{CRh}$ = 7.1 Hz, C4), 10.7 (CH_3, C5).

Dimeric Complex (n = 2)

^{1}H NMR (500 MHz, $CDCl_3$): δ 7.46 (d, $^3J_{HH}$ = 7.6 Hz, 2 H, H5), 7.13−7.07 (m[ii], 2 H, H2), 6.83 (*p*t, $^3J_{HH}$ = 7.6 Hz, 2 H, H4), 6.64 (*p*t, $^3J_{HH}$ = 7.6 Hz, 2 H, H3), 1.27 (s, 30 H, H8).

^{13}C{^{1}H} NMR (125 MHz, $CDCl_3$): δ 157.2 (C_q, C6), 139.0 (C_q, C1), 130.8 (CH, C5), 128.8 (CH, C3), 125.2 (CH, C2), 120.2 (CH, C4), 96.6 (d, $^1J_{CRh}$ = 5.7 Hz, C_q, C7), 8.1 (CH_3, C8).

MS (ES^+): *m/z* (%) 378.99 (100) $[½M+H]^+$.

IR (KBr): ν_{max}/cm^{-1} 3042w (ν_{Ar-H}), 2915m (ν_{C-H}), 1561m, 1438s, 1377s, 1239m, 1021s, 762s, 740s.

Raman (glass capillary): ν_{max}/cm^{-1} 2907m (ν_{C-H}), 1539m, 1439m, 1090s, 1020m, 613m (ν_{C-S}), 494m, 431m.

[ii] Multiplet due to overlapping signal with the mono complex.

4.2.11 – [Cp*Ir(BenzS_2] (C4-4a)

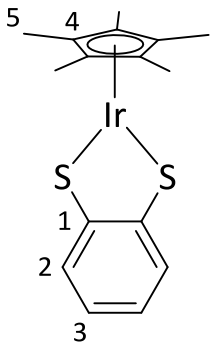

To a solution of **SM-2** (150 mg, 0.18 mmol) in THF (25 mL) was added **H_2A** (85 mg, 0.60 mmol) and the reaction refluxed for 2 h. The solution turned dark purple and the solvent was removed under vacuum. Excess ligand was removed by heating the crude product at 60 °C under vacuum. Further purification by flash column chromatography (silica gel/DCM) yielded the final product as a purple solid (101 mg, 0.13 mmol, 84%). Analytical data obtained were in good agreement with that previously reported.[162] Crystals suitable for X-ray work were obtained by slow evaporation from a DCM solution.

Anal. calcd. for $C_{16}H_{19}IrS_2$ (467.67 g mol^{-1}): C, 41.03; H, 4.09. Found: C, 41.23; H, 4.15.

^{1}H NMR (500 MHz, $CDCl_3$): δ 8.05 (dd, $^3J_{HH}$ = 6.0 Hz, $^4J_{HH}$ = 3.2 Hz, 2 H, H2), 7.03 (dd, $^3J_{HH}$ = 6.1 Hz, $^4J_{HH}$ = 3.2 Hz, 2 H, H3), 2.15 (s, 15 H, H5).

^{13}C{^{1}H} NMR (125 MHz, $CDCl_3$): δ 153.0 (C_q, C1), 129.6 (CH, C2), 122.9 (CH, C3), 91.8 (C_q, C4), 10.6 (CH_3, C5).

MS (ES^+): *m/z* (%) 468.98 (100) $[M+H]^+$.

IR (KBr): ν_{max}/cm^{-1} 2918w (ν_{C-H}), 1439m, 1382m, 1029m, 761s.

Raman (glass capillary): ν_{max}/cm^{-1} 3028w (ν_{Ar-H}), 2912m (ν_{C-H}), 1542s, 1441m, 1091s, 1019m, 669m (ν_{C-S}), 588m, 428s, 179s.

6.2.12 – [Cp*Rh(NaphthS$_2$)]$_2$ (C4-3b)

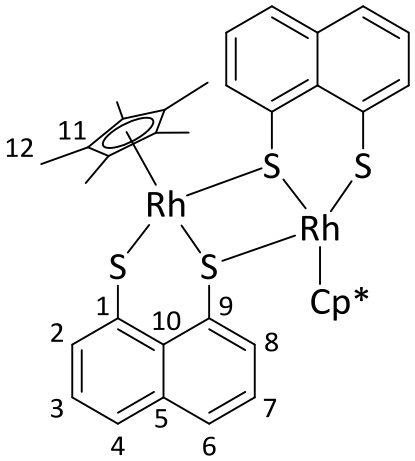

SM-1 (100 mg, 0.16 mmol) was added to THF (25 mL) followed by **H$_2$B** (100 mg, 0.52 mmol) and the reaction refluxed for 2.5 h. The red precipitate formed was filtered and washed with THF (20 mL) then diethyl ether (20 mL). Purification of the compound by flash column chromatography (silica gel/DCM) resulted in a red solid (111 mg, 0.12 mmol, 75%). Crystals suitable for X-ray work were obtained by slow evaporation from a chloroform solution.

Anal. calcd. for $C_{40}H_{42}Rh_2S_4$ (856.02 g mol^{-1}): C, 56.07; H, 4.95. Found: C, 55.94; H, 5.01.

^{1}H NMR (500 MHz, CDCl$_3$): δ 8.14 (d, $^3J_{HH}$ = 7.8 Hz, 1 H, H8), 7.78 (d, $^3J_{HH}$ = 7.2 Hz, 1 H, H2), 7.70 (d, $^3J_{HH}$ = 7.8 Hz, 1 H, H6), 7.50 (d, $^3J_{HH}$ = 7.2, 1 H, H4), 7.17 (*p*t, $^3J_{HH}$ = 7.7 Hz, 1 H, H7), 7.14 (*p*t, $^3J_{HH}$ = 7.3 Hz, 1 H, H3), 1.17 (s, 15 H, H12).

^{13}C{^{1}H} NMR (125 MHz, CDCl$_3$): δ 141.1 (C_q, C5), 136.1 (C_q, C10), 135.5 (C_q, C9), 132.0 (CH, C8), 130.5 (C_q, C1), 129.3 (CH, C6), 129.2 (CH, C7), 124.9 (CH, C4), 124.7 (CH, C3), 123.3 (CH, C42), 96.5 (d, $^1J_{CRh}$ = 5.7 Hz, C_q, C11), 8.0 (CH_3, C12).

HRMS (APCI$^+$): *m/z* (%) 857.0359 (25) $[M+H]^+$, 699.0165 (75) $[M-C_{10}H_6S+H]^+$, 667.0443 (75) $[M-C_{10}H_6S_2+H]$, 429.0215 (100) $[½M+H]^+$.

IR (KBr): ν$_{max}$/cm^{-1} 3039w (ν_{Ar-H}), 2907w (ν_{C-H}), 1537s, 1377m, 1193s, 817s, 763s.

Raman (glass capillary): ν$_{max}$/cm^{-1} 3040w (ν_{Ar-H}), 2909w (ν_{C-H}), 1540s, 1325s, 882s, 548w (ν_{C-S}), 447m, 388m.

6.2.13 – [Cp*Ir(NaphthS$_2$)]$_2$ (C4-4b)

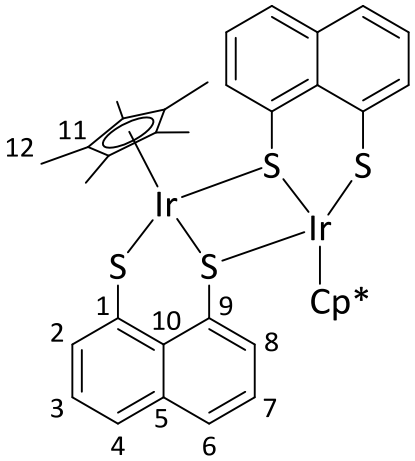

A solution of **SM-2** (150 mg, 0.18 mmol) and **H_2B** (116 mg, 0.60 mmol) in THF (25 mL) was refluxed for 4 h. A precipitate formed which was filtered and washed with THF (20 mL) then diethyl ether (20 mL). The solid was purified by flash column chromatography (silica gel/DCM) to afford the final product as a yellow solid (89 mg, 0.085 mmol, 46%). Crystals suitable for X-ray work were obtained by slow evaporation form a chloroform solution.

Anal. calcd. for $C_{40}H_{42}Ir_2S_4$ (1035.45 g mol^{-1}): C, 46.40; H, 4.09. Found: C, 46.27; H, 4.14.

^{1}H NMR (500 MHz, $CDCl_3$): δ 8.14 (dd, $^3J_{HH}$ = 7.2 Hz, $^4J_{HH}$ = 1.2 Hz, 1 H, H8), 7.76 (dd, $^3J_{HH}$ = 7.2 Hz, $^4J_{HH}$ = 1.2 Hz, 1 H, H2), 7.73 (d, $^3J_{HH}$ = 8.1 Hz, 1 H, H6), 7.50 (d, $^3J_{HH}$ = 8.1 Hz, 1 H, H4), 7.12 (*p*t, $^3J_{HH}$ = 7.6 Hz, 1 H, H7), 7.09 (*p*t, $^3J_{HH}$ = 7.6 Hz, 1 H, H3), 1.22 (s, 15 H, H12).

^{13}C{^{1}H} NMR (125 MHz, $CDCl_3$): δ 137.6 (C_q, C5), 135.7 (C_q, C10), 130.2 (CH, C8), 129.2 (CH, C6), 128.4 (CH, C7), 127.4 (C_q, C9), 125.0 (CH, C4), 124.0 (CH, C3), 123.5 (C_q, C1), 123.3 (CH, C3), 91.1 (C_q, C11), 7.7 (CH_3, C12).

HRMS (APCI+): *m/z* (%) 1037.1502 (20) $[M+H]^+$, 879.1314 (55) $[M-C_{10}H_6S+H]^+$, 519.0781 (100) $[½M+H]^+$.

IR (KBr): ν_{max}/cm^{-1} 3043w (ν_{Ar-H}), 2909m (ν_{C-H}), 1538s, 1196m, 1184m, 814s, 761s.

Raman (glass capillary): ν_{max}/cm^{-1} 3052w (ν_{Ar-H}), 2912m (ν_{C-H}), 1540s, 1417m, 1325s, 1142m, 881s, 548m (ν_{C-S}), 456m, 391m.

6.2.14 – $[(Cp^*Rh)_2(AcenapS_2)Cl]^+ Cl^-$ (C4-3c)

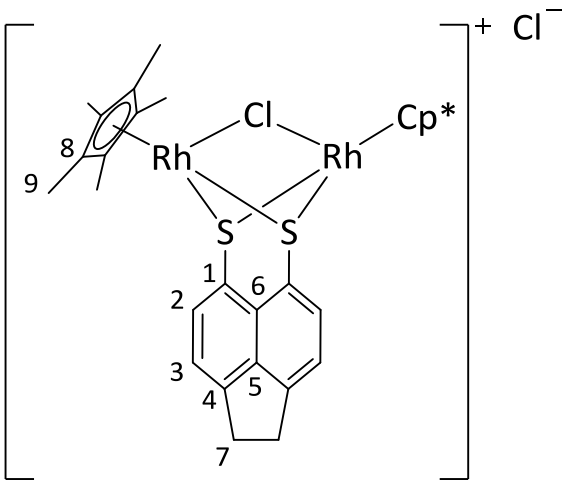

Method 1

A THF (25 mL) solution containing **SM-1** (100 mg, 0.16 mmol) and **H_2C** (113 mg, 0.51 mmol) was refluxed for 2 hrs. The reaction was cooled and filtered, washed with THF (20 mL) and diethyl ether (20 mL). The red solid obtained was dissolved in DCM and filtered to remove insoluble impurities. Removal of the solvent resulted in the product as a red/orange solid (63 mg, 0.082 mmol, 52%). Crystals suitable for X-ray work were obtained by layering a DCM solution with diethyl ether.

Method 2

A methanol (25 mL) solution containing **SM-1** (100 mg, 0.16 mmol), **H_2C** (70 mg, 0.32 mmol) and NaOMe (17 mg, 0.32 mmol) was stirred at room temperature O/N. The solvent was removed and the crude compound purified by flash column chromatography (silica gel/DCM:MeOH (9:1)) to afford the product as a red solid (101 mg, 0.13 mmol, 83%).

Anal. calcd. for $C_{32}H_{38}Cl_2Rh_2S_2$ (761.99 g mol^{-1}): C, 50.34; H, 5.01. Found: C, 50.12; H, 4.71.

^{1}H NMR (500 MHz, $CDCl_3$): δ 8.37 (d, $^3J_{HH}$ = 7.2 Hz, 2 H, H3), 7.45 (d, $^3J_{HH}$ = 7.2 Hz, 2 H, H2), 3.37 (s, 4 H, H7), 1.23 (s, 30 H, H9).

^{13}C{^{1}H} NMR (125 MHz, $CDCl_3$): δ 150.0 (C_q, C4), 139.8 (C_q, C6), 132.2 (CH, C3), 128.0 (C_q, C5), 124.5 (C_q, C1), 120.1 (CH, C2), 97.0 (d, $^1J_{CRh}$ = 7.4 Hz, C_q, C8), 30.8 (CH_2, C7), 8.2 (CH_3, C9).

MS (ES$^+$): *m/z* (%) 727.02 (100) $[M]^+$.

IR (KBr): ν_{max}/cm^{-1} 2918m (ν_{C-H}), 1591m, 1444s, 1376s, 1353s, 1024s, 733m.

Raman (glass capillary): ν_{max}/cm^{-1} 3048w (ν_{Ar-H}), 2919s (ν_{C-H}), 1592s, 1407s, 588s (ν_{C-S}), 460s, 430s, 416s, 269w (ν_{Rh-Cl}).

6.2.15 – $[(Cp^*Ir)_2(AcenapS_2)Cl]^+ Cl^-$ (C4-4c)

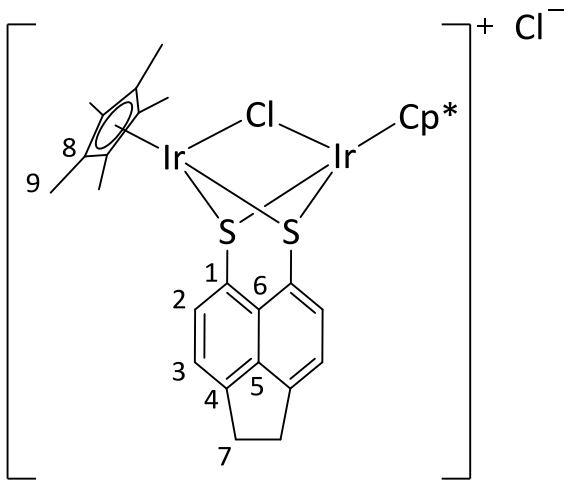

Method 1

A THF (25 mL) solution containing **SM-2** (200 mg, 0.25 mmol) and **H_2C** (137 mg, 0.63 mmol) was refluxed for 3 hrs. The reaction was cooled and the solvent removed to afford the crude product as a yellow solid which was washed with hexane. This was purified by flash column chromatography (silica gel/DCM) to afford the final compound as a light yellow solid (5 mg, 5.3 µmol, 2 %).

Method 2

A MeOH (25 mL) mixture of **SM-2** (150 mg, 0.18 mmol), **H_2C** (79 mg, 0.36 mmol) and NaOMe (20 mg, 0.36 mmol) was stirred at room temperature O/N. The solvent was removed and the crude compound purified by flash column chromatography (silica gel/DCM) to afford the product as a yellow solid (174 mg, 0.18 mmol, 98%). Crystals suitable for X-ray work were obtained by layering a DCM solution with diethyl ether.

Anal. calcd. for $C_{32}H_{38}Cl_2Ir_2S_2$ (942.10 g mol^{-1}): C, 40.75; H, 4.07. Found: C, 40.67; H, 4.12.

^{1}H NMR (500 MHz, $CDCl_3$): δ 8.27 (d, $^3J_{HH}$ = 7.1 Hz, 2 H, H3), 7.31 (d, $^3J_{HH}$ = 7.1 Hz, 2 H, H2), 3.21 (s, 4 H, H7), 1.25 (s, 30 H, H9).

$^{13}C\{^1H\}$ NMR (125 MHz, $CDCl_3$): δ 148.7 (C_q, C4), 140.0 (C_q, C6), 129.3 (CH, C3), 128.0 (C_q, C5), 122.2 (C_q, C1), 120.3 (CH, C2), 90.0 (C_q, C8), 30.8 (CH_2, C7), 8.0 (CH_3, C9).

MS (ES^+): *m/z* (%) 907.12 (100) $[M]^+$.

IR (KBr): ν_{max}/cm^{-1} 3132m (ν_{Ar-H}), 2918m (ν_{C-H}), 1592m, 1452s, 1355s, 1214m, 1030s, 860m.

Raman (glass capillary): ν_{max}/cm^{-1} 2920s (ν_{C-H}), 1593m, 1408s, 1344m, 584m (ν_{C-S}), 430s.

6.2.16 – $[(Cp^*Rh)_4(\mu^2\text{-BiphenS}_2)_2(\mu^4\text{-BiphenS}_2)]^{2+}$ $2Cl^-$ (C4-3d)

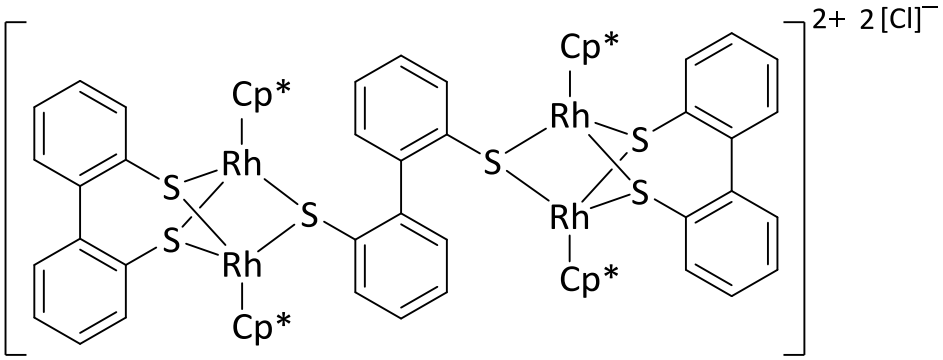

To a THF (25 mL) solution containing **SM-1** (150 mg, 0.24 mmol) was added **H_2D** (169 mg, 0.77 mmol) and the reaction refluxed for 2 h. The solvent was removed and the orange powder washed with hexane (20 mL) and diethyl ether (20 mL). The product was purified by column chromatography (silica gel/DCM:EtOH (9:1)) and the product obtained as orange crystals (155 mg, 0.096 mmol, 40%). Crystals suitable for X-ray work were obtained by layering a DCM solution with diethyl ether.

^1H NMR (500 MHz, $CDCl_3$): δ 8.32 (dd, $^3J_{HH}$ = 7.89, $^4J_{HH}$ = 1.24 Hz, 2 H, ArH), 8.07 (dd, $^3J_{HH}$ = 7.83, $^4J_{HH}$ = 1.24 Hz, 2 H, ArH), 8.02–7.97 (m, 2 H, ArH), 7.74 (t, $^3J_{HH}$ = 8.60 Hz, 4 H, ArH), 7.53–7.47 (m, 4 H, ArH), 7.46−7.26 (m, 10 H, ArH), 1.20 (s, 30 H, Cp*-CH_3), 1.17 (s, 30 H, Cp*-CH_3).

$^{13}C\{^1H\}$ NMR (125 MHz, $CDCl_3$): δ 138.5 (C_q, ArC), 138.4 (C_q, ArC), 137.4 (CH, ArC), 137.1 (CH, ArC), 136.7 (CH, ArC), 135.9 (C_q, ArC), 132.8 (CH, ArC), 132.7 (CH, ArC), 131.7 (CH, ArC), 130.4 (CH, ArC), 128.9 (CH, ArC), 128.5 (CH, ArC), 128.4 (CH, ArC), 128.3 (CH, ArC), 126.3 (CH, ArC), 126.0 (CH, ArC), 125.2 (C_q, ArC), 124.8 (CH, ArC), 98.6 (d, $^1J_{CRh}$ = 6.7 Hz, C_q, Cp*-C), 98.4 (d, $^1J_{CRh}$ = 6.5 Hz, C_q, Cp*-C), 8.7 (CH_3, Cp*-CH_3), 8.6 (CH_3, Cp*-CH_3).

MS (ES$^+$): *m/z* (%) 909.04 (100) $[M-(Cp^*_2Rh_2BiphenS_2)]^+$.

IR (KBr): ν_{max}/cm^{-1} 3047w (ν_{Ar-H}), 2917w (ν_{C-H}), 1452s, 1376m, 1021s, 754s.

Raman (glass capillary): ν_{max}/cm^{-1} 3054m (ν_{Ar-H}), 2916s (ν_{C-H}), 1582s, 1426m, 1300m, 1041s, 437m, 415s.

6.2.17 – $[(Cp^*Rh)_2(NaphthS_2)Cl]^+ Cl^-$ (C4-5b)

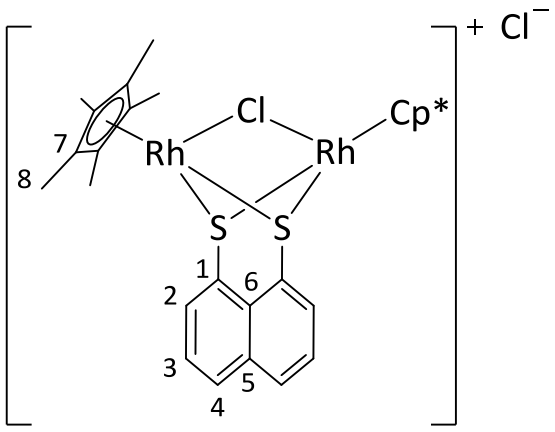

A MeOH (25 mL) mixture of **SM-1** (150 mg, 0.24 mmol), **H_2B** (116 mg, 0.60 mmol) and NaOMe (33 mg, 0.60 mmol) was stirred at room temperature O/N. The solvent was removed and the crude compound purified by flash column chromatography (silica gel/DCM:MeOH(9:1)) to afford the product as a red solid (102 mg, 0.13 mmol, 58%). Crystals suitable for X-ray work were obtained by diffusion of diethyl ether into a DCM solution.

Anal. calcd. for $C_{30}H_{36}Cl_2Rh_2S_2$ (735.97 g mol^{-1}): C, 48.91; H, 4.93. Found: C, 48.83; H, 5.04.

^{1}H NMR (500 MHz, $CDCl_3$): δ 8.44 (dd, $^3J_{HH}$ = 7.2, $^4J_{HH}$ = 1.2 Hz, 2 H, H4), 8.13 (dd, $^3J_{HH}$ = 8.2, 1.1 Hz, 2 H, H2), 7.59 (dd, $^3J_{HH}$ = 8.2, 7.2 Hz, 2 H, H3), 1.24 (s, 30 H, H8).

^{13}C{^{1}H} NMR (125 MHz, $CDCl_3$): δ 135.0 (C_q, C5), 131.8 (CH, C2), 131.3 (CH, C4), 129.3 (C_q, C6), 128.9 (C_q, C1), 125.9 (CH, C3), 97.3 (d, $^1J_{CRh}$ = 7.6 Hz, C_q, C7), 8.3 (CH_3, C8).

MS (ES$^+$): *m/z* (%) 701.00 (100) $[M]^+$.

IR (KBr): ν_{max}/cm^{-1} 2979w (ν_{C-H}), 2918m (ν_{C-H}), 1625m, 1493s, 1450s, 1377s, 1079m, 1023s, 832s, 769m.

Raman (glass capillary): ν_{max}/cm^{-1} 3065w (ν_{Ar-H}), 2919s (ν_{C-H}), 1546s, 894m, 589m (ν_{C-S}), 460m, 430s, 322m.

6.2.18 – $[(Cp^*Ir)_2(NaphthS_2)Cl]^+ Cl^-$ (C4-6b)

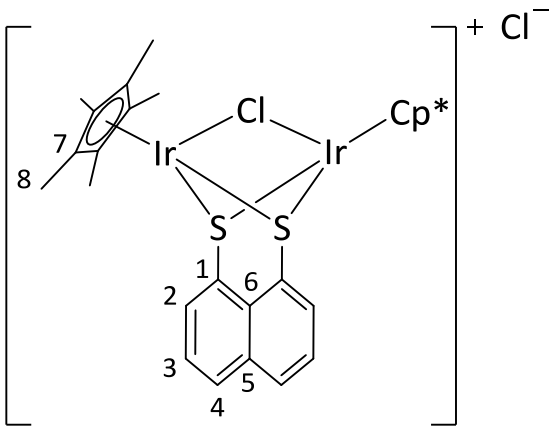

A MeOH (25 mL) mixture of, **SM-2** (150 mg, 0.18 mmol), **H_2B** (91 mg, 0.47 mmol) and NaOMe (26 mg, 0.47 mmol) was stirred at room temperature O/N. The solvent was removed and the crude product purified by flash column chromatography on silica gel. The by-product (**C4-4b**) was removed by eluting with DCM and the title compound eluted using 10% MeOH/DCM. The product was obtained as a red/orange solid (124mg, 0.13 mmol, 75%). Crystals suitable for X-ray work were obtained by diffusion of diethyl ether into a DCM solution.

Anal. calcd. for $C_{30}H_{36}Cl_2Ir_2S_2$ (916.08 g mol^{-1}): C, 39.30; H, 3.96. Found: C, 39.35; H, 4.08.

^{1}H NMR (500 MHz, $CDCl_3$): δ 8.39 (dd, $^3J_{HH}$ = 7.2 Hz, $^4J_{HH}$ = 1.2 Hz, 2 H, H4), 8.11 (dd, $^3J_{HH}$ = 8.2 Hz, $^4J_{HH}$ = 1.1 Hz, 2 H, H2), 7.50 (dd, $^3J_{HH}$ = 8.2, 7.2 Hz, 2 H, H3), 1.29 (s, 30 H, H8).

$^{13}C\{^1H\}$ NMR (125 MHz, $CDCl_3$): δ 135.2 (C_q, C5), 130.6 (CH, C2), 129.5[iii] (C_q, C1/6), 128.6 (CH, C4), 126.4 (CH, C3), 90.3 (C_q, C7), 8.1 (CH_3, C8).

MS (ES^+): *m/z* (%) 881.11 (100) $[M]^+$.

[iii] Two signals overlapping from quaternary carbons

IR (KBr): ν_{max}/cm^{-1} 2978w ($\nu_{C\text{-}H}$), 2918m ($\nu_{C\text{-}H}$), 1626m, 1490m, 1452s, 1381s, 1030s, 831s, 768s.

Raman (glass capillary): ν_{max}/cm^{-1} 3056w ($\nu_{Ar\text{-}H}$), 2921s ($\nu_{C\text{-}H}$), 1547s, 1426m, 893s, 588m ($\nu_{C\text{-}S}$), 549m, 443s, 425s.

6.3 – Chapter 5 Experimental Procedures

6.3.1 – [Cp*RhCl$_2$PEt$_3$] (C5-3)

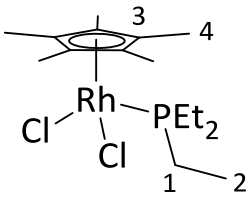

C5-3 was prepared according to the literature procedure.[259] **SM-1** (750 mg, 1.21 mmol) was added to THF (30 mL) followed by PEt_3 (318 mg, 2.7 mL, 2.66 mmol, 1M sol^n THF) and the suspension refluxed for 2 h. During this time the solid dissolved to leave a red solution which was cooled and the solvent removed *in vacuo*. Drying under vacuum for 4 h removed excess ligand to afford the product as a red solid (1.02 g, 2.38 mmol, 99%). Analytical data obtained was in good agreement with that previously reported.[259] Crystals suitable for X-ray work were obtained by slow evaporation from diethyl ether.

Anal. calcd. for $C_{16}H_{30}Cl_2PRh$ (426.05 g mol^{-1}): C, 44.98; H, 7.09. Found: C, 44.89; H, 7.20.

^{1}H NMR (500 MHz, $CDCl_3$): δ 2.10 (dq, $^2J_{HP}$ = 10.5, $^3J_{HH}$ = 7.8 Hz, 6 H, H1), 1.66 (d, $^4J_{HP}$ = 3.1 Hz, 15 H, H4), 1.15 (dt, $^3J_{HP}$ = 15.3, $^3J_{HH}$ = 7.8 Hz, 9 H, H2).

^{13}C{^{1}H} NMR (125 MHz, $CDCl_3$): δ 98.0 (dd, $^1J_{CRh}$ = 7.5, $^2J_{CP}$ = 2.8 Hz, C_q, C3), 16.8 (d, $^1J_{CP}$ = 27.3 Hz, CH_2, C1), 9.3 (CH_3, C4), 8.0 (d, $^2J_{CP}$ = 4.6 Hz, CH_3, C2).

^{31}P{^{1}H} NMR (202 MHz, $CDCl_3$): δ 28.17 (d, $^1J_{PRh}$ = 137.5 Hz).

MS (ES$^+$): *m/z* (%) 391.04 (100) [M−Cl]$^+$.

IR (KBr): ν_{max}/cm^{-1} 2964m ($\nu_{C\text{-}H}$), 2931m ($\nu_{C\text{-}H}$), 1452m, 1415m, 1034s, 748s, 724s ($\nu_{P\text{-}C}$).

Raman (glass capillary): ν_{max}/cm^{-1} 2914s ($\nu_{C\text{-}H}$), 1458m, 1423m, 725w ($\nu_{P\text{-}C}$), 591m, 437m, 396s, 282s ($\nu_{Rh\text{-}Cl}$), 179s ($\nu_{Rh\text{-}Cl}$).

6.3.2 – [Cp*IrCl$_2$PEt$_3$] (C5-4)

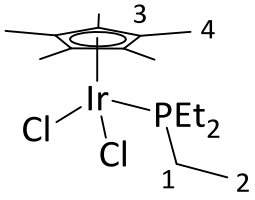

C5-4 was prepared according to the literature procedure.[259] **SM-2** (750 mg, 0.94 mmol) was added to THF (30 mL) followed by PEt_3 (245 mg, 2.1 mL, 2.07 mmol, 1M sol^n THF) and the suspension refluxed for 2 h. During this time the solid dissolved to leave a yellow solution which was cooled and the solvent removed *in vacuo*. Drying under vacuum for 4 h removed excess ligand to afford the product as a yellow solid (968 mg, 1.87 mmol, 99%). Analytical data obtained was in good agreement with that previously reported.[259] Crystals suitable for X-ray work were obtained by slow evaporation from diethyl ether.

Anal. calcd. for $C_{16}H_{30}Cl_2IrP$ (516.10 g mol^{-1}): C, 37.02; H, 5.86. Found: C, 37.09; H, 5.99.

^{1}H NMR (500 MHz, $CDCl_3$): δ 2.14−2.06 (m, 6 H, H1), 1.67 (d, $^4J_{HP}$ = 1.7 Hz, 15 H, H4), 1.11 (dt, $^3J_{HP}$ = 15.5, $^3J_{HH}$ = 7.7 Hz, 9 H, H2).

^{13}C{^{1}H} NMR (125 MHz, $CDCl_3$): δ 91.2 (d, $^2J_{CP}$ = 2.6 Hz, C_q, C3), 16.1 (d, $^1J_{CP}$ = 36.1 Hz, CH_2, C1), 8.9 (CH_3, C4), 7.5 (d, $^2J_{CP}$ = 3.96 Hz, CH_3, C2).

^{31}P{^{1}H} NMR (202 MHz, $CDCl_3$: δ −5.78 (s).

MS (ES$^+$): *m/z* (%) 481.12 (100) [M−Cl]$^+$.

IR (KBr): ν_{max}/cm^{-1} 2965m ($\nu_{C\text{-}H}$), 2931m ($\nu_{C\text{-}H}$), 1453m, 1416m, 1034s, 751s, 727s ($\nu_{P\text{-}C}$).

Raman (glass capillary): ν_{max}/cm^{-1} 2968m (ν_{C-H}), 2924s, (ν_{C-H}), 729w (ν_{P-C}), 635m, 590s, 447m, 394s, 286s (ν_{Ir-Cl}), 183s (ν_{Ir-Cl}).

6.3.3 – [Cp*RhCl$_2$PPh$_3$] (C5-5)

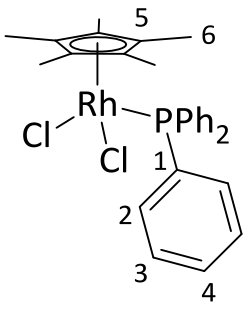

C2-5 was prepared according to the literature procedure.[258] Triphenylphosphine (0.31 g, 1.22 mmol) was added to a stirred suspension of **SM-1** (0.38 g, 0.61 mmol) in ethanol (15 mL) and heated to reflux for 5 h. The volatiles were removed *in vacuo* affording the product as a dark red solid (0.44 g, 0.85 mmol, 70%). Analytical data obtained was in good agreement with that previously reported.[258] Crystals suitable for X-ray work were obtained by slow evaporation from chloroform.

Anal. calcd. for $C_{28}H_{30}Cl_2PRh$ (570.05 g mol^{-1}): C, 58.94; H, 5.30. Found: C, 59.01; H, 5.18.

^{1}H NMR (500 MHz, $CDCl_3$): δ 7.90−7.80 (m, 6H, H2), 7.55−7.30 (m, 9H, H3/4), 1.39 (d, $^4J_{PH}$ = 3.5 Hz, 15 H, H6).

^{13}C{^{1}H} NMR (125 MHz, $CDCl_3$): δ 134.7 (d, $^2J_{CP}$ = 9.8 Hz, CH, C2), 130.4 (br s, CH, C4), 128.0 (br s, CH, C3), 99.2 (dd, $^1J_{CRh}$ = 6.7, $^2J_{CP}$ = 2.8 Hz, C_q, C5), 8.8 (s, CH_3, C6).

^{31}P{^{1}H} NMR (202 MHz, $CDCl_3$): δ 30.1 (d, $^1J_{PRh}$ = 144.1 Hz).

HRMS (NSI$^+$): *m/z* (%) 559.1262 (100) [M−Cl_2+OAc]$^+$, 535.0824 (62) [M−Cl]$^+$, 297.0357 (87) [M−Cl_2−PPh_3+OAc]$^+$.

IR (KBr): ν_{max}/cm^{-1} 3057w (ν_{Ar-H}), 2913w (ν_{C-H}), 1481m, 1435m, 1095m (ν_{P-Ar}), 749m (ν_{P-C}), 697s, 523s.

Raman (glass capillary): ν_{max}/cm^{-1} 3060m (ν_{Ar-H}), 2912s (ν_{C-H}), 1587s, 1097m, 1001s, 688w (ν_{P-C}), 618m, 401s, 285m (ν_{Rh-Cl}).

6.3.4 – [Cp*IrCl$_2$PPh$_3$] (C5-6)

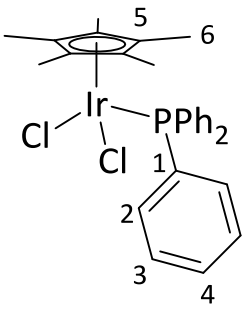

C2-6 was prepared according to the literature procedure.[258] Triphenylphosphine (0.20 g, 0.76 mmol) was added to a stirred suspension of **SM-2** (0.30 g, 0.38 mmol) in ethanol (15 mL) and heated to reflux for 5 h. The volatiles were removed *in vacuo* affording the product as an orange solid (0.35 g, 0.52 mmol, 69%). Analytical data obtained was in good agreement with that previously reported.[258] Crystals suitable for X-ray work were obtained by slow evaporation from DCM.

Anal. calcd. for $C_{28}H_{30}Cl_2IrP$ (660.63 g mol^{-1}): C, 50.90; H, 4.58. Found: C, 50.85; H, 4.46.

^{1}H NMR (500 MHz, CDCl$_3$): δ 7.77 (s, 6H, H2), 7.39 (s, 9 H, H3/4), 1.38 (d, $^4J_{HP}$ = 2.2 Hz, 15 H, H6).

^{13}C{^{1}H} NMR (125 MHz, CDCl$_3$): δ 134.8 (d, $^2J_{CP}$ = 9.9 Hz, CH, C2), 130.3 (s, CH, C4), 127.8 (d, $^3J_{CP}$ = 9.0 Hz, CH, C3), 92.7 (d, $^2J_{CP}$= 2.7 Hz, C_q, C5), 8.3 (s, CH_3, C6).

^{31}P{^{1}H} NMR (202 MHz, CDCl$_3$): δ 1.6 (s).

HRMS (NSI$^+$): *m/z* (%) 649.1842 (90) $[M-Cl_2+OAc]^+$, 606.1900 (100) $[M-2HCl+NH_4]^+$, 589.1642 (57) $[M-2HCl+H]^+$.

IR (KBr): ν_{max}/cm^{-1} 3058w (ν_{Ar-H}), 2914w (ν_{C-H}), 1482m, 1435s (ν_{P-Ar}), 1185w, 1096s, 1028m, 750m, 698s (ν_{P-C}), 529s.

Raman (glass capillary): ν_{max}/cm^{-1} 3051m (ν_{Ar-H}), 2917s (ν_{C-H}), 1588m, 1423w (ν_{P-Ar}), 1098m, 1002s, 690w (ν_{P-C}), 436w, 398m, 293m (ν_{Ir-Cl}).

6.3.5 – [Cp*RhCl$_2$P(OEt)$_3$] (C5-7)

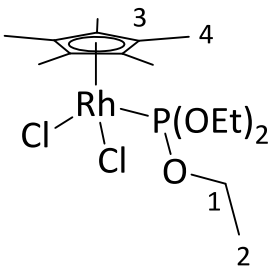

Triethylphosphite (0.20 mL, 0.20 g, 1.20 mmol) was added to a suspension of **SM-1** (0.38 g, 0.60 mmol) in toluene (8 mL) at room temperature and allowed to stir for 2 h. The volatiles were then removed *in vacuo* affording the product as a red powder (0.52 g, 91%). Crystals suitable for X-ray work were obtained by slow evaporation from chloroform.

Anal. calcd. for $C_{16}H_{30}Cl_2O_3PRh$ (475.19 g mol^{-1}): C, 40.50; H 6.38. Found: C, 40.57; H, 6.44.

^{1}H NMR (500 MHz, CDCl$_3$): δ 4.23 (*p*p, $^3J_{HH}$ = $^3J_{HP}$ = 7.0 Hz, 6H, H1), 1.68 (d, $^4J_{PH}$ = 5.1 Hz, 15 H, H4), 1.32 (t, $^3J_{HH}$ = 7.0 Hz, 9 H, H2).

^{13}C{^{1}H} NMR (125 MHz, CDCl$_3$): δ 100.3−100.2 (m, C_q, C3), 63.6 (d, $^2J_{CP}$ = 6.1 Hz, CH_2, C1), 16.2 (d, $^3J_{CP}$ = 6.1 Hz, CH_3, C2), 9.0 (d, $^4J_{CP}$ = 2.0 Hz, CH_3, C4).

^{31}P{^{1}H} NMR (202 MHz, CDCl$_3$): δ 114.0 (d, $^1J_{PRh}$ = 215.1 Hz).

HRMS (NSI$^+$): *m/z* (%) 463.1112 (100) [M−Cl_2+OAc]$^+$, 439.0673 (32) [M−Cl]$^+$, 297.0356 (70) [M−Cl_2−P(OEt)$_3$+OAc]$^+$.

IR (KBr): ν$_{max}$/cm^{-1} 2981m (ν_{C-H}), 2910m (ν_{C-H}), 1513w, 1449m, 1383m, 1063s (ν_{P-O}), 1016s (ν_{P-O}), 960s (ν_{P-O-Et} rocking)

Raman (glass capillary): ν$_{max}$/cm^{-1} 2980m (ν_{C-H}), 2915s (ν_{C-H}), 1452m (ν_{P-O}), 1034w, 590m, 400m, 290s (ν_{Rh-Cl})

6.3.6 – [Cp*IrCl$_2$P(OEt)$_3$] (C5-8)

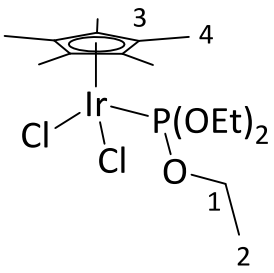

Triethylphosphite (0.16 mL, 0.15 g, 0.90 mmol) was added to a suspension of **SM-2** (0.36 g, 0.45 mmol) in toluene (8 mL) at room temperature and allowed to stir for 2 h. The volatiles were then removed *in vacuo* affording the product as a red powder (0.41 g, 0.73 mmol, 81%). Crystals suitable for X-ray work were obtained by slow evaporation from chloroform.

Anal. calcd. for $C_{16}H_{30}Cl_2IrO_3P$ (564.50 g mol^{-1}): C, 34.04; H 5.36. Found: C, 34.08; H, 5.45.

^{1}H NMR (500 MHz, CDCl$_3$): δ 4.27 (*p*p, $^3J_{HH}$ = $^3J_{HP}$ = 7.0 Hz, 6 H, H1), 1.69 (d, $^4J_{PH}$ = 3.2 Hz, 15 H, H4), 1.31 (t, $^3J_{HH}$ = 7.1 Hz, 9 H, H2).

^{13}C{^{1}H} NMR (125 MHz, CDCl$_3$): δ 94.0 (d, $^2J_{CP}$ = 4.0 Hz, C_q, C3), 62.8 (d, $^2J_{CP}$ = 5.7 Hz, CH_2, C1), 16.2 (d, $^3J_{CP}$ = 6.7 Hz, CH_3, C2), 8.6 (br s, CH_3, C4).

^{31}P{^{1}H} NMR (202 MHz, CDCl$_3$): δ 77.2 (s)

HRMS (NSI$^+$): *m/z* (%) 553.1685 (100) [M−Cl$_2$+OAc]$^+$, 529.1235 (40) [M−Cl]$^+$, 510.1744 (95).

IR (KBr): ν$_{max}$/cm^{-1} 2982m (ν_{C-H}), 2913m (ν_{C-H}), 1453m, 1385m, 1066s (ν_{P-O}), 1019s (ν_{P-O}), 960s (ν_{P-O-Et} rocking).

Raman (glass capillary): ν$_{max}$/cm^{-1} 2980m (ν_{C-H}), 2920s (ν_{C-H}), 1454w, 1421w (ν_{P-O}), 1038w, 752m, 590m, 397s, 299s (ν_{Ir-Cl}).

6.3.7 – [Cp*RhCl$_2$P(OPh)$_3$] (C5-9)

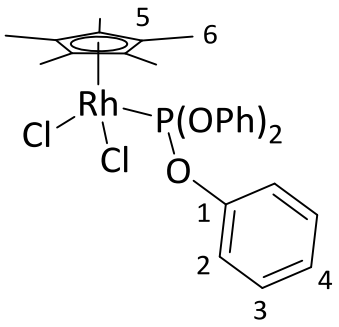

Triphenylphosphite (0.21 mL, 0.25 g, 0.80 mmol) was added to a suspension of **SM-1** (0.25 g, 0.40 mmol) in toluene (8 mL) at room temperature and allowed to stir for 2 h. The precipitate was filtered and washed with petroleum ether (15 mL) then dried *in vacuo*. The product was obtained as a red powder (0.56 g, 0.70 mmol, 88%). Crystals suitable for X-ray work were obtained by slow evaporation from diethyl ether.

Anal. calcd. for $C_{28}H_{30}Cl_2O_3PRh$ (619.32 g mol^{-1}): C, 54.37; H 4.89. Found: C, 54.38; H, 5.03.

^{1}H NMR (500 MHz, CDCl$_3$): δ 7.34−7.16 (m, 12H, H2/3), 7.14 (t, $^3J_{HH}$ = 7.2 Hz, 3 H, H4), 1.61 (d, $^4J_{HP}$ = 5.9 Hz, 15 H, H6).

^{13}C{^{1}H} NMR (125 MHz, CDCl$_3$): δ 151.3 (d, $^2J_{CP}$ = 11.9 Hz, C_q, C1), 129.4 (s, CH, C3), 125.0 (s, CH, C4), 121.4 (d, $^3J_{CP}$ = 4.0 Hz, CH, C2), 101.4 (dd, $^1J_{CRh}$ = 6.3, $^2J_{CP}$ = 4.5 Hz, C_q, C5), 9.2 (d, $^4J_{CP}$ = 2.2 Hz, CH_3, C6).

^{31}P{^{1}H} NMR (202 MHz, CDCl$_3$): δ 104.0 (d, $^1J_{PRh}$ = 240.0 Hz).

HRMS (NSI$^+$): *m/z* (%) 583.0662 (10) [M−Cl]$^+$, 547.0900 (100) [M−2HCl+H]$^+$, 485.0745 (57), 297.0358 (71) [M−Cl_2−P(OPh)$_3$+OAc]$^+$.

IR (KBr): ν_{max}/cm^{-1} 3049w (ν_{Ar-H}), 2915w (ν_{C-H}), 1588s, 1489s (ν_{P-O}), 1223s (ν_{P-O-Ar}), 1184s, 1024m, 935s (ν_{P-O}), 759s.

Raman (glass capillary): ν_{max}/cm^{-1} 3067s (ν_{Ar-H}), 2919s (ν_{C-H}), 1594m, 1425w (ν_{P-O}), 1222m, 1008s, 720s, 406s, 273m (ν_{Rh-Cl}).

6.3.8 – [Cp*IrCl$_2$P(OPh)$_3$] (C5-10)

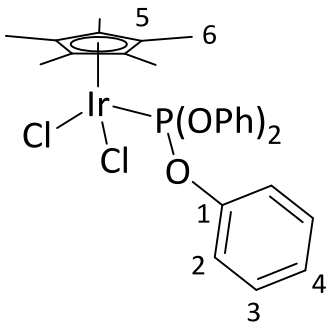

Triphenylphosphite (0.18 mL, 0.22 g, 0.70 mmol) was added to a suspension of **SM-2** (0.28 g, 0.35 mmol) in toluene (8 mL) at room temperature and allowed to stir for 2 h. The precipitate was filtered and washed with petroleum ether (15 mL) then dried *in vacuo*. The product was obtained as an orange powder (0.39 g, 0.55 mmol, 79%). Crystals suitable for X-ray work were obtained by slow evaporation from diethyl ether.

Anal. calcd. for $C_{28}H_{30}Cl_2IrO_3P$ (708.63 g mol^{-1}): C, 47.45; H 4.27. Found: C, 47.54; H, 4.36.

^{1}H NMR (500 MHz, CDCl$_3$): δ 7.38−7.26 (m, 12H, H2/3), 7.14 (t, $^3J_{HH}$ = 7.2 Hz, 3 H, H4), 1.54 (d, $^4J_{HP}$ = 3.6 Hz, 15 H, H6).

^{13}C{^{1}H} NMR (125 MHz, CDCl$_3$): δ 151.4 (d, $^2J_{CP}$ = 10.9 Hz, C_q, C1), 129.6 (s, CH, C3), 125.0 (s, CH, C4), 121.4 (d, $^3J_{CP}$ = 4.2 Hz, CH, C2), 8.9 (s, CH_3 C6).

^{31}P{^{1}H} NMR (202 MHz, CDCl$_3$): δ 65.8 (s).

HRMS (NSI$^+$): *m/z* (%) 697.1666 (5) [M−2Cl+OAc]$^+$, 654.1719 (65), 637.1472 (100) [M−2HCl+H]$^+$.

IR (KBr): ν$_{max}$/cm^{-1} 3053w (ν_{Ar-H}), 2918w (ν_{C-H}), 1588s, 1489s (ν_{P-O}), 1192s (ν_{P-O-Ar}), 1025m, 928s (ν_{P-O}), 765s, 599m, 493m.

Raman (glass capillary): ν$_{max}$/cm^{-1} 3071m (ν_{Ar-H}), 2924m (ν_{C-H}), 1595w, 1450w (ν_{P-O}), 1226w, 1008s, 731w, 402m, 298w (ν_{Rh-Cl}).

6.3.9 – [Cp*Rh(NaphthS_2)PMe_3] (C5-11b)

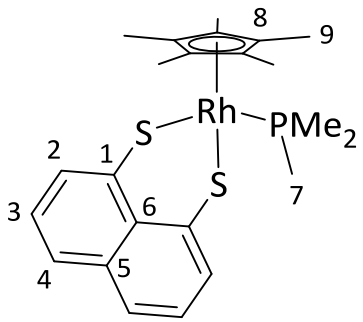

A methanol (20 mL) solution of [Cp*$RhBr_2PMe_3$] (120 mg, 0.25 mmol), Naphth$(SH)_2$ (60 mg, 0.31 mmol) and NaOMe (17 mg, 0.31 mmol) was stirred at room temperature O/N. The red precipitate was filtered, washed with MeOH then dried under vacuum for 3 h. The product was obtained as a red solid (110 mg, 0.21 mmol, 83%). Crystals suitable for X-ray work were obtained by slow evaporation from DCM.

Anal. calcd. for $C_{23}H_{30}PRhS_2$ (504.06 g mol^{-1}): C, 54.76; H, 5.99. Found: C, 54.69; H, 5.96.

^{1}H NMR (400 MHz, $CDCl_3$): δ 7.88 (dd, $^3J_{HH}$ = 7.3, $^4J_{HH}$ = 1.3 Hz, 2 H, H2), 7.47 (dd, $^3J_{HH}$ = 8.1, $^4J_{HH}$ = 1.1 Hz, 2 H, H4), 7.05 (dd, $^3J_{HH}$ = 7.9 & 7.4 Hz, 2 H, H3), 1.54 (dd, $^2J_{HP}$ = 10.3, $^3J_{HRh}$ = 0.7 Hz, 9 H, H7), 1.49 (d, $^4J_{HP}$ = 3.0 Hz, 15 H, H9).

^{13}C{^{1}H} NMR (100 MHz, $CDCl_3$): δ 139.5 (d, $^3J_{CP}$ = 5.4 Hz, C_q, C1), 136.3 (C_q, C5), 133.9 (C_q, C6), 128.1 (CH, C2), 124.9 (CH, C4), 123.8 (CH, C3), 99.7 (dd, $^1J_{CRh}$ = 4.5, $^2J_{CP}$ = 2.9 Hz, C_q, C8), 14.9 (d, $^1J_{CP}$ = 32.7 Hz, CH_3, C7), 8.9 (CH_3, C9).

^{31}P NMR (162 MHz, $CDCl_3$): δ 1.71 (br d, $^1J_{PRh}$ = 149 Hz).

^{31}P{^{1}H} NMR (162 MHz, $CDCl_3$): δ 1.71 (d, $^1J_{PRh}$ = 150 Hz).

HRMS (APCI$^+$): *m/z* (%) 429.0209 (100) $[M-PMe_3+H]^+$.

IR (KBr): ν_{max}/cm^{-1} 3040w (ν_{Ar-H}), 2907m (ν_{C-H}), 1536s, 1195m, 952s, 810m, 761m.

Raman (glass capillary): ν_{max}/cm^{-1} 3047w (ν_{Ar-H}), 2910s (ν_{C-H}), 1536s, 1315s, 886s, 439m, 374m, 325m.

6.3.10 – [Cp*Rh(AcenapS$_2$)PMe$_3$] (C5-11c)

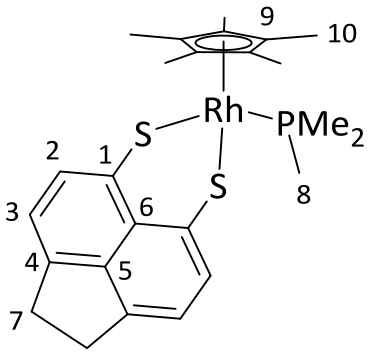

A methanol (20 mL) solution of [Cp*RhBr$_2$PMe$_3$] (120 mg, 0.25 mmol), Acenap(SH)$_2$ (68 mg, 0.31 mmol) and NaOMe (17 mg, 0.31 mmol) was stirred at room temperature O/N. The red precipitate was filtered, washed with MeOH then dried under vacuum for 3 h. The product was obtained as a red solid (121 mg, 0.22 mmol, 91%). Crystals suitable for X-ray work were obtained by slow evaporation from DCM.

Anal. calcd. for $C_{25}H_{32}PRhS_2$ (530.07 g mol^{-1}): C, 56.60; H, 6.08. Found: C, 56.49; H, 6.11.

^{1}H NMR (400 MHz, CDCl$_3$): δ 7.77 (d, $^3J_{HH}$ = 7.2 Hz, 2 H, H2), 6.91 (d, $^3J_{HH}$ = 7.2 Hz, 2 H, H3), 3.17 (s, 4 H, H7), 1.54 (dd, $^2J_{HP}$ = 10.3, $^3J_{HRh}$ = 0.7 Hz, 9 H, H8), 1.50 (d, $^4J_{HP}$ = 3.0 Hz, 15 H, H10).

^{13}C{^{1}H} NMR (100 MHz, CDCl$_3$): δ 141.7 (C_q, C4), 141.1 (C_q, C5), 134.8 (d, $^2J_{CRh}$ = 5.5 Hz, C_q, C1), 132.3 (C_q, C6), 128.6 (CH, C2), 117.9 (CH, C3), 99.5 (dd, $^1J_{CRh}$ = 4.9, $^2J_{CP}$ = 2.9 Hz, C_q, C9), 30.1 (CH_2, C7), 15.0 (d, $^1J_{CP}$ = 33.0 Hz, CH_3, C8), 8.9 (CH_3, C10).

^{31}P NMR (162 MHz, CDCl$_3$): δ 2.9 (br d, $^1J_{PRh}$ = 148 Hz).

^{31}P{^{1}H} NMR (162 MHz, CDCl$_3$): δ 2.9 (d, $^1J_{PRh}$ = 148 Hz).

HRMS (APCI$^+$): *m/z* (%) 455.0362 (80) [M−PMe$_3$+H]$^+$, 216.0060 (95) [$C_{12}H_8S_2$], 184.0339 (55) [$C_{12}H_8S$], 152.0618 (100) [$C_{12}H_8$].

IR (KBr): ν_{max}/cm^{-1} 3037w (ν_{Ar-H}), 2907m (ν_{C-H}), 1552m, 1404m, 1027m, 952s, 837m, 734m.

Raman (glass capillary): ν_{max}/cm^{-1} 3039w, (ν_{Ar-H}), 2909s (ν_{C-H}), 1594s, 1554m, 1407s, 1322s, 1031m, 827m, 727m, 579m, 375m.

6.3.11 – [Cp*Rh(BiphenS_2)PMe_3] (C5-11d)

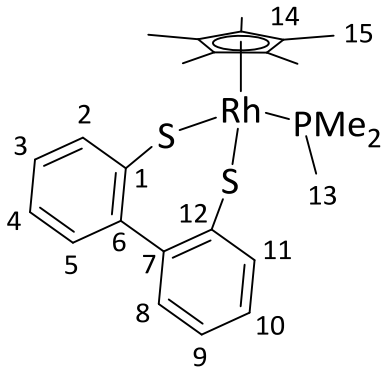

A methanol (20 mL) solution of [Cp*RhBr_2PMe_3] (120 mg, 0.25 mmol), Biphen$(SH)_2$ (71 mg, 0.33 mmol) and NaOMe (19 mg, 0.33 mmol) was stirred at room temperature O/N. The red precipitate was filtered, washed with MeOH then dried under vacuum for 3 h. The product was obtained as a red solid (110 mg, 0.21 mmol, 83%). Crystals suitable for X-ray work were obtained by slow evaporation from DCM.

Anal. calcd. for $C_{25}H_{32}PRhS_2$ (530.07 g mol^{-1}): C, 56.60; H, 6.08. Found: C, 56.49; H, 6.15.

^{1}H NMR (400 MHz, $CDCl_3$): δ 7.66 (dd, $^3J_{HH}$ = 7.6, $^4J_{HH}$ = 1.3 Hz, 1 H, H2), 7.64 (dd, $^3J_{HH}$ = 7.7, $^4J_{HH}$ = 1.3, 1 H, H11), 7.19 (*p*td, $^3J_{HH}$ = 7.4, $^4J_{HH}$ = 1.4 Hz, 1 H, H9), 7.18 (*p*td, $^3J_{HH}$ = 7.4, $^4J_{HH}$ = 1.4 Hz, 1 H, H4), 7.03 (*p*td, $^3J_{HH}$ = 7.5, $^4J_{HH}$ = 1.6 Hz, 1 H, H10), 6.98 (*p*td, $^3J_{HH}$ = 7.5, $^4J_{HH}$ = 1.6 Hz, 1 H, H3), 6.94 (dd, $^3J_{HH}$ = 7.5, $^4J_{HH}$ = 1.5 Hz, 1 H, H8), 6.86 (dd, $^3J_{HH}$ = 7.5, $^4J_{HH}$ = 1.5 Hz, 1 H, H5), 1.58 (d, $^4J_{HP}$ = 3.2 Hz, 15 H, H15), 1.39 (dd, $^2J_{HP}$ = 10.5, $^3J_{HRh}$ = 0.6 Hz, 9 H, H13).

^{13}C{^{1}H} NMR (100 MHz, $CDCl_3$): δ 151.0 (C_q, C6), 150.0 (C_q, C7), 143.0 (d, $^3J_{CP}$ = 6.5 Hz, C_q, C12), 140.2 (C_q, C1), 137.2 (CH, C2), 135.2 (CH, C11), 130.9 (CH, C8), 130.6 (CH, C5), 126.2 (CH, C3/9), 125.7 (CH, C4), 125.5 (CH, C10), 99.3 (dd, $^1J_{CRh}$ = 5.3, $^2J_{CP}$ = 3.2 Hz, C_q, C14), 15.9 (d, $^1J_{CP}$ = 31.6 Hz, CH_3, C13), 8.8 (CH_3, C15).

^{31}P NMR (162 MHz, $CDCl_3$): δ 0.3 (br d, $^1J_{PRh}$ = 153 Hz).

^{31}P{^{1}H} NMR (162 MHz, $CDCl_3$): δ 0.3 (d, $^1J_{PRh}$ = 152 Hz).

HRMS (APCI$^+$): *m/z* (%) 455.0365 (100) $[M-PMe_3+H]^+$.

IR (KBr): ν_{max}/cm^{-1} 3037w (ν_{Ar-H}), 2905m (ν_{C-H}), 1451m, 1404m, 1280w, 959s, 750s.

Raman (glass capillary): ν_{max}/cm^{-1} 3040w, (ν_{Ar-H}), 2904s (ν_{C-H}), 1584s, 1296m, 1037s, 777m, 364s, 326s.

6.3.12 – [Cp*Rh(2,2'-BinapS_2)PMe_3] (C5-11e)

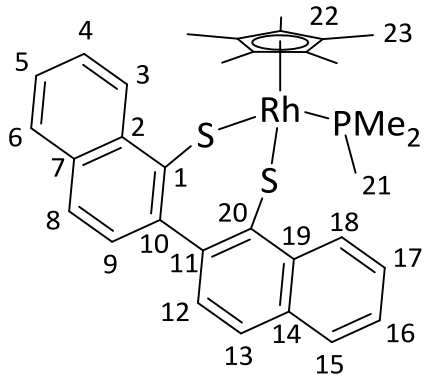

To a THF (15 mL) solution of 2,2'-BinapS_2 (117 mg, 0.37 mmol) was added lithium triethylborohydride (0.80 mL, 0.80 mmol, 1M sol^n in THF) at room temperature. The reaction was left to stir for 0.5 h during which time the solution turned from yellow to almost colourless. To this was added [Cp*Rh(PMe_3)Br_2] (148 mg, 0.31 mmol) and the solution turned instantly to a very dark red/purple colour. The reaction was left to stir at room temperature O/N. The solvent was removed under vacuum and the crude product purified by column chromatography (silica gel/DCM). The solvent was removed to afford the product as a dark purple solid (147 mg, 0.23 mmol, 82%). Crystals suitable for X-ray work were obtained by slow evaporation from DCM.

Anal. calcd. for $C_{33}H_{36}PRhS_2$ (630.11 g mol^{-1}): C, 62.84; H, 5.75. Found: C, 62.73; H, 5.66.

^{1}H NMR (500 MHz, $CDCl_3$): δ 9.20 (d, $^3J_{HH}$ = 8.6 Hz, 1 H, H3), 9.17 (d, $^3J_{HH}$ = 8.5 Hz, 1 H, H18), 7.80 (d, $^3J_{HH}$ = 8.3 Hz, 1 H, H6), 7.77 (d, $^3J_{HH}$ = 8.2 Hz, 1 H, H15), 7.65 (d, $^3J_{HH}$ = 8.3 Hz, 1 H, H13), 7.64 (d, $^3J_{HH}$ =

8.2 Hz, 1 H, H8), 7.54−7.48 (m, 2 H, H4/17), 7.45−7.39 (m, 2 H, H5/16), 7.01 (d, $^{3}J_{HH}$ = 8.3 Hz, 1 H, H9), 6.86 (d, $^{3}J_{HH}$ = 8.3 Hz, 1 H, H12), 1.42 (d, $^{4}J_{HP}$ = 3.2 Hz, 15 H, C23), 1.31 (d, $^{2}J_{HP}$ = 10.6 Hz, 9 H, C21).

$^{13}C\{^{1}H\}$ NMR (125 MHz, $CDCl_3$): δ 150.1 (C_q, C11), 148.1 (C_q, C10), 140.8 (d, $^{3}J_{CP}$ = 6.7 Hz, C_q, C1), 138.3 (C_q, C2), 138.0 (C_q, C19), 137.5 (C_q, C20), 132.9 (C_q, C14), 132.1 (C_q, C7), 129.5 (CH, C12), 129.2 (CH, C3,9), 128.0 (CH, C15), 127.9 (CH, C18), 127.7 (CH, C6), 125.4 (CH, C17), 125.0 (CH, C13), 124.8 (CH, C8,16), 124.7 (CH, C5), 124.3 (CH, C4), 99.7 (dd, $^{1}J_{CRh}$ = 5.5, $^{2}J_{CP}$ = 3.5 Hz, C_q, C22), 15.7 (d, $^{1}J_{CP}$ = 31.5 Hz, CH_3, C21), 9.2 (CH_3, C23).

^{31}P NMR (202 MHz, $CDCl_3$): δ 2.2 (br d, $^{1}J_{PRh}$ = 152 Hz).

$^{31}P\{^{1}H\}$ NMR (202 MHz, $CDCl_3$): δ 2.2 (d, $^{1}J_{PRh}$ = 152 Hz).

HRMS ($APCI^+$): *m/z* (%) 555.0729 (90) $[M-PMe_3+H]^+$, 284.0738 (100) $[C_{20}H_{12}S]$.

IR (KBr): ν_{max}/cm^{-1} 3044w (ν_{Ar-H}), 2906m (ν_{C-H}), 1493m, 1281m, 949s, 815s, 747s, 672m, 546w.

6.3.13 – [Cp*Rh(NaphthS_2)PEt_3] (C5-3b)

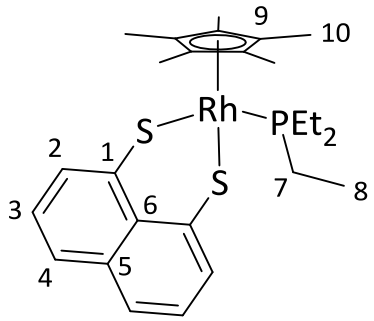

A THF (30 mL) solution containing [Cp*RhCl_2PEt_3] (150 mg, 0.35 mmol) and Naphth$(SH)_2$ (108 mg, 0.56 mmol) was refluxed for 3 h. The solution was cooled and the solvent removed to afford the crude product as a red/orange solid. Purification by flash column chromatography (silica gel/DCM) yielded the title compound as a red solid (157 mg, 0.28 mmol, 82%). Crystals suitable for X-ray work were obtained by slow evaporation from DCM.

Anal. calcd. for $C_{26}H_{36}PRhS_2$ (546.10 g mol^{-1}): C, 57.13; H, 6.64. Found: C, 56.94; H, 6.67.

^{1}H NMR (300 MHz, $CDCl_3$): δ 7.86 (dd, $^{3}J_{HH}$ = 7.3 Hz, $^{4}J_{HH}$ = 1.2 Hz, 2 H, H2), 7.43 (dd, $^{3}J_{HH}$ = 8.0, $^{4}J_{HH}$ = 1.2 Hz, 2 H, H4), 7.09 (dd, $^{3}J_{HH}$ = 8.0, 7.3 Hz, 2 H, H3), 2.08−1.95 (m, 6 H, H7), 1.45 (d, $^{4}J_{HP}$ = 2.7 Hz, 15 H, H10), 1.06 (dt, $^{3}J_{HP}$ = 15.8, $^{3}J_{HH}$ = 7.8 Hz, 9 H, H8).

^{13}C{^{1}H} NMR (125 MHz, $CDCl_3$): δ 139.7 (C_q, C1), 136.2 (C_q, C5), 134.1 (C_q, C6), 128.2 (CH, C2), 124.7 (CH, C4), 123.6 (CH, C3), 99.6 (m, C_q, C9), 15.9 (d, $^{1}J_{CP}$ = 28.1, CH_2, C7), 8.7 (s, CH_3, C10), 7.4 (d, $^{2}J_{CP}$ = 2.9 Hz, CH_3, C8).

^{31}P{^{1}H} NMR (121 MHz, $CDCl_3$): δ 24.63 (d, $^{1}J_{PRh}$ = 146.7 Hz).

MS (ES^+): *m/z* (%) 577.12 (60) $[M+OMe]^+$, 569.09 (20) $[M+Na]^+$, 547.11 (10) $[M+H]^+$, 459.03 (100) $[M-PEt_3+OMe]^+$, 428.01 (55) $[M-PEt_3+H]^+$.

IR (KBr): ν_{max}/cm^{-1} 3034w (ν_{Ar-H}), 2931m (ν_{C-H}), 1534s, 1192m, 1034m, 883m, 759s, 722m (ν_{P-C}).

Raman (glass capillary): ν_{max}/cm^{-1} 3037w (ν_{Ar-H}), 2912m (ν_{C-H}), 1582m, 1537s, 1314s, 884s, 594w (ν_{C-S}), 544m, 439s, 374m, 180m.

6.3.14 – [Cp*Ir(NaphthS_2)PEt_3] (C5-4b)

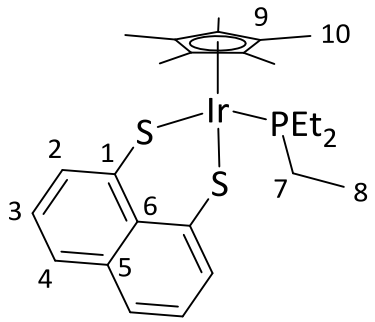

A THF (30 mL) solution containing [Cp*IrCl_2PEt_3] (150 mg, 0.29 mmol) and Naphth$(SH)_2$ (90 mg, 0.46 mmol) was refluxed for 4 h. The solution was cooled and the solvent removed to afford the crude product as a yellow solid. Purification by flash column chromatography (silica gel/DCM) yielded the title compound as a yellow solid (138 mg, 0.21 mmol, 75%). Crystals suitable for X-ray work were obtained by slow evaporation from DCM.

Anal. calcd. for $C_{26}H_{36}IrPS_2$ (636.16 g mol^{-1}): C, 49.04; H, 5.70. Found: C, 48.97; H, 5.81.

^{1}H NMR (300 MHz, $CDCl_3$): δ 7.83 (d, $^{3}J_{HH}$ = 7.3 Hz, 2 H, H2), 7.35 (d, $^{3}J_{HH}$ = 7.8 Hz, 2 H, H4), 6.87 (dd, $^{3}J_{HH}$ = 7.8, 7.5 Hz, 2 H, H3), 2.09−1.95 (m, 6 H, H7), 1.43 (d, $^{4}J_{HP}$ = 1.8 Hz, 15 H, H10), 0.96 (dt, $^{3}J_{HP}$ = 15.9, $^{3}J_{HH}$ = 7.5 Hz, 9 H, H8).

^{13}C{^{1}H} NMR (125 MHz, $CDCl_3$): δ 137.3 (C_q, C1), 136.5 (C_q, C5), 133.5 (C_q, C6), 127.3 (CH, C2), 124.3 (CH, C4), 123.8 (CH, C3), 94.7 (d, $^{2}J_{CP}$ = 2.7 Hz, C_q, C9), 15.7 (d, $^{1}J_{CP}$ = 34.9 Hz, CH_2, C7), 8.3 (CH_3, C10), 6.8 (d, $^{2}J_{CP}$ = 2.7 Hz, CH_3, C8).

^{31}P{^{1}H} NMR (121 MHz, $CDCl_3$): δ −13.97 (s).

MS (ES^+): *m/z* (%) 659.15 (15) $[M+Na]^+$, 637.17 (10) $[M+H]^+$, 549.09 (20) $[M-PEt_3+OMe]^+$, 518.07 (100) $[M-PEt_3+H]^+$.

IR (KBr): ν_{max}/cm^{-1} 3034w (ν_{Ar-H}), 2962w (ν_{C-H}), 1536s, 1192m, 1032m, 882m, 759s, 724m (ν_{P-C}).

Raman (glass capillary): ν_{max}/cm^{-1} 3037w (ν_{Ar-H}), 2914s (ν_{C-H}), 1582m, 1537s, 1315s, 1136m, 884s, 593m (ν_{C-S}), 545m, 442m, 237m.

6.3.15 – [Cp*Rh(AcenapS$_2$)PEt$_3$] (C5-3c)

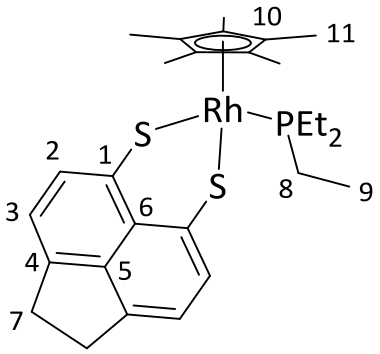

A THF (25 mL) solution containing [Cp*$RhCl_2PEt_3$] (150 mg, 0.35 mmol) and Acenap$(SH)_2$ (122 mg, 0.56 mmol) was refluxed for 5 h. The solution was cooled and the solvent removed to yield the crude compound as a red solid. Purification by flash column chromatography (silica gel/DCM) afforded the title compound as a red solid (166 mg, 0.29 mmol, 83%). Crystals suitable for X-ray work were obtained by slow evaporation from DCM.

Anal. calcd. for $C_{28}H_{38}PRhS_2$ (572.12 g mol^{-1}): C, 58.72; H, 6.70. Found: C, 58.71; H, 6.92.

^{1}H NMR (300 MHz, $CDCl_3$): δ 7.76 (d, $^{3}J_{HH}$ = 6.9 Hz, 2 H, H2), 6.87 (d, $^{3}J_{HH}$ = 6.9 Hz, 2 H, H3), 3.13 (s, 4 H, H7), 2.09–1.96 (m, 6 H, H8), 1.45 (d, $^{4}J_{HP}$ = 2.7 Hz, 15 H, H11), 1.08 (dt, $^{3}J_{HP}$ = 15.4, $^{3}J_{HH}$ = 7.6 Hz, 9 H, H9).

^{13}C{^{1}H} NMR (125 MHz, $CDCl_3$): δ 141.5 (C_q, C1), 141.0 (C_q, C4), 135.0 (C_q, C5), 132.4 (C_q, C6), 128.7 (CH, C3), 117.7 (CH, C2), 99.4 (m, C_q, C10), 30.0 (CH_2, C7), 16.14 (d, $^{1}J_{CP}$ = 28.2 Hz, C_q, C8), 8.8 (CH_3, C11), 7.5 (d, $^{2}J_{CP}$ = 2.9 Hz, CH_3, C9).

^{31}P{^{1}H} NMR (121 MHz, $CDCl_3$): δ 24.95 (d, $^{1}J_{PRh}$ = 145.9 Hz).

MS (ES^+): *m/z* (%) 595.11 (25) $[M+Na]^+$, 573.13 (35) $[M+H]^+$, 454.03 (100) $[M-PEt_3+H]^+$, 119.10 (10) $[PEt_3+H]^+$.

IR (KBr): ν_{max}/cm^{-1} 2928s (ν_{C-H}), 1458m, 1406s, 1229m, 1104m, 1033s, 831m, 758s, 721s (ν_{C-P}).

Raman (glass capillary): ν_{max}/cm^{-1} 2910m (ν_{C-H}), 1595s, 1557m, 1406s, 1323s, 1032m, 827m, 727s (ν_{C-P}), 579m (ν_{C-S}), 412m, 373m, 177m.

6.3.16 – [Cp*Ir(AcenapS_2)PEt_3] (C5-4c)

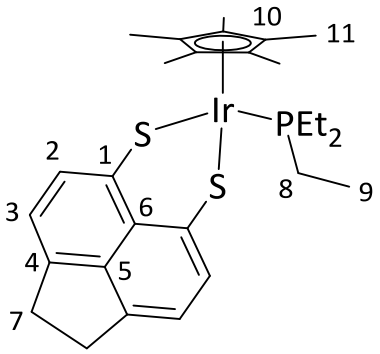

A THF (25 mL) solution containing [Cp*$IrCl_2PEt_3$] (150 mg, 0.29 mmol) and Acenap$(SH)_2$ (101 mg, 0.46 mmol) was refluxed for 6 h. The solution was cooled and the solvent removed to yield the crude product as a yellow solid. Purification by flash column chromatography (silica gel/DCM) afforded the title compound as a yellow solid (158 mg, 0.24 mmol, 83%). Crystals suitable for X-ray work were obtained by slow evaporation from DCM.

Anal. calcd. for $C_{28}H_{38}IrPS_2$ (662.17 g mol^{-1}): C, 50.74; H, 5.78. Found: C, 50.67; H, 5.89.

^{1}H NMR (300 MHz, $CDCl_3$): δ 7.84–7.69 (m, 2 H, H2), 6.81 (d, $^{3}J_{HH}$ = 7.2 Hz, 2 H, H3), 3.08 (s, 4 H, H7), 2.17–2.01 (m, 6 H, H8), 1.50 (d, $^{4}J_{HP}$ = 1.9 Hz, 15 H, H11), 1.03 (dt, $^{3}J_{HP}$ = 16.0, $^{3}J_{HH}$ = 7.6 Hz, 9 H, H9).

^{13}C{^{1}H} NMR (125 MHz, $CDCl_3$): δ 141.2 (C_q, C1), 141.0 (C_q, C4), 132.8 (C_q, C5), 131.7 (C_q, C6), 127.7 (CH, C3), 117.8 (CH, C2), 94.5 (d, $^{2}J_{CP}$ = 2.5 Hz, C_q, C10), 30.0 (CH_2, C7), 15.3 (d, $^{1}J_{CP}$ = 35.5 Hz, CH_2, C8), 8.3 (CH_3, C11), 6.9 (d, $^{2}J_{CP}$ = 2.8 Hz, CH_3, C9).

^{31}P{^{1}H} NMR (121 MHz, $CDCl_3$): δ −14.37 (s).

MS (ES^+): *m/z* (%) 663.18 (55) $[M+H]^+$, 544.08 (100) $[M-PEt_3+H]^+$.

IR (KBr): ν_{max}/cm^{-1} 2928s (ν_{C-H}), 1458m, 1407s, 1229m, 1031s, 831m, 760s, 724s (ν_{C-P}), 499m.

Raman (glass capillary): ν_{max}/cm^{-1} 2910s (ν_{C-H}), 1595s, 1406s, 1323s, 727s (ν_{C-P}), 579m (ν_{C-S}), 412s, 373s, 177s.

6.3.17 – [Cp*Rh(BiphenS_2)PEt_3] (C5-3d)

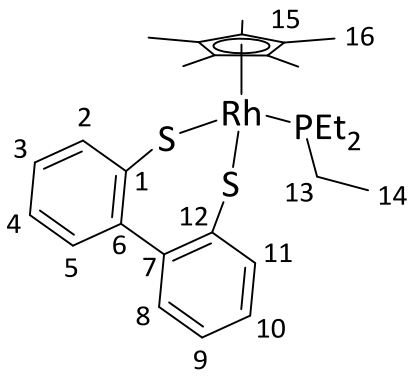

A THF (30 mL) solution containing [Cp*$RhCl_2PEt_3$] (150 mg, 0.35 mmol) and Biphen$(SH)_2$ (122 mg, 0.56 mmol) was refluxed for 5 h. The solvent was removed and the product purified by flash column chromatography (silica gel/DCM) to afford the compound as a dark purple solid (160 mg, 0.27 mmol, 80%). Crystals suitable for X-ray work were obtained by slow evaporation from DCM.

Anal. calcd. for $C_{28}H_{38}PRhS_2$ (572.12 g mol^{-1}): C, 58.72; H, 6.69. Found: C, 58.69; H, 6.74.

^{1}H NMR (300 MHz, $CDCl_3$): δ 7.69−7.61 (m, 2 H, H2/11), 7.19−7.12 (m, 2 H, H4/9), 7.01−6.92 (m, 2 H, H3/10), 6.69 (dd, $^{3}J_{HH}$ = 7.5, $^{4}J_{HH}$ = 1.6 Hz, 1 H, H5), 6.68 (dd, $^{3}J_{HH}$ = 7.5, $^{4}J_{HH}$ = 1.6 Hz, 1 H, H8), 2.04−1.86 (m, 3 H, H13), 1.73−1.58 (m, 3 H, H13), 1.52 (d, $^{4}J_{HP}$ = 2.9 Hz, 15 H, H16), 1.04 (dt, $^{3}J_{HP}$ = 15.0, $^{3}J_{HH}$ = 7.6 Hz, 9 H, H14).

^{13}C{^{1}H} NMR (125 MHz, $CDCl_3$): δ 151.1 (C_q, C6), 150.3 (C_q, C7), 140.8 (C_q, C1), 139.1 (C_q, C12), 137.4 (CH, C2), 135.5 (CH, C11), 130.9 (CH, C5), 130.6 (CH, C8), 126.1 (CH, C4), 125.9 (CH, C10), 125.7 (CH, C9), 125.3 (CH, C3), 99.2 (m, C_q, C15), 16.4 (d, $^{1}J_{CP}$ = 27.0 Hz, CH_2, C13), 8.6 (CH_3, C16), 8.1 (d, $^{2}J_{CP}$ = 3.8 Hz, CH_3, C14).

^{31}P{^{1}H} NMR (121 MHz, $CDCl_3$): δ 21.85 (d, $^{1}J_{PRh}$ = 150.8 Hz).

HRMS (APCI^{+}): *m/z* (%) 573.1277 (65) $[M+H]^{+}$, 455.0365 (20) $[M-PEt_3+H]^{+}$, 119.0981 (100) $[PEt_3+H]^{+}$.

IR (KBr): ν_{max}/cm^{-1} 3040w (ν_{Ar-H}), 2958m (ν_{C-H}), 2906m (ν_{C-H}), 1450s, 1034m, 752s, 722m (ν_{P-C}).

Raman (glass capillary): ν_{max}/cm^{-1} 3043m (ν_{Ar-H}), 2915s (ν_{C-H}), 1583s, 1477s, 1036s, 1006w (ν_{P-Ar}), 774s, 612w (ν_{C-S}), 359s, 325s.

6.3.18 – [Cp*Ir(BiphenS_2PEt_3] (C5-4d)

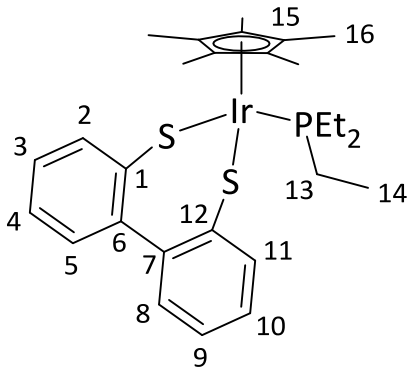

A THF (30 mL) solution containing [Cp*$IrCl_2PEt_3$] (150 mg, 0.29 mmol) and Biphen$(SH)_2$ (101 mg, 0.46 mmol) was refluxed for 5 h. The solvent was removed and the product purified by flash column chromatography (silica gel/DCM) to afford the compound as an orange solid (154 mg, 0.23 mmol, 80%). Crystals suitable for X-ray work were obtained from DCM.

Anal. calcd. for $C_{28}H_{38}IrPS_2$ (662.17 g mol^{-1}): C, 50.80; H, 5.78. Found: C, 50.71; H, 5.83.

^{1}H NMR (300 MHz, $CDCl_3$): δ 7.62 (dd, $^3J_{HH}$ = 7.6, $^4J_{HH}$ = 1.3 Hz, 1 H, H2), 7.51 (dd, $^3J_{HH}$ = 7.6, $^4J_{HH}$ = 1.3 Hz, 1 H, H11), 7.13–7.02 (m, 2 H, H4/9), 6.95–6.88 (m, 2 H, H3/10), 6.85 (dd, $^3J_{HH}$ = 7.5, $^4J_{HH}$ = 1.5 Hz, 1 H, H5), 6.73 (dd, $^3J_{HH}$ = 7.5, $^4J_{HH}$ = 1.5 Hz, 1 H, H8), 2.05–1.87 (m, 3 H, H13), 1.73–1.56 (m, 3 H, H13), 1.48 (d, $^4J_{HP}$ = 1.9 Hz, 15 H, H16), 0.95 (dt, $^3J_{HP}$ = 15.1, $^3J_{HH}$ = 7.8 Hz, 9 H, H14).

^{13}C{^{1}H} NMR (125 MHz, $CDCl_3$): δ 151.5 (C_q, C6), 150.9 (C_q, C7), 139.8 (C_q, C1), 137.2 (C_q, C12), 137.0 (CH, C2), 136.1 (CH, C11), 131.5 (CH, C5), 131.0 (CH, C8), 126.2 (CH, C4), 125.8 (CH, C10), 125.4 (CH, C9), 125.3 (CH, C3), 99.2 (d, $^2J_{CP}$ = 2.9 Hz, C_q, C15), 16.0 (d, $^1J_{CP}$ = 34.2 Hz, CH_2, C13), 8.1 (CH_3, C16), 7.75 (d, $^2J_{CP}$ = 3.8 Hz, CH_3, C14).

^{31}P{^{1}H} NMR (121 MHz, $CDCl_3$): δ −15.53 (s).

HRMS (APCI$^+$): *m/z* (%) 663.1852 (100) $[M+H]^+$, 631 (45) $[M-S+H]^+$, 545.0939 (55) $[M-PEt_3+H]^+$, 119.0981 (80) $[PEt_3+H]^+$.

IR (KBr): ν_{max}/cm^{-1} 3040w (ν_{Ar-H}), 2958w (ν_{C-H}), 2907m (ν_{C-H}), 1451s, 1414m, 1034s, 752s, 724m (ν_{P-C}).

Raman (glass capillary): ν_{max}/cm^{-1} 3043m (ν_{Ar-H}), 2917s (ν_{C-H}), 1584s, 1479s, 1295s, 1036s, 1006w (ν_{P-Ar}), 592m (ν_{C-S}), 362s.

6.3.19 – [Cp*Rh(NaphthS_2)PPh_3] (C5-5b)

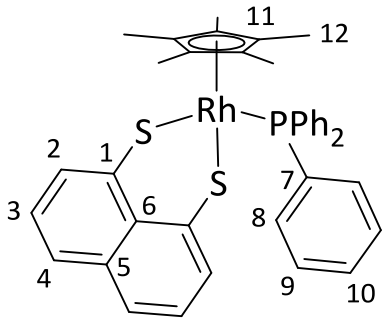

A solution of [Cp*$RhCl_2PPh_3$] (0.10 g, 0.17 mmol), Naphth$(SH)_2$ (0.04 g, 0.22 mmol) and NaOMe (0.04 g, 0.80 mmol) in methanol (20 mL) was stirred at room temperature O/N. The resulting solid was

washed with methanol to afford the product as a red solid (0.98 g, 0.14 mmol, 79%), m.p 225−226 °C (decomp.). Crystals suitable for X-ray work were obtained by slow evaporation from DCM.

Anal. calcd. for $C_{38}H_{36}PRhS_2 \cdot H_2O$ (708.71 g mol^{-1}): C, 64.39; H, 5.40. Found: C, 64.16; H, 5.63.

^{1}H NMR (400 MHz, CD_2Cl_2): δ 7.86 (dd, $^3J_{HH}$ = 7.3,$^4J_{HH}$ = 1.3 Hz, 2H, H2), 7.65−7.55 (m, 6H, H8), 7.47 (dd, $^3J_{HH}$ = 8.1,$^4J_{HH}$ = 1.2 Hz, 2H, H4), 7.45−7.38 (m, 9H, H9/10), 7.05 (dd, $^3J_{HH}$ = 7.4 Hz, 2H, H3), 1.18 (d, $^4J_{HP}$ = 3.1 Hz, 15H, H12).

^{13}C{^{1}H} NMR (100 MHz, CD_2Cl_2): δ 140.2 (d, $^3J_{CP}$ = 5.3 Hz, C_q, C1), 136.0 (C_q, C5), 134.7 (d, $^2J_{CP}$ = 10.1 Hz, CH, C8), 133.6 (C_q, C6), 131.6 (d, $^1J_{CP}$ = 45.3 Hz, C_q, C7), 130.1 (d, $^4J_{CP}$ = 1.9 Hz, CH, C10), 127.8−127.7 (m, CH, C2/11), 124.5 (CH, C4), 123.7 (CH, C3), 100.9 (dd, $^1J_{CRh}$ = 4.5, $^2J_{CP}$ = 2.9 Hz, C_q, C11), 8.0 (CH_3, C12).

^{31}P NMR (162 MHz, CD_2Cl_2): δ 36.7 (br d, $^1J_{PRh}$ 153.0 Hz).

^{31}P{^{1}H} NMR (162 MHz, CD_2Cl_2): δ 36.6 (d, $^1J_{PRh}$ 153.0 Hz).

HRMS (ASAP$^+$): *m/z* (%) 667.0446(7) $[C_{30}H_{37}S_2Rh_2]^+$, 263.1057 (100) $[PPh_3+H]^+$.

IR (KBr) data: ν_{max}/cm^{-1} 3046w (ν_{Ar-H}), 2905w (ν_{Ar-H}), 2362m, 1534s, 1482m, 1434m, 1194m, 1095m, 760s, 699s (ν_{C-S}), 525s.

6.3.20 – [Cp*Ir(NaphthS_2)PPh_3] (C5-6b)

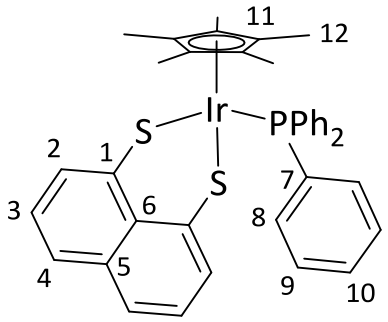

A solution of [Cp*$IrCl_2PPh_3$] (0.10 g, 0.15 mmol), Naphth$(SH)_2$ (0.04 g, 0.18 mmol) and NaOMe (0.03 g, 0.56 mmol) in methanol (20 mL) was stirred at room temperature O/N. The resulting solid was

washed with methanol, affording the product as an orange/red solid (0.90 g, 0.12 mmol, 77%), m.p 263−264 °C (decomp.). Crystals suitable for X-ray work were obtained by slow evaporation from DCM.

Anal. calcd. for $C_{38}H_{36}IrPS_2 \cdot 2H_2O$ (816.04 g mol^{-1}): C, 55.93; H, 4.94. Found: C, 56.03; H, 4.98.

^{1}H NMR (400 MHz, CD_2Cl_2): δ 7.89 (dd, $^3J_{HH}$ = 7.3, $^4J_{HH}$ = 1.2 Hz, 2H, H2), 7.61−7.56 (m, 6H, H8), 7.47 (dd, $^3J_{HH}$ = 8.0, $^4J_{HH}$ = 1.2 Hz, 2H, H4), 7.45−7.39 (m, 9H, H9/10), 6.98 (dd, $^3J_{HH}$ = 7.4 Hz, 2H, H3), 1.22 (d, $^4J_{HP}$ = 2.1 Hz, 15H, H12).

^{13}C{^{1}H} NMR (100 MHz, CD_2Cl_2): δ 137.8 (d, $^3J_{CP}$ = 5.8 Hz, C_q, C1), 136.3 (C_q, C5), 134.8 (d, $^2J_{CP}$ = 9.9 Hz, CH, C8), 133.1 (C_q, C6), 131.7 (d, $^1J_{CP}$ = 54.9 Hz, C_q, C7), 130.7 (d, $^4J_{CP}$ = 1.9 Hz, CH, C10), 127.6 (d, $^3J_{CP}$ = 10.1, CH, C11), 126.9 (CH, C2), 124.0 (CH, C4), 123.9 (CH, C3), 96.3 (d, $^2J_{CP}$ = 2.8 Hz, C_q, C11), 7.5 (CH_3, C12).

^{31}P NMR (162 MHz, CD_2Cl_2): δ 0.6 (br, s).

^{31}P{^{1}H} NMR (162 MHz, CD_2Cl_2): δ 0.6 (s).

HRMS (ASAP$^+$): *m/z* (%) 519.0786 (5) $[M-PPh_3+H]^+$, 279.0945 (20) $[OPPh_3+H]^+$, 263.0994 (100) $[PPh_3+H]^+$.

IR (KBr) data: ν_{max}/cm^{-1} 3048w (ν_{Ar-H}), 2907w (ν_{Ar-H}), 2362m, 1587w, 1537s, 1483m, 1435m, 1195m, 1094m, 811m, 760s, 700s (ν_{C-S}), 532s.

6.3.21 – [Cp*Rh(BiphenS_2)PPh_3] (C5-5d)

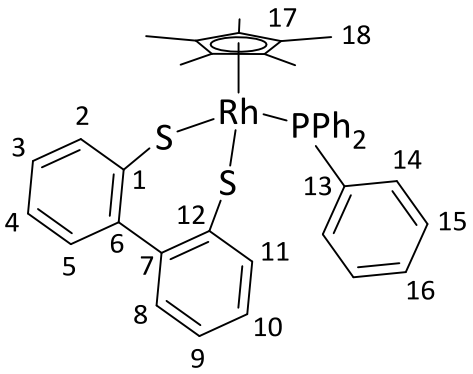

A solution of [Cp*$RhCl_2PPh_3$] (0.10 g, 0.19 mmol), Biphen$(SH)_2$ (0.05 g, 0.23 mmol) and NaOMe (0.04 g, 0.70 mmol) in methanol (20 mL) was stirred at room temperature O/N. The precipitate was filtered, washed with methanol (10 mL) and dried *in vacuo* to afford the product as a purple solid (0.10 g, 0.14 mmol, 75%). Crystals suitable for X-ray work were obtained by slow evaporation from benzene.

Anal. calcd. for $C_{40}H_{38}PRhS_2$ (716.74 g mol^{-1}): C, 67.02; H, 5.35. Found: C, 66.93; H, 5.44.

^{1}H NMR (500 MHz, CD_2Cl_2): δ 7.74 (dd, $^3J_{HH}$ = 7.68, $^4J_{HH}$ = 7.7 Hz, 1 H, H2), 7.66 (br s, 6 H, H14), 7.34 (br s, 3 H, H16), 7.27 (br s, 6 H, H15), 7.20 (*p*td, $^3J_{HH}$ = 7.4, $^4J_{HH}$ = 1.4 Hz, 1 H, H4), 7.04 (*p*td, $^3J_{HH}$ = 7.5, $^4J_{HH}$ = 1.6 Hz, 1 H, H3), 6.91−6.84 (m, 2 H, H5/9), 6.62 (dd, $^3J_{HH}$ = 7.8, $^4J_{HH}$ = 1.3 Hz, 1 H, H11), 6.59 (dd, $^3J_{HH}$ = 7.6, $^4J_{HH}$ = 1.5 Hz, 1 H, H8), 6.12 (dd, $^3J_{HH}$ = 7.5, $^4J_{HH}$ = 1.6 Hz, 1 H, H10), 1.19 (d, $^4J_{HP}$ = Hz, 15 H, H18).

^{13}C{^{1}H} NMR (125 MHz, CD_2Cl_2): δ 150.2 (C_q, C6), 150.1 (C_q, C7), 141.6 (d, $^3J_{CP}$ = 4.0 Hz, C_q, C1), 138.8 (C_q, C12), 137.3 (CH, C2), 137.2 (CH, C11), 134.4 (CH, C14), 131.0 (CH, C9), 130.3 (CH, C8), 129.6 (CH, C16), 127.7 (CH, C15), 126.1 (CH, C10), 126.0 (CH, C4), 125.2 (CH, C3), 124.4 (CH, C5), 100.6 (m, C_q, C17), 7.9 (CH_3, C18).

^{31}P NMR (202 MHz, CD_2Cl_2): δ 28.6 (br d, $^1J_{PRh}$ = 158.8 Hz).

^{31}P{^{1}H} NMR (202 MHz, CD_2Cl_2): δ 28.6 (d, $^1J_{PRh}$ = 158.8 Hz).

HRMS (APCI$^+$): *m/z* (%) 717.1273 (<1) $[M+H]^+$, 455.0362 (45) $[M-C_{12}H_8S_2+H]^+$, 263.0981 (100) $[PPh_3+H]^+$.

IR (KBr) data: ν_{max}/cm^{-1} 3046w (ν_{Ar-H}), 2905w (ν_{C-H}), 1571w, 1479m, 1432m, 1155w, 1092m, 751s, 700s (ν_{P-C}), 602w (ν_{C-S}), 527s.

Raman (glass capillary): ν_{max}/cm^{-1} 3057m (ν_{Ar-H}), 2898w (ν_{C-H}), 1586s, 1480m, 1300w, 1038s (ν_{P-Ar}), 1002s (ν_{P-Ar}), 779m, 616w (ν_{C-S}), 354s, 328s.

6.3.22 – [Cp*Ir(BiphenS$_2$)PPh$_3$] (C5-6d)

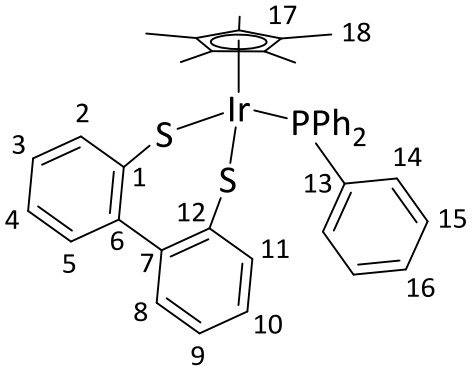

A solution of $[Cp^*IrCl_2PPh_3]$ (0.10 g, 0.15 mmol), Biphen$(SH)_2$ (0.04 g, 0.18 mmol) and NaOMe (0.03 g, 0.54 mmol) in methanol (20 mL) was stirred at room temperature O/N. The precipitate was filtered, washed with methanol (10 mL) and dried *in vacuo* to afford the product as an orange solid (0.096 g, 0.12 mmol, 79%). Crystals suitable for X-ray work were obtained by slow evaporation from diethyl ether.

Anal. calcd. for $C_{40}H_{38}IrPS_2$ (806.05 g mol^{-1}): C, 59.60; H, 4.75. Found: C, 59.78; H, 4.88.

^{1}H NMR (500 MHz, C_6D_6): δ 7.96 (dd, $^3J_{HH}$ = 7.6, $^4J_{HH}$ = 1.4 Hz, 1 H, H2), 7.86 (br s, 6 H, H14), 7.14–7.09 (m, 3 H, H4/5/8), 7.03 (*p*td, $^3J_{HH}$ = 7.3, $^4J_{HH}$ = 2.0 Hz, 1 H, H3), 6.94 (br s, 9 H, H15/16), 6.87 (*p*td, $^3J_{HH}$ = 7.4, $^4J_{HH}$ = 1.4 Hz, 1 H, H9), 6.74 (dd, $^3J_{HH}$ = 7.5, $^4J_{HH}$ = 1.6 Hz, 1 H, H8), 6.23 (*p*td, $^3J_{HH}$ = 7.5, $^4J_{HH}$ = 1.6 Hz, 1 H, H10), 1.08 (d, $^4J_{HP}$ = 2.1 Hz, 15 H, H18).

^{13}C{^{1}H} NMR (125 MHz, C_6D_6): δ 151.5 (C_q, C6), 151.1 (C_q, C7), 139.2 (d, $^3J_{CP}$ = 5.3 Hz, C_q, C1), 137.5 (CH, C11), 137.4 (CH, C2), 136.0 (C_q, C12), 134.9 (CH, C14), 132.2 (CH, C5), 131.6 (CH, C8), 129.3 (CH,

C16), 127.4 (CH, C15), 126.6 (CHs, C10), 126.0 (CH, C4), 125.0 (CH, C3), 124.0 (CH, C9), 95.6 (d, $^{2}J_{CP}$ = 3.1 Hz, C_q, C17), 7.2 (CH_3, C18).

^{31}P NMR (202 MHz, C_6D_6): δ −9.3 (br s).

^{31}P{^{1}H} NMR (202 MHz, C_6D_6): δ −9.3 (s).

HRMS (APCI$^+$): *m/z* (%) 807.1858 (5) $[M+H]^+$, 545.0939 (65) $[M-PPh_3+H]^+$, 263.0985 (100) $[PPh_3+H]^+$.

IR (KBr) data: ν_{max}/cm^{-1} 3045w (ν_{Ar-H}), 2907w (ν_{C-H}), 2361w, 1433s, 1375m, 1093s, 1027m (ν_{P-Ar}), 751s, 686s, 616w (ν_{C-S}), 533s.

Raman (glass capillary): ν_{max}/cm^{-1} 3058s (ν_{Ar-H}), 2901m (ν_{C-H}), 1587s, 1482w, 1301m, 1039s (ν_{P-Ar}), 1003s (ν_{P-Ar}), 780w, 619w (ν_{C-S}), 360s.

6.3.23 – [Cp*Rh(NaphthS_2)P(OEt)$_3$] (C5-7b)

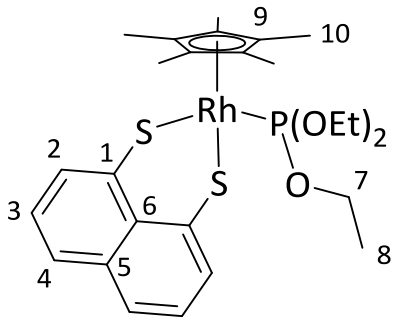

A solution of [Cp*RhCl_2P(OEt)$_3$] (0.10 g, 0.25 mmol), Naphth$(SH)_2$ (0.06 g, 0.27 mmol) and NaOMe (0.04 g, 0.80 mmol) in methanol (20 mL) was stirred at room temperature O/N. The volatiles were removed *in vacuo* and the product was purified by column chromatography (silica gel/hexane:ethyl acetate (80:20)) to afford the product as a red solid (0.11 g, 0.19 mmol, 75%), m.p 218−219 °C (decomp.). Crystals suitable for X-ray work were obtained by slow evaporation from benzene.

Anal. calcd. for $C_{26}H_{36}O_3PRhS_2$ (594.57 g mol^{-1}): C, 52.51; H, 6.10. Found: C, 52.49; H, 6.14.

^{1}H NMR (400 MHz, CD_2Cl_2): δ 7.86 (dd, $^{3}J_{HH}$ = 7.2, $^{4}J_{HH}$ = 1.3 Hz, 2H, H2), 7.47 (dd, $^{3}J_{HH}$ = 8.1,$^{4}J_{HH}$ = 1.2 Hz, 2H, H4), 7.06 (dd, $^{3}J_{HH}$ = 8.0, 7.2 Hz, 2H, H3), 4.22−4.10 (m, 6H, H7), 1.46 (d, $^{4}J_{HP}$ = 4.7 Hz, 15H, H10), 1.33 (t, $^{3}J_{HH}$ = 7.0 Hz, 9H, H8).

^{13}C{^{1}H} NMR (100 MHz, CD_2Cl_2): δ 140.4 (d, $^{3}J_{CP}$ = 5.0 Hz, C_q, C1), 136.1(C_q, C5), 133.9 (C_q, C6), 127.6 (CH, C2), 124.6 (CH, C4), 123.7 (CH, C3), 101.3-101.2 (m, C_q, C9), 62.09 (CH_2, C7), 15.9 (CH_3, C8), 8.2 (CH_3, C10).

^{31}P NMR (162 MHz, CD_2Cl_2): δ 123.5 (br d, $^{1}J_{PRh}$ = 235.0 Hz).

^{31}P{^{1}H} NMR (162 MHz, CD_2Cl_2): δ 123.5 (d, $^{1}J_{PRh}$ = 235.0 Hz).

HRMS (ASAP^{+}): *m/z* (%) 595.0976 (37) $[M+H]^+$, 428.0365 (22) $[M-P(OEt)_3+H]^+$, 284.2959 (100).

IR (KBr) data: ν_{max}/cm^{-1} 3039w (ν_{Ar-H}), 2980m (ν_{C-H}), 2901w, 1536m, 14760m, 1385m, 1157w, 1023s (ν_{P-O}), 947s ($\nu_{P-O-Et\ rocking}$), 760s (ν_{C-S}), 550m.

6.3.24 – [Cp*Ir(NaphthS_2)P(OEt)$_3$] (C5-8b)

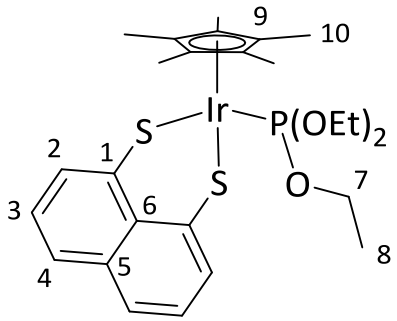

A solution of [Cp*IrCl_2P(OEt)$_3$] (0.10 g, 0.18 mmol), Naphth$(SH)_2$ (0.04 g, 0.22 mmol) and NaOMe (0.05 g, 0.85 mmol) in methanol (20 mL) was stirred at room temperature O/N. The volatiles were removed *in vacuo* and the product was purified by column chromatography (silica gel/hexane:petroleum ether (90:10)) to afford the product as an orange solid (0.07 g, 0.10 mmol, 55%), m.p 227−228 °C (decomp.). Crystals suitable for X-ray work were obtained by slow evaporation from benzene.

Anal. calcd. for $C_{26}H_{36}IrO_3PS_2$ (683.85 g mol^{-1}): C, 45.60; H, 5.30. Found: C, 45.49; H, 5.44.

^{1}H NMR (400 MHz, CD_2Cl_2): δ 7.90 (dd, $^{3}J_{HH}$ = 7.3, $^{4}J_{HH}$ = 1.3 Hz, 2H, H2), 7.48 (dd, $^{3}J_{HH}$ = 8.2, $^{4}J_{HH}$ = 1.2 Hz, 2H, H4), 7.00 (dd, $^{3}J_{HH}$ = 8.2, 7.2 Hz, 2H, H3), 4.18−4.11 (m, 6H, H7), 1.50 (d, $^{4}J_{HP}$ = 3.2 Hz, 15H, H10), 1.34 (t, $^{3}J_{HH}$ = 7.1 Hz, 9H, H8).

^{13}C{^{1}H} NMR (100 MHz, CD_2Cl_2): δ 138.1 (d, $^{3}J_{CP}$ = 5.4 Hz, C_q, C1), 136.2 (C_q, C5), 133.3 (C_q, C6), 126.7 (CH, C2), 124.2 (CH, C4), 124.0 (CH, C3), 96.8 (d, $^{2}J_{CP}$ = 4.2 Hz, C_q, C9), 61.7 (CH_2, C7), 15.8 (CH_3, C8), 7.7 (CH_3, C10).

^{31}P NMR (162 MHz, CD_2Cl_2): δ 74.2 (br s).

^{31}P{^{1}H} NMR (162 MHz, CD_2Cl_2): δ 74.2 (s).

HRMS (ASAP^{+}): *m/z* (%) 685.1550 (25) $[M+H]^{+}$, 529.1254 (100).

IR (KBr) data: ν_{max}/cm^{-1} 3039w (ν_{Ar-H}), 2979m (ν_{C-H}), 2903w, 1536m, 1385w, 1157w, 1068m, 1025s (ν_{P-O}), 947s ($\nu_{P-O-Et\ rocking}$), 761s (ν_{C-S}), 550m.

6.3.25 – [Cp*Rh(BiphenS_2)P(OEt)$_3$] (C5-7d)

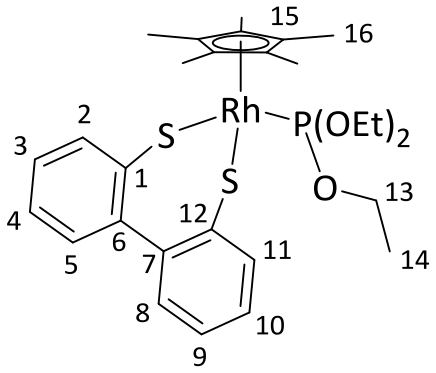

A solution of [Cp*$RhCl_2P(OEt)_3$] (0.10 g, 0.21 mmol), Biphen$(SH)_2$ (0.06 g, 0.25 mmol) and NaOMe (0.04 g, 0.80 mmol) in methanol (20 mL) was stirred at room temperature O/N. The volatiles were removed *in vacuo* and the product purified by column chromatography (silica gel/hexane:ethyl acetate (70:30)) to afford the title compound as a dark coloured solid (0.07 g, 0.11 mmol, 55%). Crystals suitable for X-ray work were obtained by slow evaporation from diethyl ether.

Anal. calcd. for $C_{28}H_{38}O_3PRhS_2$ (620.61 g mol^{-1}): C, 54.18; H, 6.17. Found: C, 54.21; H, 6.24.

^{1}H NMR (500 MHz, C_6D_6): δ 8.02 (dd, $^{3}J_{HH}$ = 7.6, $^{4}J_{HH}$ = 1.4 Hz, 1 H, H2), 7.92 (dd, $^{3}J_{HH}$ = 7.6, $^{4}J_{HH}$ = 1.3 Hz, 1 H, H11), 7.19 (*p*td, $^{3}J_{HH}$ = 7.4, $^{4}J_{HH}$ = 1.4 Hz, 1 H, H9), 7.16−7.11 (2H, m, H4/8), 7.05−6.97 (3H, m, H3/5/10), 4.03−3.94 (3H, m, H13), 3.88−3.79 (3H, m, H13), 1.46 (d, $^{4}J_{HP}$ = 4.7 Hz, 15 H, H16), 1.00 (t, $^{3}J_{HH}$ = 7.1 Hz, 9 H, H14).

^{13}C{^{1}H} NMR (125 MHz, C_6D_6): δ 152.5 (C_q, C6), 151.0 (C_q, C9), 143.0 (d, $^{3}J_{CP}$ = 4.8 Hz, C_q, C1), 141.8 (C_q, C12), 138.3 (CH, C2), 136.1 (CH, C11), 130.5 (CHs,C8), 130.3 (CH, C5), 126.1 (CH, C9), 125.9 (CH, C3), 125.5 (CH, C4), 125.3 (CH, C10), 100.4 (m, C_q, C15), 62.2 (d, $^{2}J_{CP}$ = 6.7 Hz, CH_2, C13), 16.0 (d, $^{3}J_{CP}$ = 6.0 Hz, CH_3, C14) 8.3 (CH_3, C16).

^{31}P NMR (202 MHz, C_6D_6): δ 120.5 (br d, $^{1}J_{PRh}$ = 243.6 Hz)

^{31}P{^{1}H} NMR (202 MHz, C_6D_6): δ 120.5 (d, $^{1}J_{PRh}$ = 243.0 Hz).

HRMS (APCI^{+}): *m/z* (%) 621.1119 (30) $[M+H]^{+}$, 217.0139 (100) $[C_{12}H_9S_2]^{+}$.

IR (KBr) data: ν_{max}/cm^{-1} 3051w (ν_{Ar-H}), 2975m (ν_{C-H}), 1603m, 1450m, 1385m, 1156w, 1021s (ν_{P-O}), 945s (ν_{P-O-Et} rocking), 748s, 669w (ν_{C-S}), 550m.

Raman (glass capillary): ν_{max}/cm^{-1} 3051w (ν_{Ar-H}), 2929m (ν_{C-H}), 1584m, 1477m (ν_{P-O}), 1036s, 775m, 618w (ν_{C-S}), 452m.

6.3.26 – [Cp*Ir(BiphenS_2)P(OEt)$_3$] (C5-8d)

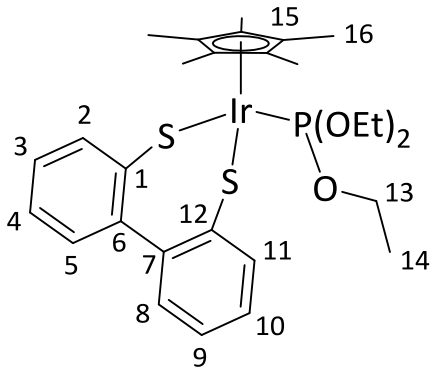

A solution of [Cp*IrCl_2P(OEt)$_3$] (0.10 g, 0.18 mmol), Biphen(SH)$_2$ (0.05 g, 0.22 mmol) and NaOMe (0.04 g, 0.65 mmol) in methanol (20 mL) was stirred at room temperature O/N. The precipitate was

filtered, washed with methanol (10 mL) and dried *in vacuo* to afford the product as an orange solid. (0.098 g, 0.14 mmol, 77%). Crystals suitable for X-ray work were obtained by slow evaporation from DCM.

Anal. calcd. for $C_{28}H_{38}IrO_3PS_2$ (709.92 g mol^{-1}): C, 47.31; H, 5.39. Found: C, 47.44; H, 5.46.

^{1}H NMR (500 MHz, C_6D_6): δ 8.05 (dd, $^3J_{HH}$ = 7.7, $^4J_{HH}$ = 1.4 Hz, 1 H, H2), 7.88 (dd, $^3J_{HH}$ = 7.5, $^4J_{HH}$ = 1.0 Hz, 1 H, H11), 7.22−7.11 (3H, m, H4/8/9), 7.09−7.02 (2H, m, H3/10), 7.00 (dd, $^3J_{HH}$ = 7.5, $^4J_{HH}$ = 1.6 Hz, 1 H, H5), 4.09−3.98 (m, 1 H, H13), 3.87−3.76 (m, 1 H, H13), 1.5 (d, $^4J_{HP}$ = 3.1 Hz, 15 H, H16), 1.03 (t, $^3J_{HH}$ = 7.1 Hz, 9 H, H14).

^{13}C{^{1}H} NMR (125 MHz, C_6D_6): δ 153.2 (C_q, C6), 151.9 (C_q, C9), 139.9 (d, $^3J_{CP}$ = 5.7 Hz, C_q, C1), 138.4 (C_q, C12), 137.9 (CH, C2), 136.5 (CH, C11), 130.9 (CH, C8), 130.8 (CH, C5), 126.1 (CH, C3), 125.9 (CH, C9), 125.5 (CH, C4), 125.3 (CH, C10), 95.8 (d, $^2J_{CP}$ = 4.6 Hz, C_q, C15), 61.5 (d, $^2J_{CP}$ = 6.2 Hz, CH_2,C13) 15.9 (d, $^3J_{CP}$ = 6.9 Hz, CH_3, C14), 7.7 (CH_3, C16).

^{31}P NMR (202 MHz, C_6D_6): δ 74.6 (br s).

^{31}P{^{1}H} NMR (202 MHz, C_6D_6): δ 74.6 (s).

HRMS (APCI$^+$): *m/z* (%) 711.1702 (100) $[M+H]^+$, 545.0939 (32) $[M-P(OEt)_3+H]^+$, 185.0418 (73) $[C_{12}H_9S]^+$.

IR (KBr) data: ν_{max}/cm^{-1} 2973m (ν_{C-H}), 1583w, 1451m (ν_{P-O}), 1386w, 1157w, 1025s, 947s, 789m, 749s, 669w (ν_{C-S}), 559m.

Raman (glass capillary): ν_{max}/cm^{-1} 3053m (ν_{Ar-H}), 2924m (ν_{C-H}), 1584m, 1478w (ν_{P-O}), 1296w, 1036s, 775m, 617w (ν_{C-S}), 364s.

6.3.27 – [Cp*Rh(NaphthS$_2$)P(OPh)$_3$] (C5-9b)

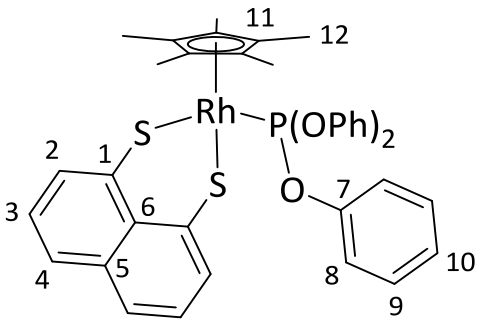

Method 1

A solution of [Cp*RhCl$_2$P(OPh)$_3$] (0.10 g, 0.17 mmol), Naphth(SH)$_2$ (0.04 g, 0.21 mmol) and NaOMe (0.04 g, 0.80 mmol) in methanol (20 mL) was stirred at room temperature O/N. The precipitate was collected by filtration and dried *in vacuo* to afford the product as a red solid (0.01 g, 0.01 mmol, 8%).

Method 2

A THF (15 mL) solution of [Cp*RhCl$_2$P(OPh)$_3$] (100 mg, 0.16 mmol), Naphth(SH)$_2$ (31 mg, 0.16 mmol) and NaOH (13 mg, 0.32 mmol) was stirred at room temperature O/N. The solvent was removed *in vacuo* and the red solid washed with MeOH then dried under vacuum for 3 h. The product was obtained as a red solid (103 mg, 0.14 mmol, 88%), m.p 202−204 °C (decomp.). Crystals suitable for X-ray work were obtained by slow evaporation from DCE.

Anal. calcd. for $C_{38}H_{36}O_3PRhS_2$ (738.70 g mol^{-1}): C, 61.79; H, 4.91. Found: C, 61.69; H, 4.91.

^{1}H NMR (400 MHz, CD_2Cl_2): δ 7.91 (dd, $^3J_{HH}$ = 7.3, $^4J_{HH}$ = 0.9 Hz, 2 H, H2), 7.53 (dd, $^3J_{HH}$ = 7.6, $^4J_{HH}$ = 0.9 Hz, 2 H, H4), 7.34−7.30 (m, 6 H, H9), 7.22−7.15 (m, 9 H, H8/10), 7.10 (*p*t, $^3J_{HH}$ = 7.6 Hz, 2 H, H3), 1.35 (d, $^4J_{HP}$ = 5.3 Hz, H12).

^{13}C{^{1}H} NMR (100 MHz, CD_2Cl_2): δ 151.6 (d, $^2J_{CP}$ = 11.8 Hz, C_q, C7), 139.9 (d, $^3J_{CP}$ = 5.6 Hz, C_q, C1), 136.0 (C_q, C5), 133.5 (C_q, C6), 129.4 (CH, C9), 127.9 (CH, C2), 124.8 (CH, C10), 124.7 (CH, C4), 123.8 (CH, C3), 121.1 (d, $^3J_{CP}$ = 4.4 Hz, CH, C8), 102.6−102.5 (m, C_q, C11), 8.2 (CH_3, C12).

^{31}P NMR (162 MHz, CD_2Cl_2): δ 112.5 (d, $^1J_{PRh}$ = 263.0 Hz).

^{31}P{^{1}H} NMR (162 MHz, CD_2Cl_2): δ 112.4 (d, $^1J_{PRh}$ = 263.0 Hz).

HRMS (ASAP$^+$): *m/z* (%) 739.0974 (<1) $[M+H]^+$, 311.0917 (100) $[P(OPh)_3+H]^+$, 217.0492 (60) $[P(OPh)_2]^+$.

IR (KBr) data: ν_{max}/cm^{-1} 3042w (ν_{Ar-H}), 2917w (ν_{Ar-H}), 1589m, 1488s, 1194s, 1024w (ν_{P-O-C}), 898s, 759s, 690s (ν_{C-S}), 491m.

6.3.28 – [Cp*Ir(NaphthS_2)P(OPh)$_3$] (C5-10b)

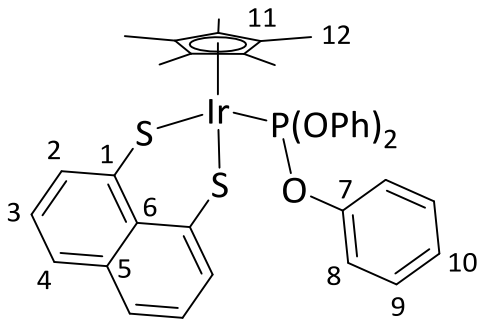

Method 1

A solution of [Cp*$IrCl_2$P(OPh)$_3$] (0.10 g, 0.14 mmol), Naphth(SH)$_2$ (0.04 g, 0.21 mmol) and NaOMe (0.03 g, 0.56 mmol) in methanol (20 mL) was stirred at room temperature O/N. The precipitate as collected by filtration and dried *in vacuo* to afford the product as a red solid (0.02 g, 0.03 mmol, 19%), m.p 235−236 °C (decomp.).

Method 2

A THF (12 mL) solution of [Cp*$IrCl_2$P(OPh)$_3$] (103 mg, 0.15 mmol), Naphth(SH)$_2$ (29 mg, 0.15 mmol) and NaOH (12 mg, 0.30 mmol) was stirred at room temperature O/N. The solvent was removed *in vacuo* and the red solid washed with MeOH then dried under vacuum for 3 h. The product was obtained as a red solid (97 mg, 0.11 mmol, 83%).

Anal. calcd. for $C_{38}H_{36}IrO_3PS_2$ (828.01 g mol^{-1}): C, 55.06; H, 4.38. Found: C, 55.03; H, 4.30.

^{1}H NMR (400 MHz, CD_2Cl_2): δ 7.98 (dd, $^3J_{HH}$ = 7.3,$^4J_{HH}$ = 1.3 Hz, 2H, H2), 7.53 (dd, $^3J_{HH}$ = 8.2,$^4J_{HH}$ 1.2 = Hz, 2H, H4), 7.34−7.31 (m, 6H, H9), 7.25−7.22 (m, 6H, H8), 7.20−7.16 (m, 3H, H10), 7.04 (dd, $^3J_{HH}$ = 7.4 Hz, 2H, H3), 1.36 (d, $^4J_{HP}$ 3.6 = Hz, 15H, H12).

$^{13}C\{^1H\}$ NMR (100 MHz, CD_2Cl_2): δ 151.7 (C_q, C7), 137.6 (d, $^3J_{CP}$ = 5.8 Hz, C_q, C1), 136.2 (C_q, C5), 133.0 (C_q, C6), 129.4 (CH, C9), 127.0 (CH, C2), 124.6 (CH, C10), 124.3 (CH, C4), 124.1 (CH, C3), 121.1 (d, $^3J_{CP}$ = 4.5 Hz, CH, C8), 98.3 ($^2J_{CP}$ = 4.4 Hz, C_q, C11), 7.8 (CH_3, C12).

^{31}P NMR (162 MHz, CD_2Cl_2): δ 60.7 (s).

$^{31}P\{^1H\}$ NMR (162 MHz, CD_2Cl_2): δ 60.6 (s).

HRMS (ASAP$^+$): *m/z* (%) 829.1555 (12) $[M+H]^+$, 519.0798 (39) $[M-P(OPh)_3+H]^+$, 311.0865 (100) $[P(OPh)_3+H]^+$.

IR (KBr) data: ν_{max}/cm^{-1} 3048w (ν_{Ar-H}), 2907w (ν_{Ar-H}), 1587w, 1537s, 1483m, 1435m, 1195m, 1094m (ν_{P-O-C}), 811m, 760s, 700s (ν_{C-S}), 532s.

6.3.29 – [Cp*Rh(BiphenS_2)P(OPh)$_3$] (C5-9d)

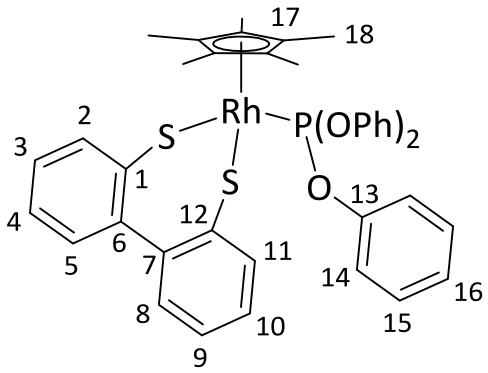

A solution of [Cp*$RhCl_2P(OPh)_3$] (0.10 g, 0.16 mmol), Biphen$(SH)_2$ (0.04 g, 0.19 mmol) and NaOMe (0.04 g, 0.80 mmol) in methanol (20 mL) was heated to reflux O/N. The volatiles were removed *in vacuo* yielding the product as a red solid (0.03 g, 0.04 mmol, 22%). Crystals suitable for X-ray work were obtained by slow evaporation from benzene.

Anal. calcd. for $C_{40}H_{38}O_3PRhS_2$ (764.74 g mol^{-1}): C, 62.82; H, 5.01. Found: C, 62.75; H, 4.95.

^1H NMR (500 MHz, CD_2Cl_2): δ 7.74−7.70 (m, 2 H, H2/12), 7.28 (*p*td, $^3J_{HH}$ = 7.4, $^4J_{HH}$ = 1.4 Hz, 1 H, H9), 7.25−7.18 (m, 6 H, H15), 7.12−7.03 (m, 11 H, H4/10/14/16), 7.02 (dd, $^3J_{HH}$ = 7.4, $^4J_{HH}$ = 1.6 Hz, 1 H,

H8), 6.91 (dd, $^{3}J_{HH}$ = 7.6, $^{4}J_{HH}$ = 1.5 Hz, 1 H, H5), 6.69 (*p*td, $^{3}J_{HH}$ = 7.5, $^{4}J_{HH}$ = 1.6 Hz, 1 H, H3), 1.45 (d, $^{4}J_{HP}$ = 5.5 Hz, 15 H, H18).

$^{13}C\{^{1}H\}$ NMR (125 MHz, CD_2Cl_2): δ 151.8 (d, $^{2}J_{CP}$ = 12.9 Hz, C_q, C13), 151.0 (C_q, C6), 150.6 (C_q, C7), 141.8 (C_q, C12), 140.2 (C_q, C1), 138.9 (CH, C2), 136.6 (CH, C11), 130.2 (CH, C8), 129.6 (CH, C5), 129.2 (CH, C15), 126.3 (CH, C9), 126.0 (CH, C3), 125.9 (CH, C4), 125.4 (CH, C10), 124.3 (CH, C16), 121.5 (d, $^{3}J_{CP}$ = 4.0 Hz, CH, C14), 102.0 (m, C_q, C17), 8.3 (CH_3, C18).

^{31}P NMR (202 MHz, CD_2Cl_2): δ 124.6 (br d, $^{1}J_{PRh}$ = 269.7 Hz).

$^{31}P\{^{1}H\}$ NMR (202 MHz, CD_2Cl_2): δ 124.6 (d, $^{1}J_{PRh}$ = 269.9 Hz).

HRMS (NSI^+): *m/z* (%) 765.1129 (30) $[M+H]^+$, 455.0365 (100) $[M-P(OPh)_3+H]^+$.

IR (KBr) data: ν_{max}/cm^{-1} 3040w (ν_{Ar-H}), 2909w (ν_{C-H}), 2361m, 1588m, 1490s (ν_{P-O}), 1191s, 1026m, 925m, 892s, 754s, 617w (ν_{C-S}).

Raman (glass capillary): ν_{max}/cm^{-1} 3058m (ν_{Ar-H}), 2915m (ν_{C-H}), 1585m, 1478m, 1037s (ν_{P-O}), 772m, 618m (ν_{C-S}), 368s, 325s.

6.3.30 – [Cp*Ir(BiphenS_2)P(OPh)$_3$] (C5-10d)

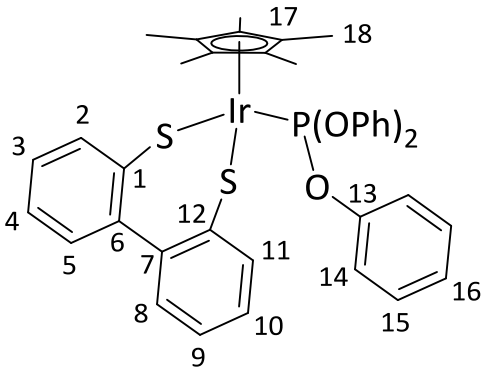

A solution of [Cp*$IrCl_2$P(OPh)$_3$] (0.10 g, 0.14 mmol), Biphen$(SH)_2$ (0.04 g, 0.17 mmol) and NaOMe (0.03 g, 0.51 mmol) in methanol (20 mL) was stirred at room temperature for 3 days to allow the reaction to reach completion. The volatiles were removed *in vacuo* and the resulting product was purified by column chromatography (10:90 ethyl acetate: hexane) yielding the desired compound as

an orange solid (0.06 g, 0.07 mmol, 48%). Crystals suitable for X-ray work were obtained by slow evaporation from diethyl ether at room temperature.

Anal. calcd. for $C_{40}H_{38}IrO_3PS_2$ (854.05 g mol^{-1}): C, 56.25; H, 4.48. Found: C, 56.18; H, 4.57.

^{1}H NMR (500 MHz, C_6D_6): δ 8.22 (dd, $^3J_{HH}$ = 7.7, $^4J_{HH}$ = 1.3 Hz, 1 H, H2), 7.95 (dd, $^3J_{HH}$ = 7.6, $^4J_{HH}$ = 1.5 Hz, 1 H, H11), 7.28 (d, $^3J_{HH}$ = 8.4 Hz, 6 H, H14), 7.25−7.18 (m, 2 H, H8/9), 7.10−7.05 (m, 2 H, H5/10), 7.03 (*p*td, $^4J_{HH}$ = 7.4, $^3J_{HH}$ = 1.3 Hz, 1 H, H4), 6.95 (*p*t, $^3J_{HH}$ = 7.5 Hz, 6 H, H15), 6.79−6.73 (m, 4 H, H3/16), 1.33 (d, $^4J_{HP}$ = 3.5 Hz, 15 H, H18).

^{13}C{^{1}H} NMR (125 MHz, C_6D_6): δ 152.2 (d, $^2J_{CP}$ = 9.6 Hz, C_q, C13), 152.1 (C_q, C6), 152.0 (C_q, C7), 139.0 (C_q, C12), 139.1 (CH, C2), 137.1 (C_q, C1), 137.0 (CH, C11), 131.4 (CH, C8), 130.7 (CH, C5), 129.1 (CH, C15), 126.4 (CH, C3), 126.3 (CH, C9), 125.9 (CH, C4), 125.2 (CH, C10), 124.1 (CH, C16), 121.3 (d, $^3J_{CP}$ = 4.1 Hz, CH, C14), 97.2 (d, $^2J_{CP}$ = 5.0 Hz, C_q, C17), 7.7 (CH_3, C18).

^{31}P NMR (202 MHz, C_6D_6): δ 62.9 (s).

^{31}P{^{1}H} NMR (202 MHz, C_6D_6): δ 62.9 (s).

HRMS (APCI$^+$): *m/z* (%) 855.1686 (10) $[M+H]^+$ 545.0927 (35) $[M-P(OPh)_3+H]^+$, 343.0543 (45), 311.0826 (100) $[P(OPh)_3+H]^+$.

IR (KBr) data: ν_{max}/cm^{-1} 3040w (ν_{Ar-H}), 2913w (ν_{C-H}), 1588m, 1491s, 1192s, 1026m (ν_{P-O}), 927s, 892s, 754s, 688m, 618w (ν_{C-S}).

Raman (glass capillary): ν_{max}/cm^{-1} 3058s (ν_{Ar-H}), 2917m (ν_{C-H}), 1586m, 1296m, 1037s (ν_{P-O}), 1007s, 772m, 616w, 368s (ν_{C-S}).

General Conclusions and Future Scope

Several rare examples of *peri*-substituted triaryl bismuthines have been prepared and spectroscopically and structurally characterised. These compound exhibit interesting spectroscopic features in so much as the *ipso*-carbon of the phenyl ring bound to the bismuth atom shows through space coupling to the adjacent phosphorus. The interaction between the phosphorus lone pair and the Bi–C σ* orbital, albeit weak, presumably allows this transfer of magnetisation to take place. The potential of these compounds as ligands could be investigated as both the phosphine and bismuthine have lone pairs capable of binding a metal centres in a bidentate (**C2**-**5**), tridentate (**C2**-**6**) and tetradentate (**C2**-**2**) fashion. Additionally altering the substituents on the bismuth centre will lead to changes in the electronics of the bismuthine which in turn may change the nature of the interaction between the *peri*-atoms.

Utilising *peri*-substitution, a series of phosphine–bismuthine donor–acceptor complexes have been synthesised. Spectroscopic and structural characterisation techniques were used to confirm the nature of the interaction between the two *peri*-atoms. Owing to the increased Lewis acidity of the bismuth centre when one aryl group is replaced with a halogen, the phosphorus lone pair now donates into the Bi–X σ* orbital. This interaction was supported by a downfield shift in the $^{31}P\{^{1}H\}$ NMR spectra and distances between the two *peri*-atoms significantly less than the sum of their van der Waals radii. The compounds were shown to be stable at room temperature indefinitely under an inert atmosphere. The Lewis acidity of the bismuth atom could be subtly altered by changing the halogen used. As you descend the halogens the resonances in the $^{31}P\{^{1}H\}$ NMR spectra shifted upfield, consistent with a decrease in the strength of the donor–acceptor interaction. The potential of **C2**-**8** as a reagent to form mixed aryl alkyl tri-substituted bismuthines could be investigated as there are few examples of such systems bound to rigid backbones. Furthermore, the effect of changing the aryl substituent could again be looked into to see how the strength of the donor–acceptor interactions varies.

Several aromatic dithiolate ligands of varying size and flexibility have been used to prepare a wide range of novel rhodium and iridium complexes. A number of the dithiol precursors have been structurally characterised for the first time using single crystal X-ray diffraction. Attempts to use these ligands in the formation of potentially stable $16e^{-}$ species resulted in three distinct structural types being formed. A subtle change in the organic backbone (naphthalene to acenaphthene) resulted in a profound difference in the structure of the complex formed. In addition, the

introduction of rotationally free backbone produced yet another type of structure. Single crystal X-ray diffraction confirmed these three distinct complex classes; such a variety is achieved through the utilisation of κ^1 and κ^2 bonding of the sulfur donor atoms and *via* chelating and bridging coordination modes of the dithiolate ligands.

The structural variation in the complexes stems from the coordinatively unsaturated nature of the starting materials (**SM**-**1** and **SM**-**2**) coupled with the flexibility of the ligand backbone. In order to test whether this was indeed the case, a series of ligands were chosen to examine whether the same change in structure between rigid and rotationally free dithiolato ligands would be seen in the coordinatively saturated complexes. This was achieved by using trimethylphosphine to occupy the vacant site in the starting material. Four complexes were prepared in high yields and fully characterised to confirm their identity and structure. Single crystal X-ray diffraction was used to examine the solid state structure and it was found that all the complexes adopted the same piano stool geometry. The presence of the phosphine ligand in the vacant coordination site results in no difference in structural type between the rigid and flexible dithiolate ligands used.

Finally, the importance of phosphorus ligand was investigated to see if changes to the size and electronics would have any effect on the synthesis and structure of the complex. It was found that two different synthetic routes were required depending on both the size and electronics of the phosphorus ligand. No changes in the solid state structure were found when using the series of phosphine and phosphites ligands selected. One interesting observation was the lack of correlation between the size of the ligand, based upon its Tolman cone angle, and the M–P bond length. In some cases, larger ligands actually had shorter M–P bond lengths. By examining the $^1J_{PRh}$ coupling constants across the series, the reason was identified. Greater π back donation in the phosphite containing complexes leads to a shorter M–P bond length and thus a larger coupling constant than in the phosphine derivatives. Hence, in this case, the electronic properties of the phosphorus ligands are overcoming any negative steric effects.

The potential of both of these series of monomeric complexes in the formation of bimetallic complexes could be investigated next. Given the interest in bimetallic systems as catalysts, this could lead to potentially catalytically active species.

Publications List

The following publications have been achieved during the course of this PhD and are available on the attached CD in PDF format. The publication marked as "*manuscript submitted*" is not included on the CD.

***Bis*(alkyl)thioethers on a biphenyl scaffold: A spectroscopic and structural insight**

Rhiann Ferguson, Phillip S. Nejman, Alexandra M. Z. Slawin and J. Derek Woollins, *manuscript submitted*.

Complexation of Aromatic Dichalcogen Ligands to Germanium

Christina B. E. Meigh, Phillip S. Nejman, Alexandra M. Z. Slawin and J. Derek Woollins, *Inorg. Chim. Acta*, **2017**, *456*, 120 – 127.

Varying the Flexibility of the Aromatic Backbone in Half Sandwich Rhodium(III) Dithiolato Complexes: A Synthetic, Spectroscopic and Structural Investigation

Phillip S. Nejman, Alexandra M. Z. Slawin, Petr Kilian and J. Derek Woollins, *Cogent Chemistry*, **2016**, *2(1)*, 1 – 14 , Article number 1245900

Geminally Substituted Tris(acenaphthyl) and Bis(acenaphthyl) Arsines, Stibines and Bismuthine: A Structural and NMR Investigation

Brian A. Chalmers, Christina B. E. Meigh, Phillip S. Nejman, Michael Bühl, Tomáš Lébl, J. Derek Woollins, Alexandra M. Z. Slawin and Petr Kilian, *Inorg. Chem.*, **2016**, *55*, 7117 – 7125.

Diphosphane 2,2'-binaphtho[1,8-*de*][1,3,2]dithiaphosphinine and the easy formation of a stable phosphorus radical cation

Christin Kirst, Bela E. Bode, David B. Cordes, Phillip S. Nejman, Alexandra M. Z. Slawin, Konstantin Karahghiosoff and J. Derek Woollins, *Dalton Trans.*, **2016**, *45*, 6348 – 6351.

Rhodium(III) and Iridium(III) Half-Sandwich Complexes with Tertiary Arsine and Stibine Ligands

Brian A. Chalmers, Michael Bühl, Phillip S. Nejman, Alexandra M. Z. Slawin, J. Derek Woollins and Petr Kilian, *J. Organomet. Chem.*, **2015**, *779-800*, 70 – 74.

Structural Diversity of Bimetallic Rhodium and Iridium Half Sandwich Dithiolato Complexes

Phillip S. Nejman, Brian Morton-Fernandez, David J. Moulding, Kasun S. A. Arachchige, David B. Cordes, Alexandra M. Z. Slawin, Petr Kilian and J. Derek Woollins, *Dalton Trans.*, **2015**, *44*, 16758 – 16766.

The Preparation and Characterisation of Rhodium(III) and Iridium(III) Half Sandwich Complexes with naphthalene-1,8-dithiolate, acenaphthene-5,6-dithiolate and biphenyl-2,2'-dithiolate

Phillip S. Nejman, Brian Morton-Fernandez, Nicholas Black, David B. Cordes, Alexandra M. Z. Slawin, Petr Kilian and J. Derek Woollins, *J. Organomet. Chem.*, **2015**, *776*, 7 – 16.

References

1. M. E. Weeks, *Discovery of the elements*, Journal of Chemical Education, USA, **1960**.
2. N. N. Greenwood, A. Earnshaw, *Chemistry of the Elements, Vol. 2nd ed*, Butterworth-Heinemann, Boston, Mass, **1997**.
3. J. E. Hoffmann, *JOM*, **1994**, *46*, 10-11.
4. N. C. Norman, *Chemistry of Arsenic, Antimony and Bismuth*, Blackie Academic & Professional, London; New york, **1998**.
5. Mineral Commodity Summaries 2015, http://minerals.usgs.gov/minerals/pubs/commodity/bismuth/mcs-2015-bismu.pdf, (accessed August 2016).
6. M. Grayson, *Kirk-Othmer Encyclopedia of Chemical Technology*, 3rd ed., John Wiley, New York, **1983**.
7. B. A. Fowler, C. H. S. J. Chou, R. L. Jones, C. J. Chen, In *Handbook on the Toxicology of Metals (Third Edition)*, Academic Press: Burlington, **2007**, pp. 367-406.
8. C. A. Tylenda, B. A. Fowler, In *Handbook on the Toxicology of Metals (Third Edition)*, Academic Press: Burlington, **2007**, pp. 353-365.
9. B. A. Fowler, M. J. Sexton, In *Handbook on the Toxicology of Metals (Third Edition)*, Academic Press: Burlington, **2007**, pp. 433-443.
10. D. A. Gidlow, *Occupational Medicine*, **2004**, *54*, 76-81.
11. P. W. Atkins, *Inorganic chemistry*, 4th ed. ed., Oxford University Press, Oxford, **2006**.
12. S. G. Shore, R. W. Parry, *J. Am. Chem. Soc.*, **1958**, *80*, 8-12.
13. R. H. Crabtree, *The Organometallic Chemistry of the Transition Metals*, 5th ed., John Wiley & Sons, **2005**.
14. A. Pelter, R. Rosser, S. Mills, *J. Chem. Soc., Chem. Commun.*, **1981**, 1014-1015.
15. P. Pellon, *Tetrahedron Lett.*, **1992**, *33*, 4451-4452.
16. M. A. Frisch, H. G. Heal, H. Mackle, I. O. Madden, *J. Chem. Soc.*, **1965**, 899-907.
17. I. R. Beattie, T. R. Gilson, G. A. Ozin, *J. Chem. Soc. A*, **1968**, 2772-2778.
18. C. Y. Wong, D. K. Kennepohl, R. G. Cavell, *Chem. Rev.*, **1996**, *96*, 1917-1952.
19. C. Chuit, C. Reyé, *Eur. J. Inorg. Chem.*, **1998**, *1998*, 1847-1857.
20. R. R. Holmes, E. F. Bertaut, *J. Am. Chem. Soc.*, **1958**, *80*, 2980-2983.
21. S. F. Spangenberg, H. H. Sisler, *Inorg. Chem.*, **1969**, *8*, 1006-1010.
22. D. K. Friesen, G. A. Ozin, *J. Mol. Struct.*, **1976**, *31*, 77-95.
23. G. Muller, H. J. Matheus, M. Winkler, *Z. Naturforsch., B: Chem. Sci.*, **2001**, *56b*, 1155-1162.
24. P. Wawrzyniak, A. L. Fuller, A. M. Z. Slawin, P. Kilian, *Inorg. Chem.*, **2009**, *48*, 2500-2506.
25. I. R. Thomas, I. J. Bruno, J. C. Cole, C. F. Macrae, E. Pidcock, P. A. Wood, *J. Appl. Crystallogr.*, **2010**, *43*, 362-366.
26. C. F. Macrae, I. J. Bruno, J. A. Chisholm, P. R. Edgington, P. McCabe, E. Pidcock, L. Rodriguez-Monge, R. Taylor, J. van de Streek, P. A. Wood, *J. Appl. Crystallogr.*, **2008**, *41*, 466-470.
27. J. C. Summers, H. H. Sisler, *Inorg. Chem.*, **1970**, *9*, 862-869.
28. G. Alonzo, M. Consiglio, N. Bertazzi, C. Preti, *Inorg. Chim. Acta*, **1985**, *105*, 51-57.
29. G. R. Willey, L. T. Daly, M. G. B. Drew, *J. Chem. Soc., Dalton Trans.*, **1996**, 1063-1067.
30. S. S. Chitnis, K. A. Vos, N. Burford, R. McDonald, M. J. Ferguson, *Chem. Commun. (Cambridge, U. K.)*, **2016**, *52*, 685-688.
31. W. Clegg, R. J. Errington, R. J. Flynn, M. E. Green, D. C. R. Hockless, N. C. Norman, V. C. Gibson, K. Tavakkoli, *J. Chem. Soc., Dalton Trans.*, **1992**, 1753-1754.
32. W. Clegg, M. R. J. Elsegood, V. Graham, N. C. Norman, N. L. Pickett, K. Tavakkoli, *J. Chem. Soc., Dalton Trans.*, **1994**, 1743-1751.

33. W. Clegg, M. R. J. Elsegood, N. C. Norman, N. L. Pickett, *J. Chem. Soc., Dalton Trans.*, **1994**, 1753-1757.
34. W. Clegg, R. John Errington, G. A. Fisher, M. E. Green, D. C. R. Hockless, N. C. Norman, *Chem. Ber.*, **1991**, *124*, 2457-2459.
35. N. L. Kilah, S. Petrie, R. Stranger, J. W. Wielandt, A. C. Willis, S. B. Wild, *Organometallics*, **2007**, *26*, 6106-6113.
36. A. R. J. Genge, N. J. Hill, W. Levason, G. Reid, *J. Chem. Soc., Dalton Trans.*, **2001**, 1007-1012.
37. A. R. J. Genge, W. Levason, G. Reid, *Chem. Commun.*, **1998**, 2159-2160.
38. A. J. Barton, A. R. J. Genge, W. Levason, G. Reid, *J. Chem. Soc.-Dalton Trans.*, **2000**, 859-865.
39. A. J. Barton, A. R. J. Genge, W. Levason, G. Reid, *J. Chem. Soc.-Dalton Trans.*, **2000**, 2163-2166.
40. A. J. Barton, N. J. Hill, W. Levason, B. Patel, G. Reid, *Chem. Commun.*, **2001**, 95-96.
41. J. Burt, W. Levason, G. Reid, *Coord. Chem. Rev.*, **2014**, *260*, 65-115.
42. P. Kilian, F. R. Knight, J. D. Woollins, *Chem. Eur. J.*, **2011**, *17*, 2302-2328.
43. C. P. Brock, J. D. Dunitz, *Acta Crystallogr. B*, **1982**, *38*, 2218-2228.
44. V. Balasubramaniyan, *Chem. Rev.*, **1966**, *66*, 567-641.
45. H. Ehrlich, *Acta Crystallographica*, **1957**, *10*, 699-705.
46. P. Kilian, F. R. Knight, J. D. Woollins, *Coord. Chem. Rev.*, **2011**, *255*, 1387-1413.
47. A. Bondi, *The Journal of Physical Chemistry*, **1964**, *68*, 441-451.
48. G. P. Schiemenz, S. Porksen, P. M. Dominiak, K. Wozniak, *Z. Naturforsch., B: Chem. Sci.*, **2002**, *57b*, 8-18.
49. D. C. Kleinfelter, P. H. Chen, *J. Org. Chem.*, **1969**, *34*, 1741-1745.
50. N. Pourahmady, E. H. Vickery, E. J. Eisenbraun, *J. Org. Chem.*, **1982**, *47*, 2590-2593.
51. G. Yamamoto, M. Suzuki, M. Ōki, *Angewandte Chemie International Edition in English*, **1981**, *20*, 607-608.
52. J. D. Hoefelmeyer, M. Schulte, M. Tschinkl, F. P. Gabbai, *Coord. Chem. Rev.*, **2002**, *235*, 93-103.
53. G. S. Hair, S. L. Battle, A. Decken, A. H. Cowley, R. A. Jones, *Inorg. Chem.*, **2000**, *39*, 27-31.
54. C. Breliere, F. Carre, R. J. P. Corriu, W. E. Douglas, M. Poirier, G. Royo, M. Wong Chi Man, *Organometallics*, **1992**, *11*, 1586-1593.
55. A. Toshimitsu, T. Saeki, K. Tamao, *J. Am. Chem. Soc.*, **2001**, *123*, 9210-9211.
56. H. Schumann, S. Dechert, M. Hummert, K. C. H. Lange, S. Schutte, B. C. Wassermann, K. Köhler, J. Eichhorn, *Z. Anorg. Allg. Chem.*, **2004**, *630*, 1196-1204.
57. S. Bontemps, M. Devillard, S. Mallet-Ladeira, G. Bouhadir, K. Miqueu, D. Bourissou, *Inorg. Chem.*, **2013**, *52*, 4714-4720.
58. F. H. Carré, C. Chuit, R. J. P. Corriu, W. E. Douglas, D. M. H. Guy, C. Reyé, *Eur. J. Inorg. Chem.*, **2000**, *2000*, 647-653.
59. E. Hupf, E. Lork, S. Mebs, L. Chęcińska, J. Beckmann, *Organometallics*, **2014**, *33*, 7247-7259.
60. A. L. Llamas-Saiz, C. Foces-Foces, J. Elguero, *J. Mol. Struct.*, **1994**, *328*, 297-323.
61. L. Sobczyk, *J. Mol. Struct.*, **2010**, *972*, 59-63.
62. H. A. Staab, T. Saupe, *Angewandte Chemie International Edition in English*, **1988**, *27*, 865-879.
63. P. R. Mallinson, K. Woźniak, C. C. Wilson, K. L. McCormack, D. S. Yufit, *J. Am. Chem. Soc.*, **1999**, *121*, 4640-4646.
64. K. Woźniak, T. M. Krygowski, B. Kariuki, W. Jones, E. Grech, *J. Mol. Struct.*, **1990**, *240*, 111-118.
65. M.-L. Lechner, K. S. Athukorala Arachchige, R. A. M. Randall, F. R. Knight, M. Bühl, A. M. Z. Slawin, J. D. Woollins, *Organometallics*, **2012**, *31*, 2922-2930.
66. M. J. Ray, A. M. Z. Slawin, M. Bühl, P. Kilian, *Organometallics*, **2013**, *32*, 3481-3492.
67. M. J. Ray, R. A. M. Randall, K. S. A. Arachchige, A. M. Z. Slawin, M. Bühl, T. Lebl, P. Kilian, *Inorg. Chem.*, **2013**, *52*, 4346-4359.

68. P. Kilian, D. Philp, Alexandra M. Z. Slawin, J. D. Woollins, *Eur. J. Inorg. Chem.*, **2003**, *2003*, 249-254.
69. M. R. StJ. Foreman, J. Novosad, A. M. Z. Slawin, J. Derek Woollins, *J. Chem. Soc., Dalton Trans.*, **1997**, 1347-1350.
70. A. Karaçar, H. Thönnessen, P. G. Jones, R. Bartsch, R. Schmutzler, *Chem. Ber.*, **1997**, *130*, 1485-1489.
71. S. A. Reiter, S. D. Nogai, K. Karaghiosoff, H. Schmidbaur, *J. Am. Chem. Soc.*, **2004**, *126*, 15833-15843.
72. P. Kilian, A. M. Z. Slawin, J. D. Woollins, *Chem. Eur. J.*, **2003**, *9*, 215-222.
73. D. M. U. K. Somisara, M. Bühl, T. Lebl, N. V. Richardson, A. M. Z. Slawin, J. D. Woollins, P. Kilian, *Chem. Eur. J.*, **2011**, *17*, 2666-2677.
74. U. Schmidt, C. Osterroht, *Angewandte Chemie International Edition in English*, **1965**, *4*, 437-437.
75. M. T. Nguyen, A. Van Keer, L. A. Eriksson, L. G. Vanquickenborne, *Chem. Phys. Lett.*, **1996**, *254*, 307-313.
76. A. Marinetti, F. Mathey, J. Fischer, A. Mitschler, *J. Am. Chem. Soc.*, **1982**, *104*, 4484-4485.
77. S. Shah, J. D. Protasiewicz, *Chem. Commun.*, **1998**, 1585-1586.
78. S. Shah, G. P. A. Yap, J. D. Protasiewicz, *J. Organomet. Chem.*, **2000**, *608*, 12-20.
79. B. A. Surgenor, M. Bühl, A. M. Z. Slawin, J. D. Woollins, P. Kilian, *Angew. Chem. Int. Ed.*, **2012**, *51*, 10150-10153.
80. B. A. Surgenor, B. A. Chalmers, K. S. Athukorala Arachchige, A. M. Z. Slawin, J. D. Woollins, M. Bühl, P. Kilian, *Inorg. Chem.*, **2014**, *53*, 6856-6866.
81. N. F. Ramsey, E. M. Purcell, *Phys. Rev.*, **1952**, *85*, 143-144.
82. A. Saika, H. S. Gutowsky, *J. Am. Chem. Soc.*, **1956**, *78*, 4818-4819.
83. D. R. Davis, R. P. Lutz, J. D. Roberts, *J. Am. Chem. Soc.*, **1961**, *83*, 246-247.
84. F. B. Mallory, C. W. Mallory, K. E. Butler, M. B. Lewis, A. Q. Xia, E. D. Luzik, L. E. Fredenburgh, M. M. Ramanjulu, Q. N. Van, M. M. Francl, D. A. Freed, C. C. Wray, C. Hann, M. Nerz-Stormes, P. J. Carroll, L. E. Chirlian, *J. Am. Chem. Soc.*, **2000**, *122*, 4108-4116.
85. R. A. Pascal, A. P. West, D. Van Engen, *J. Am. Chem. Soc.*, **1990**, *112*, 6406-6407.
86. A. Karaçar, H. Thönnessen, P. G. Jones, R. Bartsch, R. Schmutzler, *Heteroat. Chem*, **1997**, *8*, 539-550.
87. B. A. Chalmers, M. Bühl, K. S. Athukorala Arachchige, A. M. Z. Slawin, P. Kilian, *J. Am. Chem. Soc.*, **2014**, *136*, 6247-6250.
88. B. A. Chalmers, M. Bühl, K. S. Athukorala Arachchige, A. M. Z. Slawin, P. Kilian, *Chem. Eur. J.*, **2015**, *21*, 7520-7531.
89. Scifinder®, Scifinder - Explore, https://scifinder.cas.org/scifinder/view/scifinder/scifinderExplore.jsf, (accessed July 2016).
90. W. Nakanishi, S. Hayashi, *Phosphorus, Sulfur Silicon Relat. Elem.*, **2002**, *177*, 1833-1837.
91. H. Suzuki, T. Murafuji, Y. Matano, N. Azuma, *J. Chem. Soc., Perkin Trans. 1.*, **1993**, 2969-2973.
92. S. S. Batsanov, *Inorg. Mater.*, **2001**, *37*, 871-885.
93. C. J. Carmalt, A. H. Cowley, R. D. Culp, R. A. Jones, S. Kamepalli, N. C. Norman, *Inorg. Chem.*, **1997**, *36*, 2770-2776.
94. S. Kamepalli, C. J. Carmalt, R. D. Culp, A. H. Cowley, R. A. Jones, N. C. Norman, *Inorg. Chem.*, **1996**, *35*, 6179-6183.
95. C. R. Wade, M. R. Saber, F. P. Gabbaï, *Heteroat. Chem*, **2011**, *22*, 500-505.
96. R. L. Giles, J. A. K. Howard, L. G. F. Patrick, M. R. Probert, G. E. Smith, A. Whiting, *J. Organomet. Chem.*, **2003**, *680*, 257-262.
97. M. Yamashita, K. Kamura, Y. Yamamoto, K.-y. Akiba, *Chem. Eur. J.*, **2002**, *8*, 2976-2979.
98. Y. Makoto, W. Kentaro, Y. Yohsuke, A. Kin-ya, *Chem. Lett.*, **2001**, *30*, 1104-1105.
99. N. Tanaka, T. Kasai, *Bull. Chem. Soc. Jpn.*, **1981**, *54*, 3020-3025.

100. W. A. Herrmann, *Synthetic Methods of Organometallic and Inorganic Chemistry: Phosphorus, arsenic, antimony, and bismuth*, Georg Thieme Verlag, **1996**.
101. D. H. R. Barton, N. Y. Bhatnagar, J.-P. Finet, W. B. Motherwell, *Tetrahedron*, **1986**, *42*, 3111-3122.
102. J. V. Supniewski, R. Adams, *J. Am. Chem. Soc.*, **1926**, *48*, 507-517.
103. L. J. Taylor, M. Bühl, P. Wawrzyniak, B. A. Chalmers, J. D. Woollins, A. M. Z. Slawin, A. L. Fuller, P. Kilian, *Eur. J. Inorg. Chem.*, **2016**, *2016*, 659-666.
104. J.-C. Hierso, *Chem. Rev.*, **2014**, *114*, 4838-4867.
105. B. A. Chalmers, C. B. E. Meigh, P. S. Nejman, M. Buhl, T. Lebl, J. D. Woollins, A. M. Z. Slawin, P. Kilian, *Inorg. Chem.*, **2016**, *55*, 7117-7125.
106. L. J. Taylor, B. A. Surgenor, P. Wawrzyniak, M. J. Ray, D. B. Cordes, A. M. Z. Slawin, P. Kilian, *Dalton Trans.*, **2016**, *45*, 1976-1986.
107. B. A. Chalmers, PhD Thesis, University of St Andrews, **2015**.
108. C. Kirst, B. E. Bode, D. B. Cordes, P. S. Nejman, A. M. Z. Slawin, K. Karaghiosoff, J. D. Woollins, *Dalton Trans.*, **2016**, *45*, 6348-6351.
109. S. S. Chitnis, N. Burford, A. Decken, M. J. Ferguson, *Inorg. Chem.*, **2013**, *52*, 7242-7248.
110. B. Cordero, V. Gomez, A. E. Platero-Prats, M. Reves, J. Echeverria, E. Cremades, F. Barragan, S. Alvarez, *Dalton Trans.*, **2008**, 2832-2838.
111. D. M. Hawley, G. Ferguson, *J. Chem. Soc. A*, **1968**, 2539-2543.
112. V. V. Sharutin, I. V. Egorova, T. V. Tsiplukhina, T. K. Ivanenko, M. A. Pushilin, A. V. Gerasimenko, *Zh. Neorg. Khim.*, **2004**, *49*, 1475-1480.
113. Royal Society of Chemistry, Periodic Table - Sulfur, http://www.rsc.org/periodic-table/element/16/sulfur, (accessed July 2016).
114. Encylopaedia Britannica, Sulfur (S), https://www.britannica.com/science/sulfur, (accessed July 2016).
115. J. D. Woollins, In *Biological Interactions Of Sulfur Compounds*; Ed.: S. C. Mitchell, Taylor & Francis: London, **1996**, pp. 1-19.
116. G. Nickless, *Inorganic sulphur chemistry*, Elsevier Pub. Co., Amsterdam; New York, **1968**.
117. M. Schmidt, K. W. Bagnal, W. Siebert, *The chemistry of sulphur, selenium, tellurium and polonium*, Pergamon, Oxford, **1975**.
118. S. C. Mitchell, In *Biological Interactions Of Sulfur Compounds*; Ed.: S. C. Mitchell, Taylor & Francis: London, **1996**, pp. 20-41.
119. T. C. Bruice, S. J. Benkovic, *Bioorganic Mechanisms*, W. A. Benjamin, **1966**.
120. Y. Abiko, In *Metabolism of Sulfur Compounds: Metabolic Pathways,* 3rd ed.; Ed.: D. M. Greenberg, Academic Press, **1975**, *Vol. 7*.
121. R. J. Huxtable, *Biochemistry of Sulfur*, Springer US, **1986**.
122. H. Z. Sable, C. J. Gubler, *Thiamin: Twenty Years of Progress*, New York Academy of Sciences, **1982**.
123. F. A. Cotton, G. Wilkinson, *Advanced Inorganic Chemistry*, 5th ed., John Wiley & Sons, New York, **1988**.
124. H. Vahrenkamp, *Angew. Chem. Int. Ed.*, **1975**, *14*, 322-329.
125. E. Diemann, A. Müller, *Coord. Chem. Rev.*, **1973**, *10*, 79-122.
126. C. Kowala, J. Swan, *Aust. J. Chem.*, **1966**, *19*, 547-554.
127. M. G. B. Drew, R. Mandyczewsky, *J. Chem. Soc. A*, **1970**, 2815-2818.
128. H. Siebert, S. Thym, *Z. Anorg. Allg. Chem.*, **1973**, *399*, 107-114.
129. J. Roussain, *Ann. Chim. Phys.*, **1858**, *52*, 285.
130. W. Hieber, F. Seel, *Z. Anorg. Allg. Chem.*, **1942**, *249*, 308-324.
131. J. T. Thomas, J. H. Robertson, E. G. Cox, *Acta Crystallographica*, **1958**, *11*, 599-604.
132. J. Grobe, F. Kober, *Z. Naturforsch.*, **1969**, *24b*, 1346-1347.
133. L. Markó, G. Bor, G. Almásy, *Chem. Ber.*, **1961**, *94*, 847-850.
134. L. Markó, G. Bor, E. Klumpp, B. Markó, G. Almásy, *Chem. Ber.*, **1963**, *96*, 955-964.

135. E. Klumpp, L. Markó, G. Bor, *Chem. Ber.*, **1964**, *97*, 926-933.
136. J. A. De Beer, R. J. Haines, *J. Organomet. Chem.*, **1970**, *24*, 757-767.
137. J. A. McCleverty, N. Spencer, N. A. Bailey, S. L. Shackleton, *J. Chem. Soc., Dalton Trans.*, **1980**, 1939-1944.
138. J. A. McCleverty, N. J. Morrison, N. Spencer, C. C. Ashworth, N. A. Bailey, M. R. Johnson, J. M. A. Smith, B. A. Tabbiner, C. R. Taylor, *J. Chem. Soc., Dalton Trans.*, **1980**, 1945-1957.
139. J. R. Phillips, J. C. Poat, A. M. Z. Slawin, D. J. Williams, P. T. Wood, J. D. Woollins, *J. Chem. Soc., Dalton Trans.*, **1995**, 2369-2375.
140. A. M. Bond, R. L. Martin, *Coord. Chem. Rev.*, **1984**, *54*, 23-98.
141. R. Eisenberg, In *Prog. Inorg. Chem.*, John Wiley & Sons, Inc., **2007**, pp. 295-369.
142. F. Tuna, C. A. Smith, M. Bodensteiner, L. Ungur, L. F. Chibotaru, E. J. L. McInnes, R. E. P. Winpenny, D. Collison, R. A. Layfield, *Angew. Chem. Int. Ed.*, **2012**, *51*, 6976-6980.
143. C.-L. Zhou, Z.-M. Wang, B.-W. Wang, S. Gao, *Polyhedron*, **2011**, *30*, 3279-3283.
144. T. J. Kealy, P. L. Pauson, *Nature*, **1951**, *168*, 1039-1040.
145. T. Furia, *Food Technology*, **1964**, *18*, 1874-1882.
146. D. G. Shirley, S. J. Walter, F. H. Noormoahamed, *Clin. Sci.*, **2002**, *103*, 461-466.
147. M. A. Bennett, T. N. Huang, T. W. Matheson, A. K. Smith, S. Ittel, W. Nickerson, In *Inorg. Synth.*, John Wiley & Sons, Inc., **2007**, pp. 74-78.
148. R. C. Poller, J. A. Spillman, *J. Chem. Soc. A*, **1966**, 958-960.
149. J. R. Dorfman, C. P. Rao, R. H. Holm, *Inorg. Chem.*, **1985**, *24*, 453-454.
150. K. Tatsumi, Y. Sekiguchi, A. Nakamura, R. E. Cramer, J. J. Rupp, *Angew. Chem. Int. Ed.*, **1986**, *25*, 86-87.
151. K. Costuas, M. L. Valenzuela, A. Vega, Y. Moreno, O. Peña, E. Spodine, J.-Y. Saillard, C. Diaz, *Inorg. Chim. Acta*, **2002**, *329*, 129-134.
152. J. Lee, G.-B. Yi, M. A. Khan, G. B. Richter-Addo, *Inorg. Chem.*, **1999**, *38*, 4578-4584.
153. C. P. Rao, J. R. Dorfman, R. H. Holm, *Inorg. Chem.*, **1986**, *25*, 428-439.
154. R. N. Mukherjee, C. Pulla Rao, R. H. Holm, *Inorg. Chem.*, **1986**, *25*, 2979-2989.
155. T. C. Hsieh, T. Nicholson, J. Zubieta, *Inorg. Chem.*, **1988**, *27*, 241-250.
156. J. Forniés-Cámer, A. M. Masdeu-Bultó, C. Claver, C. J. Cardin, *Inorg. Chem.*, **1998**, *37*, 2626-2632.
157. T. Costa, J. R. Dorfman, K. S. Hagen, R. H. Holm, *Inorg. Chem.*, **1983**, *22*, 4091-4099.
158. A. Aaliti, A. M. Masdeu, A. Ruiz, C. Claver, *J. Organomet. Chem.*, **1995**, *489*, 101-106.
159. G. Lente, X. Shan, I. A. Guzei, J. H. Espenson, *Inorg. Chem.*, **2000**, *39*, 3572-3576.
160. M. J. Baker-Hawkes, E. Billig, H. B. Gray, *J. Am. Chem. Soc.*, **1966**, *88*, 4870-4875.
161. M. Nomura, E. Tsukano, C. Fujita-Takayama, T. Sugiyama, M. Kajitani, *J. Organomet. Chem.*, **2009**, *694*, 3116-3124.
162. R. Xi, M. Abe, T. Suzuki, T. Nishioka, K. Isobe, *J. Organomet. Chem.*, **1997**, *549*, 117-125.
163. I. K. Pandey, M. Natarajan, S. Kaur-Ghumaan, *J. Inorg. Biochem.*, **2015**, *143*, 88-110.
164. C. Topf, U. Monkowius, G. Knör, *Inorg. Chem. Commun.*, **2012**, *21*, 147-150.
165. S. M. Aucott, P. Kilian, H. L. Milton, S. D. Robertson, A. M. Z. Slawin, J. D. Woollins, *Inorg. Chem.*, **2005**, *44*, 2710-2718.
166. S. M. Aucott, P. Kilian, S. D. Robertson, A. M. Z. Slawin, J. D. Woollins, *Chem. Eur. J.*, **2006**, *12*, 895-902.
167. W. Lubitz, E. J. Reijerse, J. Messinger, *Energy & Environmental Science*, **2008**, *1*, 15-31.
168. J. W. Peters, W. N. Lanzilotta, B. J. Lemon, L. C. Seefeldt, *Science*, **1998**, *282*, 1853-1858.
169. Y. Nicolet, C. Piras, P. Legrand, C. E. Hatchikian, J. C. Fontecilla-Camps, *Structure*, **1999**, *7*, 13-23.
170. F. A. Armstrong, *Curr. Opin. Chem. Biol.*, **2004**, *8*, 133-140.
171. K. A. Vincent, A. Parkin, F. A. Armstrong, *Chem. Rev.*, **2007**, *107*, 4366-4413.
172. P. E. M. Siegbahn, J. W. Tye, M. B. Hall, *Chem. Rev.*, **2007**, *107*, 4414-4435.
173. M. Frey, *ChemBioChem*, **2002**, *3*, 153-160.

174. A. L. De Lacey, V. M. Fernández, M. Rousset, R. Cammack, *Chem. Rev.*, **2007**, *107*, 4304-4330.
175. A. J. Pierik, M. Hulstein, W. R. Hagen, S. P. J. Albracht, *Eur. J. Biochem.*, **1998**, *258*, 572-578.
176. Y. Nicolet, A. L. de Lacey, X. Vernède, V. M. Fernandez, E. C. Hatchikian, J. C. Fontecilla-Camps, *J. Am. Chem. Soc.*, **2001**, *123*, 1596-1601.
177. Y. Nicolet, C. Cavazza, J. C. Fontecilla-Camps, *J. Inorg. Biochem.*, **2002**, *91*, 1-8.
178. A. P. S. Samuel, D. T. Co, C. L. Stern, M. R. Wasielewski, *J. Am. Chem. Soc.*, **2010**, *132*, 8813-8815.
179. S. Ezzaher, A. Gogoll, C. Bruhn, S. Ott, *Chem. Commun.*, **2010**, *46*, 5775-5777.
180. B. K. Teo, F. Wudl, J. H. Marshall, A. Kruger, *J. Am. Chem. Soc.*, **1977**, *99*, 2349-2350.
181. B. K. Teo, P. A. Snyder-Robinson, *Inorg. Chem.*, **1979**, *18*, 1490-1495.
182. B. K. Teo, P. A. Snyder-Robinson, *Inorg. Chem.*, **1978**, *17*, 3489-3497.
183. B. K. Teo, P. A. Snyder-Robinson, *J. Chem. Soc., Chem. Commun.*, **1979**, 255-256.
184. B. K. Teo, P. A. Snyder-Robinson, *Inorg. Chem.*, **1981**, *20*, 4235-4239.
185. B. K. Teo, P. A. Snyder-Robinson, *Inorg. Chem.*, **1984**, *23*, 32-39.
186. B. K. Teo, F. Wudl, J. J. Hauser, A. Kruger, *J. Am. Chem. Soc.*, **1977**, *99*, 4862-4863.
187. B. K. Teo, V. Bakirtzis, P. A. Snyder-Robinson, *J. Am. Chem. Soc.*, **1983**, *105*, 6330-6332.
188. A. W. Gal, J. W. Gosselink, F. A. Vollenbroek, *Inorg. Chim. Acta*, **1979**, *32*, 235-241.
189. W. P. Bosman, H. G. M. van der Linden, *J. Chem. Soc., Chem. Commun.*, **1977**, 714-715.
190. S. M. Aucott, H. L. Milton, S. D. Robertson, A. M. Z. Slawin, G. D. Walker, J. D. Woollins, *Chem. Eur. J.*, **2004**, *10*, 1666-1676.
191. S. M. Aucott, H. L. Milton, S. D. Robertson, A. M. Slawin, J. D. Woollins, *Dalton Trans.*, **2004**, 3347-3352.
192. E. Fanghaenel, J. Bierwisch, A. Ullrich, A. Herrmann, *Chem. Ber.*, **1995**, *128*, 1047-1049.
193. S. D. Robertson, A. M. Z. Slawin, J. D. Woollins, *Polyhedron*, **2006**, *25*, 823-826.
194. S. A. Larkin, J. A. Krause Bauer, V. E. Konoplev, V. P. Dyadchenko, D. A. Lemenovskii, M. R. M. Bruce, A. E. Bruce, *Acta Crystallogr., Sect. C: Cryst. Struct. Commun.*, **2004**, *C60*, m440-m442.
195. M. R. Malachowski, M. Adams, N. Elia, A. L. Rheingold, R. S. Kelly, *J. Chem. Soc., Dalton Trans.*, **1999**, 2177-2182.
196. R. L. McNaughton, A. A. Tipton, N. D. Rubie, R. R. Conry, M. L. Kirk, *Inorg. Chem.*, **2000**, *39*, 5697-5706.
197. E. Erkizia, R. R. Conry, *Inorg. Chem.*, **2000**, *39*, 1674-1679.
198. P. R. Stafford, T. B. Rauchfuss, A. K. Verma, S. R. Wilson, *J. Organomet. Chem.*, **1996**, *526*, 203-214.
199. C. G. M. Benson, C. M. Schofield, R. A. M. Randall, L. Wakefield, F. R. Knight, A. M. Z. Slawin, J. D. Woollins, *Eur. J. Inorg. Chem.*, **2013**, 427-437.
200. L. M. Diamond, F. R. Knight, D. B. Cordes, A. C. C. Ward, A. M. Z. Slawin, J. D. Woollins, *Polyhedron*, **2015**, *85*, 395-404.
201. C. Claver, S. Castillon, N. Ruiz, G. Delogu, D. Fabbri, S. Gladiali, *J. Chem. Soc., Chem. Commun.*, **1993**, 1833-1834.
202. N. Ruiz, S. Castillon, A. Ruiz, C. Claver, A. Aaliti, A. Alvarez-Larena, J. F. Piniella, G. Germain, *J. Chem. Soc., Dalton Trans.*, **1996**, 969-973.
203. N. Ruiz, A. Aaliti, J. Forniés-Cámer, A. Ruiz, C. Claver, C. J. Cardin, D. Fabbri, S. Gladiali, *J. Organomet. Chem.*, **1997**, *545–546*, 79-87.
204. N. Ruiz, I. del Río, J. L. Jiménez, C. Claver, J. Forniés-Cámer, C. C. J. Cardin, S. Gladiali, *J. Mol. Catal. A: Chem.*, **1999**, *143*, 171-180.
205. X.-B. Wang, H.-Q. Zheng, H. Rao, H.-C. Yao, Y.-T. Fan, H.-W. Hou, *Appl. Organomet. Chem.*, **2016**, *30*, 638-644.
206. A. E. Pullen, S. Zeltner, R.-M. Olk, E. Hoyer, K. A. Abboud, J. R. Reynolds, *Inorg. Chem.*, **1997**, *36*, 4163-4171.
207. J. Ferraris, D. O. Cowan, V. Walatka, J. H. Perlstein, *J. Am. Chem. Soc.*, **1973**, *95*, 948-949.
208. J. J. Maj, A. D. Rae, L. F. Dahl, *J. Am. Chem. Soc.*, **1982**, *104*, 4278-4280.

209. X. Yang, D. D. Doxsee, T. B. Rauchfuss, S. R. Wilson, *J. Chem. Soc., Chem. Commun.*, **1994**, 821-822.
210. R. M. Moutloali, F. A. Nevondo, J. Darkwa, E. I. Iwuoha, W. Henderson, *J. Organomet. Chem.*, **2002**, *656*, 262-269.
211. T. C. Harrop, M. M. Olmstead, P. K. Mascharak, *J. Am. Chem. Soc.*, **2004**, *126*, 14714-14715.
212. C. Darnault, A. Volbeda, E. J. Kim, P. Legrand, X. Vernede, P. A. Lindahl, J. C. Fontecilla-Camps, *Nat Struct Mol Biol*, **2003**, *10*, 271-279.
213. J. Forniés-Cámer, A. M. Masdeu-Bultó, C. Claver, C. Tejel, M. A. Ciriano, C. J. Cardin, *Organometallics*, **2002**, *21*, 2609-2618.
214. J. Forniés-Cámer, C. Claver, A. M. Masdeu-Bultó, C. J. Cardin, *J. Organomet. Chem.*, **2002**, *662*, 188-191.
215. N. Nakata, M. Sakashita, C. Komatsubara, A. Ishii, *Eur. J. Inorg. Chem.*, **2010**, 447-453.
216. W. W. Seidel, M. J. Meel, F. Hupka, J. J. Weigand, *Dalton Trans.*, **2010**, *39*, 624-631.
217. S. M. Aucott, D. Duerden, Y. Li, A. M. Slawin, J. D. Woollins, *Chem. Eur. J.*, **2006**, *12*, 5495-5504.
218. S. D. Robertson, A. M. Z. Slawin, J. D. Woollins, *Eur. J. Inorg. Chem.*, **2007**, 247-253.
219. H. Xu, J. H. K. Yip, *Inorg. Chem.*, **2003**, *42*, 4492-4494.
220. I. Langmuir, *Science*, **1921**, *54*, 59-67.
221. J. Zhao, Z. Wei, X. Zeng, X. Liu, *Dalton Trans.*, **2012**, *41*, 11125-11133.
222. J. Meinwald, D. Dauplaise, F. Wudl, J. J. Hauser, *J. Am. Chem. Soc.*, **1977**, *99*, 255-257.
223. A. J. Ashe, J. W. Kampf, P. M. Savla, *Heteroat. Chem*, **1994**, *5*, 113-119.
224. S. Cossu, G. Delogu, D. Fabbri, P. Maglioli, *Org. Prep. Proced. Int.*, **1991**, *23*, 455-457.
225. H. J. Barber, S. Smiles, *J. Chem. Soc.*, **1928**, 1141-1149.
226. W. D. Neudorff, D. Lentz, M. Anibarro, A. D. Schluter, *Chem. Eur. J.*, **2003**, *9*, 2745-2757.
227. K. Yui, Y. Aso, T. Otsubo, F. Ogura, *Bull. Chem. Soc. Jpn.*, **1988**, *61*, 953-959.
228. E. Block, V. Eswarakrishnan, M. Gernon, G. Ofori-Okai, C. Saha, K. Tang, J. Zubieta, *J. Am. Chem. Soc.*, **1989**, *111*, 658-665.
229. C. White, A. Yates, P. M. Maitlis, *Inorg. Synth.*, **1992**, *29*, 228-234.
230. S. M. Aucott, H. L. Milton, S. D. Robertson, A. M. Z. Slawin, J. D. Woollins, *Heteroat. Chem*, **2004**, *15*, 530-542.
231. S. M. Aucott, H. L. Milton, S. D. Robertson, A. M. Z. Slawin, J. D. Woollins, *Heteroat. Chem*, **2005**, *16*, 346-351.
232. M. R. Churchill, S. A. Julis, F. J. Rotella, *Inorg. Chem.*, **1977**, *16*, 1137-1141.
233. M. R. Churchill, S. A. Julis, *Inorg. Chem.*, **1977**, *16*, 1488-1494.
234. D. Sellmann, M. Geck, F. Knoch, G. Ritter, J. Dengler, *J. Am. Chem. Soc.*, **1991**, *113*, 3819-3828.
235. F. A. Cotton, G. Wilkinson, C. A. Murillo, M. Bochmann, *Advanced Inorganic Chemistry*, 6th ed., Wiley & Sons, New York, **1999**.
236. L. Pauling, *J. Am. Chem. Soc.*, **1947**, *69*, 542-553.
237. A. G. Orpen, L. Brammer, F. H. Allen, O. Kennard, D. G. Watson, R. Taylor, *J. Chem. Soc., Dalton Trans.*, **1989**, S1-S83.
238. C. Janiak, *J. Chem. Soc., Dalton Trans.*, **2000**, 3885-3896.
239. J. F. Hartwig, *Organotransition Metal Chemistry: From Bonding to Catalysis*, University Science Books, **2010**.
240. A. J. Birch, D. H. Williamson, In *Organic Reactions*, John Wiley & Sons, Inc., **2004**.
241. D. A. Evans, G. C. Fu, A. H. Hoveyda, *J. Am. Chem. Soc.*, **1988**, *110*, 6917-6918.
242. I. Ojima, T. Kogure, *Tetrahedron Lett.*, **1972**, *13*, 5035-5038.
243. G. C. Vougioukalakis, R. H. Grubbs, *Chem. Rev.*, **2010**, *110*, 1746-1787.
244. P. W. N. M. van Leeuwen, *Homogeneous Catalysis: Understanding the Art*, Springer Netherlands, **2004**.

245. M. Herberhold, T. Daniel, D. Daschner, W. Milius, B. Wrackmeyer, *J. Organomet. Chem.*, **1999**, *585*, 234-240.
246. C. A. Ghilardi, F. Laschi, S. Midollini, A. Orlandini, G. Scapacci, P. Zanello, *J. Chem. Soc., Dalton Trans.*, **1995**, 531-540.
247. D. Sellmann, A. Fetz, M. Moll, F. Knoch, *J. Organomet. Chem.*, **1988**, *355*, 495-511.
248. Y. Wakatsuki, H. Yamazaki, C. Cheng, *J. Organomet. Chem.*, **1989**, *372*, 437-445.
249. M. Herberhold, G.-X. Ji, A. L. Rheingold, *Chem. Ber.*, **1991**, *124*, 2245-2248.
250. B. E. Mouatassim, C. Pearson, A. Shaver, *Inorg. Chem.*, **2001**, *40*, 5290-5291.
251. D. P. Klein, G. M. Kloster, R. G. Bergman, *J. Am. Chem. Soc.*, **1990**, *112*, 2022-2024.
252. W. D. Jones, A. D. Selmeczy, *Organometallics*, **1992**, *11*, 889-893.
253. R. P. Hughes, J. M. Smith, C. D. Incarvito, K.-C. Lam, B. Rhatigan, A. L. Rheingold, *Organometallics*, **2002**, *21*, 2136-2144.
254. A. Shaver, B. El Mouatassim, F. Mortini, F. Bélanger-Gariépy, A. Lough, *Organometallics*, **2007**, *26*, 4229-4233.
255. M. Herberhold, G.-X. Jin, A. L. Rheingold, G. F. Sheats, *Z. Naturforsch.*, **1992**, *47b*, 1091-1098.
256. K. Yang, M. J. Don, D. K. Sharma, S. G. Bott, M. G. Richmond, *J. Organomet. Chem.*, **1995**, *495*, 61-69.
257. I. Ojima, A. T. Vu, D. Bonafoux, *Science of Synthesis*, **2002**, *1*, 531-616.
258. J. W. Kang, K. Moseley, P. M. Maitlis, *J. Am. Chem. Soc.*, **1969**, *91*, 5970-5977.
259. I. Ara, J. R. Berenguer, E. Eguizábal, J. Forniés, E. Lalinde, A. Martín, F. Martínez, *Organometallics*, **1998**, *17*, 4578-4596.
260. S. Ogo, T. Suzuki, Y. Ozawa, K. Isobe, *Chem. Lett.*, **1994**, 1235-1238.
261. Y. Li, R. Ganguly, W. K. Leong, *J. Organomet. Chem.*, **2016**, *818*, 42-47.
262. K. Thommes, B. Içli, R. Scopelliti, K. Severin, *Chem. Eur. J.*, **2007**, *13*, 6899-6907.
263. B. Paz-Michel, M. Cervantes-Vazquez, M. A. Paz-Sandoval, *Inorg. Chim. Acta*, **2008**, *361*, 3094-3102.
264. S. Ogo, T. Suzuki, Y. Ozawa, K. Isobe, *Inorg. Chem.*, **1996**, *35*, 6093-6101.
265. C. A. Tolman, *Chem. Rev.*, **1977**, *77*, 313-348.
266. D. J. Darensbourg, J. R. Andreatta, S. M. Stranahan, J. H. Reibenspies, *Organometallics*, **2007**, *26*, 6832-6838.
267. B. A. Paz-Michel, F. J. González-Bravo, L. S. Hernández-Muñoz, M. A. Paz-Sandoval, *Organometallics*, **2010**, *29*, 3709-3721.
268. W. L. F. Armarego, *J. Chem. Soc.*, **1960**, 433-436.
269. X.-Q. Xiao, G.-X. Jin, *J. Organomet. Chem.*, **2008**, *693*, 316-320.
270. G.-L. Wang, Y.-J. Lin, O. Blacque, H. Berke, G.-X. Jin, *Inorg. Chem.*, **2008**, *47*, 2940-2942.
271. Z.-J. Yao, B. Xu, X.-K. Huo, G.-X. Jin, *J. Organomet. Chem.*, **2013**, *747*, 85-89.
272. S. Kuwata, T. Nagano, A. Matsubayashi, Y. Ishii, M. Hidai, *Inorg. Chem.*, **2002**, *41*, 4324-4330.
273. I. Ruppert, *Z. Anorg. Allg. Chem.*, **1981**, *477*, 59-70.
274. W. L. F. Armarego, C. L. L. Chai, *Purification of Laboratory Chemicals*, 6th ed., Butterworth-Heinemann, Oxford, **2009**.
275. I. J. Bruno, J. C. Cole, P. R. Edgington, M. Kessler, C. F. Macrae, P. McCabe, J. Pearson, R. Taylor, *Acta Crystallogr. B*, **2002**, *58*, 389-397.
276. O. V. Dolomanov, L. J. Bourhis, R. J. Gildea, J. A. K. Howard, H. Puschmann, *J. Appl. Crystallogr.*, **2009**, *42*, 339-341.
277. A. Zweig, A. K. Hoffmann, *J. Org. Chem.*, **1965**, *30*, 3997-4001.